Retinal Pigment Epithelium Derived from Mouse Embryonic Stem Cells Enhances Photoreceptor Differentiation in Retinal Organoids

Aus embryonalen Stammzellen der Maus differenziertes retinales Pigmentepithel steigert die Differenzierung von Fotorezeptoren in retinalen Organoiden

Zur Erlangung des akademischen Grades eines
DOKTORS DER NATURWISSENSCHAFTEN
(Dr. rer. nat.)
von der KIT-Fakultät für Chemie und Biowissenschaften
des Karlsruher Instituts für Technologie (KIT)

genehmigte
DISSERTATION
von

M. Sc. Kai Richler

1. Referent: Prof. Dr. Martin Bastmeyer

2. Referent: Dr. Dietmar Gradl

Tag der mündlichen Prüfung: 16.02.2023

Eidesstattliche Erklärung

Der experimentelle Teil der vorliegenden Arbeit wurde in der Zeit von August 2019 bis Dezember 2022 am Zoologischen Institut in der Abteilung für Zell- und Neurobiologie des Karlsruher Instituts für Technologie (KIT) durchgeführt.

Ich versichere hiermit, dass ich diese Arbeit selbstständig verfasst habe und keine anderen als die angegebenen Quellen und Hinweise verwendet habe. Wörtlich oder inhaltlich übernommene Stellen sind als solche gekennzeichnet und die Satzung des KITs zur Sicherung guter wissenschaftlicher Praxis habe ich in der gültigen Fassung beachtet. Diese Arbeit wurde in keiner Form einer anderen Prüfungsbehörde vorgelegt. Ich versichere außerdem, dass die beigelegte elektronische Version der Arbeit mit der schriftlichen übereinstimmt.

Datum, Ort	Unterschrift

Abstract

The vertebrate retina is a multi-layered neuronal tissue composed of the neural retina and the retinal pigment epithelium (RPE). The neural retina consists of one glial cell type and six neuronal cell types that modulate and transmit information perceived by the light-sensitive photoreceptor cells. Photoreceptors are embedded in the RPE, which has crucial functions during development and maintenance of retinal integrity. Melanosomes in the RPE contain high amounts of Melanin which absorbs scattered light to increase visual quality. In the mature retina, the RPE establishes the outer blood-retina barrier and thus has to set up a bidirectional transport between the retina and the choroid. Since photoreceptors cannot regenerate their visual pigment, many enzymatic reactions to maintain the visual cycle occur in RPE cells. Furthermore, shed photoreceptor outer segments are phagocytosed and recycled in the RPE.

Three-dimensional cell culture offers methods for the generation of organ-like structures, termed organoids. By the use of established protocols, mouse embryonic stem cells (mESCs) can develop retina-like structures by self-organization and differentiation. In retinal organoids (ROs) however, RPE cells are either completely absent or only sparsely present and not adjacent to the neural retinal tissue.

In this work, RPE cells were differentiated using a separate protocol. mESC-derived RPE cells expressed RPE-specific genes which were measured via digital droplet PCR. Immunocytochemical results demonstrated morphological as well as structural maturation. mESC-derived RPE cells were grown on permeable membranes which allowed nutrient exchange mimicking the outer blood-retina barrier. Since neuronal cell types do not fully mature in ROs, an *in vitro* co-cultivation system with mESC-derived RPE cells and ROs was established that allowed the investigation of the co-development of both tissues.

In this setup, maturating ROs were cultivated with mESC-derived RPE cells for periods of three to six days. Immunostaining of cryosectioned ROs identified more Otx2 and Crx expressing photoreceptor cells after co-cultivation. mESC-derived RPE conditioned medium had similar effects on ROs suggesting that soluble factors from RPE cells might also modulate neuronal differentiation. Expression pattern of the proliferation- and mitosis- markers Ki67 and phosphorylated Histone $H3^{ser10}$ revealed that neurogenesis in ROs follows the *in vivo* mechanism, termed interkinetic nuclear migration. In summary, co-cultivation of mESC-derived RPE strongly enhances the differentiation of photoreceptors in ROs and gives insights in the interplay between neural retina and RPE during development to understand mechanisms of *in vivo* retinogenesis.

Zusammenfassung

Die Netzhaut der Wirbeltiere ist ein mehrschichtiges neuronales Gewebe, das sich aus der Neuroretina und dem retinalen Pigmentepithel (RPE) zusammensetzt. Die Neuroretina beinhaltet einen Glia- und sechs neuronale Zelltypen, die Informationen mittels lichtsensitiver Fotorezeptorzellen aufnehmen, verarbeiten und weiterleiten. Die Fotorezeptoren sind im RPE eingebettet, das wichtige Funktionen in der Entwicklung und Instandhaltung der Retina übernimmt. Melanosomen im RPE sind Kompartimente, deren Hauptaufgabe darin besteht Licht zu absorbieren Da das RPE die Blut-Retina-Schanke aufbaut, vermittelt es den Austausch von Molekülen zwischen Retina und Aderhaut. Außerdem phagozytieren RPE-Zellen die äußeren Segmente der Fotorezeptoren und regenerieren deren Sehpigment in mehreren enzymatischen Schritten.

In der dreidimensionalen Zellkultur gibt es Methoden zur Herstellung von organähnlichen Strukturen, die Organoide genannt werden. Mithilfe etablierter Protokolle können Strukturen ähnlich der Netzhaut entwickelt werden, die sich selbstorganisierend in retinale Organoide (ROs) ausdifferenzieren. In diesen Organoiden sind RPE-Zellen jedoch zu meist nicht vorhanden oder nicht in der räumlichen Nähe und Anordnung zu den neuroretinalen Arealen.

In dieser Arbeit wurden RPE-Zellen separat aus embryonalen Stammzellen der Maus (mESZ) differenziert. Die mESZ-RPE-Zellen exprimierten RPE spezifische Markergene, deren Expression mittels *digital droplet* PCR gemessen wurde. In Immunfärbungen konnte sowohl die morphologische als auch strukturelle Maturation der Zellen gezeigt werden. Die mESZ-RPE-Zellen wurden auf permeablen Membranen kultiviert, die den Austausch von Nährstoffen erlauben, was den Aufbau der Blut-Retina-Schranke nachstellt. Da ROs kein vollständig maturiertes retinales Gewebe aufweisen, wurde ein *in vitro* Co-Kultivierungssystem mit RPE-Zellen und ROs etabliert, welches es erlaubt die gemeinsame Entwicklung der beiden Gewebe zu verfolgen und zu untersuchen.

ROs können für einen Zeitraum von drei bis sechs Tagen mit RPE-Zellen kultiviert werden. Per Immunohistochemie konnte in Gefrierschnitten von ROs eine Erhöhung der Anzahl an Otx2 und Crx exprimierenden Fotorezeptoren ermittelt werden. Lösliche Faktoren, die von den RPE-Zellen abgegeben werden, haben auf ROs einen ähnlichen Effekt. Expressionsmuster der Proliferations- und Mitosemarker Ki67 und phosphoryliertes Histon H3 ^{ser10} belegen, dass Neurogenese in ROs nach dem Mechanismus der interkinetischen Zellkernmigration erfolgt. Die Co-Kultivierung von mESZ-RPE hat einen starken Einfluss auf die Differenzierung von Fotorezeptoren in ROs und gibt Einblicke in die Interaktion von Neuroretina und RPE, um Mechanismen der *in vivo* Retinogenese besser verstehen zu können.

Content

Introduction

Animals navigate through their environment relying on the information they perceive. Of all senses, vision is probably the most important. The sensory organ to detect light is the eye which is an evolutionary conserved organ among invertebrates, which exhibit simple eyes, and vertebrates with more complex eyes. In all cases, light passes through the structures of the eye and is detected in form of photons by specialized types of neurons. In more complex eyes, the visual information can already be pre-processed before it is conveyed to brain areas involved in visual sensation.

The retina is the visual sensory tissue in the eye. For more than a century, the retina has attracted the focus of developmental biologists as well as neurobiologists. A lot of our understanding about this tissue is derived from experiments in fish or amphibian but also mammals. The retina, which is a part of the central nervous system (CNS), is easily accessible and does not fulfil vital functions in the body. This makes the retina an outstanding model for research and is now one of the most investigated and understood parts of the CNS.

The retina is a subject of high interest not only for biological research but also for medical applications. Millions of humans worldwide are affected by various diseases associated with retinal dystrophies or retinal degeneration that can cause visual impairment or even total loss of vision. Glaucoma, age-related macular degeneration (AMD), retinitis pigmentosa or diabetic retinopathy are the most prevalent diseases affecting the retina. Understanding the mechanisms in eye development and those that cause vision-affecting diseases will be essential for future therapeutic applications.

Eye Development

Patterning of the CNS is a highly conserved process in vertrebrates[1]. Neurulation and maintenance of neural fate is mediated by fibroblast growth factors (Fgfs)[2]. During and shortly after gastrulation, the forebrain arises from the anterior neuroectoderm[1] and prospective forebrain establishment requires low levels of bone morphogenic protein (Bmp)[3]. The eye field formation is achieved by the regionalization of the anterior neural plate by surrounding anterior structures[4]. In mutant zebrafish, it was observed that increased Wnt signaling causes loss of the telencephalon and eyes whereas the more posterior diencephalon expands[5]. The precise patterning of the anterior neural plate into distinct regions of telencephalon and eyes is mediated in a Wnt level dependent manner, as increasing Wnt antagonist activity can increase eye field gene expression in telencephalic regions[6]. A complete absence of Wnt however, leads to downregulation of eye field markers but an increase of telencephalon gene

expression[2]. This suggests that the patterning of the anterior neural plate is caused by an anteroposterior Wnt gradient[7].

In anterior regions, the transcription factor sine-oculis 3 (Six3) is expressed and required for the formation of telencephalon and eye field regions[8]. The striking role of Six3 in the development of the eye is the ability of ectopic eye induction by exogenous Six3[9]. There is a reciprocal suppressive interaction of Wnt activity, that downregulates Six3 expression, and Six3, which conversely represses Wnt genes[10,11]. This feedback loop results in Six3 expressing regions with low levels of Wnt, which establishes rostral forebrain development[1]. In *Xenopus*, it was found that Bmp repression is required to induce retinal fate which is mediated by Bmp antagonists Noggin, Follistatin, Cerberus and Xnr3[12]. There, a pool of retinal stem cells forms the eye field which will give rise to all neural retinal cells and structures, the retinal pigment epithelium (RPE) and in part to the iris and ciliary body[13,14]. The eye field is specified by cells with an overlapping expression pattern of a set of transcription factors, called the eye field transcription factors (EFTFs), which includes Pax6, Rax, Six3 and Lhx2 in mammals[14–16].

Prior to the onset of expression of the ETFTs, homeodomain *orthodenticle*-related transcription factor Otx2 expression is restricted to the anterior end of the embryo [17]. In Otx2$^{-/-}$ mutants, it was observed that forebrain and midbrain structures are missing[18,19]. Moreover, in Otx2$^{-/-}$ neuroectoderm of chimeric embryos, forebrain markers like Six3 were expressed but the expression has not been maintained, suggesting that Otx2 plays a role in the induction of anterior neural tissue and its patterning[20]. Together with the transcription factor Sox2, which is expressed in the neural ectoderm, Otx2 can activate Rax expression *in vitro*[21]. Mutations of both Sox2 as well as Otx2 are known to cause severe retinal dystrophy and malfunctions[22–24].

As the retinal homeobox transcription factor Rax is expressed, Otx2 expression is downregulated in the anterior neural plate[19]. Rax expression was shown to be crucial for further eye development and the expression of other ETFTs[25]. Thus, Rax drives the specification of retinal progenitor cells[26]. This essential role is highlighted in Rax mutations that cause anophthalmia[27].

Pax6 is a highly conserved paired domain-containing transcription factor, long time known as a master regulator in eye development[28–30]. Pax6 is expressed at the end of gastrulation in the anterior neural plate[31]. Mutations in this gene lead to severe eye defects in mice, rats and humans resulting in microphthalmia or aniridia[15]. Misexpression of Pax6 can induce the formation of ectopic eyes in *Drosophila*, highlighting its essential role in early eye development[32].

Lhx2 is expressed in retinal progenitor cells in the eye field[33]. It is not required for eye field establishment but Lhx2$^{-/-}$ mice fail to progress in eye development[14]. Notably, Pax6 and Lhx2

seem to regulate Six6 (Optx2) gene expression which is required for retinal fate determination and retinoblast proliferation[34,35].

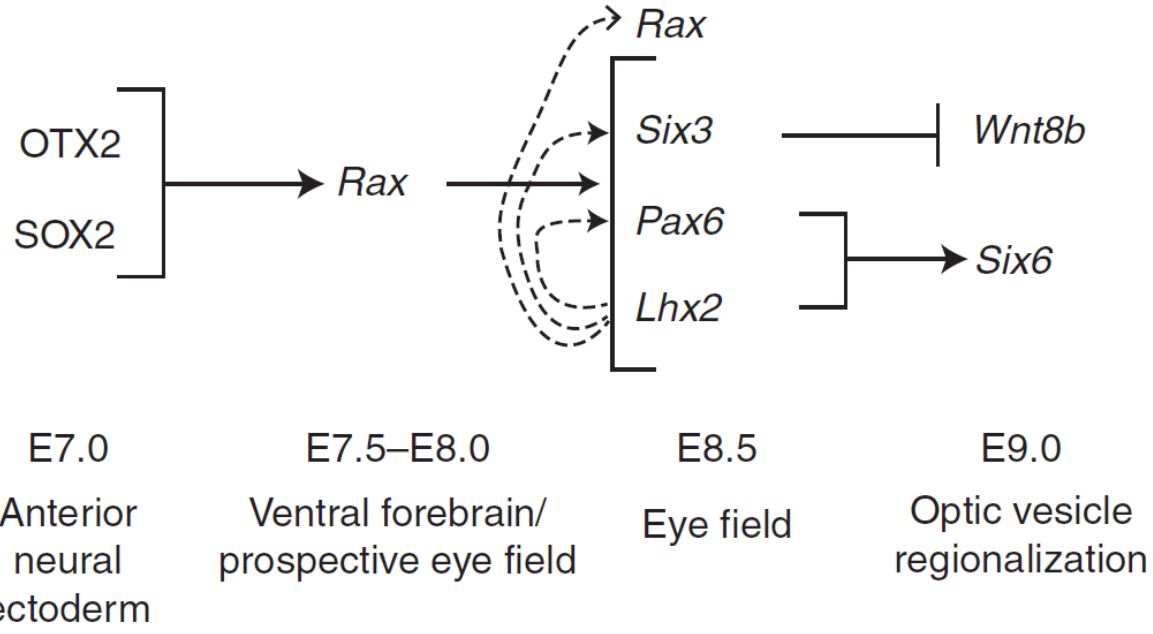

Figure 1: Eye field transcription factor network: Otx2 and Sox2 are expressed in the anterior neural ectoderm. Both co-activate Rax expression which will subsequently initiate the establishment of the eye field. This process is specified by the expression of the EFTFs. The eye field is patterned into distinct regions prior to optic vesicle evagination. Timeline describes the developmental age in mouse embryos. E: Embryonic day. (Scheme from Heavner and Pevny, 2012[14])

After specification and establishment of a single eye anlage, it is separated into two primordia. Surrounding axial tissues provide signals to split the eye field[36].Absence of these tissues leads to failure in separation of the eye field which results in cyclopia. An important factor secreted from the ventral forebrain and the underlying mesoderm is sonic hedgehog (Shh)[37]. Besides Shh, members of Transforming growth factor β (Tgf-β) , and Fibroblast growth factor (Fgf) families are involved in the separation of the eye field as well[30]. Fgf secreted at the midline was shown to mediate competence for a Shh response[38]. Additionally, Shh signaling is responsible for the formation of optic stalk regions in a gradient dependent manner, where high concentrations lead to proximal optic stalk gene expression whereas low concentrations induce ventral and dorsal neural retina[15,39]. Furthermore, Six3 was identified as a second factor to be responsible for proper eye field separation. Interestingly, loss-of-function of either Shh or Six3 leads to similar midline defects[30,40,41]. The importance of both factors is further supported by the fact that Shh expression is regulated by Six3[14]. Upon these signals, ventral diencephalic cells move anteriorly and displace cells of the forebrain laterally to separate the eye field to give rise to the bilateral eye primordia[42,43].

The earliest visible morphological feature in eye development in mice is the formation of the optic pits or optic sulci[14]. In parallel and subsequent to patterning the eye field, it enlarges in size[30]. The following step includes the evagination of the diencephalic walls to form the optic vesicles[14,30]. The transcription factor Rax plays a crucial role in this process. Its expression is shown to be required to evaginate optic vesicles, which was observed in mutant mice and fish[25,30]. Driving force of this morphogenetic process is seemingly cell migration rather than proliferation. At the site of evagination, the epithelial cells soften and cells migrate into this area and subsequently epithelialize which results in increasing size[44]. Retinal stem cells in the optic vesicles will eventually give rise to all neuroectodermal-derived structures in the eye[14]. The optic vesicles are patterned along the dorsoventral axis[14,15]. In this process, expression of identity-specific transcription factors is restricted to distinct regions. Ventral identity is established by the influence of Shh and the expression of Pax2[15,45]. Ventral presumptive optic stalk regions are specified by Pax2 expression and shape the boundary to the central presumptive neural retina where Pax6 is expressed. Both factors are able to reciprocally inhibit each other, further shaping the precise border between both regions[46]. The repressive effect results from the ability to bind to enhancer elements of the other transcription factor, respectively[46]. Dorsal to the neural retina, the presumptive RPE is established. This region is characterized by the expression of the helix-loop-helix transcription factor microphthalmia associated transcription factor (Mitf) and Otx2[14,47]. Similar to the ventral region, the borders between neural retinal and RPE are shaped by reciprocal repression. Here, Mitf can repress Vsx2, which is expressed in the presumptive neural retina, and vice versa. This is supported by the finding that regions of neural retina lose their identity at the expense of RPE in Vsx2 loss-of-function mutations[48]. Conversely, in Mitf mutants, RPE conversion to neural retina can be observed[49]. A similar observation can be made in Otx2 deficient mice[50]. Besides the transcription factor network, several signaling molecules play a role in the patterning and regionalization of the optic vesicle. Members of the Tgf-β, Fgf and Wnt family are known to be involved in the establishment of distinct regions in the optic vesicle[14]. Fgfs at the dorsal site, for example, activate Vsx2 expression while simultaneously repressing Mitf expression[47].

After optic vesicle evagination, the epithelial structure invaginates to form a cup-like structure, hence named optic cup. Lhx2 seems to play a critical role in this process as in $Lhx2^{-/-}$ mutants the progression from optic vesicle to optic cup stalls[51]. Upon expansion, the optic vesicle gets in close contact with the overlying surface ectoderm. Subsequent to this, the invagination process is observed[15]. However, the assumption about the necessity of this contact for optic cup formation is challenged with recent data suggesting independency of optic cup folding and lens placode formation[52].

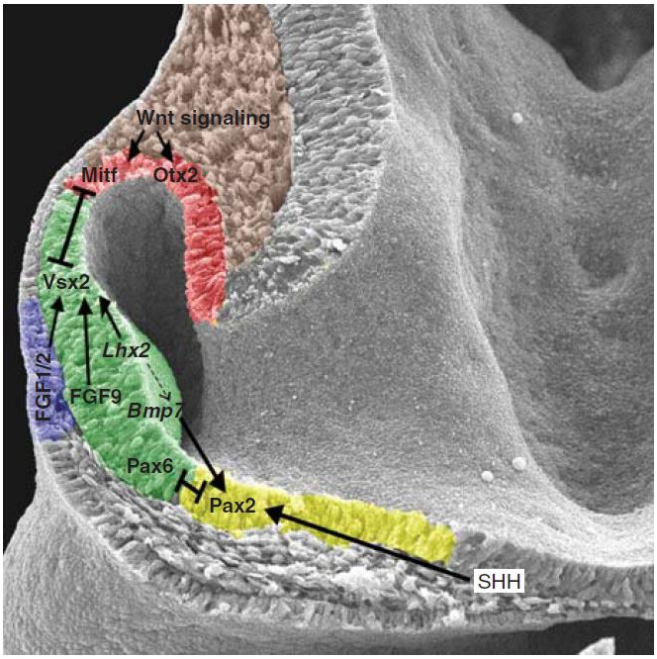

Figure 2: Optic vesicle patterning. Specific regions in the optic vesicle are highlighted with colors. Dorsal presumptive optic stalk in yellow, neural retina in green, lens placode in blue and presumptive RPE in red. Transcription factor network which specifies distinct regions and their interactions and additional signal pathways, that are active in each region, are shown (Image from Heavner and Pevny, 2012[14])

Furthermore, *in vivo* experiments without surrounding tissue show the cell intrinsic ability of optic cup formation[53]. The formation of this ball-like structures requires the bending along the anterior-posterior and dorsoventral axis[30]. At the end of this folding process, there is a two-walled cup-like structure where the proximal region becomes the RPE, which lines the outer layer of the optic cup and thus the back of the neural retina[14]. The final step is the closure of the ventral optic fissure, which is the interface between optic stalk and ventral retina that provides an exit for outgrowing axons and an entrance for the hyaloid artery[54].

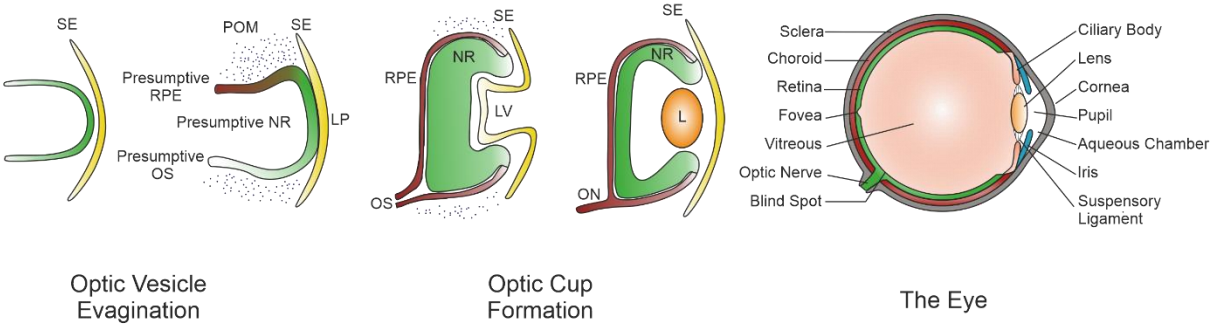

Figure 3: Eye development. After establishing and splitting the eye field in two eye primordia, they start to evaginate resulting in optic vesicles. Along the dorsoventral axis, distinct areas such as presumptive RPE (dorsal), presumptive neural retina (central) and the presumptive optic stalk (ventral) are specified. Subsequently, optic vesicles invaginate to form the bi-layered optic cups. Upon contact to the surface ectoderm, the lens placode also invaginates to form the lens vesicle which will develop into the lens. In further development, mature structures arise to eventually form the eye. SE: Surface ectoderm; POM: Periocular mesenchyme; LP: Lens placode; OS: Optic stalk; NR: Neural retina; ON: Optic nerve; L: Lens.

Alongside the formation of the optic cup, a second invagination can be observed. Here, the lens placode is invaginating to eventually form the lens. By the end of gastrulation, the surface ectoderm is biased to become lens placode[55] which consists of thickened columnar epithelial precursor cells[14]. Expression of Six3 and Pax6 is required for lens induction. Six3 can activate Pax6 expression which is in turn cooperating with Sox2 to activate lens specific gene expression[56,57]. Lens specification in *Xenopus* is acquired when the optic vesicle comes in contact with the lens placode. This is marked by αA-, αB-, δ1-, and ζ-crystallins which results in lens-like structures, named lentoids[15,58]. After invagination of the lens placode, the resulting lens vesicle pinches off from the surface ectoderm[59]. The remaining ectodermal cells proliferate to fill the gap and give rise to the corneal epithelium[14]. Forebrain and midbrain neural crest-derived cells, which form the corneal endothelium, migrate into the space between epithelium and endothelium creating a multi-layered extracellular matrix (ECM) filled structure which is populated with corneal keratocytes[14,60].

The Retina

The retina is a multilayered tissue lining the inner site of the posterior eye (**Figure 4**). It is composed of three layers containing cell bodies. The innermost layer is the ganglion cell layer (GCL) that is almost exclusively composed of retinal ganglion cells which converge their axons forming the optic nerve that projects out of the eye towards the brain[61]. The inner nuclear layer (INL) consists of interneurons which are connected to the GCL via a synaptic layer called the inner plexiform layer (IPL)[62]. Synapses with photoreceptors, which are the outermost cell types, are formed in the outer plexiform layer (OPL)[63]. Photoreceptor cell bodies make up the outer nuclear layer (ONL), while their apical outer segments extend into the interphotoreceptor matrix where they are embedded in the RPE. The RPE is a supportive cell monolayer forming the outer blood-retina barrier[64]. At their basal site, the Bruch's membrane separates the retina from the underlying choroid[65].

The Neural Retina

There are six types of neurons in the retina: Retinal ganglion cells, amacrine cells, horizontal cells, bipolar cells, rod photoreceptors and cone photoreceptor cells. Additionally, there is one glial cell type, named Müller glia[66]. Remarkably, the birth order of these cells seems to be conserved across many species[67–69]. The first type to be born are the retinal ganglion cells which are located in the innermost layer. In a second wave of differentiation, cones, horizontal cells and amacrine cells are born. Then, rod photoreceptors differentiate and the last type of

neurons to be born are bipolar cells. Finally, Müller glial cells are the last cells that differentiate[14,30,67,70].

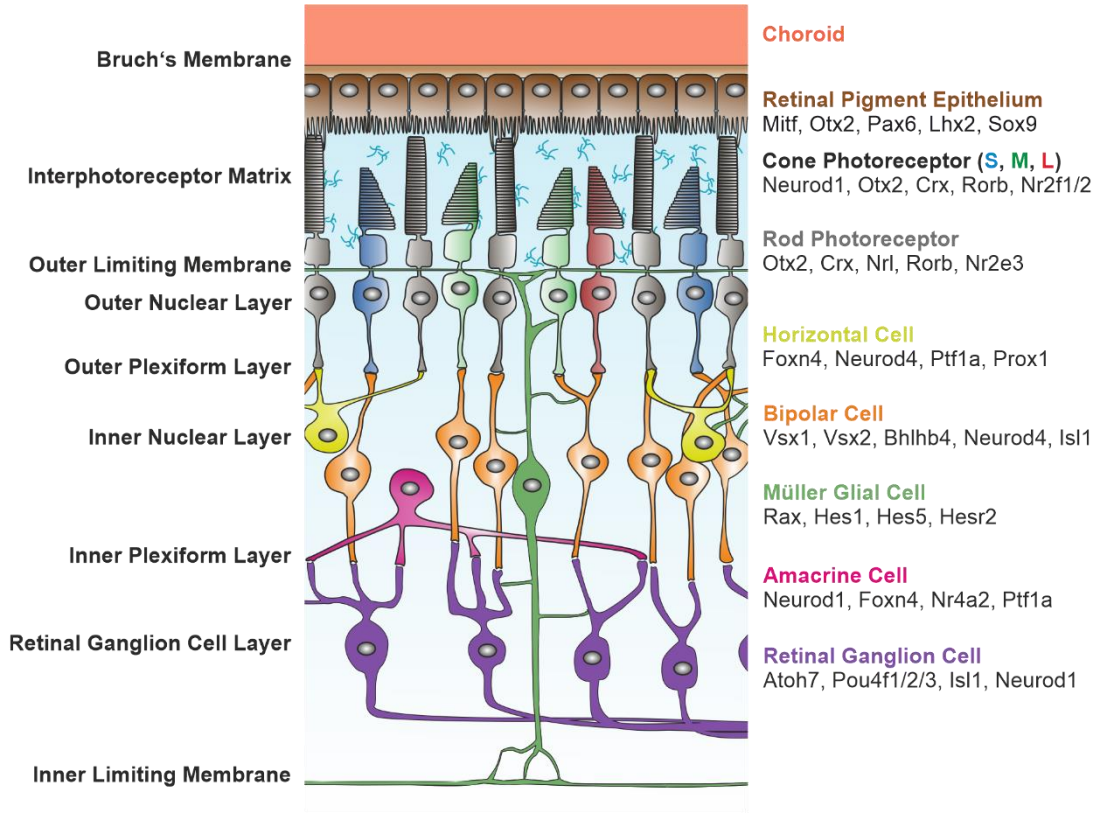

Figure 4: Schematic illustration of the retina. On the left side, major morphological features are described. The right side lists the retinal cell types in the same colors as drawn in the scheme and an excerpt of marker genes for each cell type below. The retina consists of three nuclear layers. The innermost is the ganglion cell layer composed of retinal ganglion cells. The inner nuclear layer consists of amacrine cells, horizontal cells, bipolar cells and the one glial cell type Müller glia. The outer nuclear layer is populated by cone and rod photoreceptors which are embedded in the RPE cells.

Even though neuronal differentiation follows an ordered temporal sequence, it is well known that there is a considerable overlap in the birth dating for the various cell types[68,69](**Figure 5**). All the different cell types populate distinct layers in the retina and form synapses with appropriate partners. Thus, the challenge is to create the correct number and ratio of cells at the right time that eventually migrate to their final destination[67]. How is this precise spatial and temporal neurogenesis accomplished? All retinal cell types are born from multipotent retinal progenitor cells[71]. In the mouse, it was found that a single retinal progenitor can produce a number of clones ranging from 1 up to 200 cells with an average of 40 – 50 cells[71]. In the course of time, several changes in retinal progenitor cells can be observed. The cell cycling time gradually increases from 14 hours to 30 hours in the rat retina[72]. Furthermore, it can be assumed that the cell division symmetry differs between early retinal progenitors and late progenitors. While early progenitor cells divide rather symmetrically to produce two new progenitor daughter cells, the progeny of later progenitors is shifted to give rise to one

progenitor and one postmitotic neuron. By the end of development, cell division is again symmetric but will produce two postmitotic neurons[70].

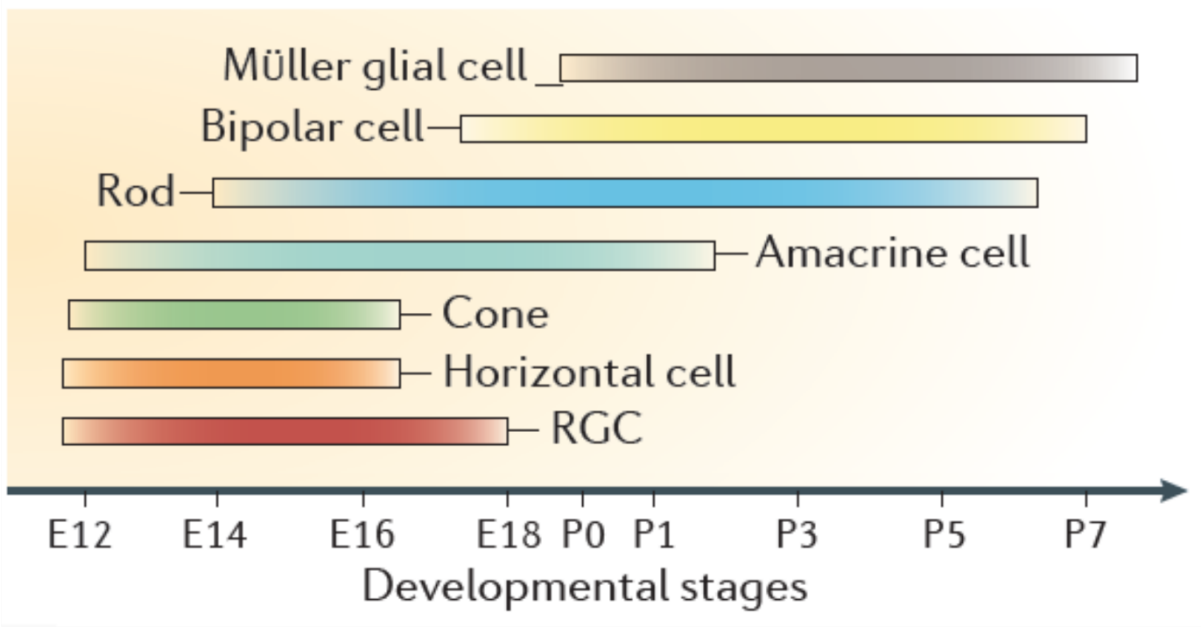

Figure 5: Differentiation of retinal cell types. Schematic illustration of birthdating of the retinal cell types. Starting from the bottom, retinal ganglion cells arise first from the multipotent progenitor cells followed by horizontal cells, cones and amacrine cells. Rods and bipolar cells are the last neurons before the differentiation of Müller glial cells which is the last cell type to be born. **(**Image adapted from Cepko, 2014[73])

Birthdating studies led to a model that describes different states of competence of retinal progenitors[67]. That is, with each cell cycle retinal progenitors can only give rise to a certain subset of postmitotic neurons[70]. This is in contrast to the progressive restriction model that is known from the development of the cortex where progenitors can give rise to all cell types in the beginning and lose their ability over time[74]. The competence of progenitors to differentiate into a subset of neurons is intrinsically regulated. However, external signals can determine the differentiation into a specific cell type from a progenitor in a certain competence state[67,70]. Intrinsic determination was highlighted in transplantation experiments where early progenitors were placed in a later stage tissue. Regardless of their environment, early progenitors gave rise to early born retinal ganglion cells[75]. Conversely, late progenitors produced rods and bipolar cells independent of their environment[76]. Additionally, studies support intrinsically different behavior of progenitor cells over time with regard to the sensitivity of Tgf-β, Egf and Fgf caused by differently expressed surface receptors[77,78].

The transcription factor network involved in early eye development, also plays a role in retinal progenitor cell states. Pax6 seems to be required to maintain multipotency in retinal progenitor cells[79].When inactivated, retinal progenitors only give rise to a single neuronal cell type which are amacrine cells[79]. This phenotype can be explained by Pax6-mediated activation of

Neurogenin 2 and Atoh7 gene expression, which is not induced in absence of Pax6[66,80]. Atoh7, in turn, is known to be required for the differentiation of retinal ganglion cells[81]. This gene shows another interesting condition in progenitor cell fate decision making. Although it is required for ganglion cell differentiation, not all cells that express Atoh7 differentiate into retinal ganglion cells[82]. This suggests the involvement of additional factors for ganglion cell fate acquisition, underlining the complexity of the gene regulatory network behind progenitor cell differentiation. Furthermore, it was shown that a temporary expression of genes required for cell identity is crucial for the temporal ordered differentiation pattern. Ikaros is expressed in early retinal progenitors but not in late[83]. Misexpression of Ikaros in late progenitors can convert the cell fate determination to produce more early born cell types. Accordingly, overexpression of Ikaros leads to a reduction of bipolar cells and even loss of Müller glial cells, suggesting that Ikaros' role is to give progenitor cells a temporal identity with the appropriate competence state during development[83].

Besides an intrinsic regulation, external signals can influence retinal progenitor differentiation. A good example is Shh, which is produced by retinal ganglion cells. Shh can induce Shh expression in neighboring cells which causes a wave of ganglion cell differentiation throughout the eye[84]. Conversely, inhibition of Shh signaling prevents retinal ganglion cell differentiation[84]. Furthermore, Shh influences proliferation and differentiation speed which was demonstrated in Brn3b$^{-/-}$ mutant mouse retinas, that lack retinal ganglion cells, which correlates with loss of Shh signaling[85]. To further emphasize the influence of external factors, neurogenesis and Shh signaling are shown to be dependent on Fgfs secreted from the optic stalk[86]. Similar to ganglion cells, a feedback loop caused by secreted factors from postmitotic neurons influences amacrine cell differentiation as well[87]. These examples describe the influence of progenitor differentiation before M-phase. However, there are also signals that can act on postmitotic cells. Leukemia inhibitory factor (LIF) and ciliary neurotrophic factor (CNTF) can increase bipolar features in cells that were prone to differentiate to rod photoreceptors[88]. Additionally, *in vitro* studies indicate that the amino acid taurine could improve rod differentiation in postmitotic neurons when added to retinal cultures[89].

One prominent and well understood mechanism is Delta-Notch signaling. Extensive work has been done to describe the Delta-Notch-mediated lateral inhibition model in which Delta is the ligand for the receptor Notch [90]. In cells initially expressing an equivalent amount of Delta and Notch, already small changes can trigger a feedback loop. Once a cell expresses more Delta than her neighbor, Notch signaling is enhanced in the neighboring cell, which in turn reduces Delta signaling in that cell. This reduced Delta signaling further amplifies the Delta-mediated effects from the first cell[90]. As Notch negatively regulates proneuronal genes, increased Notch signaling will prevent neuronal differentiation. In the retina, it was demonstrated that high Notch

activity causes cells to remain neuroepithelial or differentiate in the last born cell type Müller glia[91,92]. Conversely, in early retinas, reduction of Notch results in differentiation to retinal ganglion cells[75].

The process of mitosis in neuronal tissues often occurs in pseudostratified epithelia. That is, the nuclei of the cells in the epithelium are localized at different positions along the apico-basal axis. Progenitor cells span the thickness of the epithelium and move their nuclei to the apical (ventricular) site when they undergo mitosis. During G1, S or G2 phase, the nuclei are positioned more basally throughout the epithelium[93]. This process was already described in 1935 by Sauer and termed interkinetic nuclear migration[94]. After mitosis, differentiated neurons position their nuclei along the apico-basal axis to their final location in a process termed nuclear translocation[95]. In the retina, nuclear translocation was demonstrated in the differentiation of retinal ganglion cells and bipolar cells[95]. Both processes, interkinetic nuclear migration and nuclear translocation, can be observed in the developing retina (**Figure 6**). The underlying machinery for nuclear movements is a complex of the cytoskeletal motor protein dynein and dynactin. Dynactin activates cytoplasmic dynein which is a minus-end directed microtubule motor protein[96]. Mutations of the dynactin homolog in *Drosophila* causes M-phase of progenitors to be extended and an impairment of photoreceptor development[97]. Furthermore, photoreceptor nuclei fail to migrate apically and remain more basally. However, this can be suppressed with mutations in the plus-end directed microtubule motor protein kinesin[98]. This indicates that proper nuclear positioning is dependent on a balanced activity of plus-end and minus-end directed motor proteins. Interkinetic nuclear migration is a proliferation process that is timely connected to the cell cycle[93]. Mutational or pharmacological extension of the cell cycle disrupts nuclear localization[99,100]. In opposite to that, when nuclear migration is inhibited, the cell cycle still progresses indicating that both processes can be uncoupled[95]. While the process is known for a long time, the exact function remains unclear. There are several hypotheses that propose one or more plausible explanations for interkinetic nuclear migration. One suggestion is, that this process may be involved in the invagination process of the neuroepithelium[101]. Another reason might be, that nuclei in M-phase require space at the apical surface for cell division. To prevent this site to be too crowded, interphase cells move their nuclei away towards the basal site while still maintaining adherence junctions at the apical and basal site. Together with focal adhesions, adherence junctions provide crucial signals for differentiation and proliferation[95,102,103]. The last suggestion is, that different spatial and temporal positioning of nuclei leads to heterogeneity in the progenitor cell population. Along the apico-basal axis, various signaling cues like Delta-Notch are present. With progression of the cell cycle, the spatio-temporal encounter of extrinsic signals results in different cellular responses[95].

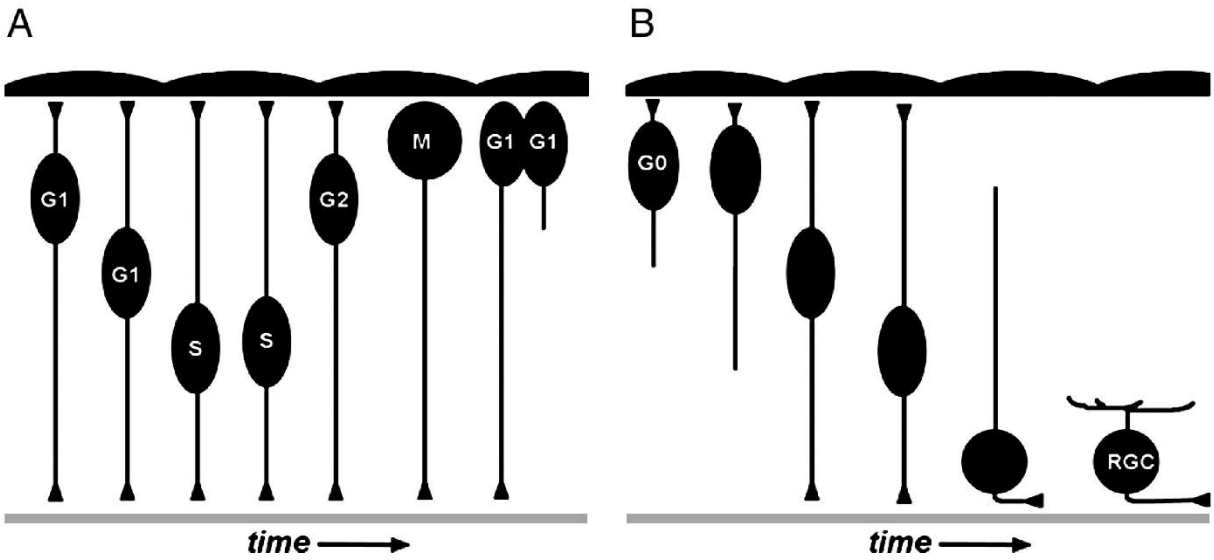

Figure 6: Interkinetic nuclear migration and nuclear translocation. **A** Interkinetic nuclear migration: Interphase nuclei are distributed along the apico-basal axis. In M-phase, cells move their nuclei to the apical surface. **B** Nuclear translocation: Postmitotic neurons remain apically adhered and position their nuclei to the final localization. Afterwards, they retract the adhering processes. (Image from Baye and Link, 2008[95])

The mature neural retina comprises six types of neurons, which in turn have various subtypes, so that a mammalian retina consists of more than 60 different cell types[63]. In the laminated structure of the retina, each cell type has a distinct localization and forms synapses in specific planes[104]. Across the retina, all neurons are approximately evenly distributed. However, exclusively in primates, the center of the retina is a specialized region, named fovea. This region is responsible for high visual acuity. Cones are the dominant photoreceptor type while rods are completely absent. In the peripheral retina, the ratio is inverted and rods outnumber cones 18:1 in humans[105]. After light detection, visual information is transmitted and already pre-processed by interneurons.

Bipolar cells form synapses with photoreceptors and transmit the information directly or indirectly to ganglion cells. There is a rod specific bipolar cell type and 11 types of cone bipolar cells, of which one is blue cone exclusive[106]. Bipolar cells can express either ionotropic or metabotropic glutamate receptors. Depending on the receptor, the response to the neurotransmitter glutamate released by photoreceptors is either depolarization or hyperpolarization of the bipolar cell[107,108]. This results in contrary responses of the cells when photoreceptors are stimulated with light. Metabotropic receptor-mediated depolarizing bipolar cells are thus termed ON cells, whereas hyperpolarizing ionotropic receptor expressing cells are termed OFF cells.

Horizontal cells also form synapses with photoreceptors but give feedback upon illumination. Excitation of a central photoreceptor leads to inhibition of the excited and neighboring photoreceptors which is known as feedback inhibition[104]. This center-surround organization

causes excitation or inhibition of retinal ganglion cells only in the center of the stimulus in the receptive field. Conversely, a stimulus of the surrounding area will have the opposite effect. Eventually, this feedback of horizontal cells is proposed to increase contrast between bright and dark regions[104].

Amacrine cells control the output of bipolar cells via inhibitory synapses on the bipolar cell axon terminals[104]. The high diversity of amacrine cells is illustrated by their morphology and branching[109]. Amacrine cells function in various ways to regulate signal transmission. Ganglion cells that receive input from a common amacrine cell tend to fire together[110]. Furthermore, amacrine cells are involved in adjustment of the retina to bright or dim light conditions[104,111].

Retinal ganglion cells are the cell type, that conveys the visual information to the brain. They arborize their dendritic trees in the inner plexiform layer. Depending on the synaptic partners, the dendrites stratify in different sub-strata of the plexiform layer[62]. In the fovea, a ganglion cell receives direct input from an individual cone which increases spatial resolution[104].

Cone and rod photoreceptors are the light-sensitive neurons in the retina. Both cell types are highly polarized and compartmentalized (**Figure 7a**). At their basal site, photoreceptors form synapses in the outer plexiform layer[112]. The cell body contains the nucleus and is continuous with the inner segment that consists of metabolic organelles[113]. The inner segment is linked to the outer segment via the connecting cilium, a modified, non-motile cilium[113]. The photoreceptor outer segments are composed of stacked membrane discs and contain the molecular components for visual perception and phototransduction[113]. Rod photoreceptors are more light sensitive than cones and are required for dim light conditions[114]. The mammalian visual pigment in rods is Rhodopsin, which has the highest sensitivity for light at wavelengths around 500 nm[115]. On the other hand, cones are responsible for high resolution and color vision. The types of cone photoreceptors differ in their opsin which is sensitive for different wavelengths. Most dichromatic mammals have S-cones, which express an opsin with a peak sensitivity at short wavelengths (S-opsin) mediating blue light detection. Additionally, there is an M-opsin, which is the most sensitive for green light at medium wavelengths. Humans have a third opsin, which has its sensitivity for long wavelengths (red) termed L-opsin, thus making humans trichromats[116]. In humans, each cone only expresses one opsin and the different types of cones are evenly distributed in the retina, resulting in a mosaic-like pattern[117]. A gene regulatory network of transcription factors controls and drives the differentiation of progenitors to specific photoreceptor cells. The initiation of differentiation into photoreceptors is regulated by Otx2 expression, committing postmitotic neurons to photoreceptor cell fate[118]. Absence of Otx2 results in a complete loss of both types of photoreceptors, rods and cones[118]. The cone and rod homeobox transcription factor (Crx) is also expressed in early photoreceptor precursors and acts downstream of Otx2[119,120]. Crx regulates the expression of photoreceptor-

specific genes and is required for maturation and formation of outer segments[121,122]. Specification and rod cell fate acquisition is mediated by neural retina leucine zipper (Nrl). In cooperation with Crx, Nrl initiates rod photoreceptor gene expression[123]. Determination of rod cell fate is facilitated by NR2E3 which is a direct target of Nrl[124]. NR2E3 suppresses cone-specific gene expression and acts together with Nrl and Crx to activate rod-specific gene expression[125–127]. Upstream to Nrl, the orphan nuclear receptor Rorβ is required for rod as well as cone differentiation. On the one hand, Rorβ$^{-/-}$ mice lack Nrl expression. On the other hand, Rorβ interacts with Crx to regulate S opsin expression[128,129]. The differentiation of M-cones in mice is dependent on the nuclear receptor TRβ2. Absence of TRβ2 results in cones that only express S-opsin[130]. On the basis of these findings, it was postulated that all photoreceptors originate from a common precursor that by default differentiates to an S-cone unless additional signals shift the cell fate to either become a rod or M-cone. The first decision is to differentiate to a rod or a cone photoreceptor. If the precursor acquired cone photoreceptor cell fate, it must be determined to express S-opsin or M-opsin[115]. In humans an additional decision to express either M-opsin or L-opsin is made. An upstream locus control region determines either of the genes to be expressed exclusively[131,132]. A number of signaling pathways has been identified that regulate photoreceptor development. Retinoic acid was found to increase photoreceptor gene expression by enhancing Nrl expression[133]. CNTF signaling is involved in photoreceptor receptor survival, even though it is known to decrease Rhodopsin expression[88,134]. Furthermore, downstream of CNTF and LIF, signal transducer and activation of transcription (STAT) also regulates the differentiation from progenitors to photoreceptors[135]. Expression of rod photoreceptor regulators persists throughout development, which takes two to four weeks in mice and up to ten weeks in humans. Afterwards, these cell fate regulators remain to be expressed in the mature retina, suggesting a homeostasis and maintenance function as well[115].

The process of converting visual information in the form of a light stimulus into an electrochemical signal in the photoreceptor cell is termed phototransduction (**Figure 7b**). The steps of this signal cascade occur in the membrane discs of the outer segments. This highly specialized compartment is almost exclusively composed of proteins involved in phototransduction while other components reside in the other parts of the photoreceptor cell[136]. Visual pigments are G-protein coupled receptors composed of a protein and a covalently attached chromophore which is 11-cis retinal[137]. The initial step in light detection is the isomerization of the chromophore when a photon is captured. This leads to a conformational change of Rhodopsin to Metarhodopsin which in turn activates the G-protein Transducin[136]. Transducin is a heterotrimer which is bound to GDP at the α-subunit in the inactive state. After activation, GDP is exchanged to GTP followed by dissociation of Metarhodopsin and Transducin. The α-subunit dissociates from the βγ-complex and further activates cGMP phosphodiesterase (PDE)[138]. PDE γ-subunits inhibit the enzymatic activity. Activation of PDE

leads to dissociation of the γ-subunits, which in turn removes the inhibition of the catalytic site. Hydrolysis and thus reduction of the intracellular cGMP level leads to cGMP-gated Ca^{2+} and Na^{+} channel closure[136,139]. As a consequence, the photoreceptor cell membrane hyperpolarizes. Photoreceptors are an exception in neuronal activity, as they are depolarized and release their neurotransmitter glutamate without light stimulation in dark conditions[140]. At a high intracellular Ca^{2+} concentration, Ca^{2+}-bound Recoverin interacts with Rhodopsin kinase to inhibit its enzymatic activity[141,142]. When the Ca^{2+} concentration drops following light detection, Recoverin dissociates from Rhodopsin kinase, which then phosphorylates Metarhodopsin. Phosphorylation diminishes Metarhodopsin activity, which is subsequently completely inactivated due to binding of Arrestin[143].

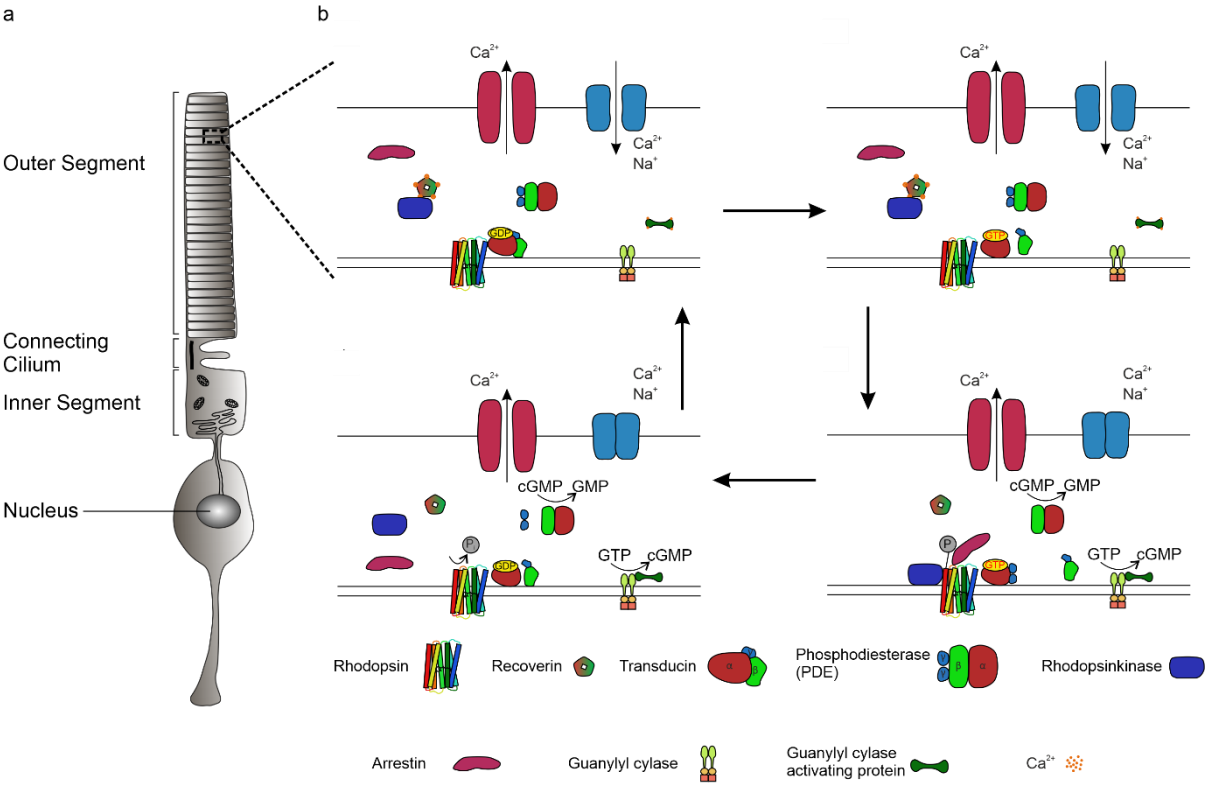

Figure 7: Schematic illustration of a rod photoreceptor and phototransduction. **a** At the basal site, photoreceptors extend to form synapses. The nucleus is localized in the cell body, while many organelles reside in the inner segment. The connecting cilium connects the inner segment to the outer segment, which is a membrane disc-filled apical elongated compartment. **b** Phototransduction occurs in the outer segments of photoreceptors and converts a photon-mediated stimulus into an electric response.

Inactivation of Transducin is rendered by a GAP complex-mediated hydrolysis of GTP to GDP[138]. The GDP-bound inactive Transducin also returns PDE to its inactive state[136]. In the meanwhile guanylyl cyclase activating protein acts on guanylyl cyclase which restores a high cGMP concentration[144]. This opens the cGMP-gated cation channels again to allow Na^{+} and Ca^{2+} influx. Finally, complete recovery is achieved when Rhodopsin is slowly dephosphorylated by phosphatases in a yet not fully understood mechanism. Several

candidate enzymes were identified to facilitate in dephosphorylation of Rhodopsin[145–147] Additionally, there is evidence that Arrestin is also involved in this process[148].

Retinal Pigment Epithelium

The RPE is a pigmented monolayer on the outer site of the retina facing the photoreceptor outer segments with its apical surface[149]. At the basal site, the RPE cells grow on the Bruch's membrane which separates the RPE and neural retina from the underlying fenestrated endothelium, thus forming the outer blood-retina barrier[64]. Hence, bidirectional transport of water and ions is mediated by RPE cells[150,151]. Nutrients from the bloodstream are taken up and passed to the photoreceptors[64,152]. Importantly, photoreceptors are unable to re-isomerize all-trans retinal back to the functional 11-cis retinal to restore their visual pigment. Thus, all-trans retinal is transported to the RPE where several enzymatic steps lead to the re-isomerization of 11-cis retinal which is then shuttled back to the photoreceptors[64]. Pigmentation of the cells absorbs scattered light that passed through the eye and hit the retina[152]. This great interaction underlines the importance of co-development of both tissues which differentiate in parallel in the early eye formation[153].

The RPE arises from the dorsal optic vesicle and is specified by the expression of Mitf and Otx2[23,154]. Mitf expression is required to establish the boundary between presumptive RPE and presumptive neural retina, by repressing Vsx2[154]. Various signaling pathways are active in this phase of development. Wnt-related transcription factor β-catenin is able to directly control Mitf and Otx2 expression[155,156]. In the absence of Wnt during the optic vesicle stage, RPE fails to differentiate at the expense of Vsx2 expressing presumptive neural retina[157]. A similar effect is observed in mice when Yap signaling was ablated resulting in RPE transdifferentiation to neural retina[158]. The surface ectoderm additionally activates Wnt signaling pathways, whereat Wnt suppresses Glycogen synthase kinase 3 (GSK3). Furthermore, Bmp from the surface ectoderm activates pSmad. Together, this enhances and promotes RPE cell fate specification[159]. Anterior retinal structures express genes of the retinal metabolism pathway such as cellular retinol binding protein (Crbp) and cellular retinaldehyde binding protein (Cralb/Rlb11) and release retinoic acid. Differentiating RPE cells on the other hand express the corresponding receptors[160,161]. With the formation of the optic cup, the RPE lines the outer side of the two walled structure. The differentiating RPE and neural retina are separated by a thin lumen which will develop into the ECM-filled interphotoreceptor matrix[162]. Interestingly, during development, retinoic acid is seemingly shuttled between RPE and neural retina through the interphotoreceptor matrix. This is mediated by the interphotoreceptor retinal binding protein (Irbp) expressed in both, differentiating photoreceptors and RPE cells[64]. Early in RPE differentiation, Pax6 activates a RPE-specific Mitf isoform and is then cooperatively

activating the genes Tyr, Dct and Tryp1 which are responsible for and involved in pigmentation[154,163,164]. Importantly, hedgehog signaling is required to drive RPE differentiation. Reduction or inhibition of hedgehog signaling in *Xenopus* or mouse results in lower Mitf expression and thus reduced pigmentation leading to improper RPE development[165,166]. Together with Otx2 and Sox9, Mitf orchestrates the expression of the calcium-dependent chloride channel Bestrophin-1 (Best1)[167]. The expression of visual cycle genes Rpe65, Rgr and Rlbp1, on the other hand, is regulated by Otx2, Sox9 and Lhx2[168]. Expression of visual cycle proteins and Best1 occurs at a time point that correlates with the first electrical activity in photoreceptors[64,169]. During differentiation, RPE cells develop an apical-basal polarity and possess small microvilli at their apical surface[170]. Additionally, other proteins localized at the apical site of the RPE cells like Na^+-K^+-ATPase and $\alpha_V\beta_5$-intrgin are found to be involved in phagocytosis[170]. For the formation of long microvilli, Ezrin expression is suggested to be required[171]. In the process of maturation, RPE cells form tight junctions starting from a rather leaky epithelium. Constant increase in junctional connections makes the RPE less permeable. By changing the composition of tight junction proteins, the formed junctional complex leads to a tightly packed epithelium that prevents free lateral diffusion[172]. With the formation of mature tight junctions which are composed of Zo-1, Occludin and numerous Claudins, the RPE acquires its final apico-basal polarity[173]. This process also marks the establishment of the outer blood-retina barrier, which in total is composed of the RPE cells and the Bruch's membrane that separates the retina from the underlying choroid. The multilayered Bruch's membrane is composed of the basal lamina of the RPE cells, an inner collagen layer, an elastin layer, an outer collagenous layer and the basement membrane of the endothelial cells[65]. As the RPE establishes the outer blood-retina barrier, transepithelial transport is mediated and regulated by RPE cells. This bidirectional transport involves many complex processes and is described in detail elsewhere[64]. Briefly summarized, a main function of RPE cells is to transport water out of the subretinal space to decrease intraocular pressure. This is facilitated by an ion gradient that drives water transportation via aquaporin-1[174,175]. Additionally, metabolic end products like lactic acid are removed from the subretinal space[176]. In turn, nutrients, oxygen and glucose are transported from the blood to the retina. Glucose transporters are expressed at the basal and apical site of RPE cells[177]. Vitamin A (all-trans retinol) is taken up by the RPE via the bloodstream as well[178]. To maintain the electrophysiology of photoreceptors, RPE cells can compensate rapid changes in ion concentration in the subretinal space which ensures and maintains excitability of photoreceptors[179].

RPE cells show morphological differences depending on the localization in the retina. RPE cells in the periphery are larger with ~60 µm in diameter. Conversely, RPE cells in the macula are 14 µm in diameter but contain higher amounts of melanin which is required for more efficient light absorption[64,152]. Because of a higher ratio of photoreceptors to RPE cells in the

macula region, the intracellular composition of enzymes, that are involved in degradation processes, differs from RPE cells in peripheral regions[180–182].

The interdependent development of neural retina and RPE is highlighted by the secretion of numerous growth factors by the RPE which are known to be required for development as well as maintenance of the retinal structural integrity[183–185]. Prominent factors secreted by RPE cells are Fgfs, Tgf-β, Insulin-like growth factor 1 (Igf1), CNTF, platelet-derived growth factor (PDGF), pigment epithelium-derived growth factor (PEDF) and VEGF[64]. The secretion pattern of RPE cells is also dependent on their apico-basal polarity. Apically secreted factors will affect the neural retinal cells, e.g. the photoreceptors. PEDF was found to be neuroprotective by preventing hypoxia-induced apoptosis in neurons[186]. In turn, VEGF is mostly secreted basally towards the choroid during development and maturation to prevent endothelial cell death and maintain the choriocapillaris[184,187]. Imbalance of this secretion profile is associated with various retinal diseases[183,188]. One of the most prominent examples is AMD, where RPE cells are found to be a major source of VEGF, which results in choroidal neovascularization, leading to primary RPE cell death and secondary photoreceptor degeneration[184,187,188].

Another important function of RPE cells is to absorb light due to their pigmentation. One function is the improvement of vision by the absorption of scattered light, that falls in the eye but the main task is to reduce phototoxicity. The combination of an oxygen rich environment as a result of high blood perfusion and the exposure to high energies of light creates the ground for photo oxidation[189,190]. To reduce the phototoxic stress, RPE cells absorb and filter light with numerous pigments that act for light at different wavelengths. The most light is absorbed by melanin which is contained in specialized compartments named melanosomes[64,191]. Additionally, photoreceptors themselves absorb light via the carotenoid pigments lutein and zeaxanthin[192–194]. Together, these pigments are able to absorb large quantities of blue light, which is the most damaging type of light. Blue light-mediated photo-oxidation of lipofuscin creates cytotoxic substances[195,196]. However, lipofuscin itself seems to be able to absorb light, which would make it beneficial in the first place and becomes cytotoxic with accumulation due to ageing[64]. Besides absorption of light, RPE cells contain various antioxidants. Melanin, glutathione but also carotenoids like lutein and zeaxanthin act as non-enzymatic antioxidants[64,197,198]. Despite the non-enzymatic antioxidants, RPE cells contain catalase and superoxide dismutase to enzymatically reduce phototoxicity[190,199,200].

RPE cells phagocytose the outer segments of photoreceptors that are constantly growing and renewed[149,201]. In the fovea of humans, one RPE cell contacts 23 photoreceptors that entirely turn over their outer segments in 10 days[202,203]. This process must be highly coordinated between RPE and photoreceptors to maintain a constant length of the photoreceptor outer segments. Due to light exposure of the photoreceptor cells, radicals, photo-damaged proteins

and lipids emerge, which accumulate in the tips of the outer segments[64]. Via phagocytosis, the RPE cells take up phototoxic substances to inactivate them as described above. Additionally, other compounds taken up by the RPE are recycled and transported back to the photoreceptors[149]. Phagocytosis is simply initiated by the presence of outer segments sensed by the RPE cells[64]. The initial step for phagocytosis is the recognition and binding of outer segments, which is mediated by $\alpha_V\beta_5$-integrin[204]. After photoreceptor binding, Focal adhesion kinase (FAK) is activated which in turn phosphorylates receptor tyrosine kinase c-mer (Mertk)[205]. Mertk transduces the signal of outer segment binding via a second messenger signal cascade to initialize the internalization[206,207]. Additionally, CD36 seems to be a regulator for the rate of ingestion[208].

The inability of photoreceptors to regenerate their visual pigment is dependent on the lack of re-isomerase activity of all-trans retinal to 11-cis retinal. Thus, retinal is shuttled between photoreceptors and RPE cells, where re-isomerization occurs to maintain a constant excitability and visual function of photoreceptors. After light absorption, 11-cis retinal is converted to all-trans retinal. Retinal dehydrogenase (Rdh) reduces all-trans retinal to all-trans retinol which is transported via Irbp into RPE cells[64,162]. There, it is bound to Crbp and an acetyl group is transferred to retinol via the lecithin retinol transferase (Lrat)[209]. An enzyme complex of Lrat, Rlbp1, Rpe65 and Rdh5 catalyzes the Rpe65-mediated re-isomerization to 11-cis retinol, which is subsequently fully regenerated to 11-cis retinal via oxidation catalyzed by Rdh5[64,210–213]. Afterwards, 11-cis retinal is translocated back and reenters photoreceptors to be incorporated in visual pigments[64].

3-Dimensional Cell Culture and Organoids

Much of what is known in biology is derived from studies in various organisms. To understand developmental processes, molecular mechanisms or drug applicability, a number of model organisms were identified that allowed researchers to address specific questions. This group of model organisms comprises lower organisms as well as higher eukaryotes including the yeast *Saccharomyces cerevisiae*, worm *Caenorhabditis elegans*, the fruit fly *Drosophila melanogaster*, zebra fish *Danio rerio* and the mouse *Mus musculus*. The advantage of model organisms is the reproducibility of experiments, as the development of the organisms follows a strict plan. Every organism was carefully chosen because of intrinsic advantages for experimental designs regarding different biological questions. *D. melanogaster* served in the past as a great organism to unravel molecular mechanisms in developmental biology as they undergo a fast reproduction cycle and allow screening for mutants in high quantities. Starting in the 1980s, mechanisms in the formation of the anterior-posterior body axis, which is driven by a set of genes, named Hox genes, in the developing fruit fly were discovered[214]. The zebra

fish embryo is transparent. Thus, fundamental questions in early embryonic development could be addressed using this organism.

However, not all findings can easily be translated to the human system. This includes the development of certain structures like the human brain. Compared to the mouse brain the human brain is by far more complex. Additionally, progenitor cells in the neo cortex, the outer radial glial cells, are fundamental in human brain development but are almost absent in the mouse brain[215]. Besides developmental biological differences, questions about medical applications and drug testing reveal substantial differences between animals and humans. This can be ascribed to different metabolic pathways resulting in a drastically varying responsiveness to certain drugs. For example, the commonly used human drug ibuprofen against pain and inflammation is toxic in rodents[216]. To partially overcome these hurdles, 2D cell culture systems were established. The use of established cell lines allows a higher experimental throughput as these cells can easily be maintained and expanded indefinitely. However, in these experiments the cells are grown in a minimalistic, artificial environment which can result in a significant deviation in their biological activities[217]. Furthermore, most of the established cells lines are cancer-derived which results in altered physiological and genetic appearance with oncogenic potential[218,219].

In 1981, it was first reported that mouse embryonic stem cells (mESCs) could be isolated and cultivated *in vitro*[220]. The next hallmark in cell biology was the establishment of the cultivation of human-derived ESCs in the year 1998[221]. However, as the isolation of these cells required human embryos, major ethical concerns were raised. But in 2006, the group of Yamanaka presented the Nobel Prize winning induction of pluripotency in somatic cells, first in mouse fibroblast and then in human cells[222,223]. Viral delivery of transcription factors from the regulatory network in pluripotency, namely Sox2, Oct4, c-Myc and Klf4, were able to reprogram somatic cells into induced pluripotent stem cells (iPSCs). These findings paved the way for a new 3D cell culture system: organoids. Organoids are stem cell grown 3D structures, containing more than one organ-specific cell type, that self-organize via cell sorting to resemble a target organ in morphology as well as function[224,225]. In the formation of organoids, stem cells recapitulate developmental processes similar to *in vivo* organogenesis. Furthermore, organoids can also be generated using adult stem cells (ASCs). The difference between iPSC/ESC-derived organoids and ASC-derived organoids is the higher complexity of iPSC/ESC-derived organoids, whereas ASC-derived organoids form largely epithelial aggregates[219]. The first step in organoid generation usually is the formation of embryoid bodies which are floating stem cell aggregates. For proper development, organoids are embedded in ECM protein mixtures. Subsequently, organoids undergo stepwise differentiation protocols that supply the organoids with cultivation media supplemented with specific signaling molecules[226].

This activates or inhibits crucial signaling pathways to induce regional patterning and shifts the stem cells towards desired cell fates. Today, various protocols have been established to generate organoids resembling colon, intestine, liver, retina, brain and many more tissues[53,227–230]. With this tool in hands, the developmental biological problem of inaccessibility of certain tissues can be overcome, to follow organogenesis *in vitro*. Additionally, developmental processes in human-like organs can be observed which were previously evaluated in animal models. Furthermore, patient-derived iPSCs allow to understand disease mechanisms in organ formation as well as the design of disease- or even patient-specific treatments. For example, intestinal organoids have been used to investigate cystic fibrosis. With the help of organoids, faithful predictions about the responsiveness to certain drugs have been made[231,232]. Nonetheless, the organoid research is still an emerging field so that many challenges need to be addressed.

The first retinal organoids (ROs) were reported in 2011. Eiraku and collegues[53] demonstrated that mESCs could form embryoid bodies in low serum conditions that developed a neuroepithelium. In the following cultivation, retinal progenitor cells were observed in the epithelium. After retinal induction, the retinal epithelium underwent morphogenetic movements resulting in optic vesicle-like evaginations. It was also reported that subsequently, the vesicle structures invaginated to form optic cup-like structures consisting of a neural retina on the inside and an RPE layer around. This breakthrough was the fundament to more protocols describing the differentiation of ROs, especially from human-derived SCs[233–235]. The combination of neural induction in 2D cell culture with subsequent aggregation to from 3D structures could further improve the generation of ROs[236,237]. Immunocytochemical experiments as well as single cell RNA sequencing (scRNA seq) could identify the majority of retinal cell types in ROs[53,238,239]. Interestingly, retinal cell types were arranged in a pseudostratified epithelium where photoreceptor cells were localized at the apical, outer site while interneurons were observed more towards the inside[53]. Recent advances in the field could further improve the structural development of human-derived ROs so that the retinal epithelium showed a lamination comparable to ONL, INL and GCL that were forming largely nuclei-free layers between them, suggesting synaptic formations comparable to IPL and OPL[239]. Furthermore, ultrastructural analysis could visualize the differentiation of mature photoreceptors by observing outer segment-like structures[240]. Additionally, photoreceptor-specific ribbon synapses could be identified at their synaptic terminals[240,241]. More interestingly, calcium imaging as well as electrode array experiments could detect neuronal activity caused by light stimuli[237,239]. Supporting the finding of mature photoreceptors that were able to detect light and convert it into electrochemical responses, neuronal responses could even be detected in cells of the inner layer upon light stimuli, suggesting the transmission of information from the photoreceptors to connected neurons[239].

Many publications successfully described the differentiation of ROs derived from human cells. However, striking differences can be identified when compared to the mESC-derived ROs. Human-derived ROs are generated in a guided differentiation protocol. That is, these protocols treat the SC aggregates by stepwise addition of signaling molecules to induce the early steps of neural induction as well as the subsequent retinal differentiation. In contrast to that, the mESC-derived ROs are cultivated in minimal media and the neural and retinal differentiation occur in an autonomous and self-organizing manner. Furthermore, maturation of ROs from mESCs takes around two weeks, while human-derived ROs start to mature at around 180 days. Notably, in both cases mature ROs largely lack the innermost retinal cell type, the retinal ganglion cells[242].Immunohistochemistry and scRNA seq data revealed an initial differentiation but a gradual loss of retinal ganglion cells during development[237,238]. This can be accounted to the fact, that many protocols prioritize the differentiation of photoreceptor cells which might not be beneficial for retinal ganglion cell differentiation[242]. A second assumption is that the inner localization of retinal ganglion cells hinders maturation as they might not receive enough nutrients. In addition to that, the target areas in the brain to which ganglion cells are connected are absent in ROs, which may also cause degeneration of retinal ganglion cells.

Transcriptomic analysis revealed that ROs mimic the *in vivo* development of retinal cell types in humans and rodents[243]. Supporting the similar development of ROs and *in vivo* retina, organoids generated from mutant cell lines showed comparable defects. In ROs derived from patients carrying a homozygous Nrl null mutation, which is the key regulator in rod cell fate determination, ROs show an overpopulation of S-cones, which is in accordance to the *in vivo* disease phenotype[244]. Further underlining the similarities of *in vivo* development and ROs, mutation in Vsx2 results in microphthalmia (small eyes) in humans and rodents. Accordingly, Vsx2$^{-/-}$ ROs contain reduced numbers of retinal cells and lower proliferation capacity[245]. Moreover, the reciprocal suppression of Vsx2 and Mitf, which determines neural retina versus RPE cell fate, could also be observed in ROs. Mutant Vsx2 ROs showed reduced neural retina regions at the expense of RPE cell differentiation[245]. Furthermore, studies in ROs could reveal that optic cup formation might be a cell autonomous process that is not dependent on the surface ectoderm which is in contrast to earlier findings in eye development[53]. However, the process of optic cup invagination is rarely seen suggesting that additional ocular tissue might still be required for proper development[242]. Nonetheless, new technologies in 3D cell culture, including microfluidic chips, allow enhanced cultivation methods and drug testing[246]. These recent advances in the field made it possible to use ROs as a valuable research tool for early eye development but also disease modelling and drug testing.

Aim of this Work

It was previously shown that mESCs can successfully be differentiated to ROs[53]. In this process, the organoids underwent crucial morphogenetic steps highly similar to *in vivo* eye development. This includes the formation of a neuroepithelium in which retinal progenitors are differentiated subsequently. The epithelium evaginated to form optic vesicle-like structures which eventually invaginated to form two-layered optic cup-like structures. There, RPE cells lined the outer side of the cup which resembles the *in vivo* situation where photoreceptors are in contact with the apically localized RPE cells. However, the formation of optic cup-like structures is extremely rare and thus lacks reliable reproducibility. Additionally, in mESC-derived ROs, the differentiation of RPE cells is only rarely induced. Similar to that, in human iPSC-derived ROs, RPE cells are formed in a bulk attached randomly at the organoid. This results in organoids composed of two almost separate instances in which one forms the neural retina and another giving rise to pigmented cells. Even though RPE cells are present, the important interaction of RPE cells and the developing neural retina and mature photoreceptor cells does not occur in ROs.

The development and maturation of mESC-derived ROs resembles a rather immature state of the retina. To recreate a more physiological, *in vivo*-like development, it was desired to co-cultivate ROs with RPE cells. On the basis of a previously described method to differentiate RPE cells from mouse-derived iPSCs[247], RPE cells should be differentiate separately and later be co-cultivated with ROs. Thus, the first step was to establish and adapt the differentiation protocol for the mESC line which was used in this work. Second, mESC-derived RO differentiation suffers from high variability, inconsistency and low reproducibility. In order to reliably generate ROs, it was fundamental to evaluate more robust conditions to increase the efficiency for retinal induction. Afterwards, ROs should be characterized at different developmental time points to understand their morphological and structural maturation as well as the differentiation of retinal cell types.

As soon as the differentiation of mESC-derived RPE cells and ROs is established, optimal co-cultivation conditions need to be assessed. The co-cultivation setup should fulfil criteria to allow the proper differentiation and maturation of mESC-derived RPE cells. Additionally, structural integrity of the ROs should be preserved to retain the RO intrinsic self-organization of the retinal epithelium. ROs have a limited cultivation time. Based on the findings of RO development, the optimal time point as well as period for a co-cultivation needs to be evaluated. As RPE cells establish the outer blood-retina barrier, the *in vitro* cultivation system was designed to recreate this *in vivo* situation. Thus, the co-cultivation of mESC-derived RPE and ROs shall reflect the *in vivo*-like co-development and maturation of both tissues in an *in vitro* system that resembles the interface of neural retina and RPE.

Results

Optimization of Early Retinal Organoid Generation

The differentiation of mESCs to early ROs is the first step for the differentiation of RPE cells and the generation of more mature ROs, respectively. In this work, a transgenic mESC line carrying a Gfp knock-in in the locus of the retinal progenitor cell marker Rx, was used. Thus, retinal induction can be monitored in real time in ROs by the onset of retinal progenitor cell differentiation via Rx-Gfp expression (**Figure 8**). Retinal differentiation and formation of epithelial structures is facilitated autonomously in organoids. To increase the efficiency of retinal induction, which was evaluated by Rx-Gfp expression, minor changes and adjustments in the cultivation of mESCs and the differentiation to ROs were applied to the existing protocols. The cultivation condition of mESCs had a considerable effect on retinal induction. The composition of the base medium as well as the combination of supplements to maintain pluripotency, namely LIF, LIF + MEK inhibitor and LIF + MEK inhibitor + GSK3 inhibitor, were evaluated to optimize the generation of ROs (See: Material & Methods). In all cultivation conditions, pluripotency was evaluated and verified (**Figure S 1**). Besides some conditions that failed to generate ROs, others could induce the differentiation of retinal progenitor cells (**Figure S 2**). Of those conditions that were able to produce Rx-Gfp$^+$ ROs, the most showed a great variation in retinal induction from one experiment to another. Besides retinal induction also the morphology depended on the previous cultivation of mESCs and the differentiation conditions. It could be observed that the addition of the retinoic acid receptor antagonist AGN 193109 at differentiation day 0 (D0) reduced the number of optic vesicle-like evaginations. This is effect was further enhanced when mESCs were cultivated in maintenance medium supplemented with MEK inhibitor prior to retinal differentiation (**Figure 8a, b**). This resulted in largely round, almost completely Rx-Gfp$^+$ aggregates with an even epithelium at D7. Cultivation of the mESC-Rx-Gfp cell line in low serum conditions supplemented with LIF and MEK inhibitor was the most robust condition to consistently obtain Rx-Gfp$^+$ ROs over time (Data quantified). Differentiating ROs were embedded in an ECM protein mix at D1. To avoid large batch-to-batch variation of the ECM protein mixtures Matrigel or Geltrex, protein concentration was adjusted to 10 mg/ml and afterwards added to the mESC aggregates with 2% as final concentration. Furthermore, it was tested whether Matrigel/Geltrex could be replaced by a controlled protein mixture. Hence, ES aggregates were embedded in laminin at D1, which is the major component of Matrigel/Geltrex (**Figure 8c**). It was observed that a partial retinal differentiation occurred in these aggregates. Nevertheless, the retinal epithelium was comparably thin and the majority of the aggregates was Rx-Gfp$^-$. However, when the aggregates were embedded in a mix of laminin and collagen, which is the second major component of Matrigel/Geltrex, more Rx-Gfp$^+$ areas were observed and the retinal epithelium was more comparable to Matrigel/Geltrex embedded organoids. Nonetheless, in both tested

conditions the aggregates did not grow in size as much and the formation of a clearly visible retinal epithelium was hampered. This suggests that a scaffold of ECM proteins alone can lead to retinal differentiation but is not sufficient to strongly induce retinal differentiation accompanied with the formation of a retinal epithelium in the whole organoid. Conversely, the more complex ECM protein mixtures Matrigel and Geltrex, that contain more ECM proteins and also a large variety of additional growth factors, were required for a strong retinal induction and proper structural maturation.

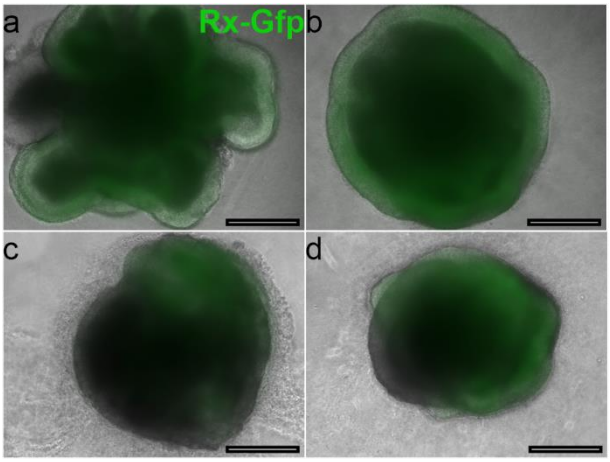

Figure 8: Retinal induction in organoids at D7. RO differentiated from mESCs cultivated in MM supplemented with LIF develops several optic vesicle-like evaginations (**a**) while supplementation with LIF + MEK inhibitor results in round organoids without evaginations (**b**). RO embedded in 100 µg laminin (**c**) and 125 µg collagen (**d**). Scale bar: 200 µm.

Differentiation of RPE from mESCs

The differentiation protocol of RPE cells is schematically depicted in **Figure 9**. The first step to differentiate RPE cells from mESCs is the generation of early ROs that function as a source of retinal progenitor cells. At D7, Rx-Gfp$^+$ ROs (**Figure 9b**) were mechanically broken up by shear forces exerted on the organoids when passed through needles and syringes. The fragments and single cells were allowed to adhere and grow on laminin coated well plates (**Figure 9c**). To avoid reduced proliferation due to contact inhibition, only ~16 aggregates were transferred into one well of a 6-well plate. The enzymatic and mechanic detachment of less adhesive cells at D11 left the more adhesive RPE precursor cells in the well plate. The remaining RPE precursors were detached afterwards and dissociated to single cells. From initially ~64 aggregates, the number of purified cells was sufficient to prepare three to five Transwells or wells of a 96-well plate (~300.000 – 500.000 cells; Data not shown). From D11 until ~D13, the cells proliferated and could form a confluent monolayer (**Figure 9d**). After the final medium change at D15, the cells differentiated into RPE cells adopting the characteristic cobble stone shaped morphology which could be first observed from D18 onwards (**Figure 9e**). When the cells were not able to cover the whole surface of a well plate, the cells failed to differentiate properly (Data not shown). The differentiated mESC-derived RPE cells could be maintained in a long-term cultivation with a constant medium change every two or three days.

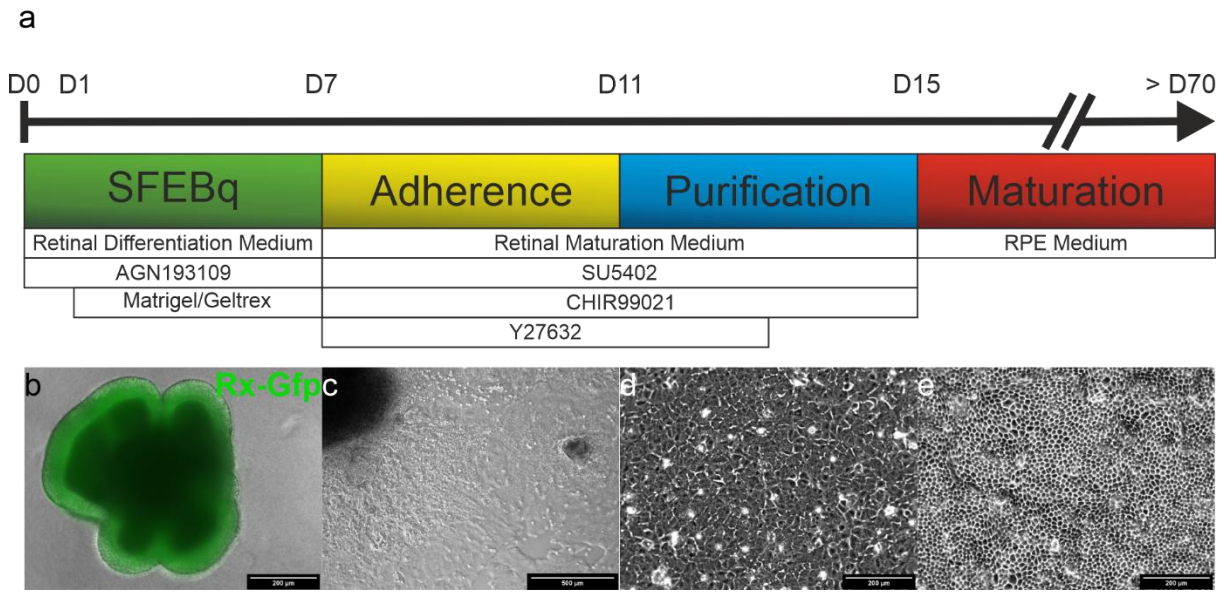

Figure 9: Differentiation of RPE cells from mESCs. **a** Schematic description of the differentiation protocol for RPE cells from mESCs. Colored boxes represent the single steps and cultivation conditions. Small boxes describe cultivation media and added supplements. **b** Early ROs at D7 with Rx-Gfp^{+} epithelium. **c** Adherent broken up RO with outgrowing cells. **d** After purification, RPE precursor cells are allowed to grow to confluency forming a monolayer. **e** After switching to RPE Medium, cells adopt a characteristic cobble stone shaped morphology. (Figure taken and adapted from Richler, 2019[248]).

mESC-derived RPE Cells Express RPE-specific Marker Genes

To further validate that the differentiated cells indeed resemble RPE, it was next investigated whether RPE-specific gene expression could be detected via immunostaining. Immunocytochemical labeling of the cytoskeleton revealed more clearly the RPE cell morphology and the formation of a tight monolayered epithelium, indicated by the expression of the tight junction marker Zo-1 (**Figure 10a, b**). Early expressed transcription factors Mitf and Otx2, involved in the correct differentiation and cell fate adoption in RPE cells, were detected as well as later expressed Sox9. Mitf, Otx2 and Sox9 showed a strong nuclear localization, respectively (**Figure 10b-d**). The key isomerase in the visual cycle, Rpe65, was ubiquitously expressed in mESC-derived RPE cells and was localized in the cytoplasm. To test whether mESC-derived RPE cells were still able to undergo cell division, proliferation marker Ki67 was stained. However, only in a few cells signal for Ki67 could be detected indicating terminally differentiated RPE cells with very limited proliferation capacity (**Figure 10c, arrows**).

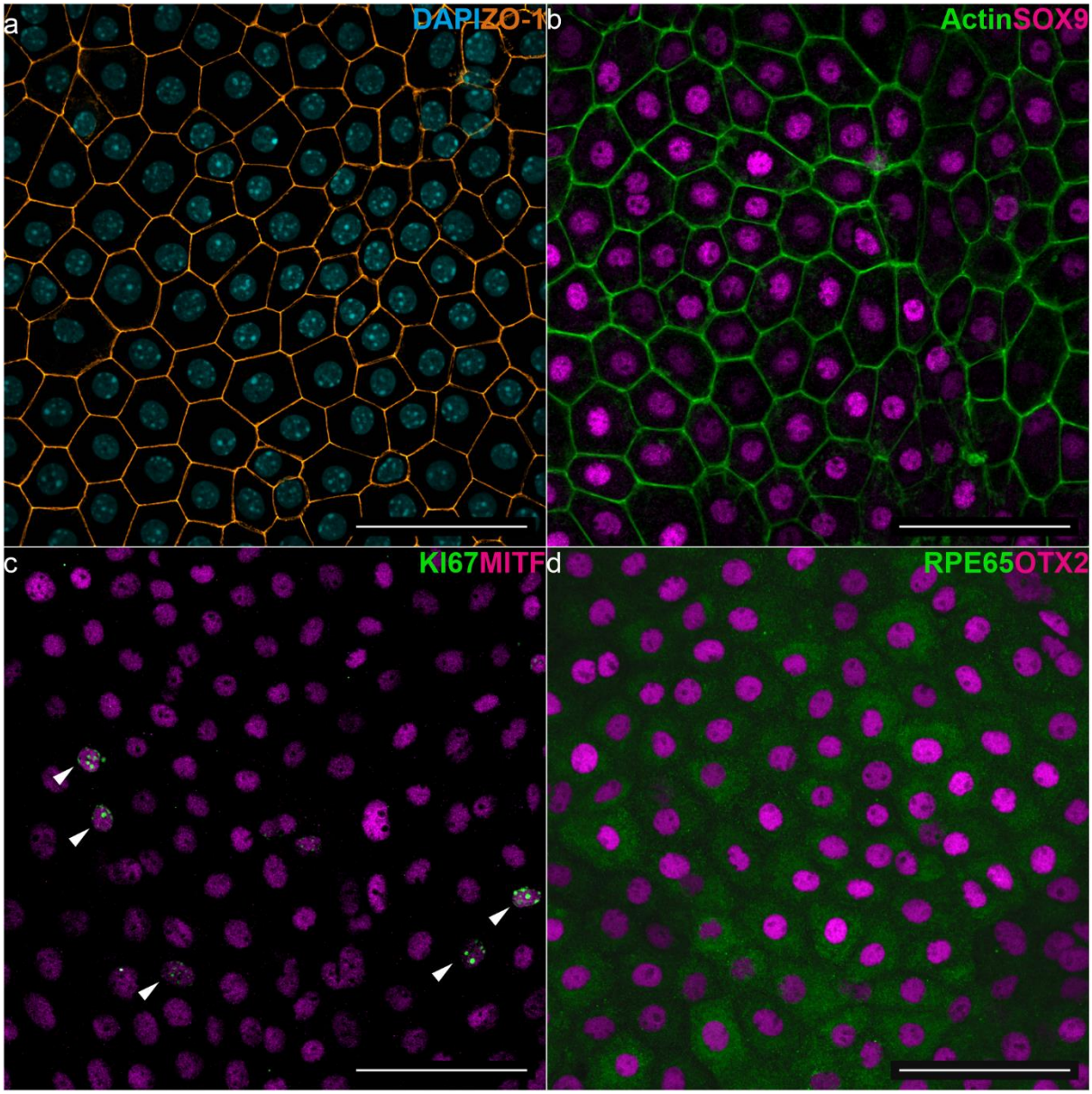

Figure 10: Immunocytochemical staining of RPE marker proteins. RPE marker genes are expressed in mESC-derived RPE cells at D26 (**a**,**d**), D36 (**b**) and D19 (**c**). Actin and ZO-1 mark the cytoskeleton while transcription factors SOX9, OTX2 and MITF have a nuclear localization. RPE65 is detected in the cytoplasm. Arrows highlight KI67^{+} cells. Scale bar: 50 µm.

To fulfil functions as an epithelial layer, RPE cells are required to form an apico-basal polarity. The microvilli marker Ezrin showed a dotted pattern widely distributed across all mESC-derived RPE cells. Furthermore, the orthogonal view reveals that elongated Ezrin^{+} structures line the apical site of the cells. The 3D reconstruction highlights these elongated Ezrin^{+} structures supporting the assumption that microvilli are present at the apical surface (**Figure 11a, b**). In addition to that, apical localization of Zo-1 also indicates the proper apico-basal polarity of the RPE cells (**Figure 11b**). These results suggest that mESC-derived RPE cells are highly

polarized and form a tight monolayer. Additionally, Ezrin$^+$ microvilli indicate structural maturation.

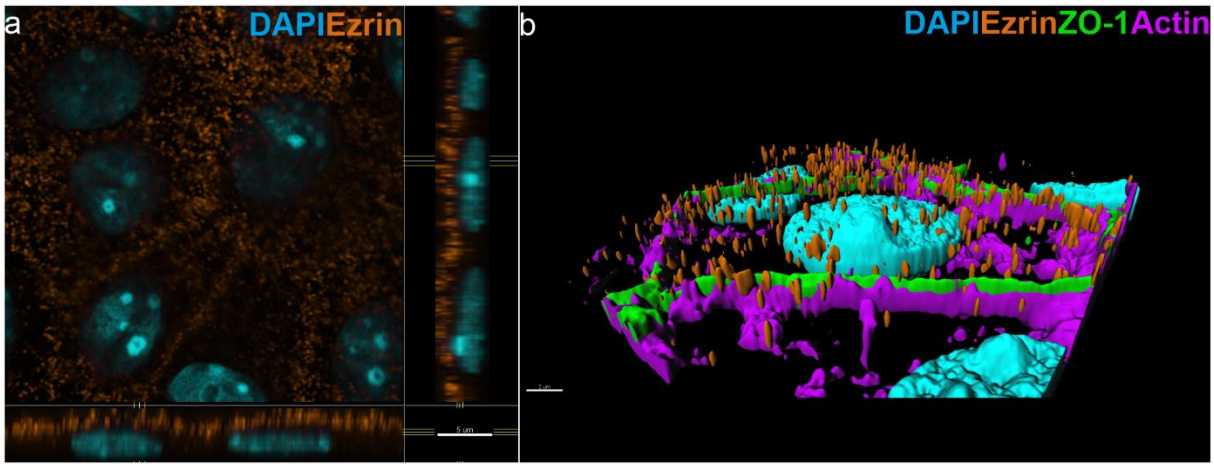

Figure 11: Apico-basal polarity of mESC-derived RPE cells. **a** Top view and orthogonal view of a z-stack. **b** 3D reconstruction of image shown in **a**. Widely expressed Ezrin in a dotted pattern. Elongated structures can be observed in the orthogonal view and 3D reconstruction. Scale bar: 5 µm (**e**); 2 µm (**f**).

Differentiation and Cultivation of Mature ROs

After retinal induction, Rx-Gfp expression could be observed as early as D5 (Data not shown) increasing until D7 resulting in a strong Rx-Gfp$^+$ signal in the whole organoid. An even, clearly visible neuroepithelium lined the outside of the organoids. However, the distinct formation of optic vesicle-like evaginations was rarely observed. The majority of the ROs remained round with slight bending in the epithelium. In the next step, ROs were transferred to a serum-free floating culture at D7 (**Figure 12b**). In the following four days, organoids continued to increase in size. Rx-Gfp$^+$ epithelial structures that grew out from the organoid could clearly be seen. At D11, Rx-Gfp$^+$ areas were dissected from the aggregate and transferred into a new petri dish while Rx-Gfp$^-$ areas were discarded (**Figure 12c**). After the dissection step, the isolated structures again formed aggregates consisting of a continuous epithelium with smooth surface (**Figure 12d**). ROs were then further cultivated in floating culture where they increased in size while showing a strong Rx-Gfp signal (**Figure 12e-f**). From D25, the surface of the epithelium became rougher and small evaginating substructures could be observed as a result of outgrowing and potentially apoptotic cells indicating loss of epithelial integrity (**Figure 12g, g'**). Interestingly, the organoids retained Rx-Gfp expression even in prolonged cultivation time while the epithelial structure continued to degenerate (Data not shown). In cross-sections of ROs a compact Rx-Gfp$^+$ retinal epithelium can be observed, while cells on the inside decrease in density (**Figure 12h**). These observations suggest, the successful differentiation of ROs from mESCs. During maturation, the formation a retinal epithelium with high structural integrity can be observed until D21. Loss of epithelial structure with increasing cultivation time suggests

that the developmental peak is at around D21 and thus indicates the limited maturation capability of ROs.

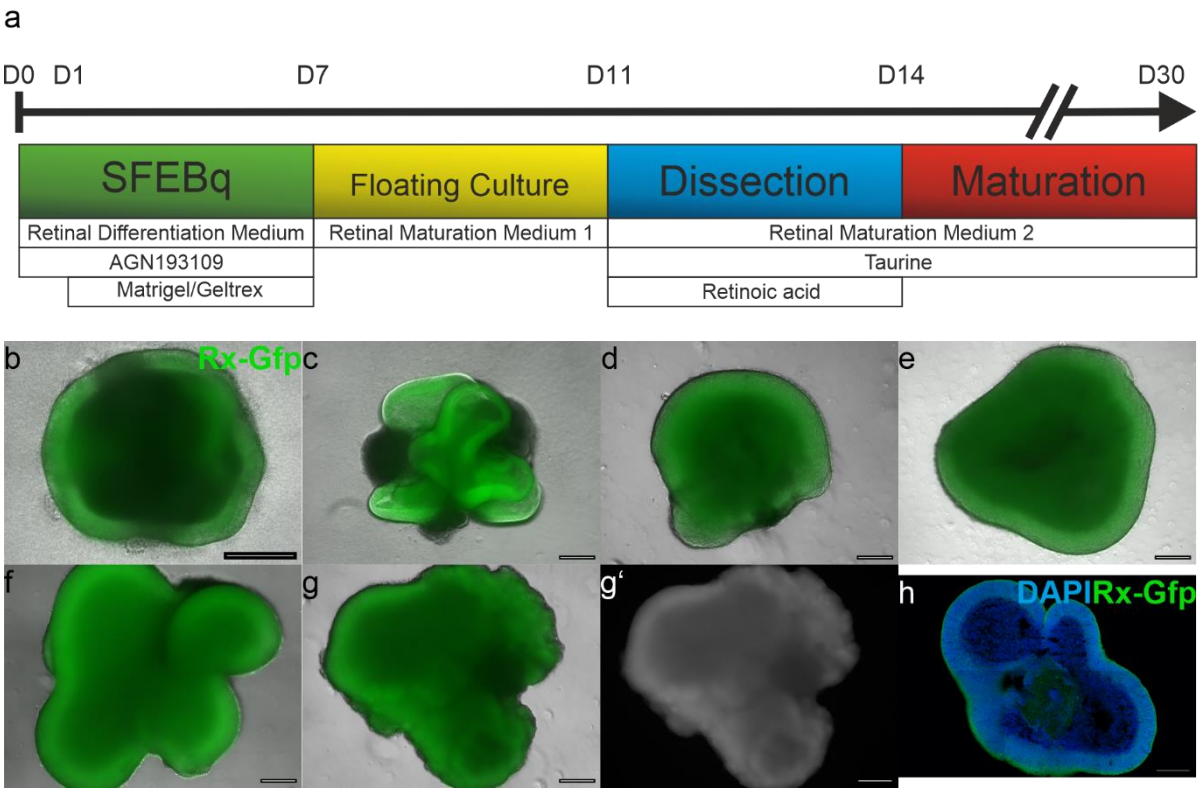

Figure 12: Generation of ROs from mESCs. **a** Scheme for the differentiation of ROs from mESCs. **b-g** Maturation of Rx-Gfp^{+} Ros at D7 (**b**), D11 before sectioning (**c**), D15 (**d**), D18 (**e**), D21 (**f**) and D25 (**g**). **g'** Rx-Gfp signal of RO shown in **g**. **h** Cryosection of a RO at D21. Scale bar: 200 µm.

One of the most outstanding structural features of the retina is the formation of distinct layers with individual cell type composition. Notably, the epithelium of ROs has the capability to self-organize to form a pseudostratified retinal epithelium with apico-basal polarity. Prior to immunohistochemical experiments, cryosections of 20 µm thickness were prepared. These cross-sections allowed to visualize the structural and cellular composition of the ROs. Cell density and Rx-Gfp signal clearly indicated the retinal epithelium which could be distinguished from apparently non-retinal cells inside the organoid (**Figure 13a**). It was observed that the nuclei in the epithelium had an elongated morphology along the apico-basal axis. Nuclei inside the organoid appeared to be round and lined the basal site of the epithelium. Interestingly, nuclei of the cells that formed the basal border of the retinal epithelium tended to be oriented laterally to the epithelium (**Figure 13b**). The Rx-Gfp channel showed a diffuse signal in the whole retinal epithelium (**Figure 13c**). This is most likely caused by diffusion of free Gfp which then localized in the nucleus as well as the cytoplasm. Nonetheless, a strong Rx-Gfp signal was restricted to the retinal epithelium and thus allowed to distinguish between retinal and non-retinal areas. Based on the Rx-Gfp signal, the basal border of the epithelium was identified.

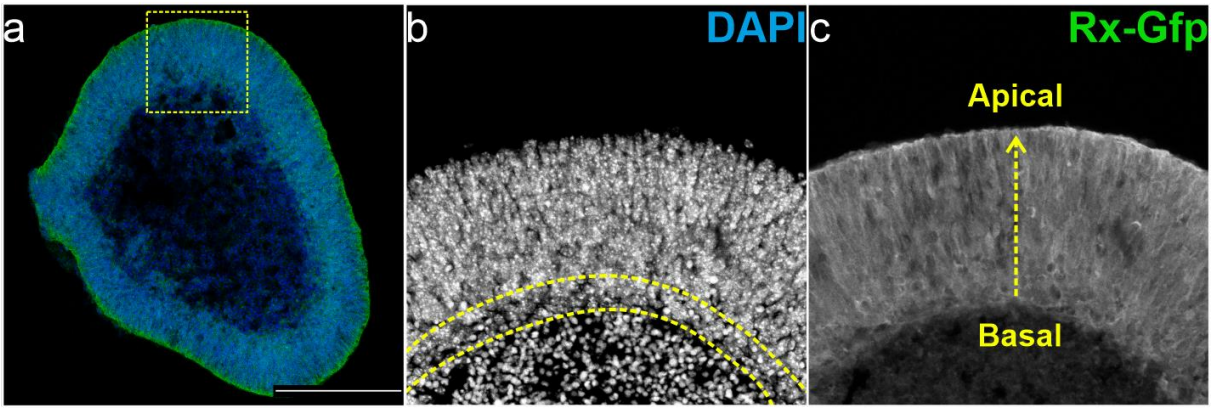

Figure 13: Retinal epithelium of a cryosectioned RO. The retinal epithelium of a RO can be distinguished by Rx-Gfp signal. The cell density in the epithelium is higher than on the inside of the organoid. **a** Section of a whole RO. **b** Exemplary magnification image of the region marked in **a**. Nuclei in the epithelium appear elongated along the apico-basal axis while nuclei on the inside are round. Nuclei within the dotted lines tend to be elongated lateral to the epithelium. Lower dotted line marks the border of the retinal epithelium. **c** Rx-Gfp signal indicates the borders of the retinal epithelium. Dotted arrow describes the apico-basal axis in the epithelium. Scale bar: 200 µm.

Immunostaining of cryosectioned ROs shown in **Figure 14** revealed that most of the nuclei of cells immunoreactive for the photoreceptor marker Otx2 were localized on the outer side of the organoid and thus at the apical site of the epithelium. In turn, the number of $Otx2^+$ nuclei decreased at the basal site where only a few single nuclei could be observed (**Figure 14a**). Neural retina progenitor cell marker Vsx2 showed signal throughout the epithelium. Interestingly, $Vsx2^+$ nuclei seemed to form a border that separated the most basal nuclei of the retinal epithelium from the apical part (**Figure 14b**). Notably, less $Vsx2^+$ nuclei were observed at the most apical site. Cells positive for the bipolar and ganglion cell marker Isl1 tended to be localized at the basal site of the retinal epithelium. Additionally, a low number of single $Isl1^+$ nuclei could be observed that were localized more inside of the organoid and hence not in the retinal epithelium (**Figure 14c**). These observations in ROs show that retinal cell types differentiate in the retinal epithelium and self-organize themselves along the apico-basal axis. Interestingly, this pseudo-stratification was facilitated without formation of optic vesicle or optic cup-like structures and in the absence of RPE suggesting that this process in autonomously driven by retinal progenitor cells and is independent of other ocular tissue.

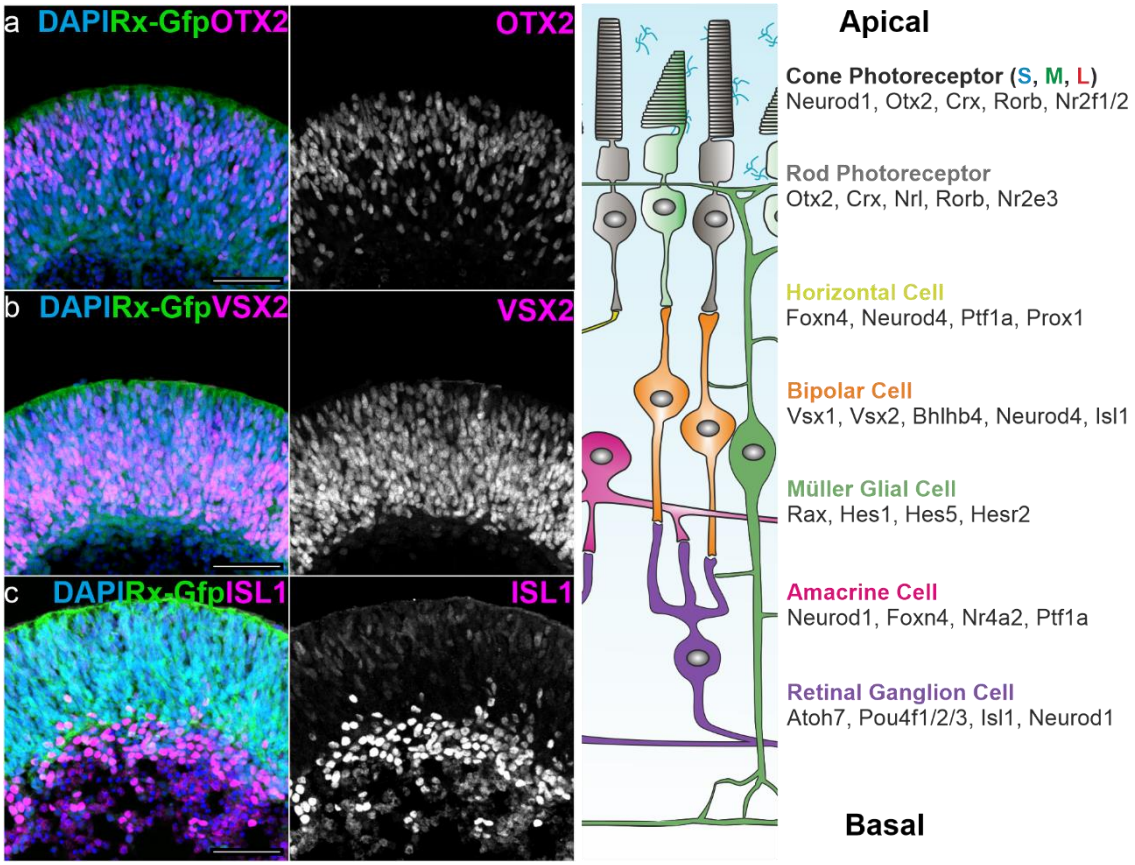

Figure 14: Pseudostratified neuroepithelium in ROs. Different retinal cell types arrange their nuclei along the apico-basal axis resulting in a pseudo-stratification of the retinal epithelium in ROs. **a** Otx2, a marker for photoreceptor cells, is detected at the apical site of the retinal epithelium. **b** Nuclei of neural retina progenitor cells stained with Vsx2 mark a clear border at the basal site. $Vsx2^+$ nuclei density is reduced at the apical site. **c** Nuclei positively stained for bipolar and ganglion cell marker Isl1 can be detected at the basal site of the retinal epithelium. Scale bar: 50 µm.

Photoreceptor Development can be Observed from D15 in ROs

To get insights in photoreceptor development in ROs, aggregates were fixed at D15, D18 and D21. Immunostaining for early photoreceptor marker Otx2, its downstream target Crx and the neural retina progenitor cell marker Vsx2 was conducted. Confocal images of fluorescently labeled ROs were digitally processed and the cell composition of the retinal epithelium was analyzed. As depicted in **Figure 15b**, it was measured that 44.73 ± 3.63% cells in the retinal epithelium were $Vsx2^+$ at D15. With increasing cultivation time, the number of $Vsx2^+$ cells declined to 38.12 ± 1.96% at D18 and even further down to 29.22 ± 2.36% at D21. In contrast, photoreceptor marker Otx2 was initially expressed only in 18.99 ± 3.63% of the cells at D15 but increased to 36.86 ± 4.32% $Otx2^+$ cells at D21. Notably, the amount of Crx expressing cells increased as well (9.37 ± 1.29% at D15, 31.12 ± 1.72% at D21). However, the number of Crx^+ cells was always slightly lower compared to that of Otx2 expressing cells. This indicates that Otx2 is expressed before Crx in photoreceptors and suggests the dependency of Crx on Otx2 expression.

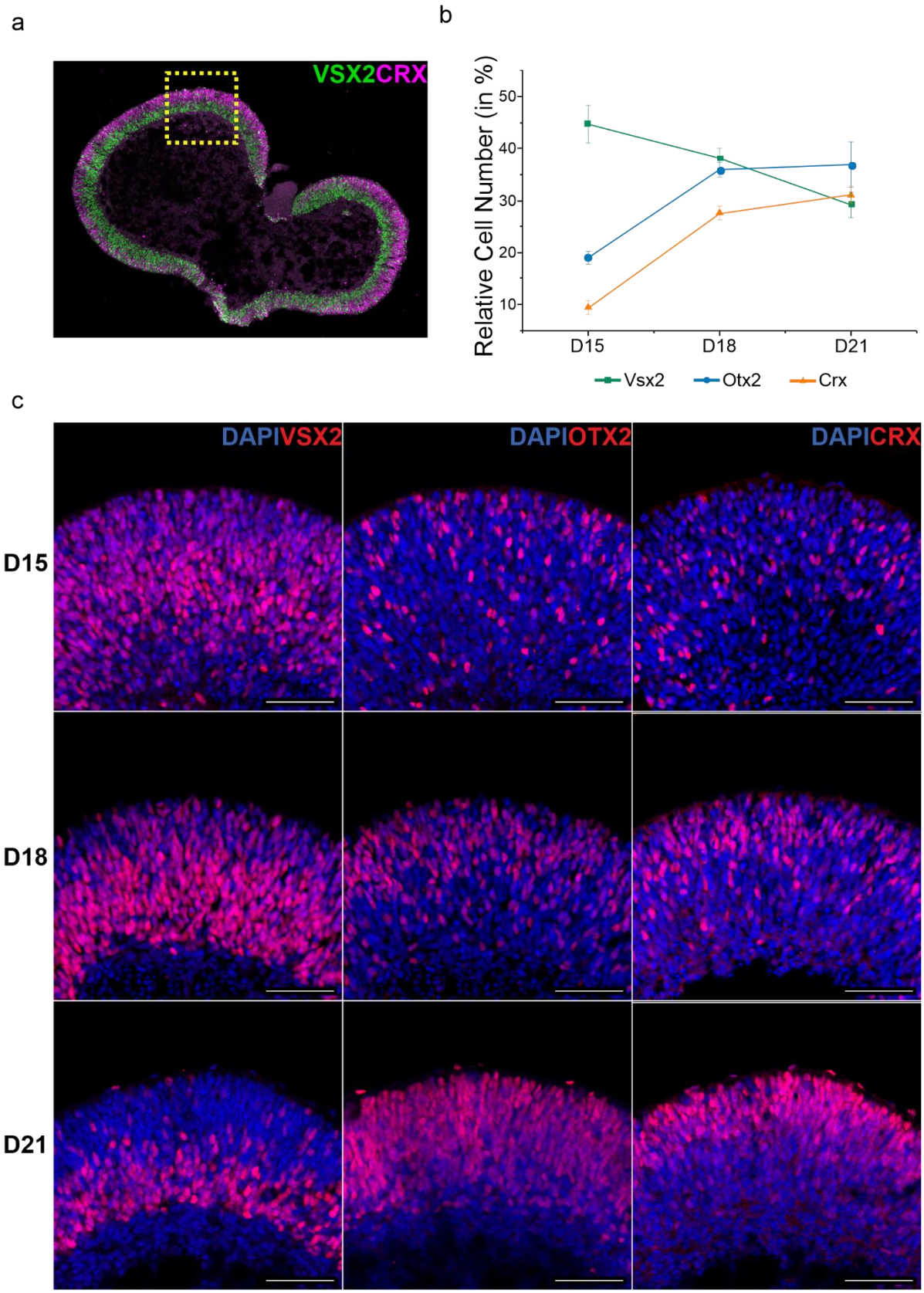

Figure 15: Photoreceptor development in ROs. **a** Exemplary cryosectioned RO at D21. Yellow dotted rectangle illustrates an exemplarily drawn crop area **b** Diagram depicting the amount of Vsx2, Otx2 and Crx immunoreactive cells in ROs at D15 (*N* = 3; *n* = 7), D18 (*N* = 3; *n* = 12) and D21 (*N* = 3; *n* = 9). **c** Crop images of the retinal epithelium Scale bar: 50 µm.

As shown in **Figure 15c**, the localization of the immunoreactive nuclei changed over of time. $Vsx2^+$ nuclei were broadly distributed in the epithelium at D15 but began to restrict their localization to the basal site at D18. At D21, only a few single nuclei of Vsx2 expressing cells could be observed apically (**Figure 16a**). Plot profile measurements give information about the localization of fluorescence signal along a drawn line in a region of interest in a fluorescence micrograph. When measured along the apico-basal axis in the retinal epithelium, the data supported the observation of a continuous shift of $Vsx2^+$ progenitor cells nuclei to the basal site during development. At D15, Vsx2 signal had an almost even distribution with a peak around the center of the epithelium. With increasing maturation, the curve's maximum was shifted to the left in the plot profile diagram, reflecting the more basal localization of $Vsx2^+$ nuclei, which was also observed in the fluorescence images. In contrast to that, nuclei of photoreceptor cells positive for Otx2 as well as Crx appeared apically with a low number of basal nuclei. There was only a short period at around D18 in which slightly more $Otx2^+$ nuclei were located more basally. At D21 however, the majority of the nuclei of Otx2 expressing cells was detected at the apical site. Similar, but less evident findings were made in the localization pattern of Crx (**Figure 16b, c**). These results additionally show the self-organization of the cells in the retinal epithelium. The arrangement of their nuclei along the apico-basal axis resulted in a pseudostratified epithelium in which nuclei of photoreceptors were localized at the most apical, and thus outermost site of the epithelium.

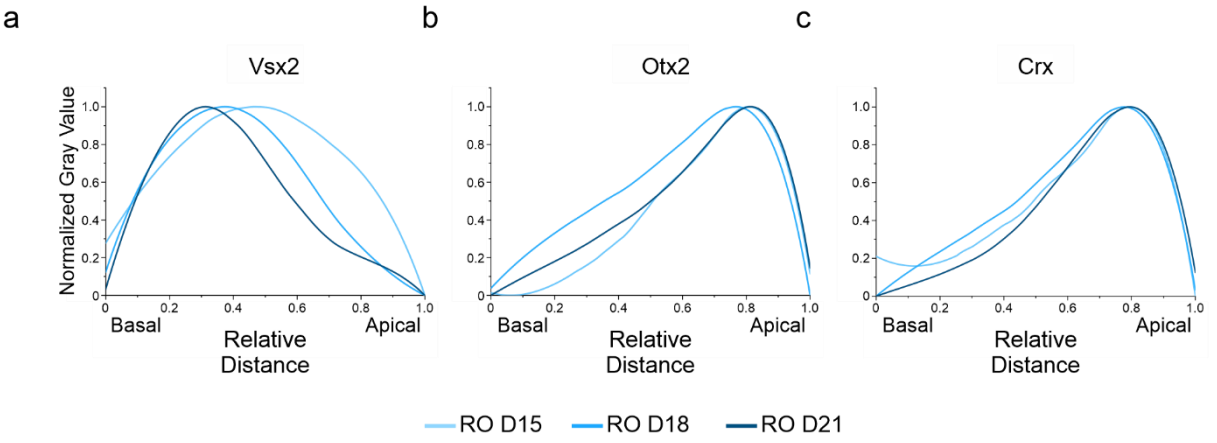

Figure 16: Photoreceptor cells are localized apical in the retinal epithelium. **a** Plot profile measurements along the apico-basal axis of the retinal epithelium in ROs. $Vsx2^+$ nuclei are detected throughout the epithelium but their localization is shifted towards the basal site during maturation. $Otx2^+$ and Crx^+ nuclei have a similar distribution pattern at the apical site.

Establishing a Co-Cultivation System for RPE Cells and ROs

To allow an interaction of apically localized photoreceptor cells with RPE, which does not occur in ROs alone, an *in vitro* co-cultivation system was set up (**Figure 17**). To mimic the outer blood-retina barrier, RPE cells were seeded on porous membranes of Transwell inserts after

purification at D11. When grown to a confluent monolayer, the RPE cells were supposed to create a barrier between the lower and the upper compartment so that nutrient exchange from the basal site to the apical site was mediated by the RPE cells. ROs were placed in the upper compartment, so that apically localized photoreceptors in the retinal epithelium faced the apical site of the RPE cells. The porous membrane was intended to allow a polar secretion of factors from mESC-derived RPE. Basally secreted factors can diffuse through the pores of the membrane into the lower compartment, while apically secreted factors were released into the upper compartment, which contained the ROs.

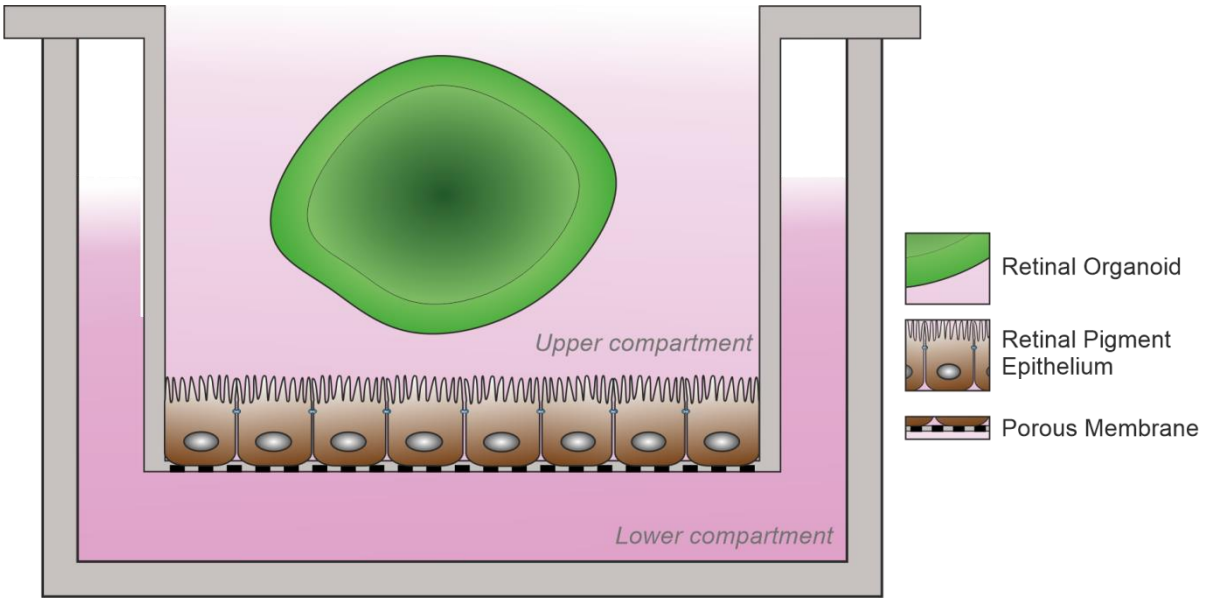

Figure 17: In vitro co-cultivation system for RPE cells and ROs. RPE cells are grown on a porous membrane of Transwell inserts. RPE cells receive nutrients from RPE medium in the lower compartment as well as RMM2 in the upper compartment. At the apical site of the RPE cells, ROs are cultivated floating in the upper compartment.

As RPE cells receive a different cultivation medium than ROs, it was first tested whether RPE cells could be maintained in the RO cultivation medium RMM2. **Figure S 3a** and **b** show a comparison of RPE cells grown on laminin-coated plastic surface of a 96-well plate with either RPE medium or RMM2. Under regular cultivation conditions, RPE cells appeared with characteristic morphology. When changing the medium to RMM2, the cells retained their morphology which suggests a good acceptance of the different cultivation medium. As photoreceptors outer segments *in vivo* are embedded in RPE cells surrounded by the interphotoreceptor matrix, it was next tested whether an ECM layer could be deposited on top of the RPE cells. This layer would also prevent potential outgrowth of retinal cells from the organoid by creating a physical barrier from RPE cells to the ROs, while still being permissive to smaller molecules. However, when a layer of Matrigel was polymerized on the RPE cells, the cobble stone morphology was lost after a few days of cultivation, suggesting incorrect differentiation or de-differentiation (**Figure S 3c**). At last, it was tested whether RPE cells could

be grown and maintained on Transwell insert membranes cultivated with RMM2 in the upper compartment and RPE medium in the lower compartment (**Figure S 3d, b**). Under these conditions, mESC-derived RPE cells were clearly recognized by their proper cell shape. Furthermore, RPE cells could be cultivated for several days without showing negative phenotypic effects.

Besides morphological properties that indicated differentiation and maintenance of RPE cells, gene expression was measured to evaluate the effect of the co-cultivation system. Therefore, regular cultivated mESC-derived RPE cells at D21 grown in a 96-well plate (**Figure 18a**) were compared to D21 mESC-derived RPE cells seeded on Transwell membranes receiving RMM2 in the upper compartment and RPE medium in the lower compartment either for three days (D18 – D21) or six days (D15 – D21) (**Figure 18b**). Notably, almost all RPE-specific genes, that have been measured, were upregulated when RPE cells were grown on Transwells and maintained with RMM2 apically and RPE medium at the basal site (**Figure 18c, Figure S 5**). Taken together these findings indicate that mESC-derived RPE cells in the co-cultivation setup can be grown and maintained for short-term cultivation of three days as well as long-term cultivation of six days. Furthermore, gene expression measurements revealed that RPE-specific genes were upregulated in the co-cultivation setup compared to regular cultivated mESC-derived RPE cells suggesting enhanced maturation when grown on porous membranes accessing both media.

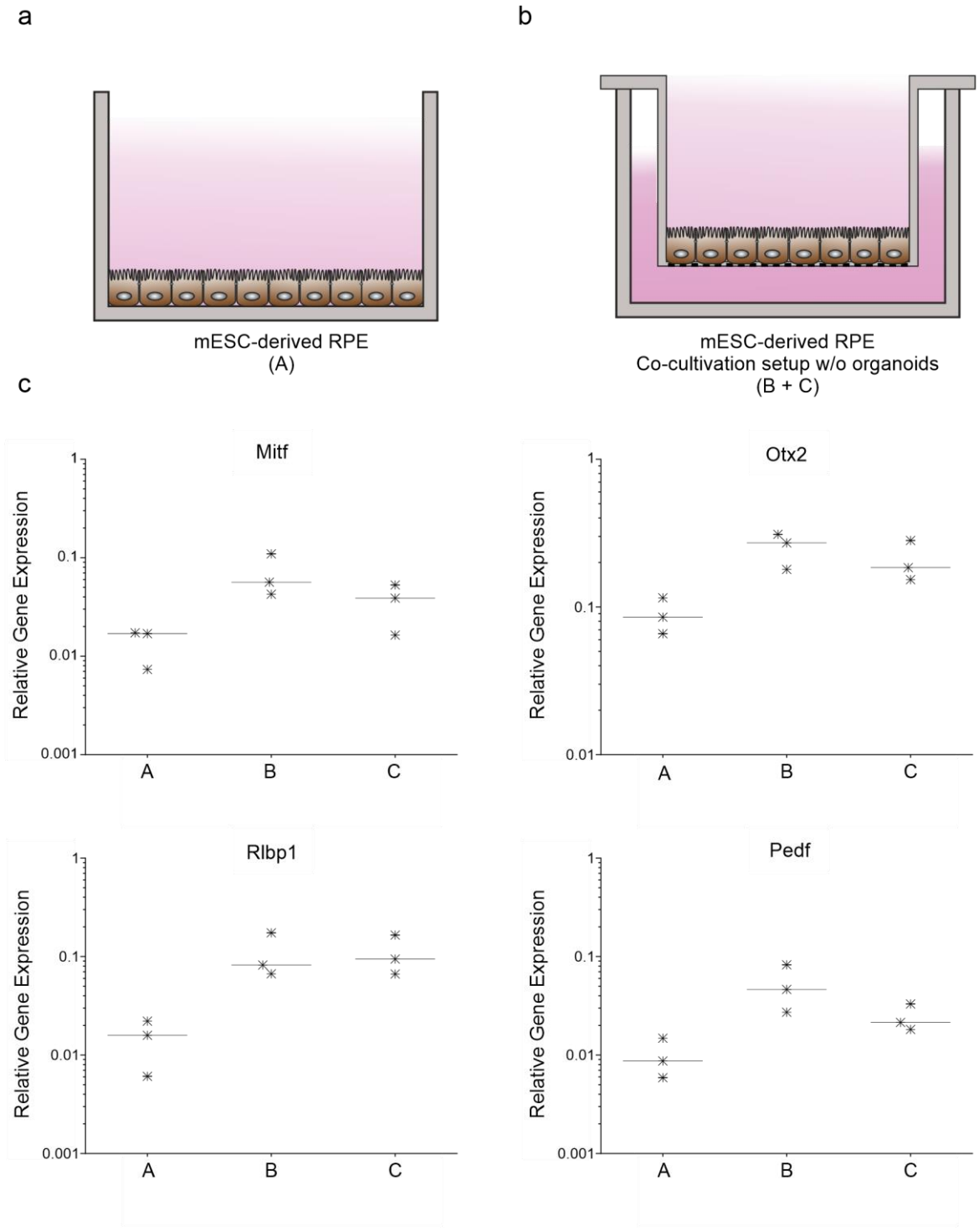

Figure 18: Enhanced RPE gene expression in the co-cultivation system. **a** Schematic drawing of mESC-derived RPE cells grown in regular cultivation conditions. **b** mESC-derived RPE cells cultivated on a Transwell membrane with RPE medium in the lower compartment and RMM2 in the upper compartment. **c** ddPCR measurements show an increase in RPE-specific gene expression. A: mESC-derived RPE grown in a 96-well plate with RPE Medium at D21; B: mESC-derived RPE grown on a Transwell membrane cultivated with RMM2 in the upper compartment from D18-D21; C: mESC-derived RPE grown on a Transwell membrane cultivated with RMM2 in the upper compartment from D15-D21.

Next, it was tested whether and how long ROs could be cultivated with mESC-derived RPE cells. In one Transwell, three to four ROs were cultivated floating at the apical site of the RPE

cells to allow direct contact. Attachment of ROs to RPE cells was not observed as long as ROs had a smooth surface at the retinal epithelium (**Figure 19a, b**). When ROs contained larger Rx-Gfp$^-$ areas and an uneven rough surface, the aggregates tended to adhere to the underlying RPE cells. This resulted in rapid decrease of Rx-Gfp expression and outgrowth of cells from the ROs which led to a loss of the epithelial structure (Data not shown). Thus, only ROs that were largely Rx-Gfp$^+$ and surrounded almost completely with an intact retinal epithelium, were identified to be suited for co-cultivation. It was found that ROs could be co-cultivated for up to six days with a daily medium change. Organoids remained Rx-Gfp$^+$ and retained their retinal epithelial integrity. As a control experiment, ROs were co-cultivated with the epithelial osteosarcoma cell line U2OS (**Figure 19c**).

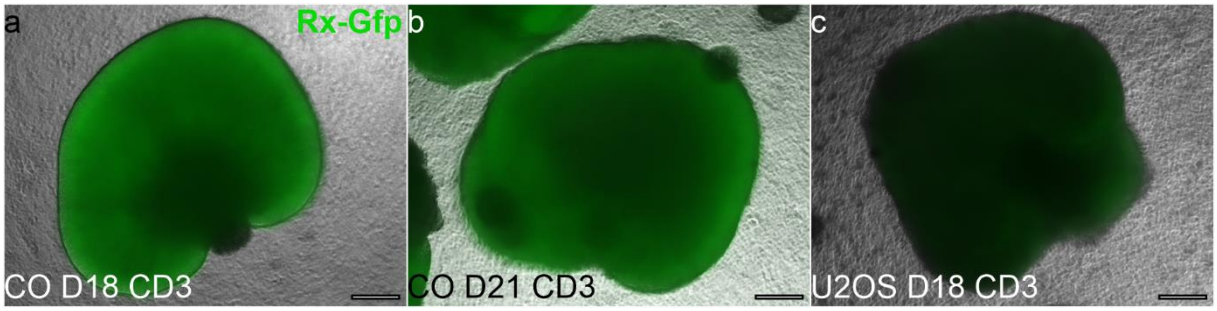

Figure 19: Floating co-cultivation of ROs with RPE cells. **a** Rx-Gfp$^+$ RO at D18 co-cultivated for three days. **b** RO at D21 co-cultivated for three days. **c** Negative control experiment in which ROs were cultivated on U2OS cells for three days from D15 – D18. CO: Co-cultivated RO; CD: Co-cultivation day. Scale bar: 200 µm.

To investigate the influence of RPE cells on developing ROs, organoids were co-cultivated at different time points. Differentiation of mESC-derived RPE cells and ROs was synchronized that both tissues were at the same differentiation day, thus simulating an *in vivo*-like co-development of both tissues during co-cultivation. The results of the immunostaining in ROs shown above suggested the presence of differentiating photoreceptors already at D15, which is also the last day in the RPE differentiation protocol. Thus, D15 was determined as the earliest time point for co-cultivation (**Figure 20**). As ROs at D21 had a certain degree of maturation while still having an intact retinal epithelium before they started to degenerate, D21 marked the end point of the co-cultivation period. Hence, a co-cultivation should occur between D15 and D21.

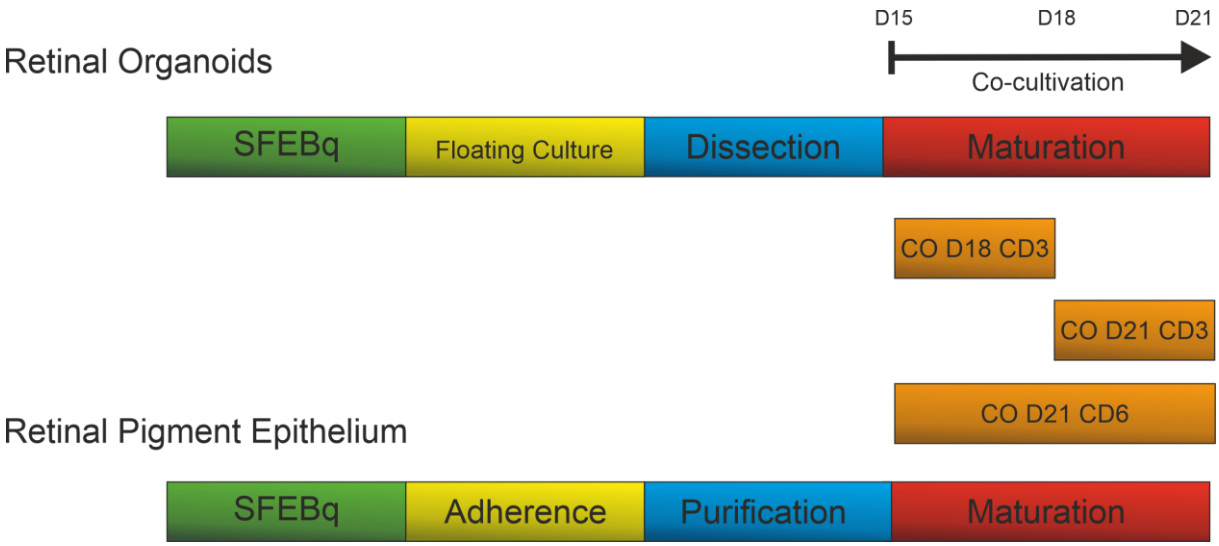

Figure 20: Co-cultivation periods. Differentiation schemes of ROs (top) and RPE (bottom) are depicted. Co-Cultivation periods are visualized with orange boxes.

Co-Cultivation has Insignificant Effect on mESC-derived RPE Gene Expression

To evaluate the effect of neural retinal tissue on mESC-derived RPE during maturation, RPE gene expression was measured. Therefore, mESC-derived RPE cells were lysed after co-cultivation and RNA was isolated and reverse transcribed to cDNA. Control samples were mESC-derived RPE cells grown in the co-cultivation setup for the same period without ROs. Reference samples were mESCs and isolated RPE (iRPE) from p28+ mouse eyes. Relative gene expression was measured via ddPCR and is shown in **Figure 21** (detailed measurements: **Figure S 11**, **Figure S 12** and **Figure S 13**). As expected, mESCs expressed RPE genes only on low levels. In mESC-derived RPE cells, all genes of interest were detected. Notably, Rpe65 expression was extremely low in all conditions, especially compared to iRPE. The relative gene expression of mESC-derived RPE was only slightly affected by co-cultivation resulting in no recognizable upregulation or downregulation pattern of gene expression. Neither co-cultivation time point, nor co-cultivation period could lead to a gene expression pattern in mESC-derived RPE comparable to iRPE. Remarkably, the number of co-cultivated organoids had also no significant effect on the gene expression of the RPE cells as no outstanding influence was observed in co-cultivation of single ROs with mESC-RPE cells (***Figure S 14***). These results suggest that floating ROs cannot increase RPE-specific gene expression and thus do not promote RPE cell maturation.

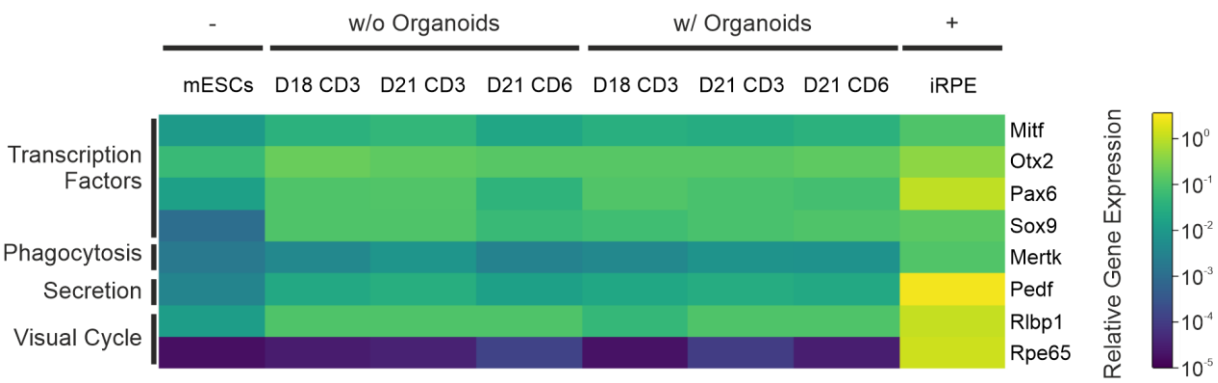

Figure 21: Relative gene expression of co-cultivated mESC-derived RPE cells. ddPCR measurements of RPE marker genes normalized to the housekeeping gene Pgk1.

Co-Cultivation of RPE and ROs Increases Photoreceptor Cell Number

After co-cultivating ROs with RPE cells for three days from D15 to D18 (CO D18 CD3; CO: Co-cultivated Organoid; CD: Co-cultivation day), organoids were fixed and immunostained. **Figure 22** clearly shows that $Vsx2^+$ retinal progenitor cells were localized throughout the entire retinal epithelium. While ROs at D18 started to restrict $Vsx2^+$ nuclei to the basal site in the epithelium, co-cultivation with mESC-derived RPE cells prevented the basal shift and apical $Vsx2^+$ nuclei were observed. Strikingly, photoreceptors ($Otx2^+$, Crx^+) were also widely present in the epithelium in CO D18 CD3. As D21 marked a peak in RO development, it was interesting to see the effect on ROs co-cultivated from D18 until D21 (CO D21 CD3). Similar to COs D18 CD3, organoids at D21 CD3 contained an abundancy of photoreceptors as well as a broad distribution of progenitor cells. Next, it was tested whether a prolonged co-cultivation period could further increase the observed effects. Thus, ROs were co-cultivated from D15 until D21 (CO D21 CD6). Similarly, COs D21 CD6 showed widely abundant photoreceptors as well as progenitor cells. These observations suggest that RPE mediates enhancing effects for the differentiation of photoreceptors in ROs in co-cultivation periods of three days and six days. Additionally, it can be stated that mESC-derived RPE influences earlier ROs at D15 as well as more mature ROs at D18.

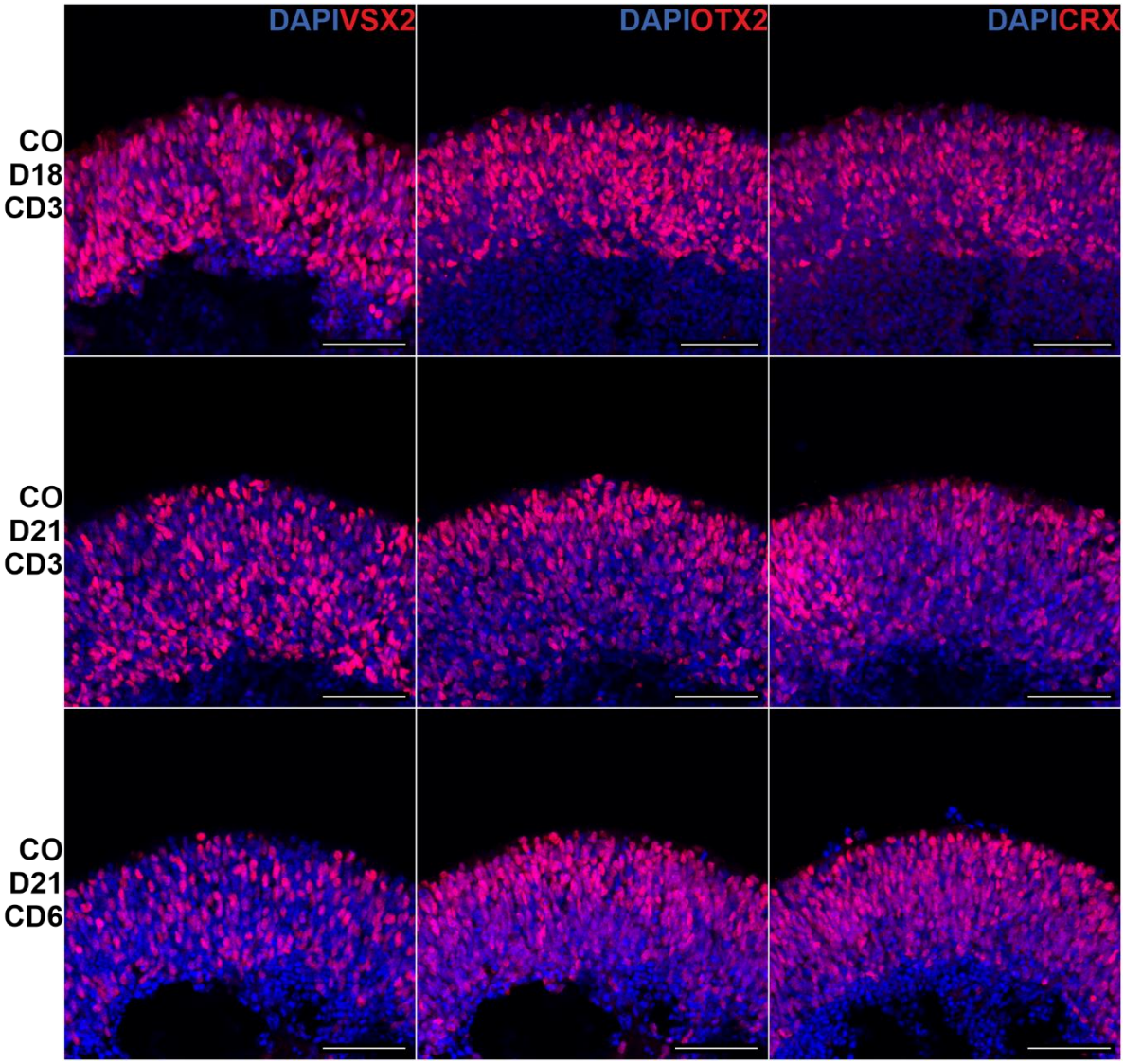

Figure 22: Co-cultivation with RPE leads to more photoreceptors in ROs. Fluorescence images of co-cultivated ROs. In all cases progenitor cells are seen being more distributed in the epithelium and the number photoreceptor cells is increased. Scale bar: 50 µm.

Soluble Factors in mESC-derived RPE Conditioned Medium Mediate an Increase in Photoreceptor Cells

Co-cultivated ROs were in direct contact with the underlying mESC-derived RPE layer. However, as there was no attachment and organoids remained floating, the contact surface of the round ROs to the RPE cells was minimal. Thus, it was assumed that besides a physical interaction also factors secreted from the RPE cells could elicit the effects of increased photoreceptor cell numbers which have been observed in the co-cultivation. To test whether there are influential soluble factors in the medium, conditioned medium from mESC-derived RPE cells grown in the co-cultivation setup was collected daily. ROs treated with conditioned medium at D15 only received medium from mESC-derived RPE cells grown in the co-

cultivation setup from D15 onwards. ROs treated with conditioned medium at D18 also only received medium from mESC-derived RPE cells grown in the co-cultivation setup from D18. Thus, any potential maturation-dependent effects of mESC-derived RPE cells at varying differentiation days were excluded. To simulate the co-cultivation conditions in a Transwell insert, ROs were transferred into a low adhesion 96-well plate for the conditioned medium treatment. According to the co-cultivation periods, ROs were treated with conditioned medium from D15 until D18 (CM D18 D3), from D18 until D21 (CM D21 D3) and from D15 until D21 (CM D21 D6). **Figure 23** shows that ROs treated with conditioned medium had a strong Rx-Gfp signal and a clearly visible retinal epithelium. Neither short-term treatment from either D15 or D18 nor the long-term treatment caused structural degeneration in ROs.

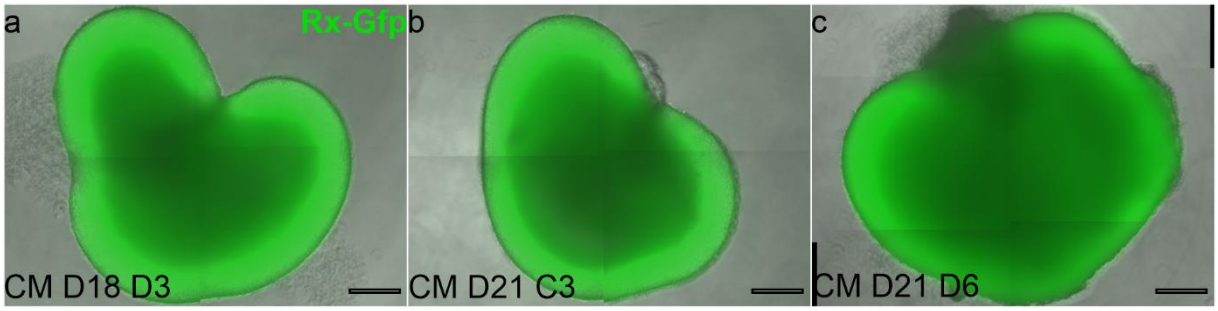

Figure 23: ROs treated with mESC-derived RPE conditioned medium. **a** RO at D18 cultivated with mESC-derived RPE conditioned medium for three days. **b** RO at D21 treated with conditioned medium for three days and **c** RO treated with conditioned medium from D15 to D21. Scale bar: 200 µm.

ROs treated with conditioned medium from D15 until D18 and from D18 until D21 showed an effect that is comparable to co-cultivated ROs in same periods, respectively (**Figure 24a** and **b)**. Immunohistochemical results showed more apical $Vsx2^+$ nuclei resulting in a less prominent restriction to the basal site. Furthermore, an increase in cells expressing photoreceptor cell markers Otx2 and Crx can be observed. Similar to co-cultivation, conditioned medium treatment results in a broad distribution of photoreceptor nuclei in the retinal epithelium. However, treating ROs for six days with conditioned medium influenced the localization of progenitors and photoreceptor cells but did not significantly increase the number photoreceptor cells (**Figure 24c**).

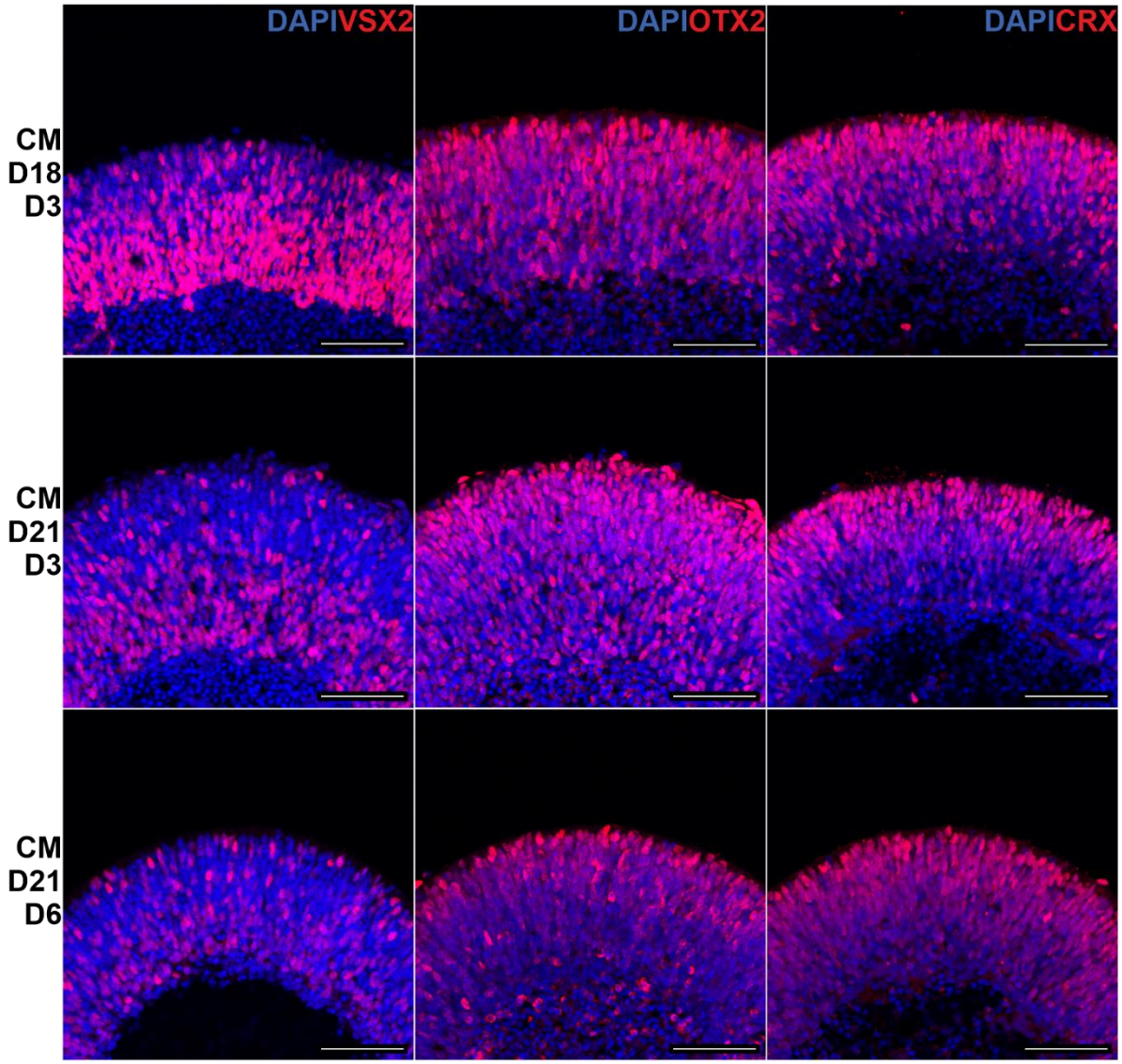

Figure 24: Fluorescence images of ROs treated with mESC-derived RPE conditioned medium. Slightly increased number of apical progenitor cells can be observed as well as more basal photoreceptor cells compared to untreated ROs at the same differentiation days.

mESC-derived RPE Mediates Enhanced Photoreceptor Differentiation in ROs

Quantification of the relative number of $Vsx2^+$ neural retina progenitor cells and photoreceptors expressing Otx2 and Crx showed a significant increase in $Otx2^+$ cells (42.50 ± 1.32%) as well as Crx^+ cells (36.02 ± 1.5%) in D18 ROs after co-cultivation with RPE cells. A similar increase could be seen in ROs which were treated with conditioned medium in the same period (44.23 ± 2.81% $Otx2^+$, 38.09 ± 2.5% Crx^+, **Figure 25a**). ROs that were co-cultivated from D18 until D21 also had significantly increased numbers of photoreceptor cells (51.17 ± 3.86% $Otx2^+$, 49.39 ± 4.61% Crx^+). Conditioned medium in this case also led to an increase of $Otx2^+$ cells (50.91 ± 2.13%) as well as Crx^+ cells (41.19 ± 2.47%, **Figure 25b**). Interestingly, when organoids were co-cultivated or treated with conditioned medium from D15 for three days, the

number of photoreceptors increased stronger than in organoids treated from D18 until D21. In contrast to that, co-cultivation of ROs for six days only affects the number of Crx$^+$ cells. Notably, the treatment with conditioned medium seemingly had almost no effect on the relative cell number for this period. To exclude that these observations were due to the cultivation setup itself and not the RPE cells, ROs were also co-cultivated with U2OS cells. There however, Rx-Gfp signal was often decreasing rapidly accompanied with loss of epithelial integrity (**Figure 19c**). Immunocytochemical evaluation further validated these observations as a strong decrease in progenitor cells as well as photoreceptors was measured (**Figure 25**).

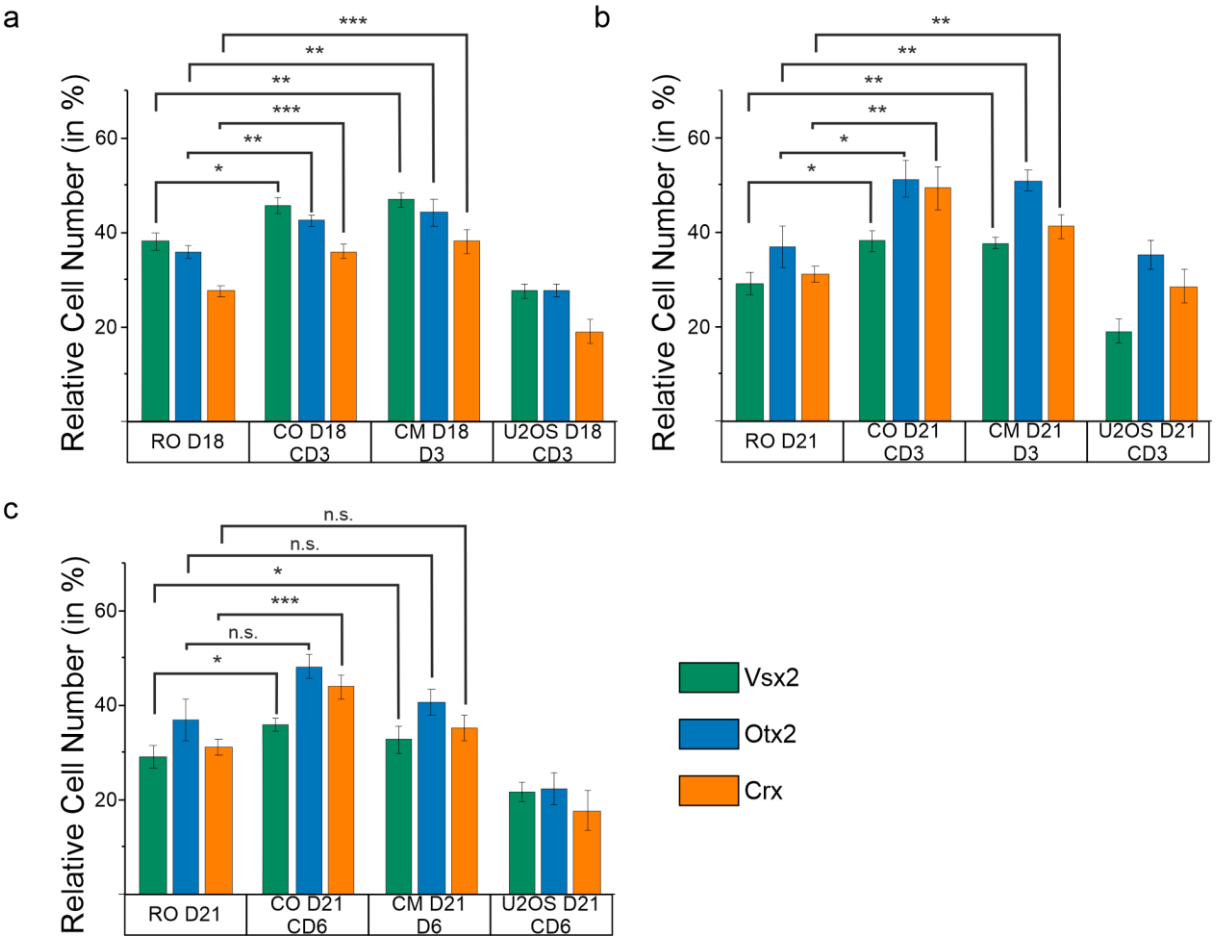

Figure 25: Quantification of relative cell numbers in ROs. Relative cell numbers in ROs which were regular cultivated, co-cultivated, conditioned medium treated or co-cultivated with U2OS cells. Increased photoreceptor cell numbers can be observed for co-cultivation and conditioned medium treatment for three days. **a** RO D18: *N* = 3, *n* = 12; CO D18 CD3: *N* = 3, *n* = 9; CM D18 D3: *N* = 3, *n* = 8; U2OS D18 CD3: *N* = 3, *n* = 10. **b** RO D21 *N* = 3, *n* = 9; CO D21 CD3: *N* = 3, *n* = 8; CM D21 D3: *N* = 3, *n* = 9; U2OS D21 CD3: *N* = 3, *n* = 6. **c** RO D21 *N* = 3, *n* = 9; CO D21 CD6: *N* = 3, *n* = 6; CM D21 D3: *N* = 3, *n* = 9; U2OS D21 CD6: *N* = 3, *n* = 6. Two sample t-test: * p ≤ 0.05; ** p ≤ 0.01; *** p ≤ 0.001.

These results suggest that a co-cultivation as well as conditioned medium treatment for three days yields better results to increase photoreceptor cell numbers. Notably, co-cultivation and conditioned medium treatment for six days seemed to exceed a beneficial period that enhances photoreceptor differentiation and thus the positive effects could not be increased by

prolonged cultivation periods. It was also observed that ROs at D15 were more acceptive to these effects than ROs at D18 as the increase in photoreceptors was stronger in both, co-cultivation as well as conditioned medium treatment.

Co-staining of the three retinal markers showed a largely non-overlapping pattern of $Vsx2^+$ and $Otx2^+$ or Crx^+ nuclei. Contrary to that, a strong co-localization of both photoreceptor markers could be seen (**Figure 26**, **Figure 27**). The shift of retinal progenitor cells to the basal site while photoreceptors populate the apical site of the epithelium during RO development was also highlighted (**Figure 26a**). Strikingly, in co-cultivated organoids the non-overlapping pattern of the photoreceptor markers and progenitor cell marker was the same even though the localization of the nuclei was different. $Vsx2^+$ nuclei as well as $Otx2^+$ and Crx^+ nuclei were widely distributed along the apico-basal axis, which resulted in a mosaic-like pattern of progenitor cells and photoreceptors. In conditioned medium treated ROs, the same co-localization pattern was observed (**Figure S 4**).

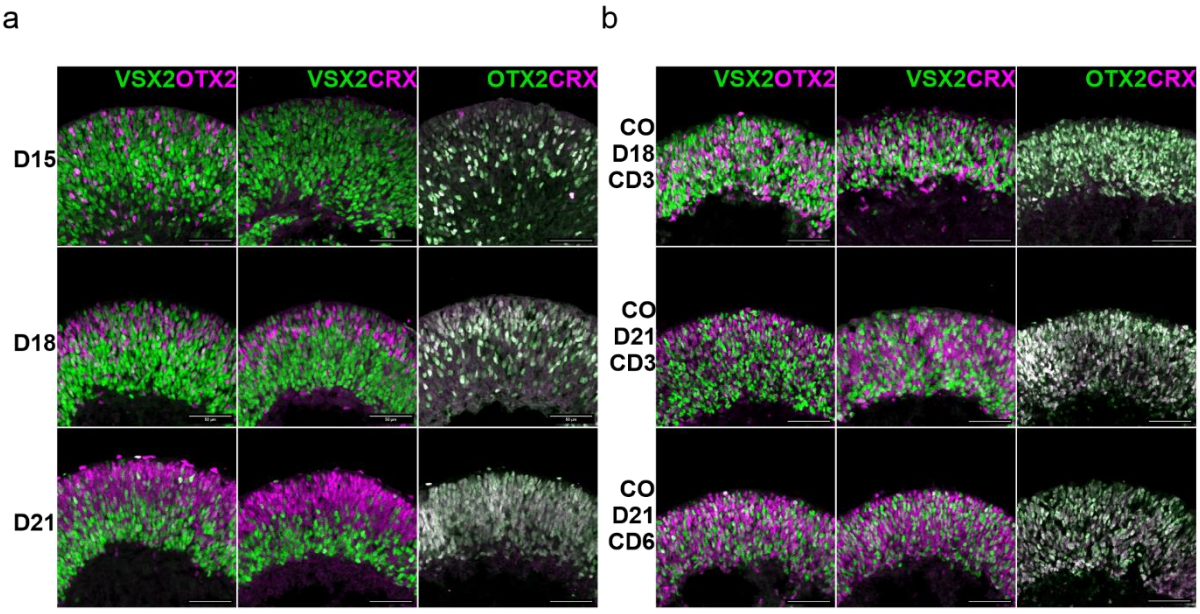

Figure 26: Co-staining of retinal cell markers Vsx2, Otx2 and Crx. Immunofluorescence merge images of co-stained ROs (**a**) and COs (**b**). $Vsx2^+$ progenitor cell nuclei do not overlap with photoreceptor cell markers, while Otx2 and Crx signal strongly co-localizes. Scale bar: 50 µm.

The immunohistochemical staining revealed that there were more $Otx2^+$ cells than Crx^+ cells. As Crx expression depends on Otx2, the co-expression of both marker genes can indicate more mature photoreceptors. Thus, the co-localization of Otx2 and Crx signal was measured and is graphically displayed in **Figure 27a**. In D18 ROs, ~76% of Otx2 expressing cells were positive for Crx. Organoids that were co-cultivated with RPE cells however, contained 81% of $Otx2^+$ and Crx^+ cells whereas ROs treated with conditioned medium showed only a minor increase of co-expression. A similar but even enhanced effect could be observed in ROs that

were co-cultivated from D18 to D21. Notably, in the six-day co-cultivation period, the ratio of $Otx2^+/Crx^+$ cells was on the same level like in ROs at D21. Furthermore, there were even less Otx2 and Crx co-expressing cells observed in CM D21 D6 (**Figure 27a**).

It can be noted, that there was always a small portion of cells that expressed Otx2 and Vsx2. Both genes are required for late born bipolar cell differentiation. Thus, the question was raised, whether this co-expression was observed in cells which were in transition from progenitor state to photoreceptors or whether co-localization of Otx2 and Vsx2 could potentially indicate the presence of bipolar cells. In **Figure 27**, it can be seen that in ROs the amount of $Otx2^+/Vsx2^+$ cells decreased from 33% at D18 to 21% at D21. Co-cultivated and conditioned medium treated organoids always consisted of more Otx2 and Vsx2 co-expressing cells. which decreased at a later time.

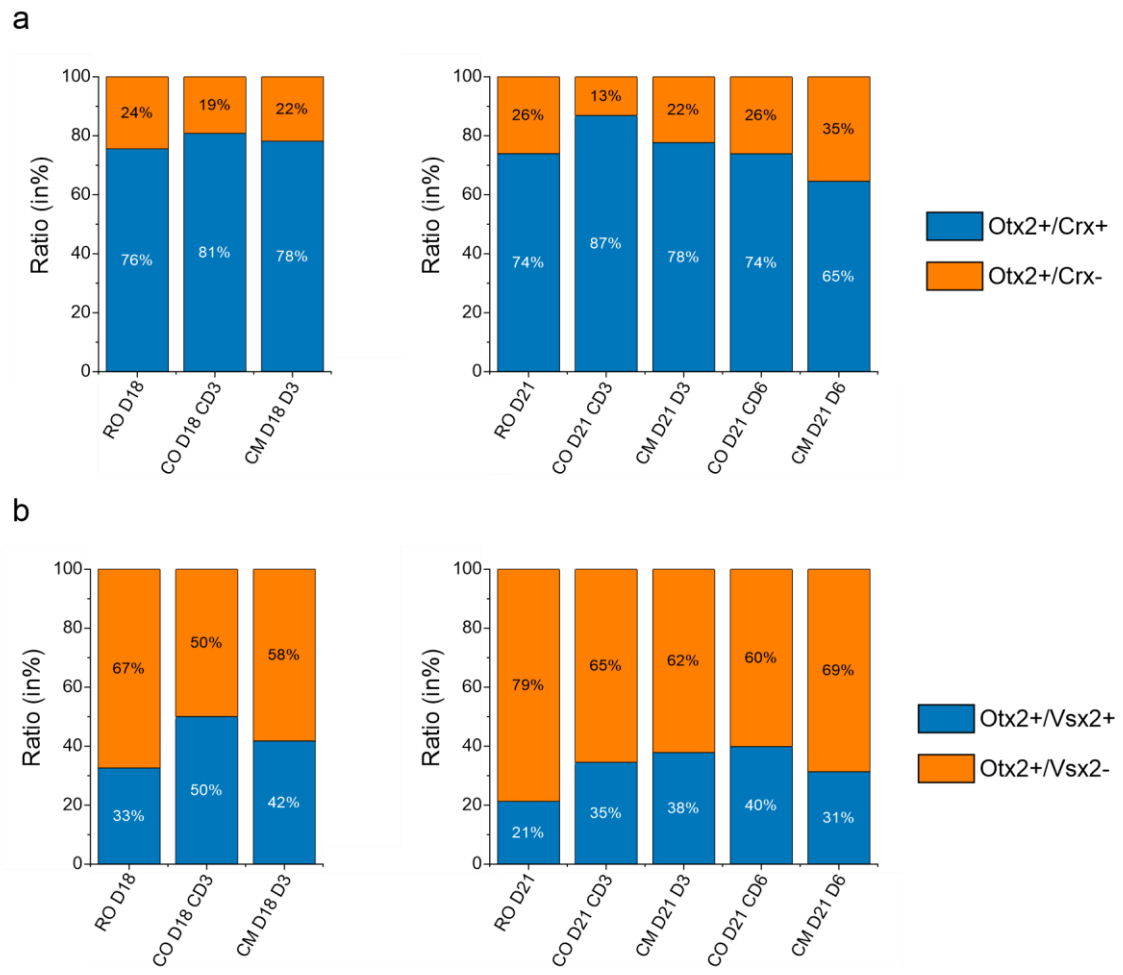

Figure 27: Co-expression of retinal cell markers Vsx2, Otx2 and Crx. **a** Ratio of cells positive for Otx2 that are also positive for Crx (blue) compared to $Otx2^+$ cells which do not co-localize with Crx (orange). **b** Ratio of $Otx2^+$ cells that co-localize with Vsx2 (blue) and $Otx2^+$ without Vsx2 co-localization (orange). For sample size (N, n) see: ***Figure 25***.

Taken together, the results show that co-cultivation of ROs for three days, either from D15 or from D18 onwards, increased the amount of more mature, $Otx2^+/Crx^+$ expressing photoreceptor cells. Comparable effects were observed in organoids that were treated with conditioned medium for the same periods, respectively. These co-localization measurements of Otx2 and Crx further emphasize the accelerated differentiation of photoreceptors in COs compared to regular cultivated ROs. The decrease of Otx2 and Vsx2 co-expressing cells over time indicate that these cells can represent the transition from progenitor cells to photoreceptors or the presence of bipolar cells. Nonetheless, the increased number of $Otx2^+/Vsx2^+$ in co-cultivated and conditioned medium treated organoids suggests an accelerated neuronal differentiation from progenitors to either photoreceptors or potentially bipolar cells.

Mature Photoreceptors Develop in ROs and COs

Expression of the transcription factors Otx2 and Crx indicates the differentiation of photoreceptors. However, it does not provide evidence for the development of fully maturated and potential functional photoreceptor cells. Thus, crucial proteins involved in light perception could reveal the state of maturation of photoreceptors in ROs. Two prominent marker genes are Rhodopsin (Rhod) and Recoverin (Rcvrn). To evaluate their expression, organoids at D21 were used for immunohistochemical experiments. As **Figure 28** shows, Rcvrn and Rhod were expressed in ROs and COs at D21. Rcvrn had a strong cytoplasmic localization but was also detected around the nucleus in the cell body. Interestingly, the cytoplasmic signal gave a clear impression about the cell morphology. $Rcvrn^+$ cells had an elongated cell shape where the cell body is rather basally and the apical part is a thin, almost straight elongation. Notably, $Rcvrn^+$ photoreceptors were only sparsely detected in both conditions. However, it can be noted that in COs D21, many more $Rcvrn^+$ cells without or with only a short apical elongation were observed compared to ROs D21 (Data not quantified). Rhod was also detected in both conditions. Similar to Rcvrn, Rhod was only expressed in a few cells in ROs D21, but is detected throughout large parts of the retinal epithelium in COs D21. Nonetheless, it needs to be mentioned, that most of the $Rhod^+$ photoreceptors consist only of short apical elongations. Similar to the Rcvrn signal, also Rhod marked only a few single cells that were fully elongated. These observations suggest that mature photoreceptors can be found in ROs and COs. Moreover, these immunohistochemical experiments might indicate that the terminal differentiation to photoreceptors is initiated earlier in COs than in ROs

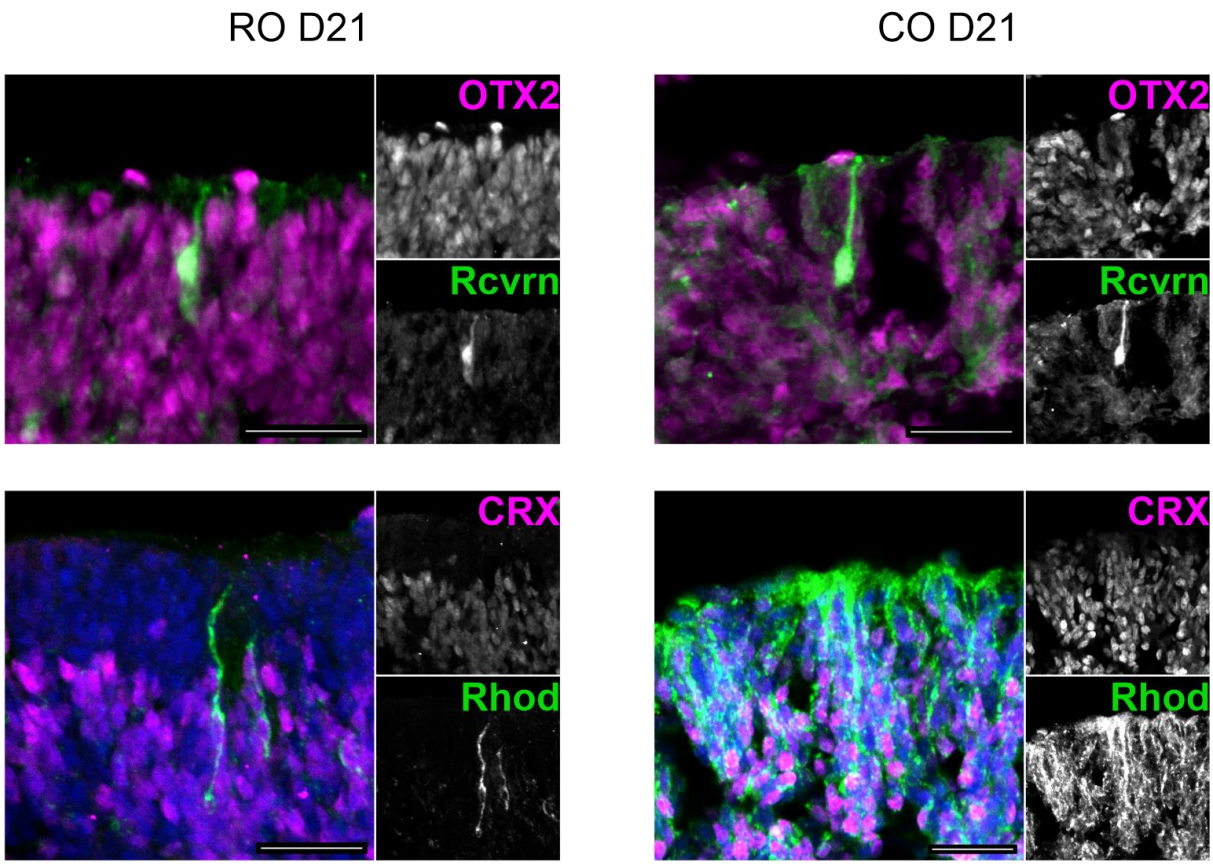

Figure 28: Mature photoreceptors in ROs: Rcvrn and Rhod expression can be detected in ROs and COs at D21. Both proteins show cytoplasmic localization which highlights an elongated cell shape. Co-cultivation period was three days (top) and six days (bottom). Scale bar: 25 µm.

Vsx2$^+$ Nuclei Localize More Apically in COs

In the process of maturation from D15 to D21, Vsx2$^+$ nuclei were observed to be localized more at the basal site in ROs. However, in immunohistochemically stained COs, Vsx2$^+$ nuclei were more evenly distributed along the apico-basal axis (**Figure 29**). This effect was enhanced in organoids that were co-cultivated from D15 onwards (**Figure 29b, d**) compared to ROs at D18 (**Figure 29c**). Interestingly, the Vsx2 distribution curve in ROs at D18 already shows a shift of the nuclei to the basal site which gets more prominent at D21. However, after co-cultivating organoids from D18 to D21, more apical Vsx2$^+$ nuclei appeared, indicating an active apical movement rather than a remaining at the apical site. Prolonged co-cultivation increased the number of apically localized progenitor cell nuclei. Notably, plot profile data from retinal epithelia of ROs treated with conditioned medium display an intermediate distribution curve between ROs and COs (**Figure S 6**).

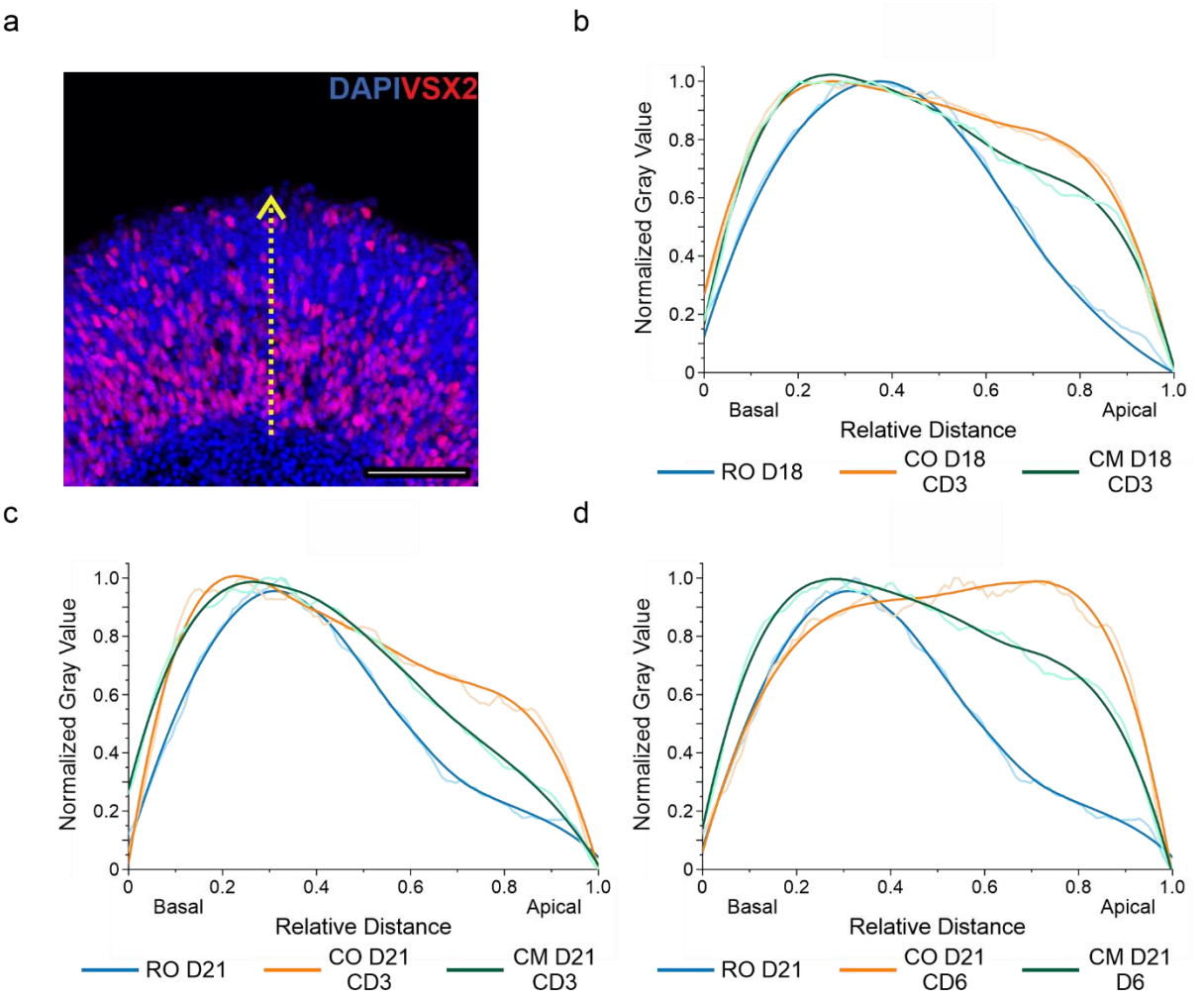

Figure 29: mESC-derived RPE mediates apical localization of Vsx2⁺ nuclei. **a** Exemplarly drawn line for plot measuremnts from the basal site of the retinal epithelium to the apical site (yellow dotted arrow). **b-d** Plot profile graphs for Vsx2 localization. Light colored lines: Normalized plot profiles; Bold lines: Smoothed curves of normalized plot profiles. For sample sizes see ***Table S 1***. Scale bar 50 µm.

Broad Distribution of Photoreceptors Along the Apico-Basal Axis in the Retinal Epithelium in COs

The localization of photoreceptor cell nuclei produced an inverted pattern compared to the localization of Vsx2⁺ nuclei in ROs. Photoreceptors seemed to differentiate at the apical site and slightly moved their nuclei more towards the apical end of the retinal epithelium. However, co-cultivation affected the localization of both Otx2⁺ and Crx⁺ nuclei resulting in more basal nuclei (**Figure 30**, **Figure 31**). This effect was observed in COs D18 CD3 and COs D21 CD3 but is much more evident in COs D21 CD6 (**Figure 30b, c, Figure 31b, c, Figure S 7**, **Figure S 8**).

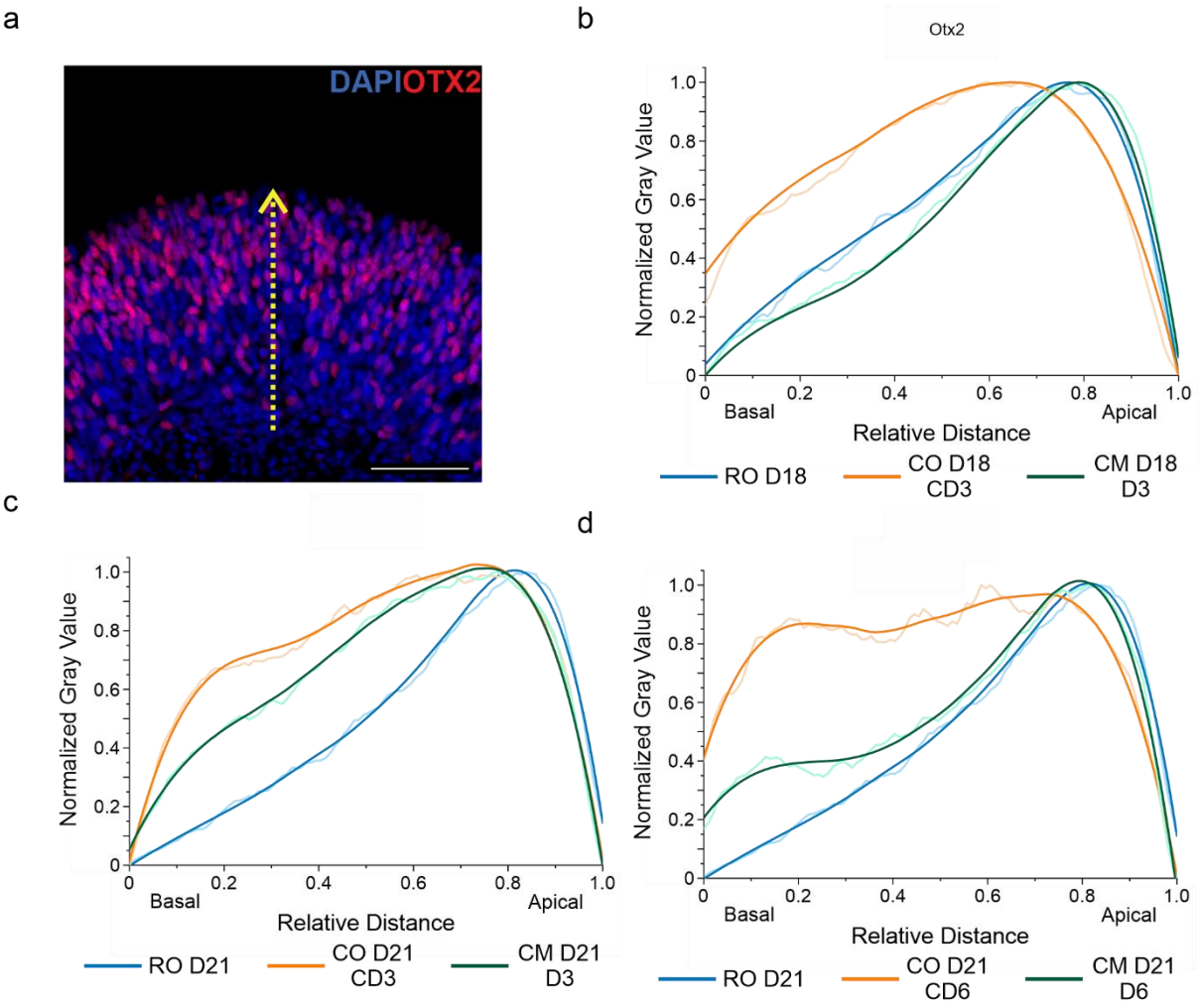

Figure 30: Distribution of Otx2⁺ Nuclei. **a** Exemplarly drawn line for plot measurements from the basal site of the retinal epithelium to the apical site (yellow dotted arrow). **b-d** Plot profile graphs for Otx2 localization. Light colored lines: Normalized plot profiles; Bold lines: Smoothed curves of normalized plot profiles. For sample sizes see ***Table S 1***. Scale bar 50 µm.

Moreover, the restricted apical pattern of photoreceptor nuclei at D18 is also lost by co-cultivation from D18 until D21 which indicates that photoreceptors move their nuclei basally as a consequence of co-cultivation with RPE cells. Despite CM D18 D3, where no increased basal nuclear localization is observed, treating ROs with conditioned medium has a similar but slightly reduced effect, resulting in more basal photoreceptor nuclei.

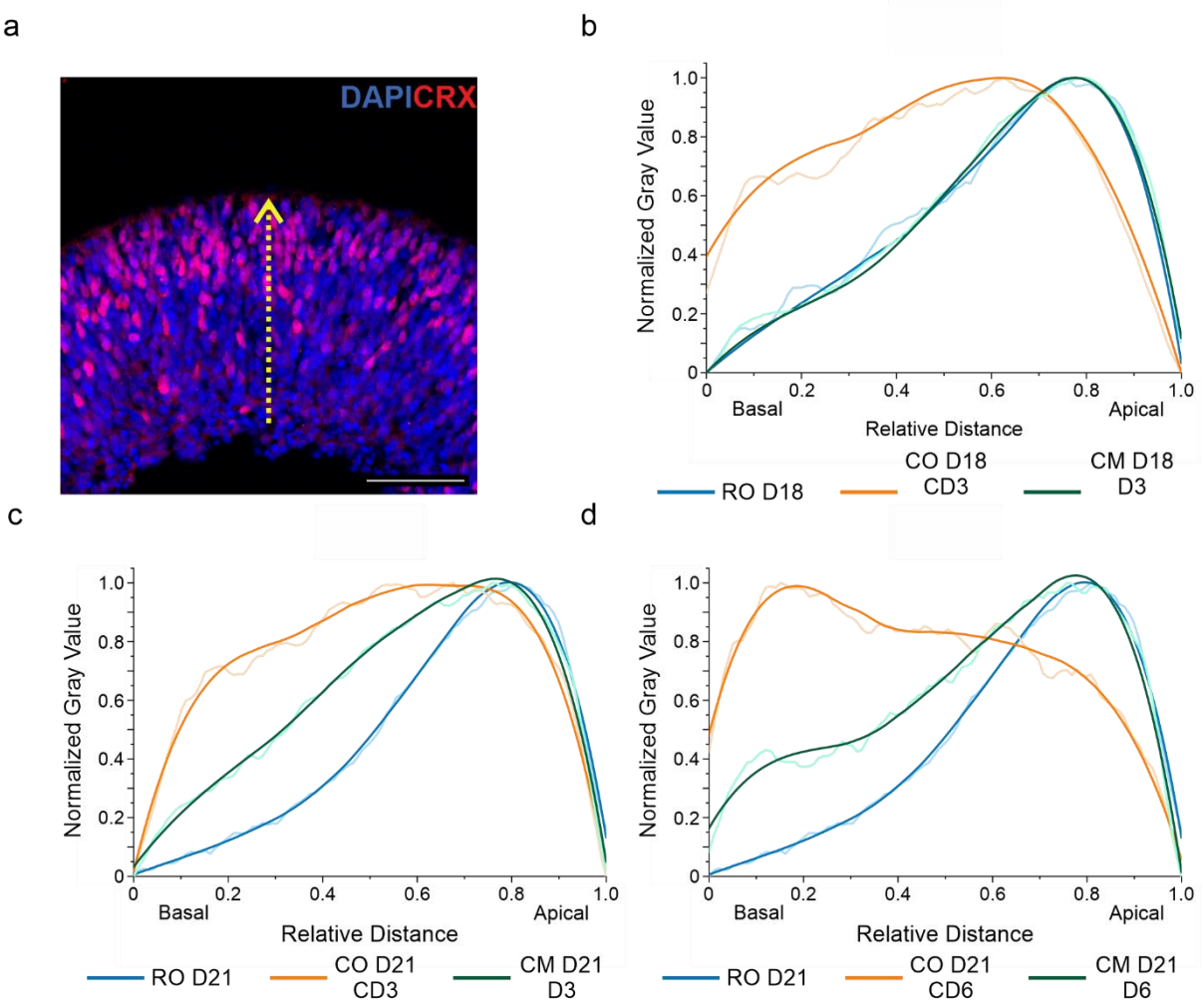

Figure 31: Distribution of Crx⁺ nuclei. **a** Exemplarly drawn line from the basal site of the retinal epithelium to the apical site (yellow dotted arrow). **b-d** Plot profile graphs for Crx localization. For sample sizes see ***Table S 1***. Scale bar 50 µm.

Co-Cultivation Accelerates Cell Cycle Exit of Progenitor Cells in ROs

To validate the observations of increased photoreceptor cell numbers and, thus accelerated differentiation to neurons, it was interesting to evaluate proliferation and cell division capacity of progenitor cells in ROs. A first striking indicator of proliferating progenitors that give rise to at least one progenitor daughter cell is the thickness of the retinal epithelium (**Figure 32**). The retinal epithelium thickness was assessed by measuring the length along the apico-basal axis. The first measurement in ROs at D15 revealed a large deviation around the median of a 93.94 ± 7.77 µm thick epithelium. At D18, the retinal epithelium became more refined with a distinct separation from cells inside of the organoid resulting in a thinner epithelium (median = 90.04 ± 3.77 µm). In the next days of cultivation until D21, the epithelium thickens to 97.77 ± 3.12 µm. This indicated that progenitors in ROs still proliferated from D18 until D21. Remarkably, co-cultivated ROs had a much thinner epithelium. When ROs were co-cultivated for three days from D15 (CO D18 CD3), the epithelium was 68.54 ± 2.62 µm thick. The effect of epithelial

thinning is reduced when co-cultivation began at D18 (75.63 ± 3.04 µm). Notably, in CO D21 CD6, it was observed that with prolonged co-cultivation period the epithelium is thinner (66.73 ±4.37 µm). Treatment with mESC-derived RPE conditioned medium also reduced epithelial thickness. Interestingly, the trend for the different conditioned medium treatment periods was similar compared to co-cultivated organoids. Epithelial thinning after three days of conditioned medium treatment was slightly more visible in CM D18 D3 (84.4 ± 1.57 µm) than in CM D21 D3 (85.88 ± 2.52 µm). Similar to six days of co-cultivation, treatment with conditioned medium for six days showed the strongest effect in epithelial thinning to 73.12 ± 1.92 µm. Notably, co-cultivation led to thinner epithelia than conditioned medium treatment. In control experiments where ROs were co-cultivated with U2OS cells, it could also be observed that the thickness of the retinal epithelium decreased. U2OS D18 CD3 (75.4 ± 2.9 µm) and U2OS D21 CD3 (69.7 ± 5.65 µm) had a retinal epithelium of comparable thickness like COs. However, after six days of co-cultivation with U2OS cells, the retinal epithelium was severely thinned to only 51.422 ± 3.44 µm, which is in accordance with the previous observation of degeneration and loss of structural integrity (**Figure 19c**).

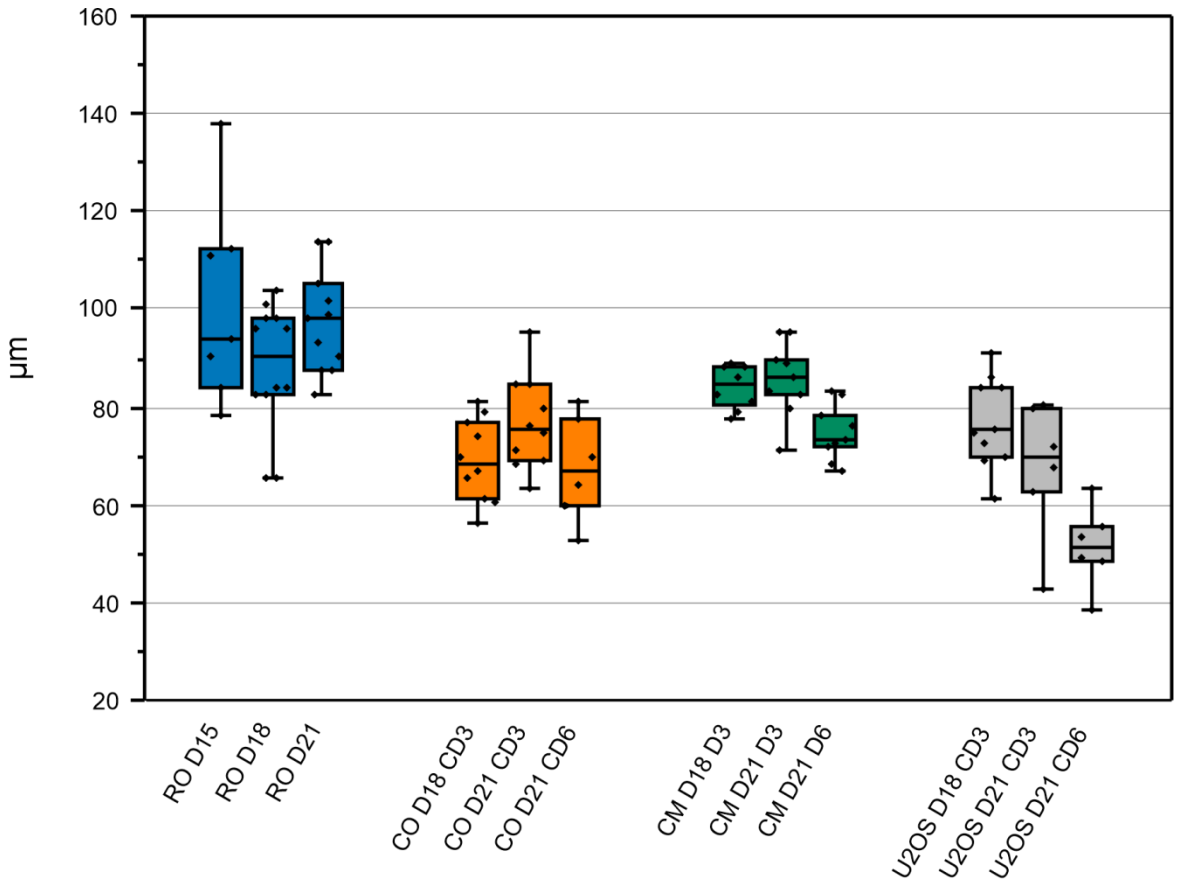

Figure 32: Retinal epithelium thickness. Epithelial thickness was measured in fluorescence micrographs of cryosectioned organoids. For sample sizes see ***Table S 1***.

Epithelial thickness measurements gave a first indication that ROs would normally proliferate until D21. However, co-cultivation or treatment with mESC-derived RPE conditioned medium, resulted in thinner epithelia. Thus, it can be assumed that mESC-derived RPE signaling cues seem to prevent proliferation or induce postmitotic neuronal differentiation in ROs.

Thinner retinal epithelia after co-cultivation as well as conditioned medium treatment suggest that cells in these organoids had a reduced proliferative capability compared to ROs. Immunohistochemical staining of the marker Ki67 can give insights into the percentage of proliferative cells (**Figure 33a**).

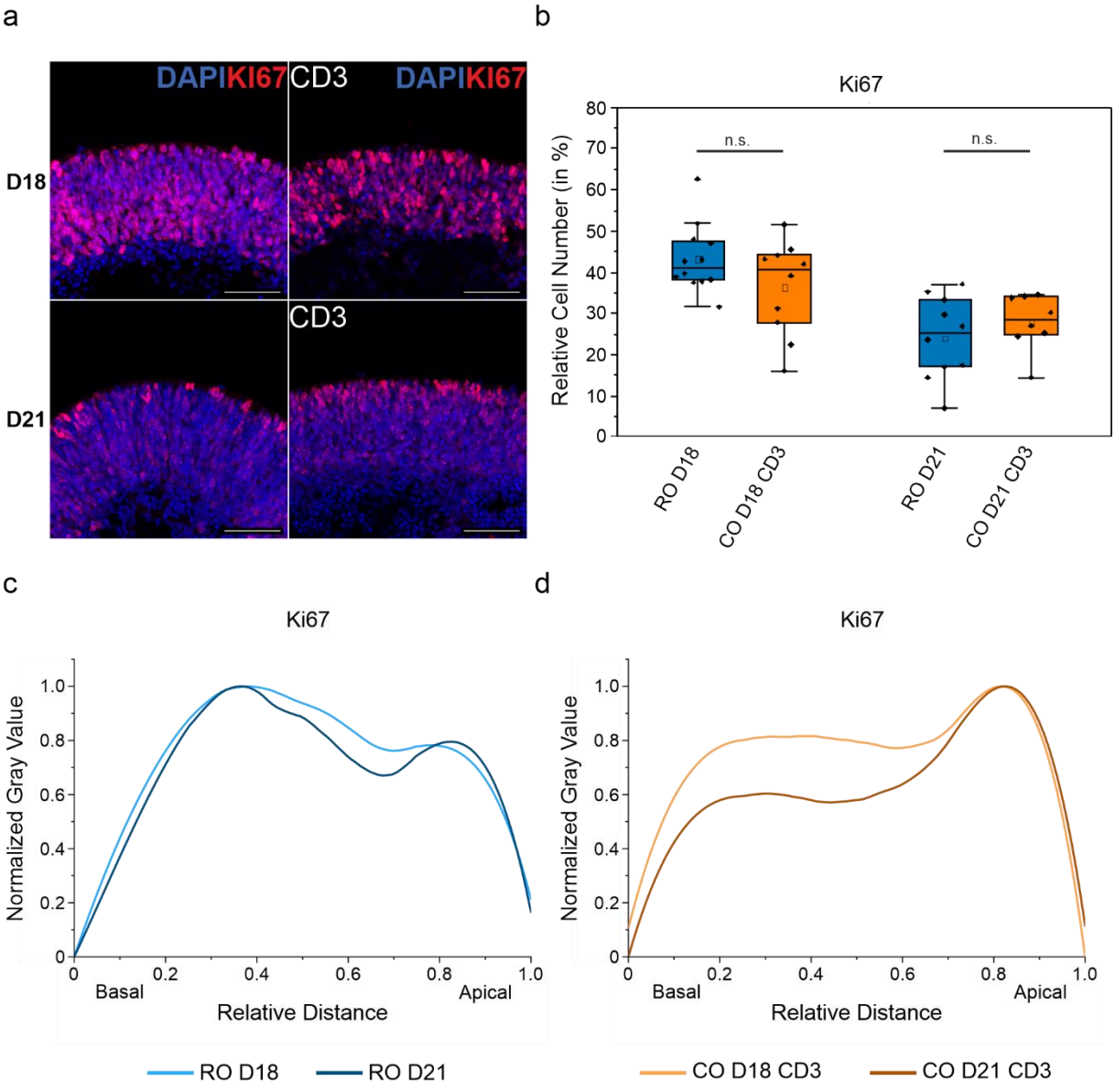

Figure 33: Proliferation capacity of retinal cells. **a** Immunohistochemical staining of proliferation marker Ki67 in ROs at D18 and D21 (left) and co-cultivated ROs (right). **b** Quantification of Ki67$^+$ labeled cells (RO D18: $N = 3$, $n = 12$; CO D18 CD3: $N = 4$, $n = 10$; RO D21: $N = 3$, $n = 10$; CO D21 CD3: $N = 3$, $n = 8$). **c-d** Plot profile measurement of the retinal epithelium in ROs and COs.

At D18 in ROs, 41.2 ± 2.37% of the cells in the retinal epithelium were $Ki67^+$. At D21, the expression of Ki67 was detected only in 25.2 ± 3.15% of the cells. Surprisingly, no significant difference in $Ki67^+$ cell number could be observed in the retinal epithelium in CO D18 CD3 (40.58 ± 3.6%) or CO D21 CD3 (28.65 ± 2.4%), when compared to regular ROs, respectively (**Figure 33b**). The distribution pattern of $Ki67^+$ nuclei in ROs and COs showed some similarities, which was a peak at the apical site and a peak at the basal site of the epithelium. However, whereas ROs had their maximum in the basal half, co-cultivated organoids only showed a flat local maximum at this position and had their maxima at the apical site (**Figure 33c**, **d**). This suggests that more proliferating cells were localized apical after co-cultivation.

As the relative number of proliferating cells in COs did not differ from that of ROs, it was next investigated whether there was a difference in mitotically active cells. The marker for dividing cells phosphorylated Histone $H3^{ser10}$ (pH3) can be labeled immunohistochemically. Remarkably, in ROs at D18 and D21, $pH3^+$ signal was mostly detected in the outermost nuclei of the epithelium while only a minority of partially labeled nuclei could be observed more basally. In contrast, though fully $pH3^+$ nuclei are also at the most apical site, there was an increase in partially labeled nuclei which were distributed more basally in CO D18 CD3. In CO D21 CD3, only a few apical nuclei positive for pH3 were observed (**Figure 34a**). Notably, at D18 were significantly more $pH3^+$ cells after co-cultivation (5.53 ± 0.57%) than in ROs (3.33 ± 0.29%). On the other hand, the number of $pH3^+$ was decreased at D21 and significantly reduced in COs (0.43 ± 0.12%) compared to ROs (1.73 ± 0.4%) (**Figure 34b**). Plot profile measurements in **Figure 34c-d** highlight the apical localization of $pH3^+$ nuclei in both, ROs and COs. However, in CO D18 CD3, there were more basally localized $pH3^+$ partially labeled nuclei than in ROs at D18. In turn, at D21 almost no pH3 signal was detected at more basal localizations after co-cultivation. In contrast, ROs at D21 showed a small peak shifted to the basal site (**Figure S 10**).

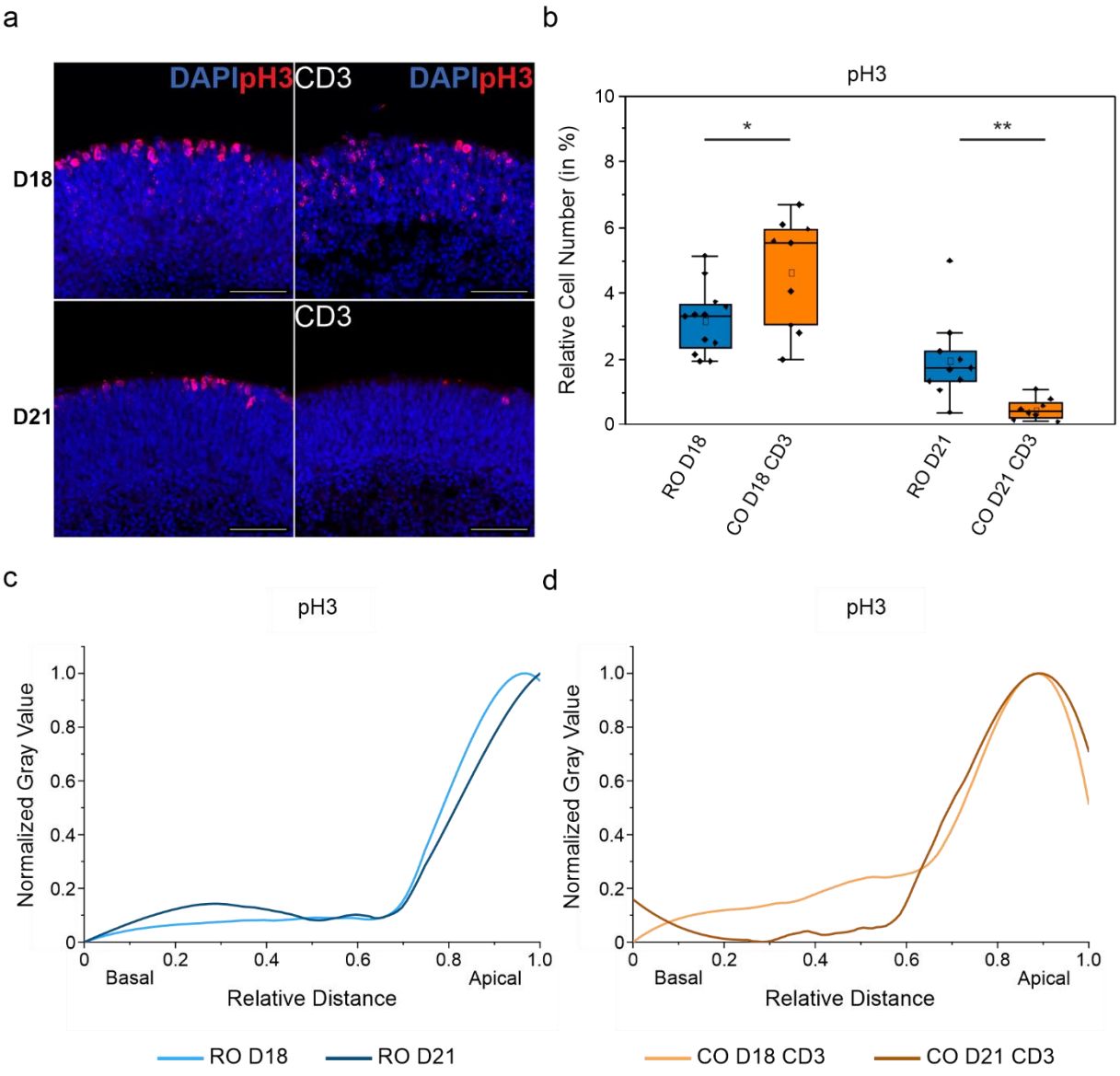

Figure 34: Cell division occurs at the apical site in the retinal epithelium. **a** Immunohistochemical staining of dividing cells via phosphorylated Histone $H3^{Ser10}$ (pH3) in ROs at D18 and D21 (left) and COs (right). **b** Quantification of $pH3^{+}$ labeled cells (RO D18: *N* = 3, *n* = 12; CO D18 CD3: *N* = 4, *n* = 9; RO D21: *N* = 3, *n* = 10; CO D21 CD3: *N* = 3, *n* = 8; Two sample t-test: * p ≤ 0.05; ** p ≤ 0.01). **c-d** Plot profile measurement of the retinal epithelium in ROs and COs.

In was noted that nuclei of proliferating cells in the epithelium vary in their morphology (**Figure 35a**). While fully $pH3^{+}$ labeled nuclei appeared round at the apical site, the partially labeled nuclei tended to be elongated along the apico-basal axis. Interestingly, the amount of pH3 per nucleus seemed to correlate in many cells with the apico-basal localization in the epithelium. That is, the more apical proliferating cells were, the more pH3 signal was observed. Immunostaining of the neuronal cell type specific β3-Tubulin (Tubb3) revealed that the cells in the retinal epithelium had a strong apico-basal polarity (**Figure 35b**). The majority of the cells formed long thin processes that in some cases spanned the entire distance from the basal site to the apical site. Magnification images highlight that the localization of a cell's nucleus varied

with regard to the apico-basal axis while the cells still remained attached at the basal and apical site.

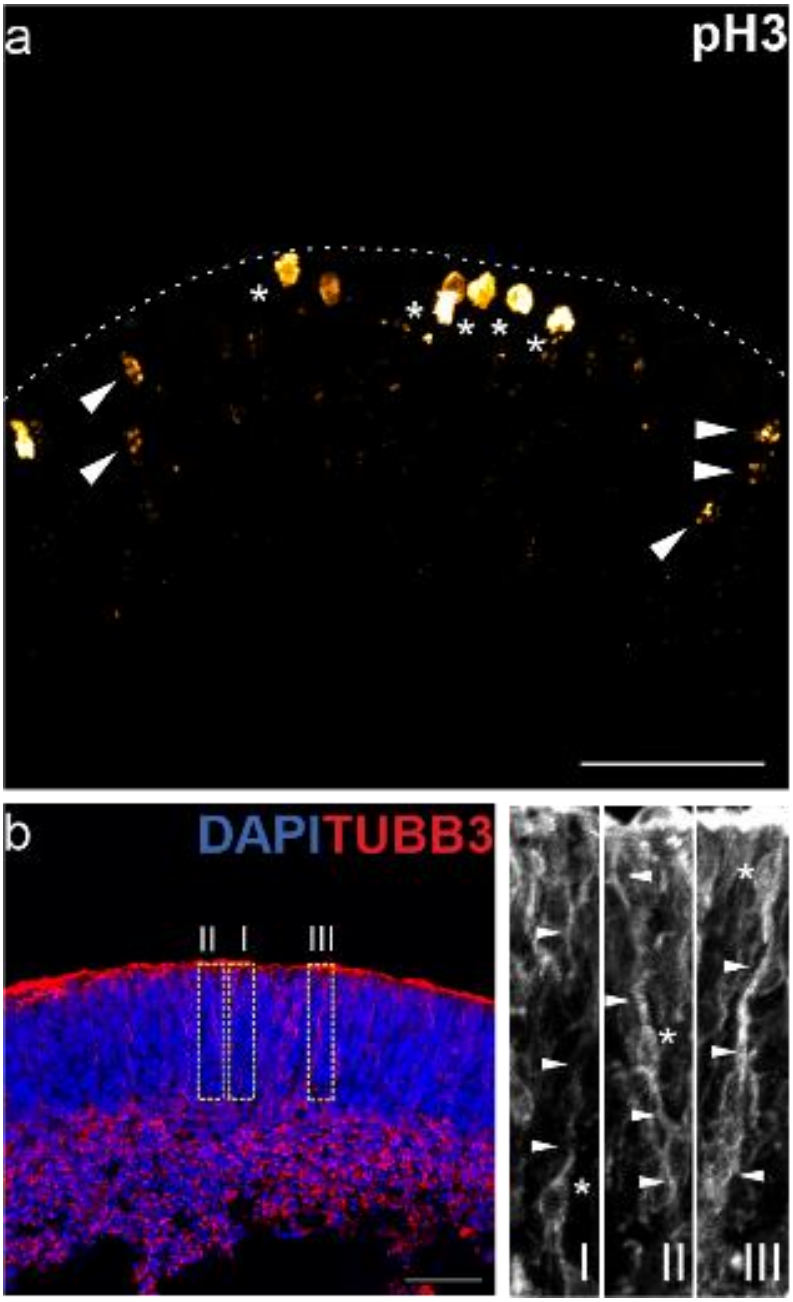

Figure 35: Nuclear positioning in the retinal epithelium. **a** Localization of pH3^{+} nuclei along the apico-basal axis. Completely stained round nuclei are localized at the apical site (asterisks). Partially labeled elongated nuclei are located more basally (arrows). Dashed line indicates the apical surface of the epithelium. **b** β3-tubulin (Tubb3) signal identifies neuronal cytoskeletal structures. Cells in the boxes with dashed lines are shown in higher magnification on the right. Asterisks mark the position of the nucleus. Arrows indicate elongated processes of the single cells. Scale bar: 50 µm.

These findings additionally support the previous observations of accelerated neuronal differentiation after co-cultivation with mESC-derived RPE cells. Thinning of the retinal epithelium was most likely caused by an earlier exit from the cell cycle as a result of co-cultivation. Partially pH3^{+} labeled nuclei in CO D18 CD3, which were more widely distributed along the apico-basal axis, presumably represent cells at the onset of Histone H3^{ser10} phosphorylation. This further indicates early exit from the cell cycle during co-cultivation with mESC-derived RPE cells. Detection of almost no mitotically active cells in COs D21 CD3 was presumably the result of terminal differentiation of most of the cells during the co-cultivation

period, which also suggests an accelerated differentiation. Notably, in ROs at D21, a small peak of partially $pH3^+$ nuclei localized more basally was observed which might indicate that the transition to M-phase in ROs is delayed compared to COs.

Discussion

This work could demonstrate an improved method to generate early ROs from mESCs. On the one hand, these early ROs can be subsequently differentiated into RPE cells in a stepwise differentiation protocol that involves successive dissociation to eventually purify RPE precursor cells. Activation and inhibition of critical signaling pathways shifts the initial retinal progenitor cells to acquire RPE cell fate. In the end, a polarized monolayer of epithelial cells expressing prominent RPE marker genes can be obtained. On the other hand, early ROs can be maintained in a floating culture to develop more mature ROs. Retinal progenitors have the potential to self-organize and form a pseudostratified retinal epithelium with photoreceptor cells on the outer side while interneurons or potential ganglion cells are localized more on the inside. Synchronized generation of ROs allowed the co-development of mESC-derived RPE cells and ROs in an *in vitro* co-cultivation system that resembles the interface of neural retina and RPE, which forms the outer blood-retina barrier *in vivo*. It was found that ROs can be co-cultivated for three to six days, while still maintaining the retinal epithelial structure. Co-cultivation resulted in increased numbers of photoreceptor cells in ROs due to accelerated differentiation. Treatment of ROs with mESC-derived RPE conditioned medium could induce similar effects suggesting that secreted factors from RPE cells drive photoreceptor differentiation. Furthermore, differentiation of retinal progenitors to postmitotic neurons in ROs follows a comparable pattern like *in vivo*, underlining the relevance of ROs as a tool to supplement research in developmental biological principles.

Generation of Early ROs from mESCs

The improvement of the efficiency in retinal induction to generate early ROs from mESCs was the first crucial step to increase reproducibility. It is known that organoid differentiation and maturation is highly dependent on the cell line which is used. In a study, multiple cell lines were tested in parallel to generate ROs. It was found that the ROs differentiated from different cell lines in a common protocol shared many structural and cellular features. However, some inconsistencies among the ROs derived from different cell lines were observed regarding morphology, structure and cellular composition. Additionally, even within the same RO population different developmental progress was noted[249]. In another publication, ROs differentiated from 23 iPSC lines were screened for desired mature structures. There it was

found, that only eight out of the 23 cell lines could form a potentially laminated epithelium, of those only four iPSC lines could differentiate into ROs with three layers[239]. For iPSCs, many genetic differences can be accounted to donor effects. Epigenetic memory and different transcriptomic states vary between different cell lines resulting in different molecular and phenotypic appearance which influences subsequent differentiation[250]. In this work, a mESC line was used which was previously reported to be capable to produce ROs[53]. mESCs are commonly cultivated and maintained in a pluripotent state by supplementing the cultivation media with LIF, MEK inhibitor and GSK3 inhibitor, together termed LIF+2i. LIF was identified first as a pluripotency regulator by activating JAK3-STAT signaling resulting in the expression of pluripotency factors Oct4, Nanog and ERR2[251,252]. The addition of an inhibitor for MEK signaling was found to enhance stability and self-renewal capacity in mESCs[253]. Additional application of GSK3 inhibitor, mimicking Wnt signaling, further stabilized mESCs growth and increased proliferation[254]. The mESC-Rx-Gfp cell line used in this work is derived from the 129/ola mouse strain. ESCs from this mouse strain can be propagated in LIF and fetal bovine serum (FBS) supplemented medium whereas other cell lines from different mouse strains are reliant on the supplementation of the other two inhibitors[255]. Thus, previously mESC-Rx-Gfp were maintained by supplementation with LIF only[53,256]. Notably, the recommended medium composition for this cell line describes only a low FBS concentration[257]. A defined serum replacement, named KnockOut Serum Replacement, is the major ingredient, while FBS is only added with 1% as final concentration. This serum replacement is stated to be more consistent to increase reproducibility compared to the biologically derived FBS which is known to have a great lot-to-lot variability. In order to test the influence of different cultivation conditions for mESCs on retinal induction, the low-serum based medium (Riken MM) and an FBS based medium (MM), described in Völkner et al.[258], were used to maintain the mESCs. Second, both media were supplemented with LIF, LIF and MEK inhibitor (LIF+1i) or LIF, MEK inhibitor and GSK3 inhibitor (LIF+2i), respectively (***Figure 8***, **Figure S 1** and **Figure S 2**). It was noted that ROs at D7, generated from mESCs maintained with LIF, developed more optic vesicle-like structures which is in accordance with previously described results[53]. However, it was also observed that the ROs, which were generated in one experiment, had a large variability with regard to retinal induction and morphology. This resulted in Rx-Gfp$^+$ ROs with optic vesicle structures on the one hand but also only weakly retinal induced or completely Rx-Gfp$^-$ aggregates on the other hand. Furthermore, while retinal induction was observed in one experiment, in following experiments RO generation could completely fail to produce any Rx-Gfp$^+$ organoids[259]. Contrary to that, ROs that were differentiated from mESCs, which were maintained with LIF+1i or LIF+2i, had a drastic reduction in evaginating structures. Conversely, the aggregates remained round and only slightly bended the retinal epithelium. Hence, vesicle-like structures were only rarely seen. Interestingly, these morphological developments were

independent from the base cultivation medium. More importantly, in repeated experiments, the retinal induction seemed to be more consistent, especially with mESCs maintained with LIF+1i. It can now be hypothesized that MEK inhibition might influence the differentiation of ROs. However, when mESCs supplemented with LIF received MEK inhibitor at D0 of the differentiation protocol, no difference in retinal induction could be observed (Data not shown). Thus, it can be assumed that inhibition of the MEK pathway is either not sufficient to increase retinal induction efficiency, or that MEK inhibition is temporal and/or dosage dependent. Therefore, it needs to be evaluated whether and how long the inhibition of this signaling pathway might persist after transferring the mESCs into the differentiation medium until it is depleted. Nevertheless, a precise mechanism to induce retinal differentiation remains unclear. Moreover, it was shown that the MEK pathway is crucial in neurulation[260,261] which is the initial step before cells can acquire retinal fate. This suggests that differences in the retinal induction might rather be caused by the pluripotency state of mESCs. ESCs from the inner cell mass exhibit distinct characteristics of the pre-implantation embryo which is referred to naïve pluripotency. In contrast, post-implantation configuration is termed primed pluripotency. Differences of both states involve for example global DNA hypomethylation and increased expression of pluripotency markers in naïve SCs whereas X chromosomal inactivation and ablation of epigenetic repressors for differentiation has occurred in primed pluripotent cells[254]. Although both mESC maintenance conditions, LIF + FBS and LIF+2i, are described to represent naïve pluripotency, respectively, there are fine differences known between these conditions. While LIF+2i represents complete naïve pluripotency, mESCs maintained with LIF + FBS share features of primed SCs with regard to their methylation pattern and can thus be considered to be less naïve[254]. It can now be speculated that LIF+1i might represent an intermediate between both conditions, that promotes more consistent retinal differentiation compared to LIF + FBS in a yet unknown mechanism.

Furthermore, the mESC cultivation medium seems to influence the reproducibility of ROs. Cultivating mESCs in maintenance medium with low serum concentration and supplementation of the defined serum replacement (Riken MM) delivered the most robust and consistent results regarding retinal induction. In contrast, the serum based medium (MM) caused more variability and thus reduced reproducibility. This could be explained by the variable composition of serum ingredients as it is a biological product. However, the exact influence remains elusive.

The differentiation to ROs was originally described to be mediated by cell autonomous mechanisms in a minimalistic differentiation medium[53]. In a second publication, using mouse iPSCs, minor changes have been applied to the differentiation step, which include an increase in KnockOut Serum Replacement and the addition of a retinoic acid receptor antagonist[247].

Applied to our system, it resulted in higher retinal induction efficiency and increased consistency between different experiments. While the authors did comment on their adjustments, it can be assumed that antagonizing retinoic acid signaling serves to maintain anterior neural plate specification. In zebrafish, it was demonstrated that retinoic acid initializes the posteriorization of the neural ectoderm[262]. As the eye field is established in the anterior neural plate, suppression of retinoic acid signaling in differentiating ROs might increase retinal induction. However, the source of retinoic acid in the differentiation protocol remains unclear as no vitamin A derivate is actively added or known to be included in either of the components. Remarkably, when it was tested to increase the KnockOut Serum Replacement concentration without supplementation with the retinoic acid receptor antagonist, retinal induction was not observed[259]. This suggests an interplay between the serum replacement and retinoic acid receptor inhibition. Another potential candidate, that influences RO generation, can be the ECM compound Matrigel or Geltrex which is added to the aggregates at D1. As this protein mixture is derived from cell culture supernatants, it consists of various more factors than ECM proteins. However, the exact composition of KnockOut Serum Replacement and Matrigel/Geltex is unknown.

The addition of the ECM protein mixtures is on the one hand necessary, as in its absence ROs will not properly develop a neuroepithelium and will not differentiate into retinal cells. On the other hand, it adds variability and uncertainty to the system as Matrigel/Geltrex are poorly defined and known to have a large lot-to-lot variability[263]. The main ingredients of Matrigel/Geltrex are laminin, collagen, heparan sulfate, and entactin among a variety of growth factors including Igf-1, Vegf, EGF, Tgf-β, Pdgf, Fgf and Ngf[264]. The differentiation of ROs relies on autonomous differentiation and self-organization which is intended to be largely driven by cell intrinsic programs instead of external signaling cues. Hence, the introduction of this highly complex and undefined compound can drastically influence the outcome of an experiment. To reduce one aspect of variability, the protein concentration was adjusted to 10 mg/ml in all experiments, which is in accordance of the range that has previously been recommended[265]. The rigidity of the surrounding protein matrix plays a crucial role in the formation of the neuroepithelium[266]. Nonetheless, this adjustment does not compensate the relative amount of the different proteins and growth factors. Therefore, a more controlled and precisely composed compound would eliminate uncertainties regarding undesired ingredients that cause a high fluctuation in retinal induction efficiency. In the past, it was shown that Matrigel can be replaced to embed differentiating ROs. A composition of the ECM proteins laminin and entactin and the growth factor Nodal could also induce retinal differentiation, resulting in Rx-Gfp^{+} aggregates with retinal epithelium[53]. In this work, it could be shown that laminin alone is sufficient to observe retinal differentiation (**Figure 8c**). Furthermore, when combined with collagen, the structural development of a neuroepithelium was improved (***Figure 8*d**). Remarkably, no

further signaling molecules were added, which again underlines the intrinsic capability of mESCs to differentiate and form a retinal epithelium. Although organoids embedded in Matrigel/Geltrex displayed a stronger retinal induction and formed epithelia with a higher degree of structural integrity, these findings highly suggest that there is a potential to establish alternatives to Matrigel/Geltrex to generate ROs in the future. However, the main drawback in this approach is that purified proteins are much more expensive than the ECM basement membrane protein mix. In another publication using human-derived iPSCs, differentiation of ROs in the absence of Matrigel/Geltrex was shown. Igf-1 or Bmp4 was applied to embryoid bodies, which subsequently induced retinal differentiation[267]. Although the efficiency was cell line dependent, it demonstrated that more controlled conditions to generate ROs can be found.

Taken together, all adjustments in mESC maintenance and initial differentiation steps could drastically increase the robustness of the differentiation protocol to generate early ROs at D7. This allowed a reliable reproduction and high throughput of experiments. Furthermore, the different mESC cultivation conditions as well as adjusted differentiation steps to generate ROs heavily affected retinal induction and the morphology of organoids. It would be interesting to know whether different conditions not only affect the early steps in RO differentiation but also cause differences in molecular and cellular composition of the RO.

RPE Differentiation from mESCs

Establishment of the differentiation of RPE cells from the mESC-Rx-Gfp cell line has been described previously[248]. This work focused on the verification of previous observations to validate the use of mESC-derived RPE cells for co-cultivation systems. The differentiation protocol has critical steps that determine the outcome of the experiment. The first important step is the generation of D7 ROs which will serve as a source of retinal progenitor cells that will stepwise differentiate to RPE cells. The aforementioned improvements helped to increase the number ROs at D7. The second step required to break up the ROs mechanically and let them adhere to laminin coated well plates. At this point, the cells were actively shifted towards RPE cell fate by application of a Wnt activator and Fgf receptor inhibitor. Wnt signaling is active in the optic vesicle stage and drives RPE cell specification[159]. Conversely, Fgf signaling needs to be inhibited as it activates neural retina-specific Vsx2 expression and suppresses Mitf expression, which in turn is required for RPE differentiation. After four days, RPE precursors were purified enzymatically. This is a non-standardized step which involves the experience of the experimenter to decide how rigorously the cells need to be purified. Hence, a great deviation can be caused by different experimenters. It was described that on average ~$2x10^6$ RPE precursor cells can be purified from initially 60 aggregates[247]. However, in this work, it could only rarely be achieved to purify more than 10^6 cells. Moreover, the average cell number

of RPE precursor cells purified from ~64 aggregates was around $5x10^5$ cells, which is drastically less than described. A potential reason for that could be too harsh purification conditions. In the previous publication, it was stated that RPE precursor cells could be identified due to their pigmentation. This allowed, besides the enzymatical detachment of less adhesive cells, a precise mechanical removal of undesired non-pigmented cells, whereas RPE precursors remained attached. However, the mESC-Rx-Gfp cell line used in his work is non-pigmented. Thus, the clear indicator to distinguish properly differentiating cells from non-RPE precursor cells was lacking. Therefore, the cells could only be purified due to their adhesiveness. In order to avoid impurities caused by contaminations of non-RPE precursors, the cells have been treated more rigorously, which might have caused an undesired detachment of differentiating RPE cells. Second, it can be speculated that the ROs, which do not form optic vesicle-like structures, do not contain many retinal progenitors that will give rise to RPE cells. Instead, by D7 the Rx-Gfp^+ progenitor cells might have already acquired neural retina cell fate and thus are not competent to differentiate to RPE cells when they receive RPE cell fate signaling cues. To test this, it would be interesting to continue with the second step of the RPE differentiation protocol already at D6, which is one day after the onset of Rx-Gfp expression in the organoids. This assumption can be challenged by observations of transdifferentiation of neural retina to RPE via ablation of the Fgf signaling pathway[268], which is simulated in the differentiation protocol with the addition of an Fgf receptor inhibitor. However, the Fgf-mediated regulation of neural retina differentiation is temporally restricted to the optic-vesicle formation during eye development. Thus, Fgf inhibition can only transdifferentiate neural retina cell to RPE in a narrow time frame.

The last critical point is the seeding density of purified RPE precursor cells on a new substrate at D11. It is mandatory to seed a sufficient number of cells, that can cover the surface of the growth substrate within one or two days. Otherwise, the cells will not form a monolayer and will not adopt the hexagonal RPE-specific cell shape. Around D18, the first regions of RPE-shaped cells can be observed and by D21 onward all cells are differentiated to RPE cells. Usually, the cells form an even monolayer. Nonetheless, improperly purified or not completely dissociated cells can contaminate the RPE cells, which can be identified by spherical structures on the RPE cell layer.

It was previously shown that mESC-derived RPE cells can be cultivated for up to 70 days without recognizable morphological degeneration[248]. Immunocytochemical staining could detect RPE-specific proteins Mitf and Otx2 which are required for RPE cell fate specification[23,154]. Additionally, Sox9 and its downstream target Rpe65 have been identified to be expressed in mESC-derived RPE cells. As expected, the transcription factors Mitf, Otx2 and Sox9 showed a prominent nuclear localization pattern while Rpe65 has a cytoplasmic

localization (**Figure 10**). The cytoskeleton marker proteins revealed expression of mature RPE markers as well as a proper apico-basal polarity (**Figure 11**). ZO-1 localization indicates the presence fully mature tight junctions which are formed at the apical site of the cells[173]. Confluency and the formation of mature tight junctions indicate that mESC-derived RPE cells could also form a barrier which is non-permissive for lateral diffusion. To validate the epithelial integrity, the transepithelial electrical resistance (TEER) could be measured, which serves as a strong indicator for the barrier function of epithelial cells. This is a non-invasive method that does not harm the cells and hence can be monitored in real-time. It requires a monolayer of cells to be grown on porous membrane inserts that electrodes, or Epithelial Voltohmeters, can be placed in an apical upper compartment and a basal lower compartment, respectively[269]. After application of a defined voltage, the resulting current can be measured to evaluate the Ohmic resistance[270]. This method is highly sensitive and error prone, as the position of the electrodes can influence the measurement[270]. Thus, this technique is a valuable method that can give insightful results when used with caution. Furthermore, Ezrin expression marks the onset of the formation of secondary long microvilli[171]. In the immunocytochemical experiments, a dotted pattern on the apical surface of mESC-derived RPE cells could be observed. A 3D reconstruction revealed an elongated shape of $Ezrin^+$ structures indicating the presence of long microvilli. These findings suggested that mESC-RPE cells resemble the *in vivo* phenotype. However, gene expression analysis revealed that the transcriptional level of RPE-specific genes is relatively low compared to iRPE cells. Notably, the expression of early marker genes Mitf, Otx2 and Sox9, with exception of Pax6, is only slightly reduced. In contrast to that, transcripts of late expressed, functional genes can only be detected in low quantities. A contradictory observation is, that Rpe65 gives an abundant immunofluorescent signal whereas Rpe65 transcripts are only barely detected or absent in ddPCR measurements. The detection and quantification of RPE marker genes leads to the suggestion that mESC-derived RPE cells are properly differentiated but resemble still maturating RPE cells rather than fully mature RPE. This assumption is further supported by previous gene expression analyses which revealed a maturation process of the mESC-derived RPE cells, in which RPE-specific gene expression increased over time[271]. Nonetheless, mESC-derived RPE cells can be considered as terminally differentiated which is indicated by the lack of proliferation capability. The active cell cycle marker Ki67 is expressed only in a few mESC-derived RPE cells, while the majority represents dormant non-dividing cells which resembles the *in vivo* cell behavior[272]. Gene expression pattern as well as incapability to proliferate are to a large extend in accordance to the previous findings[247]. It must be noted however, that RPE cells differentiated from human-derived iPSCs are able to be passaged multiple times[273–275]. Nonetheless, with increasing passage number, human iPSC-derived RPE cells tend to dedifferentiate. It remains unclear why human iPSC-

derived RPE can be passaged while RPE cells differentiated from mouse SCs fail to be expanded.

Cultivation and Maturation of ROs

Besides the differentiation of RPE cells, early ROs from D7 can be further cultivated to develop more mature organoids. With continued cultivation, ROs increase in size and retinal Rx-Gfp$^+$ epithelial structures grow out of the main aggregates which is often composed of non-retinal cells. At D11, the ROs can be precisely dissected under a fluorescence microscope to isolate Rx-Gfp$^+$ areas and discard Rx-Gfp$^-$ regions. Accurate and careful preparation allows to preserve retinal epithelial structures. The cutting points of the Rx-Gfp$^+$ epithelium can regenerate within one or two days, that the newly formed ROs can eventually develop a spherical aggregate with a continuous retinal epithelium. The size of the resulting aggregates is on the one hand determined by the size of Rx-Gfp$^+$ regions. On the other hand, it highly dependents on the experimenter so that mature ROs, from D18 onwards, can have a size ranging from 0.5 mm up to 1 mm in diameter. Too large aggregates however, bear the risk to develop a necrotic core. That is, cells in the center of the organoid cannot be supplied sufficiently with oxygen, nutrients and metabolites via diffusion. Apoptotic cells on the inside of the organoid can lead to premature differentiation and improper development of outer epithelial structures[276]. Until D14, ROs were treated with taurine and retinoic acid. The sulfuric amino acid taurine was described to promote rod photoreceptor differentiation[89]. More recent studies pointed out that taurine deficiency leads to degeneration of cone photoreceptors and retinal ganglion cells in the retina[277]. Additionally, it is suggested that taurine possesses neuroprotective properties and counteracting effects against oxidative stress[278]. However, removal of taurine from the cultivation medium had only minor effects on ROs[265]. Contrary to that, absence of retinoic acid leads to structural disorders related to photoreceptor development and thus is important for the structural and cellular development of the retinal epithelium[265]. This is supported by previous findings that show that retinoic acid leads to upregulation of rod photoreceptor-specific Nrl expression[133]. Previously, it was described that mESC-derived ROs can be maintained for up to 30 days before showing signs of degeneration[259]. In this work however, retinal epithelial impairment was observed already at D25 which involved the loss of epithelial structure caused by cellular outgrowth and apoptosis. It remains to be investigated what caused the premature degeneration compared to previous experiments described in literature. It was demonstrated that RO development and maintenance was improved by increasing oxygen supplementation from 20% to 40%[265]. However in another work, ROs were cultivated under atmospheric oxygen conditions and could be maintained until D30[259]. Notably, the ROs were generated from mESCs that have been

cultivated in medium with high FBS concentration, which also resulted in ROs of a different morphology, as described above. It can only be speculated whether different mESC cultivation conditions influence the maturation capabilities. Furthermore, another study reported a prolonged cultivation method for mESC-derived ROs. Slight variations to the initial RO differentiation protocol by Eiraku and colleagues[53] were applied which involved a prolonged SFEBq step, skipping dissection and replacing retinoic acid with a synthetic retinoid analog which was applied to the ROs throughout the entire development[279]. Thus, adjusting differentiation and maintenance conditions for ROs could help to increase the maximum cultivation time and thus improve maturation.

The ROs in this work have the capability to form a pseudostratified epithelium. The nuclei of different cell types organize and position themselves along the apico-basal axis. The inner or basal site of the epithelium in ROs represents the inner cells of the retina. Conversely, the apical site in ROs resembles the outer site of the retina. This becomes evident in immunohistochemical labeling of retinal cell type-specific marker proteins. Retinal ganglion cell and bipolar cell marker Isl1 stains nuclei at the inner border of the retinal epithelium (**Figure 14c**). Retinal ganglion cells can be found in the innermost layer of the retina while bipolar cells populate the inner nuclear layer. In contrast, photoreceptor marker Otx2 was mostly localized at the apical site (**Figure 14a**). Thus, the apico-basal orientation in the retinal epithelium of ROs is the same as in the retina. Nevertheless, it can be noted, that if it was assumed that ROs evaginate optic vesicles which subsequently invaginate to form optic cup-like structures, then the pattern is inverted as photoreceptor cells would be the innermost cell types. However, as the invagination process did not occur in ROs in this work and in other publications using human[237,239,249] or mouse-derived[258,279] SCs, this fact can be neglected.

A lamination which would involve the formation of three distinct layers, that has previously been reported[53], could not be observed. However, a separation of the outer retinal epithelium and inner retinal cells, indicative of premature layer-like structures, was existent, which is in accordance with other reports[258]. Interestingly, although the retinal epithelium in the ROs in this work did not undergo optic vesicle-like or optic cup-like formations and is thus not in contact with an outer RPE layer, the retinal cells were able to form a stratified epithelium. This suggests that orientation and localization along the apico-basal axis is a retinal progenitor cell-intrinsic and autonomous process. The maturation to form a multi-layered tissue however seems to require more ocular tissue.

In vitro Co-Cultivation System for mESC-derived RPE and ROs

The differentiation of RPE in ROs is largely lacking or limited to regions that are non-adjacent to neural retinal tissue. Although it was reported that RPE regions and neural retinal regions arise during invagination of optic cup-like structures in mESC-derived ROs[53], the reproduction of these events could not reliably be achieved. This is in accordance to other publications using mouse-derived ROs that do also not describe optic cup formation or presence of RPE cells[258,279]. However, literature has underlined the importance of reciprocal interactions between neural retina and RPE during development and maintenance of the mature retina[64,152]. Thus, it is desired to combine both tissues *in vitro* to investigate their co-development *ex vivo*. The decision to use porous membrane inserts to grow RPE cells on is based on their *in vivo* function to establish the outer blood-retina barrier. In this setup, the RPE cells form a monolayer on a permeable substrate that mimics the Bruch's membrane. In the eye, this membrane separates the retina from the underlying choroid[65]. In the co-cultivation system, the RPE cells form a barrier between the lower compartment at their basal site and the upper compartment at their apical site. Next, the cultivation media must be evaluated that allow the differentiation and maturation of both the RPE cells as well as the ROs. In the final maturation stage of the differentiation protocols, both tissues would normally receive differently composed cultivation media. The RPE medium strongly differs from the RO cultivation medium. The only common ingredient is taurine. However, it was previously reported that the effect of taurine is neglectable in the maintenance of ROs[265]. Despite that, the RPE medium is composed of a different base medium supplemented with 1% FBS. In cell culture experiments, high serum concentrations are commonly used in maintenance but also to induce cell proliferation[280]. Primary RPE cells or the RPE cell line ARPE-19 are also initially cultivated in medium with high serum concentrations until reaching confluency. After the expansion phase however, RPE cells are commonly maintained at low serum concentrations comparable to the RPE medium in this work[281,282]. Additionally, RPE medium is supplemented with hydrocortisone and triiodothyronine. The former is a glucocorticoid, that is widely applied to growth media of epithelial cells. It was shown to upregulate genes involved in the formation of tight junctions, which is critical to establish barrier functions such as in the blood-brain or blood-retina barrier[283,284]. On the other hand, triiodothyronine is a thyroid hormone which is involved in the development of the brain and the retina[285]. It acts via binding to its receptors TRα or TRβ which are ligand dependent nuclear transcription factors[286]. During retinogenesis triiodothyronine binding to the retina-specific isoform TRβ2 in cone photoreceptors is required for the expression of M-opsin[130,287]. In later stages however, triiodothyronine is reduced or absent in photoreceptors and gets restricted to inner cell types of the retina[288]. It was demonstrated, that excessive signaling could lead to photoreceptor cell death. Conversely, in AMD affected eyes, increased levels of triiodothyronine were detected and its suppression

could promote cell survival[289]. Taken together, low serum concentrations which do not favor cell proliferation, and the application of signaling molecules that can alter gene expression, suggest that RPE medium is not suited for proper RO development. Thus, it was decided not to use RPE medium to co-cultivate ROs with RPE cells. The immunohistochemistry results as well as previous gene expression analysis indicated that mESC-derived RPE cells are terminally differentiated[271]. Furthermore, it was demonstrated that the cells can be robustly maintained in culture[248]. Thus, it was assumed that mESC-derived RPE cells can rather adapt to a different cultivation medium than the highly sensitive ROs. Therefore, the RO cultivation medium RMM2 was tested on mESC-derived RPE cells. The maintenance of mESC-derived RPE cells in RMM2 was approved as no obvious morphological deficits could be observed (**Figure S 3**). The use of Transwell inserts, on which the RPE cells grow, leads to an upper and lower compartment. As the mESC-derived RPE cells are intended to establish a barrier between these compartments, it was decided to apply RPE medium to the lower compartment where it supplies the RPE cells from the basal site. RMM2 was applied to the upper compartment which will eventually contain the ROs. Furthermore, it was evaluated whether an ECM layer between mESC-derived RPE cells and ROs can be polymerized which would resemble the interphotoreceptor matrix. In a previous study, it was demonstrated that ROs could be cultivated on human-derived iPSC-RPE cells which were separated by a thin hydrogel matrix[246]. This matrix allowed perfusion of diffusible signaling molecules and prevented cellular outgrowth from the RO[246]. However, when a layer of Matrigel was deposited, the mESC-derived RPE cells lost their characteristic morphology (**Figure S 3c**). The previous report used a synthetic and neutral hydrogel, which did not contain other signaling molecules unlike Matrigel. Thus, it can be assumed that the use of a defined, growth factor free matrix allows to recreate an interphotoreceptor matrix-like environment.

After determining the co-cultivation conditions, it was tested whether this setup influences the mESC-derived RPE cells on a transcriptional level. Therefore, normally in 96-well plates cultivated mESC-derived RPE cells at D21 were compared to the RPE cells that were cultivated in the co-cultivation system from D15 until D21 or D18 until D21 without ROs. Remarkably, almost all measured genes were upregulated in mESC-derived RPE cells grown in the co-cultivation setup (**Figure 18** and ***Figure S 5***). This is in line with previous findings that could demonstrate that RPE cells form highly polarized and functional epithelial monolayers on various porous substrates including electro spun fibers and Transwell inserts[282,290]. However, most studies focused on morphological features, while this work could show the upregulation of genes involved in differentiation as well as functional genes in mature RPE cells.

Next, it was assessed how ROs can be co-cultivated with mESC-derived RPE cells. Regular maturating ROs are maintained in an excess of cultivation medium. A Transwell however with a surface area of 0.33 cm^2, has a very limited volume capacity which is less than 10% of the volume that is usually applied to ROs. In initial attempts to co-cultivate ROs in Transwells with mESC-derived RPE cells, it was observed that daily medium changes were required to maintain the ROs. Recent technological advances solve this problem by microfluidic chips that can continuously supply cell culture systems by pumping fresh medium with a constant flow into the devices. In such a system, ARPE-19 cells and the human umbilical vein endothelial cells (HUVEC) could be co-cultivated to resemble the outer blood-retina barrier[291]. Another study combined human iPSC-derived RPE and ROs and demonstrated a successful co-cultivation[246]. In both cases, the microfluidic system allowed a continuous medium flow-through to resemble the bloodstream. However, the latter study also reported that even with a permanent medium exchange, the cultivation period for ROs was drastically reduced when co-cultivated with RPE cells. While human iPSC-derived ROs can be maintained for up to one year normally, the co-cultivation period in the microfluidic chip system was restricted to ~30 days[246]. Organoids can attach to each other resulting loss of epithelial integrity followed by degeneration. As it was also of interest to investigate the co-cultivation effect of neural retina on RPE, it was decided to increase the contact surface of ROs to the RPE cells by raising the number of ROs without interfering each other. It was found that at most three to four ROs could be co-cultivated simultaneously without observing morphological degenerative effects on ROs or mESC-derived RPE cells.

It could be identified that ROs which possessed a retinal epithelium of high structural integrity were qualified for co-cultivation, as these organoids did not adhere to the RPE cell layer. In contrast, structural disorders or ruptures in the epithelium led to attachment of the ROs. This resulted in cellular outgrowth and a complete loss of the epithelial structure followed by a rapid decrease in Rx-Gfp expression. Thus, these criteria reduced the number of available ROs which were qualified for co-cultivation. From usually ~32 aggregates that were initially generated, it was possible to obtain enough ROs for two to five experiments (Not quantified).

At last, it was elucidated when and how long ROs could be co-cultivated. At D11, ROs undergo a dissection step to discard non-retinal tissue. The Rx-Gfp^+ ROs need to regenerate the lesions inflicted by the mechanical stress. This process takes around two days until the sites of injury are completely closed and form a retinal epithelium. Until D14, ROs are treated with retinoic acid, which was reported to play a crucial role in the formation of an ordered epithelium[265]. Thus, D15 was defined to be the earliest time point for co-cultivation. When considering the latest time point, ROs started to show signs of degeneration at around D25 while ROs at D21 show the highest epithelial integrity and strong Rx-Gfp expression without being fully

maturated. Because it was of interest to investigate the role of RPE on ROs during development, it was decided to examine D21 ROs at latest. Thus, an early co-cultivation from D15 until D18 and a late co-cultivation from D18 until D21 should give insights in short-term co-cultivation effects. In attempts to elucidate the maximal co-cultivation period, it was observed that ROs could be maintained for up to six days before degeneration. Therefore, long-term effects were evaluated when ROs were co-cultivated from the earliest time point at D15 until D21.

The advantage of using whole organoids for co-cultivation is the formation of the retinal epithelium that contains neural retinal progenitor cells that can eventually differentiate into retinal cell types. Furthermore, this epithelium has already the intrinsic capability to form a stratified structure resulting in a microenvironment that contains a plethora of cell types influencing each other which closely resembles the *in vivo* environment. However, it was also hypothesized whether ROs can be dissociated to single retinal progenitor cells which can subsequently be co-cultivated with mESC-derived RPE cells. It is known that dissociated cells have the capability to re-aggregate[292]. Dissociated retinal cells from six days old embryonic chicks formed clusters in suspension[293]. In these so formed retinospheroids, multipotent progenitors proliferated to give rise to other retinal cell types. Primary photoreceptors differentiated followed by more inner retinal cell types such as amacrine cells, horizontal cells and bipolar cells[293,294]. Interestingly, cell sorting led to a stratified organization in these rosettes[295]. Moreover, in the presence of RPE the retinospheroids were able to form a laminated structure resembling the retinal outer nuclear layer and inner nuclear layer, connected via plexiform layers[294,296]. Previously, it was demonstrated that single retinal progenitor cells isolated from mESC-derived ROs showed signs of self-organization when grown in 3D scaffolds[259]. In preliminary experiments, which have not been described in this work, dissociated retinal progenitors formed spherical colonies on mESC-derived RPE cells. A prolonged Rx-Gfp expression compared to ROs could be observed (Data not shown). However, the retinal progenitors did not proliferate and showed no signs of stratification inside these retinal colonies. Thus, these experiments have not been further followed. Nevertheless, it could be possible to reaggregate dissociated retinal progenitor cells derived from ROs and afterwards co-cultivate these spheroids with RPE. This could give insights in the degree of self-organization and cell sorting capability of mouse-derived retinal progenitors at different stages and the role of RPE in this process. So far, reaggregation of retinal cells to form retinospheroids was only reported by using embryonic cells from chick or quail[293,297].

Photoreceptor Development in ROs and COs

Differentiation of the majority of the retinal cell types in mESC-derived ROs has already been demonstrated[53,258,279]. This study focused mainly on the differentiation of photoreceptors in ROs. *In vivo*, photoreceptors are born in two waves. Early-born cone photoreceptors can be first detected at embryonic day 11 (E11) in mice. Expression of S-opsin continues until late stages of embryonic development[115]. In turn, rod photoreceptor genesis occurs at around E13 with a peak at birth and is persisting until postnatal day 5 (P5)[298]. In mouse-derived ROs, photoreceptor-specific gene expression could be detected as early as D10[258]. Visual cycle genes Rhodopsin and Recoverin were expressed later at around D18[53]. A comparative study using transcriptomic data revealed similarities in retinogenesis in native mouse retina and mouse SC-derived ROs. It was found that cone-specific transcription factors were expressed from E14 until P6 in native retinas and from D12 until D25 in ROs. Rod-related genes were expressed from E16 until P10 and from D15 until D32 in ROs,[299]. These findings indicate a similar developmental generation of retinal cell types in ROs compared to the native retina. In this work, photoreceptors could be detected at D15 in ROs. In accordance with the previous report, photoreceptor genes were already expressed at this stage. Otx2 expression is required for photoreceptor cell fate specification and activates expression of Crx[118]. Similar to the native retina, Otx2 was expressed in more cells in earlier differentiation days in ROs compared to Crx. As both markers strongly overlap in their expression, it can be stated that co-expression of Otx2 and Crx indicates more mature photoreceptors. Supporting this finding, the amount of $Otx2^+$ cells simultaneously expressing Crx increased over time. The expression of both markers increased until D21. While Crx expressing cells strongly increased until D21, the Otx2 curve starts to flatten, indicating that D21 marks the peak of photoreceptor differentiation (**Figure 15**). According to the strong co-localization, it can be assumed that most of the Otx2 expressing cells will eventually co-express Crx. Thus, the retinal epithelium will consist of ~40% differentiating photoreceptors. A previous study reported that the retinal epithelium in their ROs consists of ~25% photoreceptors at the same differentiation day but with prolonged cultivation, photoreceptors eventually make up ~70% of the total cell population in mouse ROs at D35[300]. Thus, it would be necessary to examine ROs at later stages to elucidate photoreceptor differentiation in more mature ROs. Interestingly, most of the photoreceptor cell bodies were localized apically at the outer side of the retinal epithelium. During development, the photoreceptor cell nuclei were continuously restricted towards the apical site. This localization pattern leads to an outer nuclear layer-like organization.

Co-cultivation of ROs with mESC-derived RPE cells resulted in increased numbers of photoreceptors compared to ROs of the same age without the presence of RPE. Interestingly, co-cultivation of ROs from D15 until D18 resulted not only in more photoreceptors compared to D18 ROs but also D21 ROs. Moreover, the relative photoreceptor cell number in CO D21

CD3 exceeded the number of photoreceptors in ROs D21 even more. This suggests that mESC-derived RPE cells induce the differentiation of photoreceptors in ROs during a period from D15 until D21. This does not only result in accelerated photoreceptor differentiation in earlier ROs but also leads to an increase beyond the number of photoreceptors in regular cultivated ROs. It was also found that the portion of Otx2 and Crx co-expressing cells was higher in co-cultivated ROs, which indicates earlier progression in photoreceptor development and thus accelerated differentiation. In a previous study, isolated primary RPE cells from mouse eyes were directly co-cultivated with human-derived ROs. The authors described similar results, which showed accelerated differentiation and enhanced photoreceptor gene expression. However, as a result of the direct contact, the organoids attached to the RPE cells and lost the stratification and displayed structural disorganization[301]. A second publication, in which a hydrogel layer was used to prevent attachment, RPE co-cultivation enhanced photoreceptor maturation resulting in the formation of more outer segments[246].

It was demonstrated that co-cultivation for three days had a significant effect on photoreceptor development. It was then speculated whether increased co-cultivation periods could increase this effect. It must be noted however, that ROs co-cultivated with mESC-derived RPE from D15 to D21 did not contain more photoreceptors than ROs at D21 co-cultivated for three days. This can be explained by the competence model for retinal progenitor cells, which describes the ability to give rise to a small subset of retinal neurons at distinct phases during development[66]. The state of competence is intrinsically determined in retinal progenitors and cannot be significantly altered by the molecular or cellular environment[70]. In turn, extrinsic factors can drive the differentiation of only a certain cell type from the competence subset[67]. Thus, it can be assumed, that retinal progenitor cells in ROs represent a competence state that can give rise to photoreceptor cells within the time frame from D15 to D21. This is not unexpected as cones are early-born neurons, while rods belong to the late late-born cells in the retina. Birthdating experiments indicate temporal overlap in the development of both cell types during retinogenesis[66,73]. This assumption is supported by the aforementioned transcriptomic analysis in mouse ROs that detected cone- and rod-related gene expression starting at D12 and D15 respectively[299]. It can be hypothesized, that prolonged co-cultivation does not further increase photoreceptor cell numbers because retinal progenitors moved on from the transient competence to produce photoreceptors to a late retinal progenitor state that will give rise to the later-born cell types. This hypothesis is supported by the observation that co-cultivation increases the relative number of cells expressing Vsx2, which can also be used as a marker for bipolar cells. $Vsx2^+$ is initially expressed in neural retinal progenitor cells but becomes restricted to bipolar cells in later stages[302]. Bipolar cells are the last-born retinal neurons and arise from a tripotential pool of progenitor cells which express Otx2[153]. Vsx2 is a downstream target of Otx2 and suppresses photoreceptor development[303]. It was found, that

high levels of Otx2 expression result in photoreceptor differentiation, while null mutants fail to differentiate bipolar cells[304]. This suggests that after initiation of bipolar cell fate acquisition, Otx2 is downregulated in bipolar cells. To evaluate potential bipolar cell differentiation in ROs, the relative number of $Otx2^+$ cells which co-express Vsx2 was measured. Expectedly, this value was always higher in COs than in regular cultivated ROs (**Figure 27b**). Notably, the number of $Otx2^+/Vsx2^+$ cells declined with increased cultivation time. It is unclear whether this could indicate a transition of differentiating retinal progenitors to photoreceptors that still express Vsx2 while already upregulating Otx2 expression. Or, whether this illustrates the Otx2-mediated bipolar cell differentiation, that retains Vsx2 expression, while downregulating Otx2.

Many observations that underline the crucial influence of RPE cells on neural retinal tissue are derived from studies that focused on secreted factors. The RPE secretes a variety of growth factors that are required for the correct differentiation of the neural retina as well as the underlying choriocapillaris[64]. While some act as neuroprotective factors, others promote angiogenesis and neovascularization. Thus, secretion occurs in a polarized manner that needs to be precisely controlled to maintain the structural integrity of the retina. In the co-cultivation system described in this work, mESC-derived RPE cells grew on porous membrane inserts that allowed the secretion of basal factors into the lower compartment, while apically secreted factors were given into the upper compartment containing ROs. During development and maintenance, RPE cells release VEGF primarily at the basal site to promote differentiation and maintenance of endothelial cells of the chroroid[184,187]. In turn, apically secreted VEGF is endocytosed and released basally via a transcytosis mechanism resulting in low but essential concentrations of VEGF in the subretinal space[305]. Conversely, apically secreted factors affect the neural retinal development. ATP released from the RPE was found to promote proliferation and speeds up differentiation of retinal progenitor cells[306]. This could in part explain the observed effects in a previous study[301] and in this work, which indicate accelerated differentiation of photoreceptors after co-cultivation with RPE cells. Another known secreted growth factor is CNTF. It was described to reduce Rhodopsin expression but enhances photoreceptor cell survival[307]. Contradictory, in cooperation with LIF, which is secreted in low concentrations, it was observed that CNTF could promote bipolar and Müller glial cell fate in differentiating rod photoreceptors[308]. This is in line with the observations in this work, that showed a potential increase in bipolar cells aside with photoreceptor differentiation. A prominent factor secreted by RPE cells is PEDF which is known to have neuroprotective fuctions[186]. The gene expression profile of mESC-derived RPE cells shows that Pedf is expressed by these cells. It was also found that Crx, which is required for photoreceptor development and maintenance, is a potential downstream target of Pedf signaling[309]. Its main functions nevertheless, are to maintain photoreceptors and to prevent degeneration and cell death[310]. At last, it was reported that decellularized peptides derived from RPE cells could

promote the formation of outer segments of photoreceptors[311]. In contrast to a previous publication, that treated ROs with RPE-derived conditioned medium which did not affect RO devlopment[301], this work could clearly show increased differentiation of photoreceptors upon treatment with conditioned medium. This suggests that mESC-derived RPE cells secrete factors that promote and enhance neuronal differentiation in ROs. However, more detailed work needs to be done to evaluate the secretome of mESC-derived RPE cells. Enzyme-linked immunosorbent assay (ELISA) can reveal secreted factors, their concentration and polarity which allows to better understand the secretion profile.

Besides neuronal differentiation, it was previously found that RPE cells could induce and maintain lamination in retinal tissue[312]. Retinospheroids from chick embryonic retinal cells form laminated organotypic retinal tissue. Interestingly, the presence of RPE cells could invert the orientation and also induce the formation of Müller glia endfeet and a basal lamina[313,314]. The mESC-derived ROs already possess a stratified epithelium with the correct orientation for co-cultivation. A clear lamination however, with distinct cellular layers is often lacking. It could only be observed that there was a separation of the retinal epithelium and closely associated retinal cells that were localized basally of the epithelium. It remains elusive whether these cells represent an inner nuclear layer or ganglion cell layer-like structure. PEDF was described to protect cells of the inner layers of the retina from cell death[310]. However, neither co-cultivation nor treatment with conditioned medium could induce a more prominent lamination in ROs. In turn, photoreceptor cells differentiated and populated the retinal epithelium along the entire apico-basal axis. This rather suggests that RPE-induced photoreceptor differentiation can promote the transformation of the retinal epithelium into an outer nuclear layer-like structure. It can be speculated whether the formation of a laminated structure in ROs requires more inductive signals from the inside of the ROs. The co-cultivation with mESC-derived RPE might represent an imbalance of signaling cues in which the RPE induces the formation of an outer nuclear layer and late born neurons while other ocular tissue provides signals for the formation of inner nuclear and ganglion cell layer.

Co-cultivation and conditioned medium increased the differentiation of photoreceptors at an early and a late stage during RO development. As cones differentiate earlier than rod photoreceptors, it can be speculated which cell type arises due to co-cultivation at different time points. Cone or rod-specific markers could give insights in the RPE-mediated differentiation pattern. The conducted immunohistochemical experiments could only give information of one specific time point. To follow the differentiation of certain progenitor cells, lineage tracing methods could reveal more dependable results. Furthermore, the advent of scRNA seq allows the synchronous transcriptional evaluation of thousands of single cells derived from a tissue. This method has been successfully applied to retinal samples revealing

clusters of cells with similar transcription profiles representing distinct cell types in the retina[315]. Even more sophisticated approaches that integrate single cell assays for transposon accessible chromatin (scATAC) seq are powerful tools to unravel the temporal patterning and genetic regulation in retinogenesis[316].

Neural retina and RPE reciprocally influence each other during development. Thus, the effect of ROs on maturating mESC-derived RPE was elucidated via relative gene expression measurements. Previous studies could demonstrate that proper RPE differentiation and maturation is mediated by secreted factors from the neural retina[317]. These factors increased epithelial integrity by upregulation of tight junction proteins and fostered polarization of the cells[173]. However, visual cycle proteins were largely unaffected[317] which is in accordance to the findings in this work. Even though ROs were directly co-cultivated on mESC-derived RPE cells, it could not be observed that RPE-specific gene expression was upregulated to resemble native mature RPE. However, it must be considered that although ROs and mESC-derived RPE cells were directly co-cultivated, the close contact of both tissues like it occurs *in vivo* is not established. It was found that besides secreted factors, the direct cell-cell contact enhanced RPE maturation[290]. In the co-cultivation system, ROs remained floating and thus could potentially only influence the RPE cells to a limited degree.

Differentiation of Retinal Progenitor Cells in the Retinal Epithelium of ROs

Even more striking than the increase of photoreceptor cell number was the localization pattern of their nuclei. While photoreceptor cell bodies were found at the apical site of the retinal epithelium in ROs, co-cultivation resulted in a broad distribution of their cell bodies in the epithelium. Similarly, $Vsx2^{+}$ progenitors that were restricted to the basal site during development were found more apically after co-cultivation (**Figure 22**, **Figure 26** and **Figure 29**,). It could be stated that mESC-derived RPE cells caused loss of stratification of the retinal epithelium in ROs. This would be a drawback from the aim to recreate tissue which highly resembles a target organ *in vitro*. However, in mouse-derived ROs, the cells do not form a retina-like layered tissue. Therefore, the changes in the localization pattern might be an indicator for enhanced cell division, which supports the findings of accelerated neuronal differentiation to produce more photoreceptors. Already since the last century, it was observed that progenitor cells in neuronal tissue undergo nuclear movements[94]. This phenomenon is also seen in the developing retina[95]. In this process, progenitor cells form adhesions at the apical as well as the basal site and thus span the entire thickness of the epithelium. While progressing through cell cycle, their nuclei move in an oscillatory manner basally and apically. M-phase nuclei are found at the apical surface of the epithelium, while G1-, S-, or G2-phase nuclei are located more basally[95]. This process is driven by the microtubule motor proteins

kinesin and dynein[318]. Lateral inhibition mediated by the Notch pathway in the retina is required to retain a population of cells in the progenitor cell state[319]. It was proposed that a Notch gradient is established along the apico-basal axis. Notch signaling is increased at the apical surface while Delta is concentrated at the basal site[320]. Thus, progenitor cells encounter different concentrations of Notch while they move their nuclei in phase with the cell cycle. Progenitors whose nuclei remain more apically will give rise to progenitor daughter cells, while a deep basal movement will produce postmitotic neurons[321]. After co-cultivation of ROs with mESC-derived RPE, differentiating photoreceptor nuclei are found to be located more basally (**Figure 30** and **Figure 31**). It could be speculated that co-cultivation with RPE cells causes progenitor nuclei to move more basally to initiate the differentiation of neurons. Contradictory, *in vivo* RPE cells act as a source of Notch signaling, and are proposed to enable asymmetric cell division of progenitor cells in which one daughter cell will retain the progenitor cell fate[322]. However, this is observed in adjacent RPE and progenitor cells. Notch signaling requires direct cell-cell contact[323]. Although ROs are cultivated directly on RPE cells, they do not adhere and it is thus questionable whether cell-cell contacts are formed in the interface between both cell types. The facts that ROs remain floating and that the altered apico-basal localization pattern is observed in every region of the retinal epithelium even though not all areas directly faced the RPE cells, it can rather be assumed that Notch activation from RPE cells does not occur in this co-cultivation setup. Taken together, it can be assumed that an intra-retinal Notch gradient is supported by an RPE-mediated Notch signaling niche[322]. In the co-cultivation system the RPE-mediated Notch activation in apical progenitors is absent resulting in lower Notch concentrations at the apical surface in the retinal epithelium of ROs compared to the *in vivo* retina. It must be noted however, that RPE cells are absent in regular cultivated ROs without resulting in a similar localization pattern. It can thus be hypothesized that factors from the RPE cells drive the nuclear migration. This is supported by the findings that photoreceptor nuclei as well as progenitor cell nuclei in conditioned medium treated ROs show a similar localization pattern as in the co-cultivation experiments. It is yet unknown which signals exactly drive this process. It can be noted however, that ATP released from the RPE cells binds to P2Y receptors on retinal progenitor cells[306]. A pharmacological activation of these receptors resulted in increased calcium levels which have been shown to be involved in interkinetic nuclear migration[324]. In turn, Ca^{2+} can modulate Ras signaling which is part of the atypical Protein Kinase C (aPKC) signaling pathway[325,326]. There is evidence that aPKC signaling is connected to nuclear migration in the retina as well[321]. Thus, these previous findings and the results of this work suggest that RPE-mediated signals are involved in the nuclear migration and differentiation in the developing retina.

Nonetheless, it is still unclear why photoreceptor cells move their nuclei towards the basal site although they are eventually localized apically. However, a study reported highly motile

photoreceptor nuclei in early retinogenesis and proposed that this movement serves to create more space for dividing progenitors at the apical site of the retina[327]. This could also be the case in co-cultivated ROs where cell division occurs at the apical surface of the epithelium like in regular cultivated ROs and the native retina. The basal shift of photoreceptor nuclei due to co-cultivation allowed more progenitor cells to divide. Increased signal for mitosis marker $pH3^+$ indicated more actively dividing cells in COs compared to ROs at D18. It was observed that nuclei, which are not completely labeled with pH3 antibody, were localized more basally (**Figure 34** and **Figure 35**). Phosphorylation of Serine 10 at Histone H3 can first be detected in late G2 phase in pericentromeric heterochromatin and then spreads over the whole chromosome during mitosis[328]. Subsequent dephosphorylation of histone H3 is initiated in anaphase and completed in telophase[328]. Time-lapse imaging allowed to observe that migrating nuclei of proliferative cells are tear drop-shaped, while dividing nuclei are round at the apical surface[329]. In congruency with these findings, that interphase nuclei are located more basally, partially phosphorylated chromosomes of retinal cell nuclei were elongated and found more basally, whereas the apical $pH3^+$ nuclei were round. In CO D18 CD3 more nuclei in late G2 phase were observed compared to RO D18, which suggests an acceleration of the cell cycle. In contrast, in COs D21 CD3 almost no basal late G2-phase nuclei could be detected while in RO D21 more partially pH3 labeled nuclei could be found. This could demonstrate that around D21 a new wave of differentiation is initiated in ROs whereas co-cultivation from D18 results in terminal postmitotic differentiation in the majority of progenitor cells until D21. This is supported by the finding that almost no M-phase nuclei were seen in CO D21 CD3. Moreover, measurements of retinal epithelial thickness showed, that in ROs the epithelial thickness increased until D21 indicating production of progenitor daughter cells. Conversely, co-cultivation and treatment with conditioned medium resulted in comparably thinner epithelia caused by increased production of postmitotic neurons at the expense of progenitor daughter cells. Surprisingly, the percentage of cells positive for proliferation marker Ki67 was not significantly reduced after co-cultivation neither at D18 nor D21. This could be due to the fact that Ki67 is not only expressed in all phases of the cell cycle of progenitors in the retina, but the protein can also be detected in new-born postmitotic neurons for a certain period of time[330]. Thus, it could be that cells, that did already exit the cell cycle, were measured in immunocytochemical experiments (**Figure 33**). To evaluate the quantity of Ki67 expressing cells, it requires methods like in-situ hybridization which detect RNA transcription rather than presence of protein.

At last, Tubb3 is a neuronal marker expressed in early-born retinal cell types but decreases in the mature retina[331]. Immunostaining of this protein visualizes the cytoskeletal architecture which is oriented along the apico-basal axis. The cells appear elongated with apical and basal processes. Some cells seem to span the entire thickness of the epithelium with attachments

at the basal site as well as the apical surface. Furthermore, it could be observed that nuclei of these cells can be localized in different sub-strata in the retinal epithelium ranging from deep at the basal site to the apical site (**Figure 35**). This observation could indicate cells that undergo nuclear translocation. During this process, postmitotic neurons remain attached via adherence junction at the apical and basal site and position their nuclei to the final localization in the retina[95]. However, immunohistochemical experiments on fixed ROs represent a snapshot of a certain time point. Live cell- and time-lapse imaging experiments are needed to faithfully follow nuclear translocation in the retinal epithelium in ROs.

Conclusion

This work could successfully demonstrate the differentiation of ROs and RPE derived from one mESC line and a subsequent co-cultivation of both tissues. Minor adjustments to initial protocols that describe the generation of early ROs[53,247] could increase retinal induction efficiency and the robustness of the differentiation protocol which improved reproducibility. Mouse-derived ROs developed a pseudostratified retinal epithelium with an apico-basal polarity. Nuclei of photoreceptors were localized at the apical site while nuclei for interneurons could be observed more basally. mESC-derived RPE cells represent terminally differentiated cells in a maturating process that express RPE-specific marker genes and exhibit mature structural features. It was decided to differentiate RPE cells from mESCs, instead of using the mouse RPE cell line RPEJ because these cells failed to maintain retinal integrity in *ex vivo* experiments[332]. Additionally, the focus of this work was the development of retinal tissue which cannot be mimicked by cell lines.

An *in vitro* co-cultivation system that resembles the interface of neural retina and RPE cells grown on permeable membrane inserts which mimics the outer blood-retina barrier, was established. Synchronized differentiation of RPE and ROs allowed the co-development of both tissues that contained cells in a similar developmental state. ROs were co-cultivated for up to six days before showing signs of degeneration. Co-cultivation of ROs with mESC-derived RPE cells led to accelerated neuronal differentiation resulting in increased numbers of photoreceptor cells in early as well as later stage ROs. Comparable effects were elicited by treating ROs with mESC-derived RPE conditioned medium. While the retinal epithelium in regular cultivated ROs rather resembles the neuroblast layer that contains cells which will eventually give rise to cells of the outer nuclear layer and inner nuclear layer, co-cultivation resulted in photoreceptor cells that are localized in the entire epithelium.

Lastly, the results of this work suggest that the process of neurogenesis in ROs is highly similar to *in vivo* retinogenesis. Progenitor cells move their nuclei to apical and basal positions in

phase with cell cycle. Basal nuclei represent cells in G1, S and G2 phase while the most apical cells are dividing M-phase nuclei. Co-cultivation strongly enhanced nuclear migration in the retinal epithelium of ROs. Treatment of ROs with conditioned medium from mESC-derived RPE cells showed similar effects which suggests that besides contact depending signals, also secreted factors are involved in accelerated differentiation and nuclear migration. Thus, ROs can be considered as an important tool to investigate the process of retinogenesis, as they can be generated in larger quantities, are more accessible and easier to manipulate than animal models.

Materials & Methods

Materials

Chemicals

All chemicals or compounds were, if necessary, diluted and stored as recommended by the manufacturer.

Table 1: Chemicals

Reagent	**Manufacturer** **Prod. Number**
AGN193109	Sigma Aldrich SML-2034-5MG
Accutase	Pan Biotech P10-21100
β-Mercaptoethanol	Sigma Aldrich M6250
Blasticidin	InvivoGen Ant-bl-05
Bovine Growth Serum Supplemented Calf (FCS/FBS)	GE Healthcare Hyclone SH30541.03
Bovine serum albumin (BSA)	Sigma Aldrich A4503
CHIR99021	Sigma Aldrich SML1046
Chloroform (Dichloromethane)	Carl Roth 6053.1
DAPI (4',6-Diamidino-2-phenylindol Dihydrochlorid)	Carl Roth 6335.1
Dimethylsulfoxid (DMSO)	Sigma Aldrich D2650-5X5ML
Dulbecco’s Modified Eagle Medium (DMEM)	Pan Biotech P04-03590
DMEM/F12 + GlutaMAX (1X)	Gibco 10565-018
dNTPs	Carl Roth 0178.1/2
Ethanol	Carl Roth

	9065.2
Surgipath	Leica FSC 22 Frozen Section Media
Gelatin	Sigma Aldrich G6144
Geltrex	ThermoFisher A14132
Glasgow's Minimum Essential Medium (GMEM)	Gibco/ThermoFisher Scientific 21710-025
Hydrocortisone	Sigma Aldrich H0396
KAPA SYBR® FAST Universal	SFUKB Roche KK4601
KnockOut Serum Replacement (KSR)	ThermoFisher Scientific 10828010
Laminin 111	Sigma Aldrich L2020
Leukemia inhibitory factor (LIF)	ESGRO ESG1107
Matrigel	Corning 356230, 354230, 356255
Minimum Essential Medium (MEM) alpha	Gibco 12561-056
Mowiol	Merck 475904
N1-Supplements	Sigma Aldrich N6530-5ML
N2-Supplements	Sigma Aldrich 17502048
Non-essential amino acids (100x) (NEAA)	Gibco 11140050
PanSerum	Pan Biotech P30-2602
Paraformaldehyde (PFA)	Merck 30525-89-4
Penicillin/Streptomycin (P/S)	Gibco 15140-122

PD0325901	Sigma Aldrich PZ0162
Phosphate Buffered Saline w/o Ca and Mg	Pan Biotech P04-36500
Phosphate Buffered Saline with Ca and Mg ($PBS^{+/+}$)	Corning 21-030-CVR
Sodium Pyruvate	Gibco/ThermoFisher Scientific 11360-070
Random Primers/Hexamers	Invitrogen (P/N 58875)
Retinoic acid	Sigma Aldrich R2625
SU5402	Sigma Aldrich SML0443
Sucrose	Carl Roth 9097.1
Taurine	Sigma Aldrich T8691
3,3′,5-Triiodo-L-thyronine sodium salt	Sigma Aldrich T5516
Triton-X	Carl Roth 3051.1
TRIzol	Thermo Fisher Scientific 15596026
Trypsin/EDTA	Gibco 15400-054
Tween20	Carl Roth 9127.1
Y27632 (ROCK inhibitor)	StemCell Technologies 72304

Media and Solutions

Media were prepared sterile and stored at 4°C.

Table 2: Media

Medium	Composition
Maintenance Medium (MM)	DMEM 15% PanSera 1% NEAA (0.1 mM) 1% P/S 0.1 mM β-Mercaptoethanol
Riken Maintenance Medium (Riken MM)	GMEM 10% KSR 1% FCS 1% NEAA (0.1 mM) 1% Sodium Pyruvate (1 mM) 0.1 mM β-Mercaptoethanol
Retinal Differentiation Medium (RDM)	GMEM 5% KSR 1% NEAA 1% Sodium pyruvate 0.1 mM β-Mercaptoethanol
Retinal Maturation Medium 1 (RMM1)	DMEM/F12 1% N2 Supplements 1% P/S
Retinal Maturation Medium 2 (RMM2)	DMEM/F12 1% N2 Supplements 1% P/S 10% PanSera
RPE Medium (RPE M)	MEM alpha 1% N1 Supplements 1% PanSera 1% NEAA (0.1 mM)

Table 3: Buffers and Solutions

Solution	Ingredients
15% Sucrose solution	150 mg sucrose in 10 ml H_2O
30% Sucrose solutuon	300 mg sucrose in 10 ml H_2O
PBS-T	0.1 % Triton-X in PBS
Sodium Citrate Buffer	10 mM Tri-sodium citrate (dihydrate) 1 L dH2O Adjust to pH 6 with 1N HCl 0.05% ml Tween 20

Antibodies

All antibodies were reconstituted and stored as recommended by the manufacturer.

Table 4: Primary Antibodies

Antigen	Manufacturer	Product Number	Dilution
CRX	R&D	AF7085	1:200
E-CADHERIN	Abcam	ab15148	1:200
Ki67	abcam	ab15580	1:400
MITF	Exalpha Biologicals Inc	X1405M	1:200
OCT4	Santa Cruz	sc-5279	1:200
OTX2	R&D Systems	AF1979	1:200
Phosphorylated Histone $H3^{Ser10}$	Sigma Aldrich	06-570	1:400
RAX	Santa Cruz	Sc-271889	1:100
RPE65	Invitrogen	MA116578	1:100
SOX2	abcam	ab97959	1:200
SOX9	R&D Systems	AF3075-SP	1:200
ZO-1	Santa Cruz	R40.76 sc-33725	1:100

Table 5: Secondary Antibodies and affinity markers

Molecule/Specificity	Conjugate	Manufacturer	Productno.	Dilution
PAF- 488	AlexaFluor 488	Molecular Probes	A12379	1:200
PAF- 568	AlexaFluor 568	Molecular Probes	A12380	1:200
PAF- 647	AlexaFluor 647	Molecular Probes	A22287	1:100
DAPI		Carl Roth	6335.1	1:1000
mouse	AlexaFluor 488	Molecular Probes	A11029	1:200
mouse	AlexaFluor 488	JacksonImmunoResearch	715-545-151	1:200
mouse	Cy3	JacksonImmunoResearch	715-165-151	1:200
rabbit	568	Invitrogen	A10042	1:300
rabbit	Cy5	JacksonImmunoResearch	711-175-152	1:200
rat	AlexaFluor 488	Life technologies	A11006	1:200
rat	AlexaFluor 568	Life technologies	A11077	1:200
goat	AlexaFluor 568	JacksonImmunoResearch	711-175-152	1:300
goat	AlexaFluor 647	Invitrogen	A21447	1:200
sheep	AlexaFluor 568	Abcam	ab175712	1:200

Primers

Primers were designed previously (Winklhofer, 2021[271]) and synthesized by eurofins Genomics and reconstituted as recommended to 100 pmol/µl (100 µM). For ddPCR experiments, primer working solutions of 1 µM were prepared and stored at -20°C.

Table 6: Primers

Gene Primer	Sequence	Tm [°C]	Amplicon [bp]
Mertk Fwd	ATCAAAGTAATCCCCTCCCCGCC	57.37	270
Mertk Rev	TGCAGACCAGCCAATCTCATTCC	57.7	270
Mitf Fwd	CAGCGTGTATTTTCCCCACAGAGT	57.61	246
Mitf Rev	CAAGGTCCTTAGCTCGTTGCTG	57.73	246

Rpe65 Fwd	CAGGACTTCCCCTTTCAATCTCTTCC	58.19	249
Rpe65 Rev	GGCAGTGTGACTAAATTTCTGCCTG	58	249
Rlbp1 Fwd	CGGATACCCTGGTGTCCTTTCCA	57.04	154
Rlbp1 Rev	GGTTTCCTCATTTTCCAGCAGTTTCT	57.06	154
Pax6 Fwd	GGAGGGGGAGAGAACACCAACTCC	58.51	257
Pax6 Rev	CTTCTCCATTTGGCCCTTCGATTAG	58.16	257
Pedf Fwd	AGAAAGACGACCCTCCAGGATTTTC	57.3	170
Pedf Rev	AGGGGCAGGAAGAAGATGATGC	57.09	170
Sox9 Fwd	AGGAAGCTGGCAGACCAGTACC	57.84	195
Sox9 Rev	TCCGTTCTTCACCGACTTCCTCC	57.93	195
Otx2 Fwd	AAAGCAACCGCCTTACGCAGT	57.72	156
Otx2 Rev	TGTGCCCTAGTAAATGTCGTCCTCT	58.27	156
Pgk1 Fwd	GCCAAGGCTTTGGAGAGTCCAG	58.11	178
Pgk1 Rev	GAGATGTGCCAATCTCCATGTTGTTG	57.8	178

Methods

Maintenance of mESC-Rx-Gfp

New T-25-Flasks are coated with 5 ml 0.1% Gelatin in PBS. Medium of the flask containing the cells is aspirated, rinsed with 4 - 5 ml PBS and the PBS is aspirated. 200 µl 0.25% trypsin/EDTA are added to the cells and incubated for 1 - 2 minutes at 37°C to detach the cells. To neutralize the trypsin reaction, 5 ml MM are added. By pipetting up and down, (~3 - 5 times) remaining cells will be detached mechanically. Afterwards, the cell suspension is transferred into a 15 ml reaction vessel and centrifuged for 5 minutes at 500 rpm at room temperature Supernatant is aspirated, the pellet is resuspended in the remaining medium and the cells are taken up in 3 - 6 ml MM depending on the size of the pellet. To assess the cell number, 10 µl cell suspension are put on a Neubauer chamber. Gelatin solution is aspirated and the flask is washed with PBS. 5 ml Riken MM are added to one flask freshly supplemented with 2000 U/ml LIF, 1 µM PD0325901 and 20 µg/ml Blasticidin. For a two-day cultivation, $4x10^5$ cells, for a

three-day cultivation add 1x10^5 cells are added per flask. Cells are incubated at 37°C and 5% CO_2.

Differentiation of mESCs to RPE

The Protocol is based on Iwasaki et al: Differentiation/Purification Protocol for Retinal Pigment Epithelium from Mouse Induced Pluripotent Stem Cells as a Research Tool[247].

Retinal Induction (SFEBq)

At **D0**, regularly 3000 mESCs per well are seeded in a 96-low adhesion well plate (Nunclon Sphera 96U Bottom Plate, Thermo Fisher Scientific, 174925) in 100 µl RDM freshly supplemented with 0.1 µM AGN193109. mESCs are detached and counted as described in the previous section. Cells are incubated at 37°C and 5% CO_2.

At **D1**, Matrigel/Geltrex is adjusted to 10 mg/ml, if possible, and added in a final concentration of 2%.

The aggregates are cultivated at 37°C and 5% CO_2 until **D7**.

Adherent culture

At **D7**, the aggregates are transferred from floating culture to adherent culture. One well of a 6-Well Plate is coated with 1 µg/cm^2 laminin in PBS for 16 aggregates. Before transferring the aggregates, they are screened for Rx-Gfp Signal. Gfp^- aggregates are discarded. To break up the aggregates, they are taken up by pipetting with a cut tip and transferred into a 1.5 ml reaction tube (16 aggregates per tube). Afterwards, they are taken up by a syringe with a 23G needle and given back into the vessel. Then the aggregates are taken up by a syringe with a 26G needle and again put back into the reaction vessel and centrifuged for 2 minutes at 100 g with slow acceleration and deceleration. The supernatant is aspirated and the aggregates are resuspended in the remaining medium and taken up in 500 µl DMEM/F12 + 10% FCS or RMM2. Aggregates are again centrifuged for 2 minutes at 100 g with slow acceleration and deceleration. The supernatant is aspirated and the aggregates are resuspended and taken up in 500 µl RMM2 + 10 µM Y27632, 5 µM SU5402 and 3 µM CHIR99021. The laminin solution is aspirated and the wells are washed with PBS. PBS is replaced by 1.5 ml of RMM2 + 10 µM Y27632, 5 µM SU5402 and 3 µM CHIR99021. Afterwards, the aggregates are transferred into the wells and the plate is carefully shaken for an even distribution. The aggregates are incubated at 37°C and 5% CO_2.

Purification

At **D11**, RPE-precursor cells are purified. A sufficient number of wells or Transwells (Corning, CLS3470) is coated for 2h at 37°C with laminin as described in **Table 7**. Medium of the cells is aspirated and the cells are rinsed with PBS. To detach less-adhesive cells, 250 µl Accutase are added per well and incubated at 37°C for 5 minutes. The reaction is stopped by adding 2 ml DMEM/F12 + 10% FCS or RMM2 to each well. Intensive, repeated pipetting (~ 20 times) in the well plate will detach less-adhesive cells. The medium is aspirated and the remaining cells are rinsed with PBS. Afterwards, 200 µl 0.25% trypsin/EDTA are added and the cells are incubated for 2 minutes at 37°C. To neutralize the trypsin reaction, 2 ml DMEM/F12 + 10% FCS or RMM2 are added and the remaining adherent cells are detached and dissociated by pipetting. The cell suspension is transferred into a 15 ml reaction vessel and centrifuged for 5 minutes at 100 g with slow acceleration and deceleration. The supernatant is aspirated and the cells are resuspended and taken up in 2 ml RMM2 + 10 µM Y27632, 5 µM SU5402 and 3 µM CHIR99021. Cell number is assessed with a Neubauer chamber. The laminin solution is aspirated and the wells are rinsed with PBS. The correct cell number and volume of medium is given in the wells as indicated in **Table 7**. Cells are incubated at 37°C and 5% CO_2.

Table 7: Laminin coating and volume of cultivation media

Substrate	Surface area	Laminin (1 mg/ml)	Cell number	Volume of Medium
24-Well	1.9 cm^2	2 µl in 300 µl PBS	$5x10^5$	500 µl
96-Well	0.32 cm^2	0.33 µl in 100 µl PBS	$1x10^5$	150 - 200 µl
24-Well-Transwell	0.33 cm^2	0.66 µl in 100 µl PBS	$1x10^5$	Upper Compartment: 200 µl Lower Compartment: 750 µl

Maturation

At **D13**, the medium is completely changed to RMM2 + 5 µM SU5402 and 3 µM CHIR99021. At **D15**, the medium is changed to RPE medium freshly supplemented with 250 mg/L taurine, 20 µg/L hydrocortisone and 0.013 µg/L triiodothyronine. The medium is changed three times per week.

Differentiation of mESCs to ROs

The Protocol is based on Eiraku et al: Self-organizing optic-cup morphogenesis in three-dimensional culture[53].

Retinal Induction (SFEBq)

See Retinal Induction (SFEBq) in the previous section for **D0** and **D1** step.

Floating culture in RMM1

At **D7**, aggregates are transferred into 6 cm petri dishes with 5 ml RMM1 using cut pipette tips.

Dissection and Maturation

At **D11**, Rx-Gfp+ neuroepithelia and optic vesicle-like structures were dissected with forceps and cultivated in a new petri dish with RMM2 supplemented with 1 mM taurine and 1 µM retinoic acid. At **D14**, the medium was changed to RMM2 supplemented with 1 mM taurine only. In continued cultivation, a half medium change was conducted three times per week.

Co-Cultivation of ROs and mESC-derived RPE cells

ROs are co-cultivated with mESC-derived RPE cells grown on Transwell membranes. Co-cultivation periods are D15 to D18, D18 to D21 and D15 to D21. For co-cultivation, the medium in the upper compartment was changed to RMM2 + 1 mM Taurine. RPE Medium + 250 mg/L Taurine, 20 µg/L Hydrocortisone and 0.013 µg/L triiodothyronine was added to the lower compartment. Usually, 3 to 4 ROs are carefully transferred into one well. Medium in the upper compartment was changed daily while medium in the lower compartment was changed every second day.

Conditioned Medium Collection and Treatment

Conditioned medium from mESC-derived RPE cells was collected and transferred into a 1.5 ml tube and quickly frozen and stored at -20°C.

Single ROs that are treated with conditioned medium are transferred into wells of a low adhesion 96-well plate containing 200 µl of a 1:1 RMM2 + 1 mM Taurine and conditioned medium mixture. A half medium change was conducted every day.

Cryopreservation and Cryosectioning of ROs

ROs are carefully taken with cut pipette tips and transferred into 1.5 ml tubes. Medium residues are aspirated and the aggregates are washed with PBS. Subsequently, PBS is discarded and ROs are fixed with 4% PFA for 30 minutes at room temperature in the dark. Afterwards, ROs are washed with 15% sucrose solution and then incubated in 15% sucrose for 3 hours at room temperature in the dark. The solution is changed to 30% sucrose and ROs are incubated over-night at 4°C. Next, the solution is changed to Sucrose + Surgipath solution and the ROs are carefully mixed. Aggregates are incubated over-night at 4°C or maintained for short-term storage in this solution at 4°C. Samples that should be cryosectioned are transferred into a 1.5 ml tube containing Surgipath and carefully mixed to dilute sucrose solution residues. This step is repeated and ROs are transferred into a small volume of Surgipath and placed at -20°C. Cryosections of 20 µm thickness are prepared using the Leica Cryotome (Leica, CM3050) and placed on glass slides (SuperFrost Plus, VWR, 631-0108). To dry the sections, the glass slides are incubated at 60°C for 3 hours. Cryosections can be used afterwards for immunohistochemistry or long-term stored at -80°C.

Immunocytochemistry

Cells on coverslips are fixed with 4% PFA for 15 minutes. Cryosections are fixed with 4% PFA for 20 minutes. Subsequently, cryosections are placed into a vessel with a slide holder and Sodium Citrate Buffer is added to cover the glass slides. Cryosections are incubated at 60°C for 5 hours. Samples were permeabilized 3 times for 10 minutes with PBS-T. Primary antibodies are diluted as recommended (see: **Table 4**) in PBS + 1% BSA and cells on coverslips are incubated for one to two hours at room temperature while cryosections were incubated overnight at 4°C. Samples are again washed 3 times for 10 minutes with PBS-T and secondary antibodies, DAPI and fluorescently labeled Phalloidin are diluted (see: **Table 5**) in PBS + 1% BSA and incubated for 2 hours at room temperature. Samples are washed with PBS 3 times and embedded in Mowiol.

Confocal Microscopy and Image Acquisition

Fluorescence images are acquired using the confocal laser scanning microscope (LSM) 800 by Carl Zeiss. Cryosectioned organoids were imaged with Plan-Achromat 20x/0.8 Air objective. Tiles were stitched using the ZEN software stitching tool. Sections were acquired by z-stacks of usually 5 – 10 µm. Afterwards, maximum intensity projections of the z-stacks were made using ZEN orthogonal projection tool.

Calculation of Relative Cell Numbers and Plot Measurements in ROs

Immunolabeled cryosections of organoids are processed using imagej. Images are split in single channels (**Figure M 1** top row and center row; top right shows the merged image of the proteins of interest). To exclude background or unspecific signal, a threshold is set for the fluorescently labeled proteins and DAPI to create binary images. Threshold is set manually for each image. The GFP channel showing Rx-Gfp is used to specify regions of interest (ROI) in an unbiased manner. The first Rx-Gfp image exemplarily shows 50 pixels wide lines drawn from the basal (inner) site of the epithelium towards to apical (outer) site (**Figure M 1** center row). Per section, multiple lines (usually 4 – 7) are drawn to representatively measure the epithelium. Drawn lines are saved in the ROI manager. Next, using the GFP channel, a mask is created by drawing a ROI around only the Rx-Gfp$^+$ epithelium. This mask is applied to the other channels to cut off non-retinal cells. Afterwards, the multi plot function of imagej is applied to the channels with labeled proteins. Therefore, the previously saved lines from the ROI manager function as templates. Resulting tables give values for multiple x- and y-axes which are saved afterwards (**Figure M 1** exemplary plot measurement). The binary images are then used for co-localization measurements using the imagej plugin JACoP. To quantify the amount of immunoreactive cells, the relative number of pixels in the DAPI channel overlapping with pixels from the fluorescently labeled proteins is calculated. To calculate the ratio of immunostained proteins, the overlap of their channels is calculated as well (**Figure M 1** bottom row).

Multiplot measurements are further processed using Origin2021. Multiple curves from one image are imported into the software. First, all x-axes are normalized from 0 to 1 using the Origin tool *Normalize.* All curves measured in one image are then averaged using *Average Curves* with 100 data points, resulting in one curve for one image. Multiple sections of the same staining from one organoid were processed as batch resulting in one curve for all images. All curves for one protein of one condition are eventually averaged to the final data set. The values for the y-axis are then normalized to the maximum gray value 255. Plots are smoothed using the *smoothen* function in Origin with default settings.

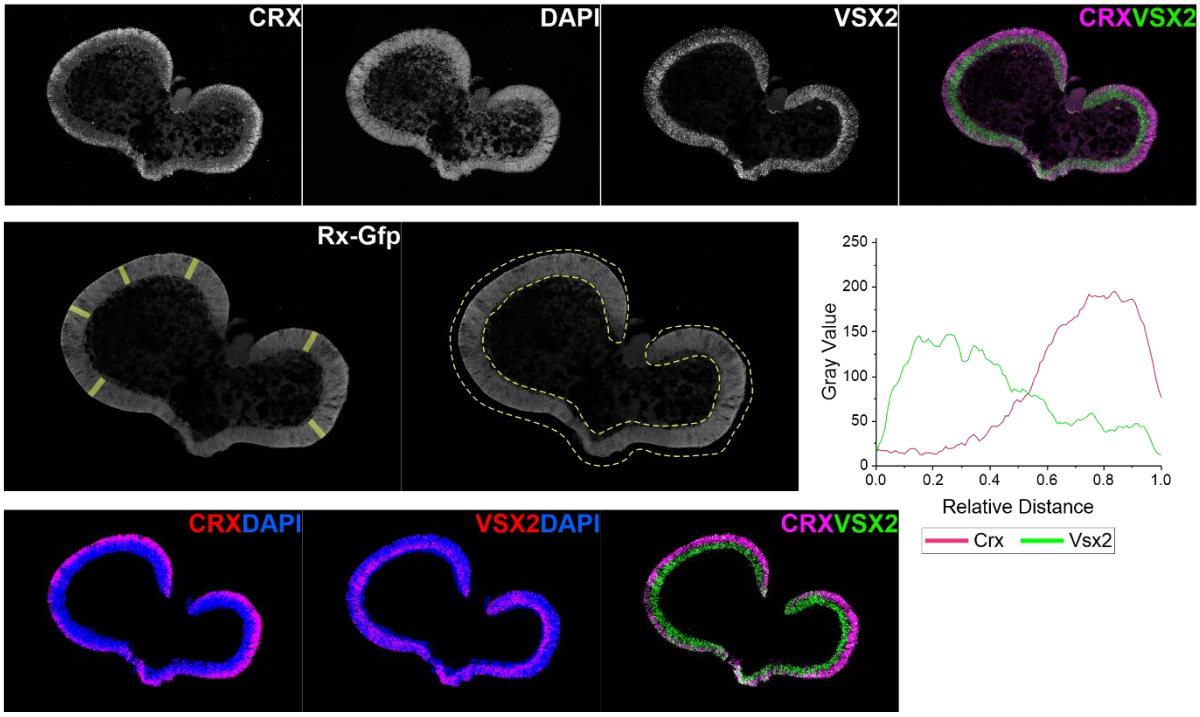

Figure M 1: Image processing. Fluorescently labeled proteins and nuclei in single channels and a merge image. Rx-Gfp signal was used to specify ROIs. Diagram shows an exemplary plot measurement. Co-localization images are depicted in the bottom row.

Isolation of primary RPE cells from mouse eyes

Provided eyes are placed in PBS and are immediately dissected after explantation. Remaining residuals of surrounding tissue is removed with forceps. The eye is kept in place using forceps with a grip. Then the eye is cut open with scissors by starting from the emersion point of the optic nerve to the cornea on two sides. To obtain the neural retina, the sclera (with RPE and choroid) is held with one forceps and pulled through second forceps. By this, the neural retina is peeled off from the Sclera/Choroid/RPE. For isolation of the RPE, the pigmented cells that are still attached to the sclera are dissected with forceps and scratched off. The desired cells and/or tissue are placed in TRIzol and homogenized. The cell lysate is used for RNA isolation immediately or stored at -20°C.

RNA Purification and cDNA Synthesis

Cells grown in 96-well plates are detached first with trypsin at 37°C for 2 minutes. For detachment, the cells are pipetted up and down a few times and are then transferred into a 1.5 ml reaction vessel and centrifuged for 2 -3 minutes with 13.000 rpm. Discard the supernatant and resuspend the pellet. When cells are grown on Transwell membranes, the insert can be taken out of plate and TRIzol is added directly to the cells in the well. Per well 4x200 µl TRIzol

are added to the cells and pipetted up and down to homogenize the lysate and transferred into another 1.5 ml tube. Samples can be stored at 4°C overnight or at -20°C for up to one year.

For RNA purification, the RNeasy MinElute Cleanup Kit (Qiagen, 74204) and RNase-Free DNase Set (Qiagen, 79254) was used and proceeded as described with minor changes to the protocol:

- 200 µl Chloroform are added and the samples were vortexed
- 10 min centrifugation at 10.000 rpm at RT
- Samples are separated into phases
- The aqueous phase is taken while being cautious not to transfer the red phase and transferred into a new 1.5 ml tube
- 240 µl 100% EtOH are added and mixed. Afterwards, the samples are transferred on a RNeasy spinning column and centrifuged 15s, 10.000 rpm
- Flow-through is discarded and 500 µl RW1 buffer are added and centrifuged 15s,10.000 rpm (incubate 5min before centrifugation)
- Flow-Through is discarded and 10 µl DNase in 70 µl RDD buffer are added and centrifuged 15min, 10.000 rpm
- Flow-Through is discarded and 350 µl RW1 buffer are added and centrifuged 15s, 10.000 rpm
- Flow-Through is discarded and 500 µl RPE buffer are added and centrifuged 15s, 10.000 rpm
- Flow-Through is discarded and 500 µl 80% EtOH are added and centrifuged 15s, 10.000 rpm
- Flow-Through is discarded and for drying the column is centrifuged 5 min, 10.000 rpm
- Flow-Through is discarded. Spinning column is placed into a 1.5 ml collection tube.
- For elution, 12 µl RNase-free H_2O are added and centrifuged 1 min, 10.000 rpm 4°C
- Flow-Through was collected and RNA concentration was measured with the Fluorometer Qubit 3.0 (Thermo Fisher Scientific, Q10211)

Samples can be quick-frozen in liquid nitrogen and stored at -80°C.

First stand cDNA synthesis was achieved by using Thermo Scientific RevertAid H Minus Reverse Transcriptase (Thermo Fisher Scientific, 10121360). After thawing random hexamers, dNTPs and the reaction buffer, the components are briefly mixed, centrifuged and placed on ice. To prepare one sample, the following components are added into sterile, nuclease-free tubes on ice:

Table 8: Random hexamer mix

Component	Volume
Template RNA: usually 250 - 500 ng; (10 pg - 5 µg total RNA)	up to 11 µl
Random hexamers (250 ng/µl)	0.4 - 0.8 µl
DEPC-treated water	to 12.5 µl
Final Volume	**12.5 µl**

The components are mixed and centrifuged briefly and afterwards incubated at 65°C for 5 minutes in a PCR cycler. Samples are placed on ice for 1 minute and centrifuged briefly. To prepare the reverse transcriptase reaction mix, the components are combined as shown in the table below.

Table 9: Reverse Transcription mix

Component	Volume
5x Reaction Buffer	4 µl
RNase Inhibitor (RiboLock)	0.5 µl (20 U)
10 mM dNTP mix	2 µl (1 mM)
RevertAid H Minus Reverse Transcriptase	1 µl (200 U)
Final Volume	**20 µl**

The components are mixed and centrifuged and then incubated at 25°C for 10 minutes. Afterwards, the PCR cycler is turned to 42°C for 60 minutes. In the end, the mix is incubated at 70°C for 10 minutes. Every sample that is reverse transcribed had a negative control containing H_2O instead of reverse transcriptase.

After reverse transcription, cDNA was purified using the DNA Clean & Concentrator-5 Kit (ZymoResearch) with minor changes to the protocol. At first, cDNA is diluted 1:7 with DNA Binding Buffer, mixed by vortexing and briefly centrifuged. The mixture is transferred into a Zymo-Spin Column in a Collection Tube and centrifuged for 30 seconds. Flow-through is discarded and 200 µl Wash Buffer are added to the column and centrifuged for 30 seconds. This step is repeated once again, before placing the Spin Column into a new 1.5 ml tube. 13 µl Elution Buffer are added to the column and incubated for 5 minutes at room temperature.

To elute the cDNA, the column was centrifuged for 30 seconds and concentration was measured three times with the Nanodrop. Samples can be frozen and stored at -20°C.

digital droplet PCR (ddPCR) and Relative Gene Expression Measurement

To prepare one sample, the following components are pipetted in a well of a ddPCR 96-well plate on ice:

Table 10: ddPCR Mix

Component	Volume
QX200 ddPCR EvaGreen Supermix (Bio Rad)	10 µl
Forward Primer (1 µM)	2 µl
Reverse Primer (1 µM)	2 µl
cDNA (5 ng/µl)	0.5 µl
H_2O	5.5 µl

After preparation of all samples, the well plate is sealed with a foil. The whole plate is briefly vortexed and centrifuged afterwards. Droplets are generated using the automated droplet generator Auto DG (Bio Rad). The droplets are generated in a new 96-well plate which is sealed as well afterwards. The plate is handled cautiously to preserve single droplets and is carefully placed in a PCR cycler. The two-step PCR program is shown in the table below:

Table 11: ddPCR program recommended and taken from Bio Rad

Step	Temperature	Time	Cycles
Enzyme activation	95°C	5 min	1
Denaturation	95°C	30 sec	40
Annealing and Extension	60°C	1 min	
Signal stabilization	4°C	5 min	1
	90°C	5 min	1
Hold	4°C	∞	1

Next, the plate was placed in the Droplet Reader (QX200 Droplet Reader, Bio Rad) to evaluate the number of positive droplets. Data is analyzed using QuantaSoft software (Bio Rad). In 1D Amplitude graphs, the quality of the reaction for each sample can be viewed. Ideally, a clear separation of two clusters can be seen. One cluster representing all droplets, in which no PCR amplification occurs (**Figure M 2** left graph; gray dots). The other cluster indicates positive

droplets that are detected via a fluorescent dye that intercalates in dsDNA. From the number of positive droplets, the copy number can be calculated and the concentration (copies/µl) can be derived (**Figure M 2** right graph).

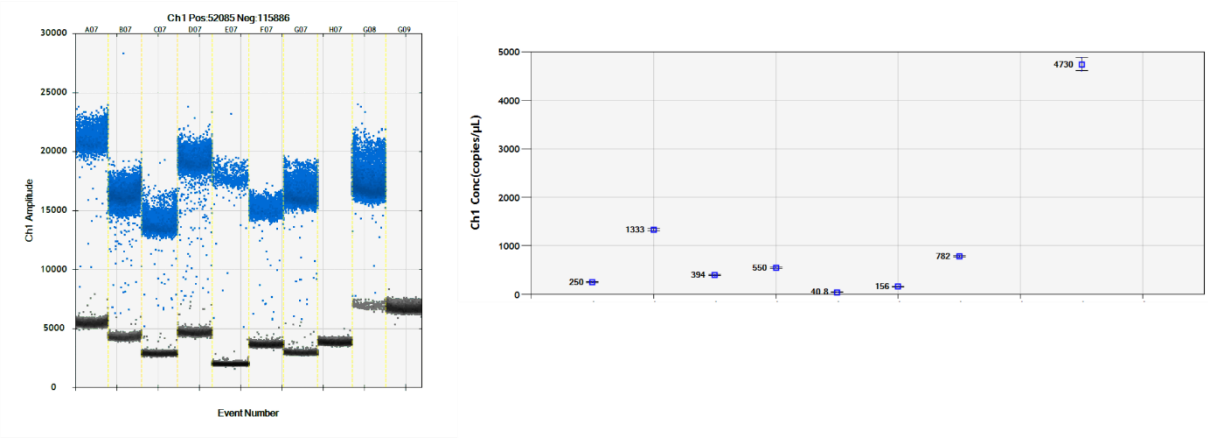

Figure M 2: ddPCR read-out. The left graph shows all droplets that were generated in one exemplary sample. The genes that are measured are Mitf, Otx2, Pax6, Sox9, Mertk, Pedf, Rlbp1, Rpe65, Pgk1 and Pgk1 in the NoRT control (from left to right). Blue dots are considered to be positive, while gray dots represent negatives. In the right diagram the concentration in copies/µl are calculated.

Relative gene expression is calculated by normalizing the values for copies/µl of each gene to the value from Pgk1 which serves as housekeeping gene. At least three independent samples per condition are measured. For the heatmap, the three values are averaged.

Statistical Analysis

The preparation of one batch of organoids is considered as one independent experiment (N). Single organoids from independent experiments are considered as samples (n). For mESC-derived RPE, one independent experiment is considered as one sample (N = n). Calculation of relative cell numbers in the retinal epithelium is described above. For statistical analyses, all values from different cryosections of one organoid measured for one protein are averaged to one value. Area under the distribution curve is measured using the Origin2021 software. In order to calculate the relative area under the curves, the function *Minitools: Integrate* was used to calculate the area under the whole curve first. Next, the area under the curve from x_1 to x_2 is calculated. Average values, median, standard deviation, SEM and maxima as well as the statistical tests are calculated in Origin2021.

Supplementary Information

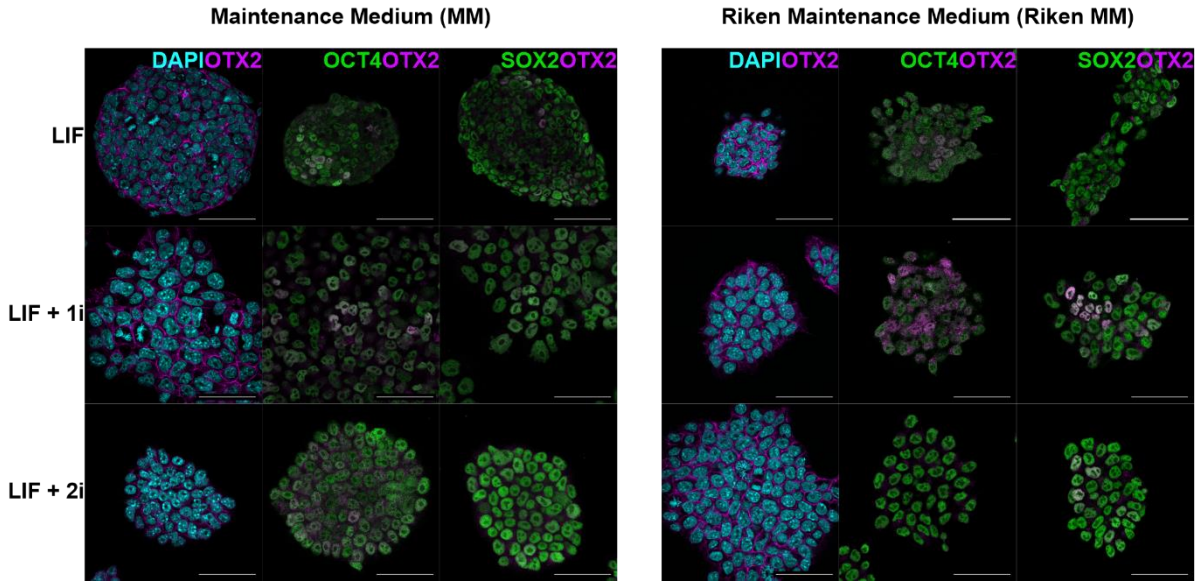

Figure S 1: mESC cultivation conditions. mESCs can be maintened in MM (left) or Riken MM (right) supplemented with LIF, LIF + MEK inhibitor (LIF + 1i) or LIF + MEK iinhibitor + GSK3 inhibitor (LIF + 2i).

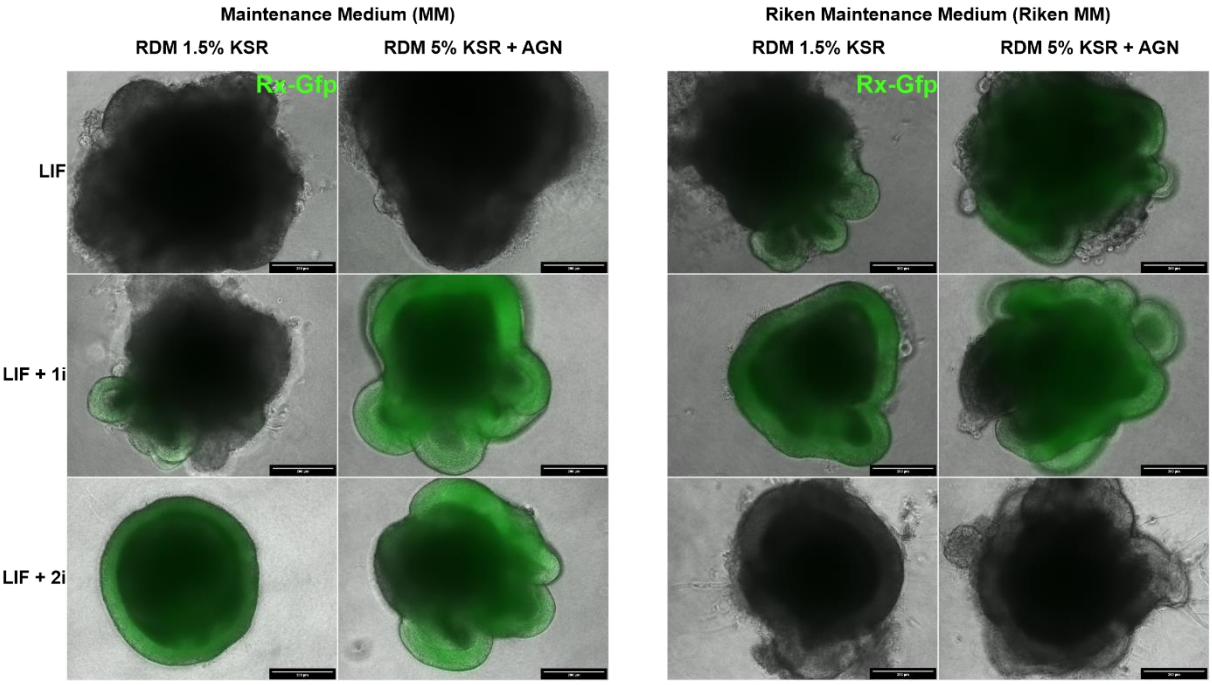

Figure S 2: ROs generated from differently cultivated mESCs. ROs were imaged at D7 to visualize retinal induction in two different RDMs. mESCs have been maintained in MM (left) or Riken MM (right) supplemented with LIF, LIF + MEK inhibitor (LIF + 1i) or LIF + MEK inhibitor + GSK3 inhibitor (LIF + 2i) prior to seeding in low adhesion well plates.

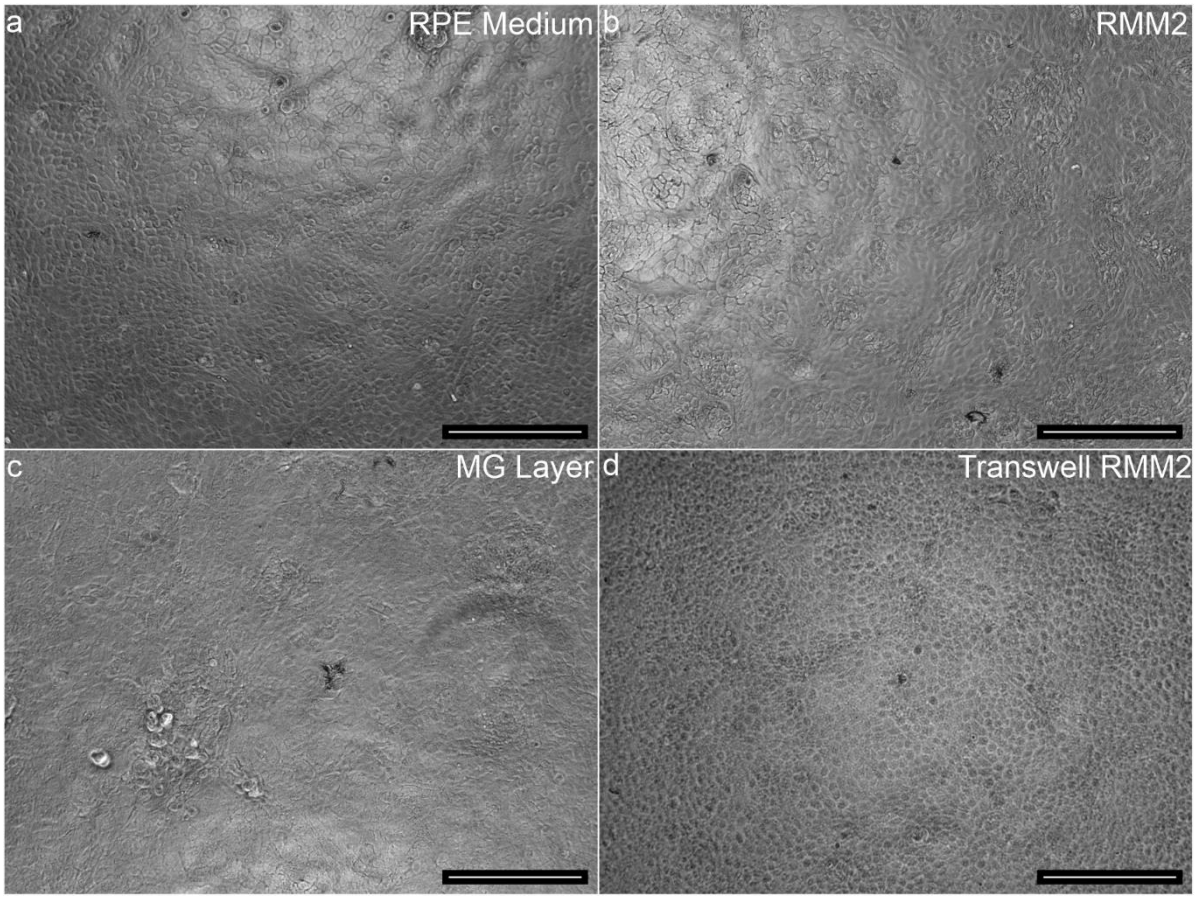

Figure S 3: Establishing co-cultivation conditions for RPE cells. **a** mESC-derived RPE cells at D20 cultivated with RPE Medium with characteristic hexagonal morphology. **b** mESC-derived RPE cells at D20 cultivated in RMM2 for 5 days. **c** Matrigel layer on top of mESC-derived RPE cells D20 and cultivated in RMM2 for 5 days. **d** mESC-derived RPE cells at D22 on a Transwell membrane. Scale bars: 200 µm.

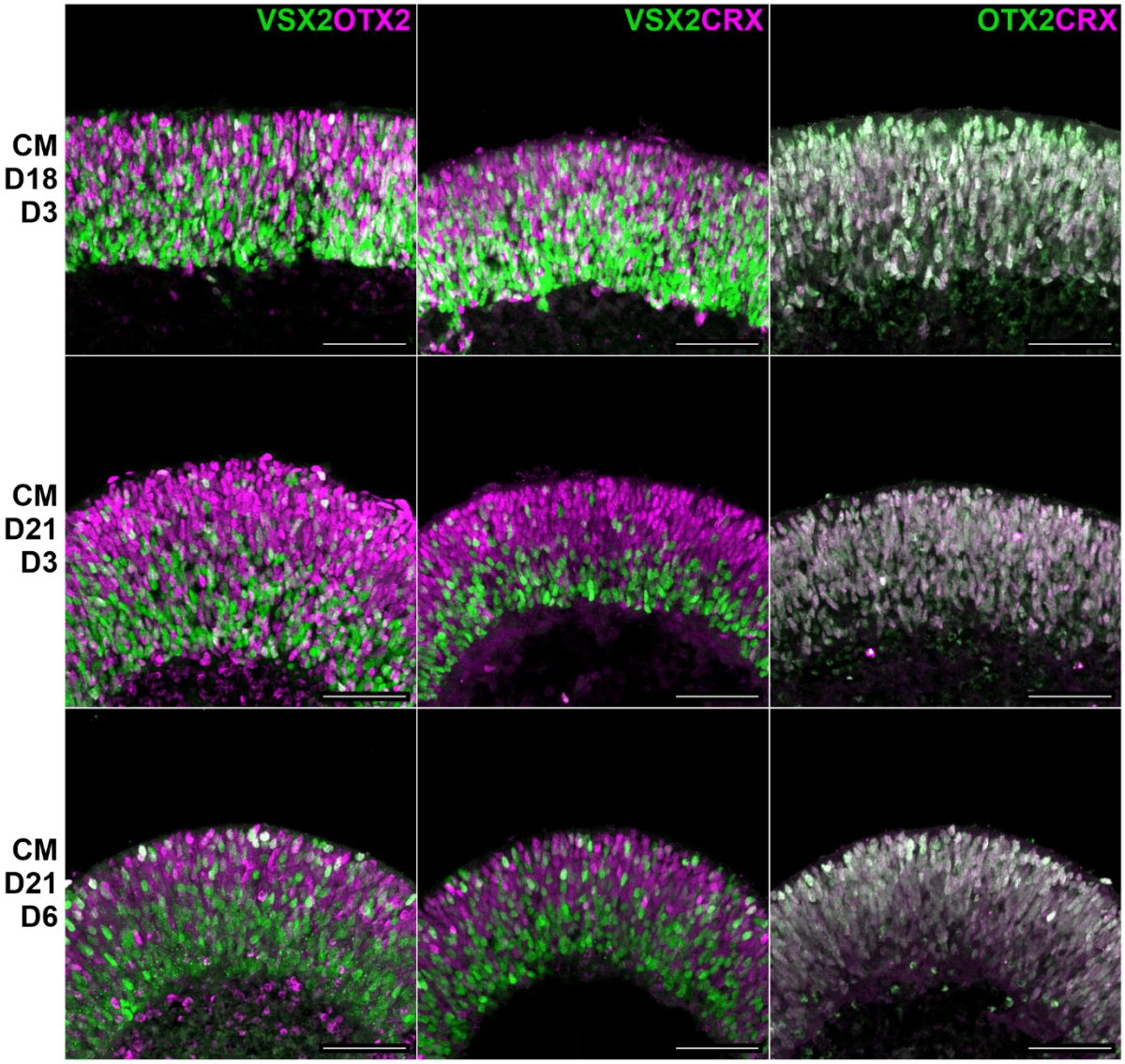

Figure S 4: Co-expression of retinal markers in ROs treated with mESC-derived RPE conditioned medium. ROs were treated with conditioned medium from D15 to D18 (CM D18 D3; top row), D18 to D21 (CM D21 D3; middle row) and from D15 to D21 (CM D21 D6; bottom row).

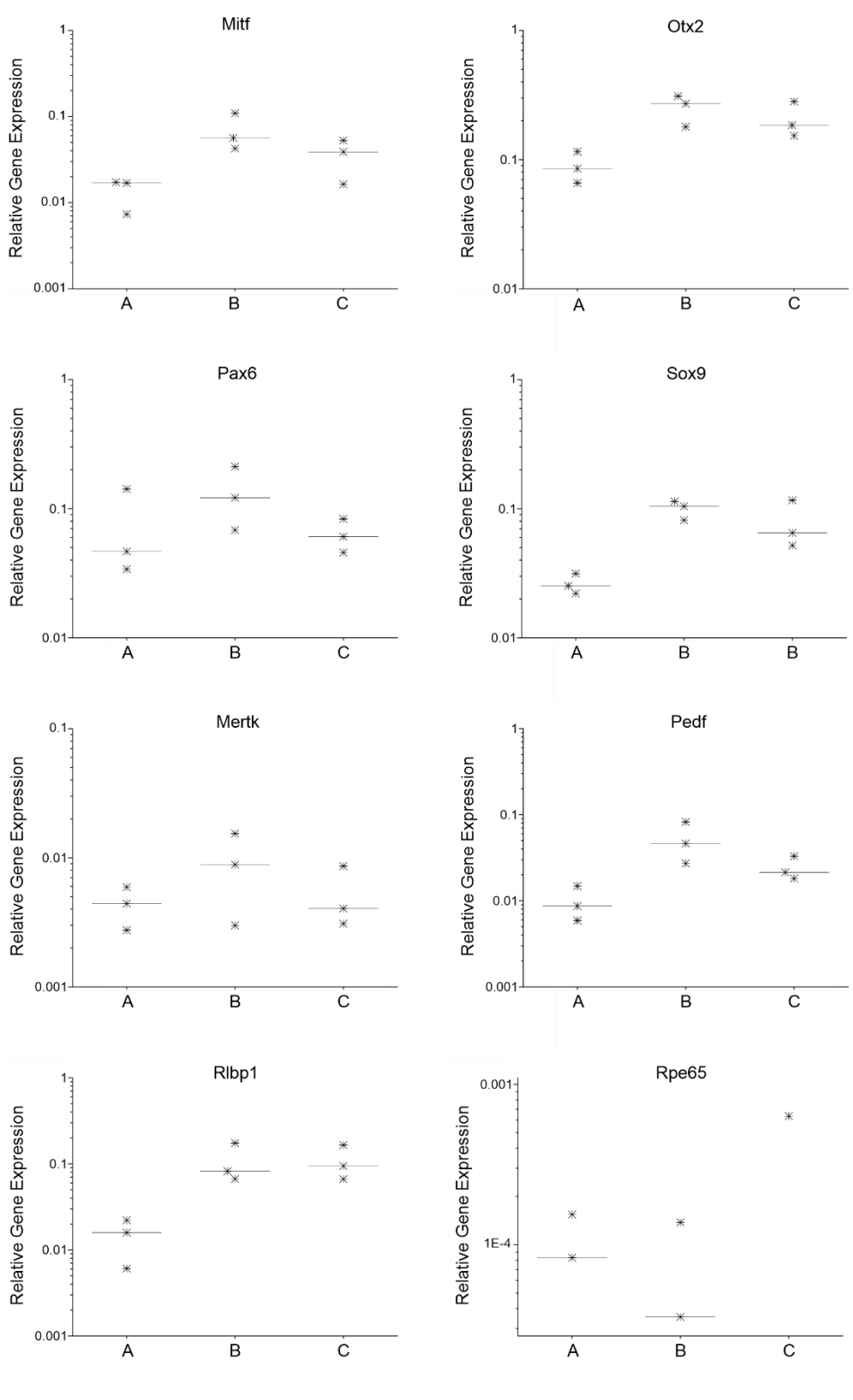

***Figure S 5: Extended gene expression measurements for mESC-derived RPE cells*.** All Graphs for **Figure 18**. ddPCR measurements show an increase in RPE specific gene expression. A: mESC-derived RPE grown in a 96-well plate with RPE Medium at D21; B: mESC-derived RPE grown on a Transwell membrane cultivated with RMM2 in the upper compartment from D18-D21; C: mESC-derived RPE grown on a Transwell membrane cultivated with RMM2 in the upper compartment from D15-D21.

Table S 1: Experiments and sample sizes for plot measurements and epithelial thickness.

Sample	Experiments	Sample size
RO D15	N = 3	n = 7
RO D18	N = 3	n = 12
RO D21	N = 4	n = 11
CO D18 CD3	N = 4	n = 10
CO D21 CD3	N = 4	n = 10
CO D21 CD6	N = 3	n = 6
CM D18 D3	N = 3	n = 8
CM D21 D3	N = 3	n = 9
CM D21 D6	N = 3	n = 9
U2OS D18 CD3	N = 3	n = 10
U2OS D21 CD3	N = 3	n = 6
U2OS D21 CD6	N = 3	n = 6

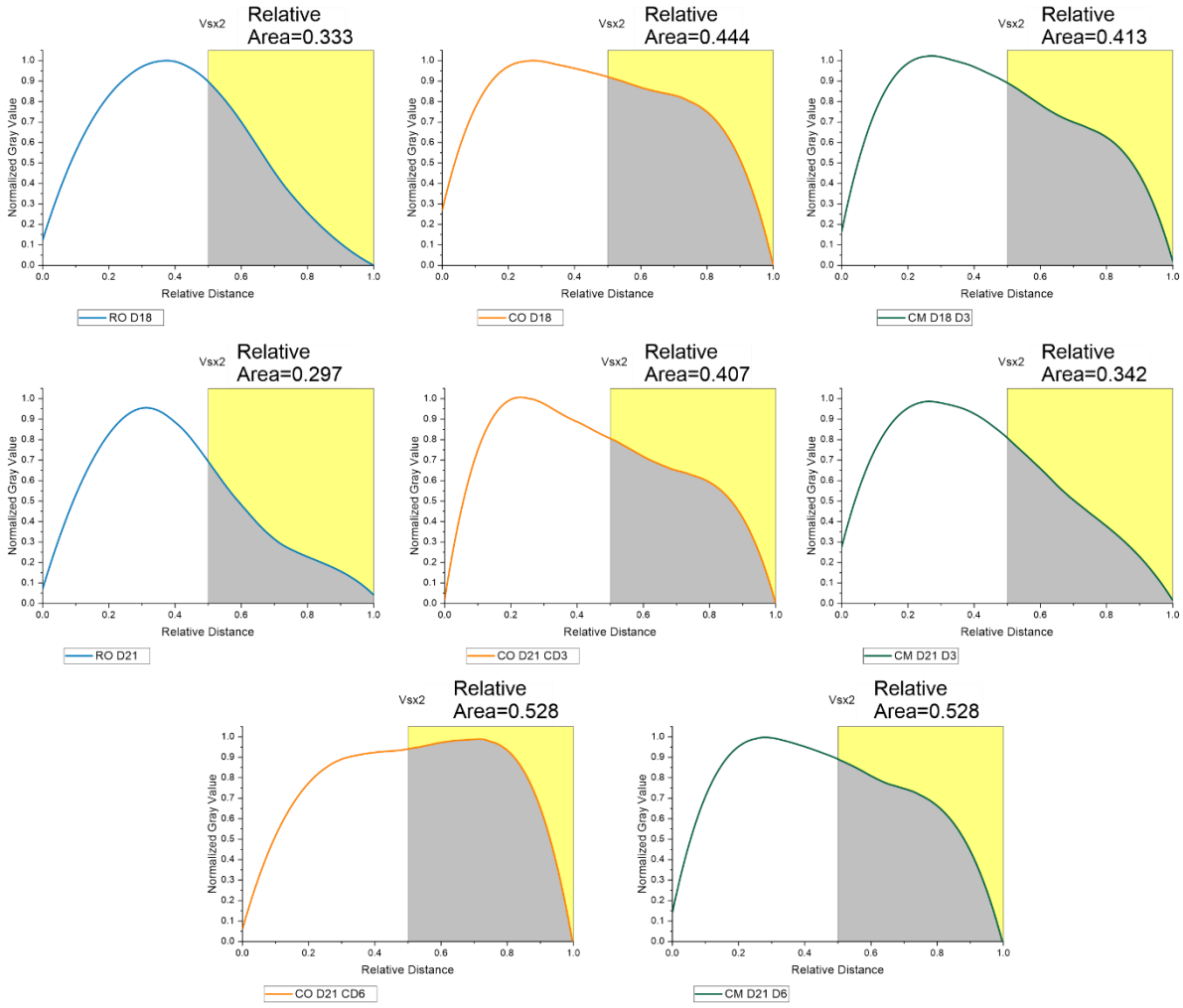

Figure S 6: Apical distribution of Vsx2⁺ nuclei. Relative area under the curves from x = 0.5 to x = 1 was calculated (gray) representing the apical half of the retinal epithelium.

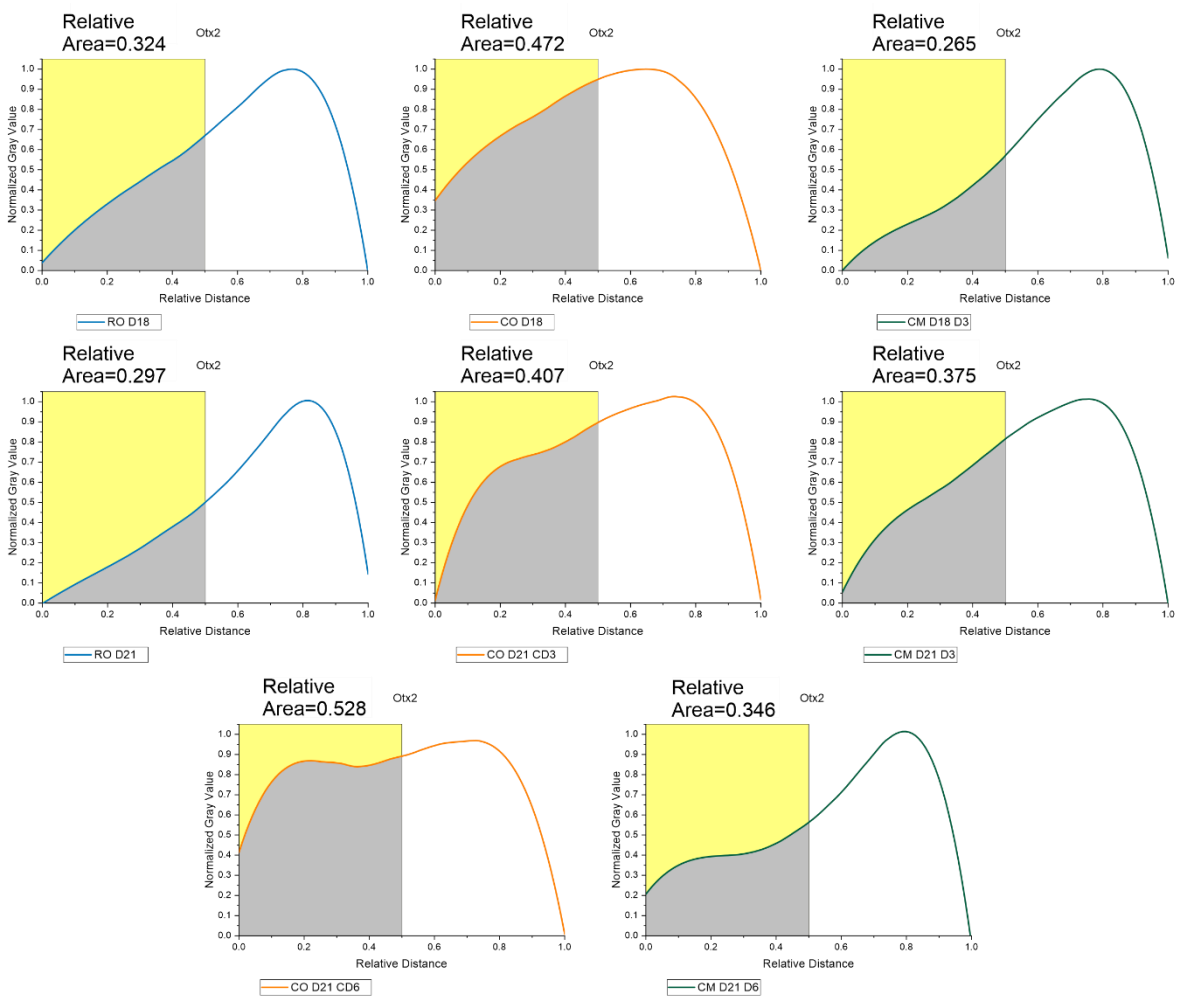

Figure S 7: Basal distribution of Otx2⁺ nuclei. Relative area under the curves from x = 0 to x = 0.5 was calculated (gray) representing the basal half of the retinal epithelium.

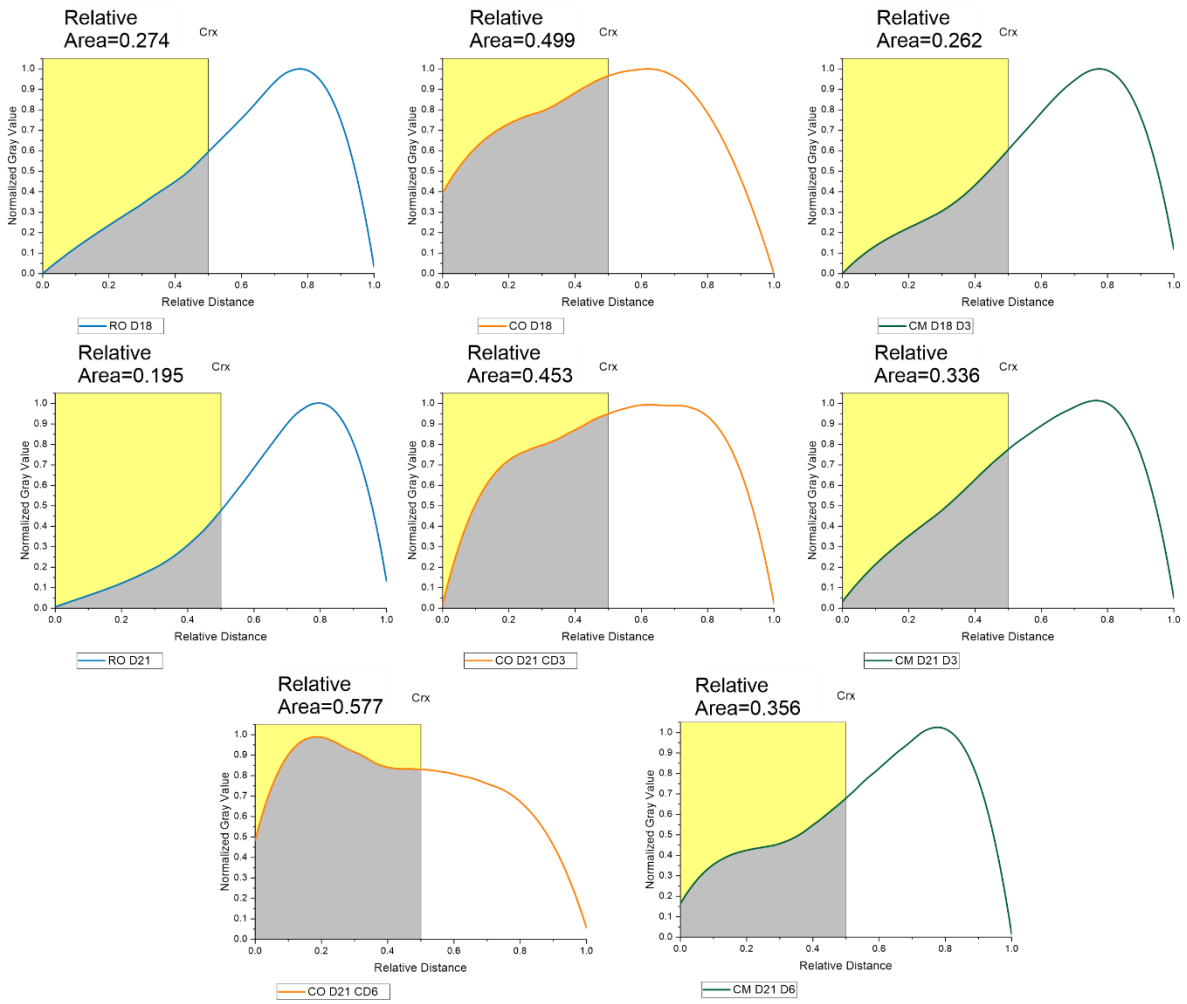

Figure S 8: Basal distribution of Crx⁺ nuclei. Relative area under the curves from x = 0 to x = 0.5 was calculated (gray) representing the basal half of the retinal epithelium.

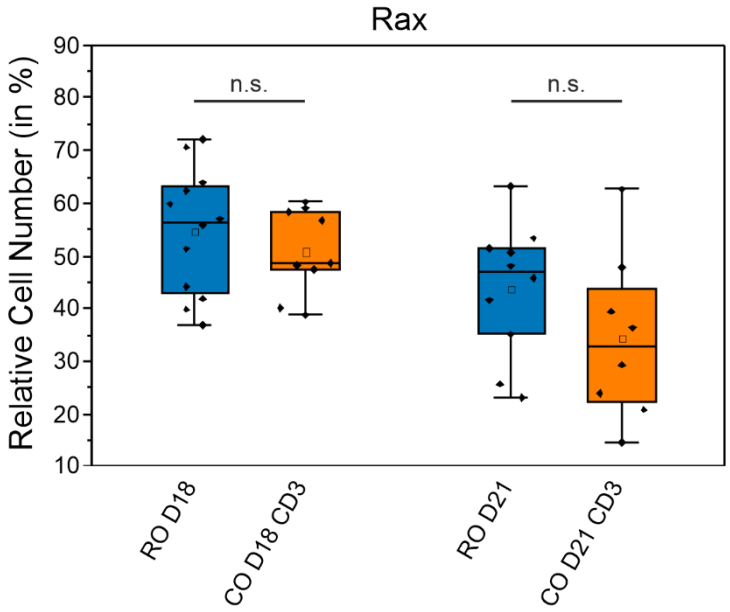

Figure S 9: Relative cell number of immunostained Rax⁺ Cells. Quantification of pH3⁺ labeled cells (RO D18: *N* = 3, *n* = 12; CO D18 CD3: *N* = 4, *n* = 9; RO D21: *N* = 3, *n* = 10; CO D21 CD3: *N* = 3, *n* = 8

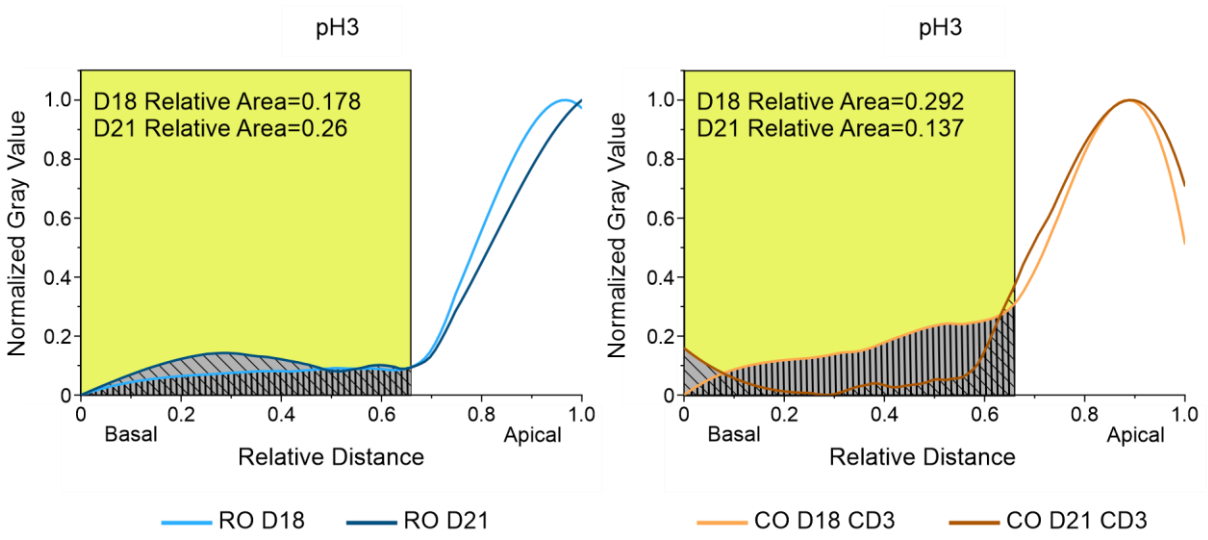

Figure S 10: Basal Distribution of pH3⁺ nuclei. Relative area under the curves from x = 0 to x = 0.66 was calculated (gray) representing the basal portion of the retinal epithelium.

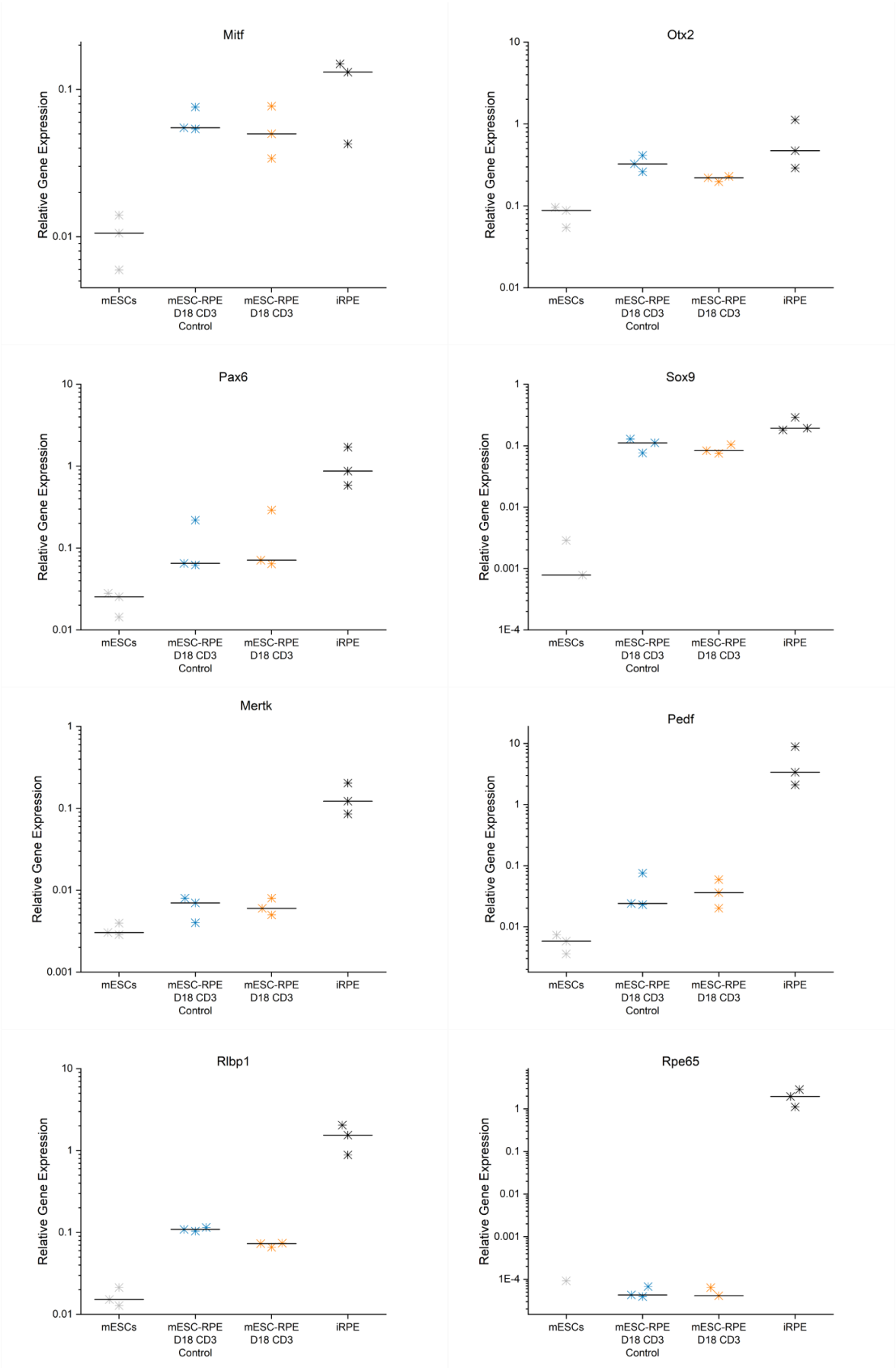

Figure S 11: Detailed gene expression of co-cultivated mESC-RPE CO D18 CD3. Single graphs for Heatmap shown in ***Figure 21***

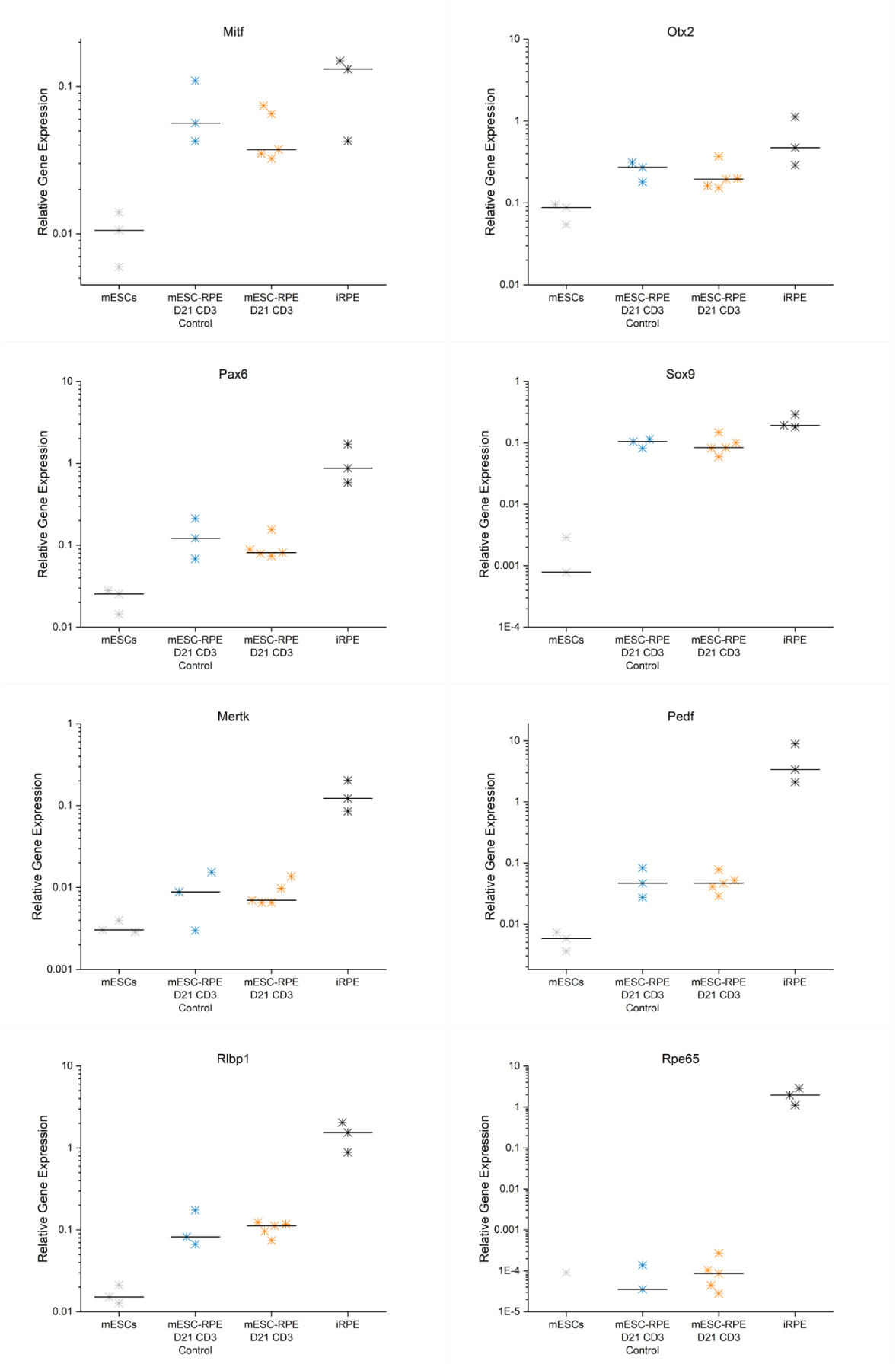

Figure S 12: Detailed gene expression of co-cultivated mESC-RPE CO D21 CD3. Single graphs for Heatmap shown in ***Figure 21***.

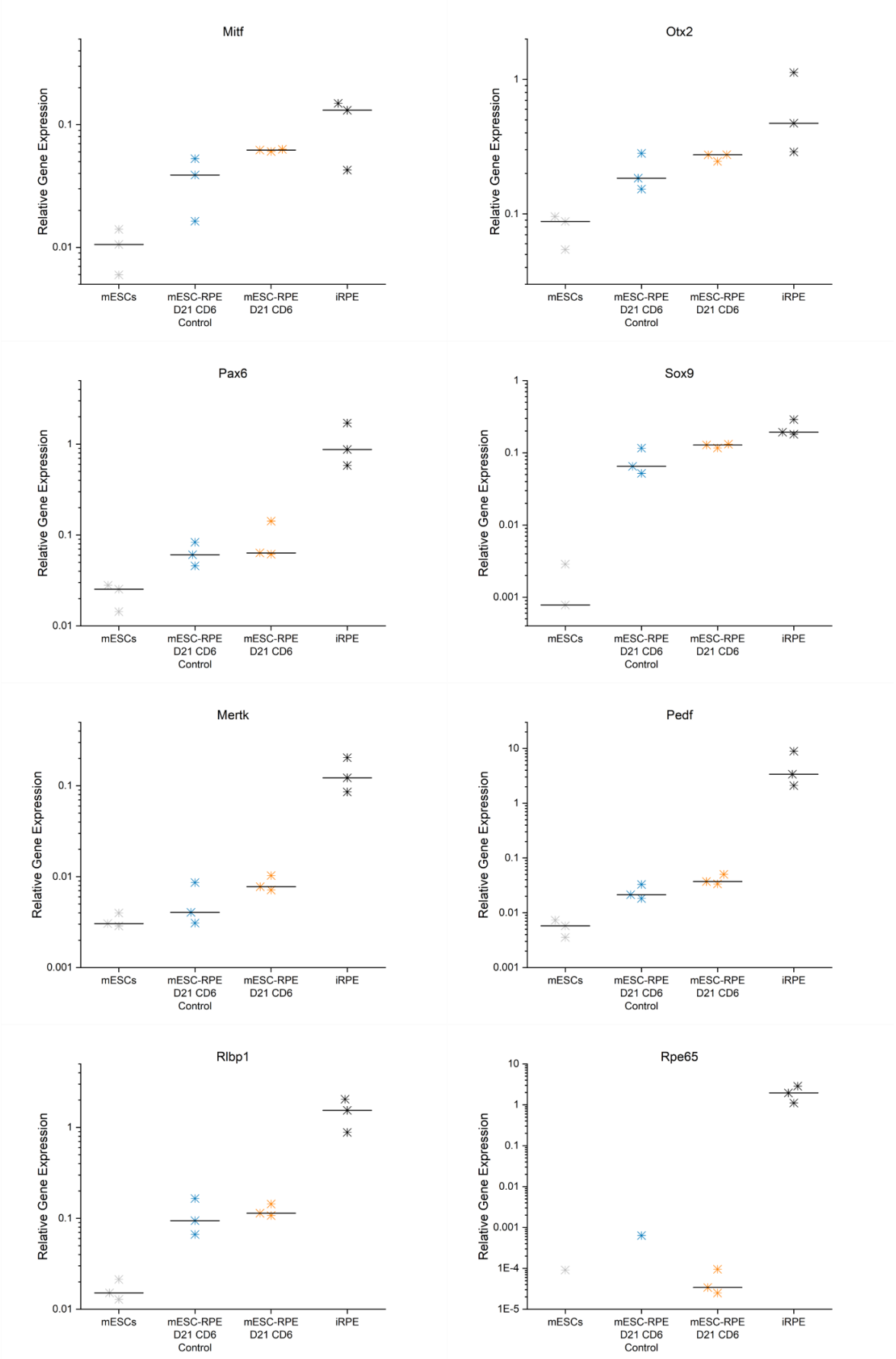

Figure S 13: Detailed gene expression of co-cultivated mESC-RPE CO D21 CD6. Single graphs for Heatmap shown in ***Figure 21***.

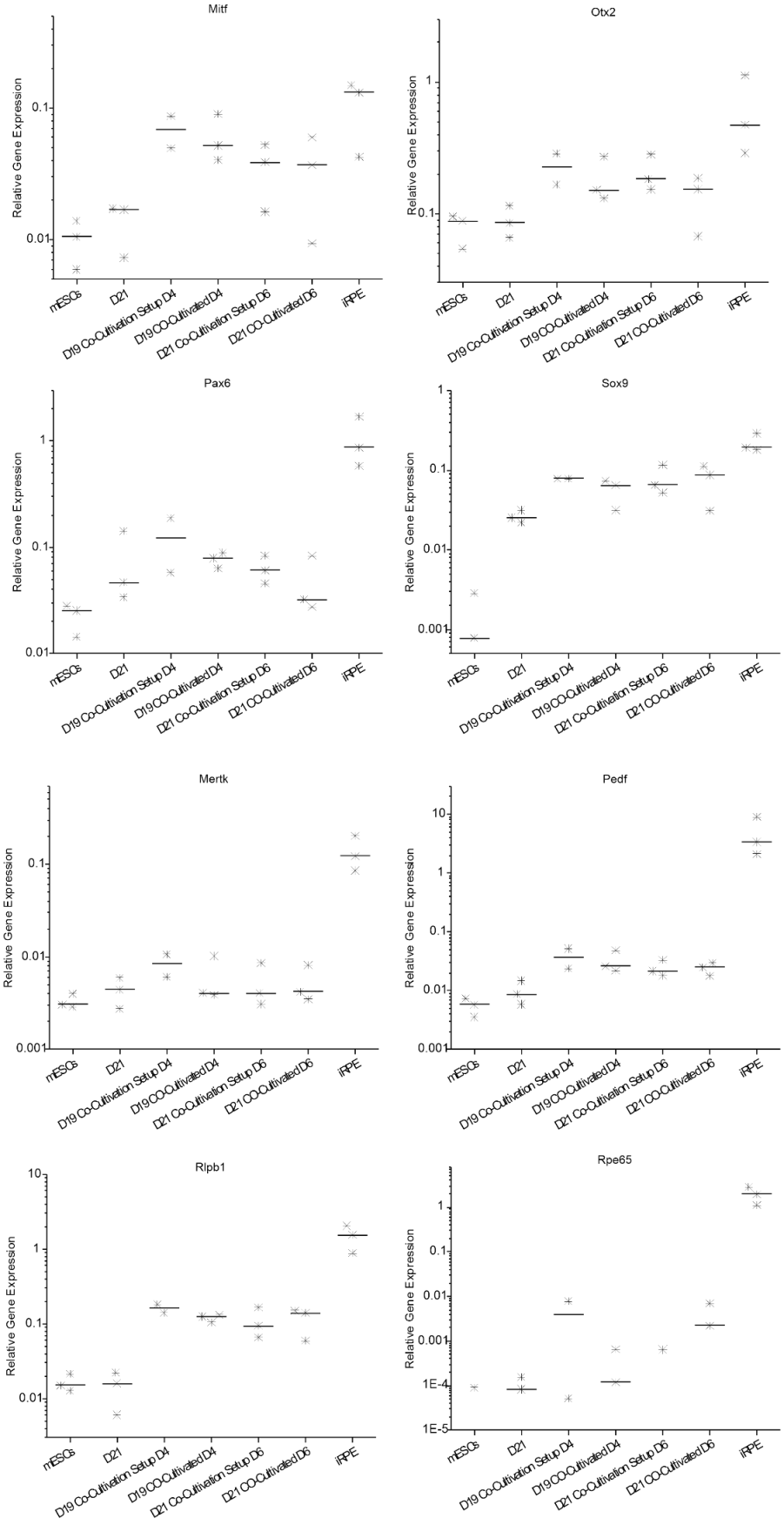

Figure S 14: RPE gene expression measurements with a single co-cultivated RO. Gene Expression measured in mESC-derived RPE cells that have been co-cultivated with only a single RO compared to mESC-derived RPE cells that were not co-cultivated.

Acknowledgements

I wish to express my gratefulness to everyone who supported me throughout the time. It was a pleasure to meet such great and kind people, so that it was a joy to work in this group everyday.

At first, I want to thank Prof. Dr. Martin Bastmeyer for giving me the opportunity to work on this exciting and interesting topic and write my PhD thesis at his institute. I want to thank for the trust and support during the time as a doctoral student.

I also want to thank Dr. Dietmar Gradl who took the responsibility to be co-referee for my work.

Furthermore, I want to thank Prof. Dr. Holger Puchta for kindly providing me the opportunity to conduct ddPCR experiments.

I want to thank all my colleagues who were present during my time at the institute. I could rely on excellent scientific expertise whenever I needed help. But moreover, being surrounded by kind and friendly people made me enjoy every single day. Thanks to Martina and Elisa for proofreading and being the best partners in the stem cell lab.

A special thanks goes to Dr. Stephan Keppler who supervised me during my master thesis and supported me throughout all his time at the institute. His experience and advices helped me to conduct and improve my experiments and together we could handle the retinal organoids.

Additionally, I want to thank the Cluster of excellence 3DMM2O and the members of the thrust C3, especially Dr. Lucie Zilova for being part of my Mentoring Committee and for her critical and helpful input.

I also wish to thank Magdalena Winkhofer for the excellent work which also helped me a lot for my thesis. Always being highly motivated and in a good mood made it a great pleasure to supervise her master thesis.

Tamara, Nicole and Rebecca, I want to thank you for all the great times during our time at the university and for not only being fellow students but also good friends!

At last, I want to thank all my friends and family who supported me all the time. Especially, I want to thank my wife Michelle. Without you I would have never achieved all of this.

List of Publications

Hippler, Marc; Weißenbruch, Kai; Richler, Kai; Lemma, Enrico D.; Nakahata, Masaki; Richter, Benjamin; Barner-Kowollik, Christopher; Takashima, Yoshinori; Harada, Akira; Blasco, Eva; Wegener, Martin; Tanaka, Motomu, Bastmeyer, Martin

Mechanical stimulation of single cells by reversible host-guest interactions in 3D microscaffolds.

In: Science advances 6 (39). DOI: 10.1126/sciadv.abc2648. .(2020):

Contribution: Cell culture experiments and live-cell imaging

References

1. Wilson, S. W. & Houart, C. Early Steps in the Development of the Forebrain. *Developmental Cell* **6,** 167–181; 10.1016/S1534-5807(04)00027-9 (2004).
2. Wilson, S. I., Graziano, E., Harland, R., Jessell, T. M. & Edlund, T. An early requirement for FGF signalling in the acquisition of neural cell fate in the chick embryo. *Current biology : CB* **10,** 421–429; 10.1016/s0960-9822(00)00431-0 (2000).
3. Bachiller, D. *et al.* The organizer factors Chordin and Noggin are required for mouse forebrain development. *Nature* **403,** 658–661; 10.1038/35001072 (2000).
4. Perron, M. & Harris, W. A. 23 - Cellular Determination in Amphibian Retina. In *Cell fate and lineage,* edited by S. A. Moody (Academic Press, San Diego, 1998), pp. 353–368.
5. Masai, I. *et al.* floating head and masterblind regulate neuronal patterning in the roof of the forebrain. *Neuron* **18,** 43–57; 10.1016/S0896-6273(01)80045-3 (1997).
6. Houart, C. *et al.* Establishment of the telencephalon during gastrulation by local antagonism of Wnt signaling. *Neuron* **35,** 255–265; 10.1016/S0896-6273(02)00751-1 (2002).
7. Kiecker, C. & Niehrs, C. A morphogen gradient of Wnt/beta-catenin signalling regulates anteroposterior neural patterning in Xenopus. *Development* **128,** 4189–4201; 10.1242/dev.128.21.4189 (2001).
8. Carl, M., Loosli, F. & Wittbrodt, J. Six3 inactivation reveals its essential role for the formation and patterning of the vertebrate eye. *Development* **129,** 4057–4063; 10.1242/dev.129.17.4057 (2002).

9. Loosli, F., Winkler, S. & Wittbrodt, J. Six3 overexpression initiates the formation of ectopic retina. *Genes Dev.* **13,** 649–654; 10.1101/gad.13.6.649 (1999).

10. Lagutin, O. V. *et al.* Six3 repression of Wnt signaling in the anterior neuroectoderm is essential for vertebrate forebrain development. *Genes Dev.* **17,** 368–379; 10.1101/gad.1059403 (2003).

11. Braun, M. M., Etheridge, A., Bernard, A., Robertson, C. P. & Roelink, H. Wnt signaling is required at distinct stages of development for the induction of the posterior forebrain. *Development* **130,** 5579–5587; 10.1242/dev.00685 (2003).

12. Harland, R. Neural induction. *Current opinion in genetics & development* **10,** 357–362; 10.1016/S0959-437X(00)00096-4 (2000).

13. Zaghloul, N. A., Yan, B. & Moody, S. A. Step-wise specification of retinal stem cells during normal embryogenesis. *Biology of the Cell* **97,** 321–337; 10.1042/BC20040521 (2005).

14. Heavner, W. & Pevny, L. Eye development and retinogenesis. *Cold Spring Harbor Perspectives in Biology* **4**; 10.1101/cshperspect.a008391 (2012).

15. Chow, R. L. & Lang, R. A. Early eye development in vertebrates. *Annual review of cell and developmental biology* **17,** 255–296; 10.1146/annurev.cellbio.17.1.255 (2001).

16. Zuber, M. E., Gestri, G., Viczian, A. S., Barsacchi, G. & Harris, W. A. Specification of the vertebrate eye by a network of eye field transcription factors. *Development* **130,** 5155–5167; 10.1242/dev.00723 (2003).

17. Simeone, A. *et al.* A vertebrate gene related to orthodenticle contains a homeodomain of the bicoid class and demarcates anterior neuroectoderm in the gastrulating mouse embryo. *The EMBO journal* **12,** 2735–2747; 10.1002/j.1460-2075.1993.tb05935.x (1993).

18. Matsuo, I., Kuratani, S., Kimura, C., Takeda, N. & Aizawa, S. Mouse Otx2 functions in the formation and patterning of rostral head. *Genes & development* **9,** 2646–2658; 10.1101/gad.9.21.2646 (1995).

19. Andreazzoli, M., Gestri, G., Angeloni, D., Menna, E. & Barsacchi, G. Role of Xrx1 in Xenopus eye and anterior brain development. *Development* **126,** 2451–2460; 10.1242/dev.126.11.2451 (1999).

20. Rhinn, M. *et al.* Sequential roles for Otx2 in visceral endoderm and neuroectoderm for forebrain and midbrain induction and specification. *Development* **125,** 845–856; 10.1242/dev.125.5.845 (1998).

21. Danno, H. *et al.* Molecular links among the causative genes for ocular malformation: Otx2 and Sox2 coregulate Rax expression. *Proceedings of the National Academy of Sciences of the United States of America* **105,** 5408–5413; 10.1073/pnas.0710954105 (2008).

22. Ragge, N. K. *et al.* Heterozygous mutations of OTX2 cause severe ocular malformations. *American Journal of Human Genetics* **76,** 1008–1022; 10.1086/430721 (2005).

23. Martínez-Morales, J. R. *et al.* OTX2 activates the molecular network underlying retina pigment epithelium differentiation. *The Journal of biological chemistry* **278,** 21721–21731; 10.1074/jbc.M301708200 (2003).

24. Ragge, N. K. *et al.* SOX2 anophthalmia syndrome. *American journal of medical genetics. Part A* **135,** 1-7; discussion 8; 10.1002/ajmg.a.30642 (2005).

25. Mathers, P. H., Grinberg, A., Mahon, K. A. & Jamrich, M. The Rx homeobox gene is essential for vertebrate eye development. *Nature* **387,** 603–607; 10.1038/42475 (1997).

26. Zhang, L., Mathers, P. H. & Jamrich, M. Function ofRx, but notPax6, is essential for the formation of retinal progenitor cells in mice. *genesis* **28,** 135–142; 10.1002/1526-968X(200011/12)28:3/4<135::AID-GENE70>3.0.CO;2-P (2000).

27. Voronina, V. A. *et al.* Mutations in the human RAX homeobox gene in a patient with anophthalmia and sclerocornea. *Human molecular genetics* **13,** 315–322; 10.1093/hmg/ddh025 (2004).

28. Walther, C. & Gruss, P. Pax-6, a murine paired box gene, is expressed in the developing CNS. *Development* **113,** 1435–1449; 10.1242/dev.113.4.1435 (1991).

29. Grocott, T., Lozano-Velasco, E., Mok, G. F. & Münsterberg, A. E. The Pax6 master control gene initiates spontaneous retinal development via a self-organising Turing network. *Development* **147**; 10.1242/dev.185827 (2020).

30. Sinn, R. & Wittbrodt, J. An eye on eye development. *Mechanisms of Development* **130,** 347–358; 10.1016/j.mod.2013.05.001 (2013).

31. Li, H. S., Yang, J. M., Jacobson, R. D., Pasko, D. & Sundin, O. Pax-6 is first expressed in a region of ectoderm anterior to the early neural plate: implications for stepwise determination of the lens. *Developmental biology* **162,** 181–194; 10.1006/dbio.1994.1077 (1994).

32. Halder, G., Callaerts, P. & Gehring, W. J. Induction of ectopic eyes by targeted expression of the eyeless gene in Drosophila. *Science (New York, N.Y.)* **267,** 1788–1792; 10.1126/science.7892602 (1995).

33. Hägglund, A.-C., Dahl, L. & Carlsson, L. Lhx2 is required for patterning and expansion of a distinct progenitor cell population committed to eye development. *PLoS ONE* **6,** e23387; 10.1371/journal.pone.0023387 (2011).

34. Tétreault, N., Champagne, M.-P. & Bernier, G. The LIM homeobox transcription factor Lhx2 is required to specify the retina field and synergistically cooperates with Pax6 for Six6 trans-activation. *Developmental biology* **327,** 541–550; 10.1016/j.ydbio.2008.12.022 (2009).

35. Zuber, M. E., Perron, M., Philpott, A., Bang, A. & Harris, W. A. Giant eyes in Xenopus laevis by overexpression of XOptx2. *Cell* **98,** 341–352; 10.1016/s0092-8674(00)81963-7 (1999).

36. Adelmann, H. B. The Problem of Cyclopia. Part I. *The Quarterly Review of Biology* **11,** 161–182; 10.1086/394504 (1936).

37. Echelard, Y. *et al.* Sonic hedgehog, a member of a family of putative signaling molecules, is implicated in the regulation of CNS polarity. *Cell* **75,** 1417–1430; 10.1016/0092-8674(93)90627-3 (1993).

38. Carl, M. & Wittbrodt, J. Graded interference with FGF signalling reveals its dorsoventral asymmetry at the mid-hindbrain boundary. *Development* **126,** 5659–5667; 10.1242/dev.126.24.5659 (1999).

39. Sasagawa, S., Takabatake, T., Takabatake, Y., Muramatsu, T. & Takeshima, K. Axes establishment during eye morphogenesis in Xenopus by coordinate and antagonistic actions of BMP4, Shh, and RA. *genesis* **33,** 86–96; 10.1002/gene.10095 (2002).

40. Belloni, E. *et al.* Identification of Sonic hedgehog as a candidate gene responsible for holoprosencephaly. *Nature genetics* **14,** 353–356; 10.1038/ng1196-353 (1996).

41. Muenke, M. & Cohen, M. M. Genetic approaches to understanding brain development: Holoprosencephaly as a model. *Ment. Retard. Dev. Disabil. Res. Rev.* **6,** 15–21; 10.1002/(SICI)1098-2779(2000)6:1<15::AID-MRDD3>3.0.CO;2-8 (2000).

42. Varga, Z. M., Wegner, J. & Westerfield, M. Anterior movement of ventral diencephalic precursors separates the primordial eye field in the neural plate and requires cyclops. *Development* **126,** 5533–5546; 10.1242/dev.126.24.5533 (1999).

43. Li, H., Tierney, C., Wen, L., Wu, J. Y. & Rao, Y. A single morphogenetic field gives rise to two retina primordia under the influence of the prechordal plate. *Development* **124,** 603–615; 10.1242/dev.124.3.603 (1997).

44. Rembold, M., Loosli, F., Adams, R. J. & Wittbrodt, J. Individual cell migration serves as the driving force for optic vesicle evagination. *Science (New York, N.Y.)* **313,** 1130–1134; 10.1126/science.1127144 (2006).

45. Nornes, H. O., Dressler, G. R., Knapik, E. W., Deutsch, U. & Gruss, P. Spatially and temporally restricted expression of Pax2 during murine neurogenesis. *Development* **109,** 797–809; 10.1242/dev.109.4.797 (1990).

46. Schwarz, M. *et al.* Spatial specification of mammalian eye territories by reciprocal transcriptional repression of Pax2 and Pax6. *Development* **127,** 4325–4334; 10.1242/dev.127.20.4325 (2000).

47. Nguyen, M. & Arnheiter, H. Signaling and transcriptional regulation in early mammalian eye development: a link between FGF and MITF. *Development* **127,** 3581–3591; 10.1242/dev.127.16.3581 (2000).

48. Horsford, D. J. *et al.* Chx10 repression of Mitf is required for the maintenance of mammalian neuroretinal identity. *Development* **132,** 177–187; 10.1242/dev.01571 (2005).

49. Bumsted, K. M. & Barnstable, C. J. Dorsal retinal pigment epithelium differentiates as neural retina in the microphthalmia (mi/mi) mouse. *Investigative ophthalmology & visual science* **41,** 903–908 (2000).

50. Martinez-Morales, J. R., Signore, M., Acampora, D., Simeone, A. & Bovolenta, P. Otx genes are required for tissue specification in the developing eye. *Development* **128,** 2019–2030; 10.1242/dev.128.11.2019 (2001).

51. Porter, F. D. *et al.* Lhx2, a LIM homeobox gene, is required for eye, forebrain, and definitive erythrocyte development. *Development* **124,** 2935–2944; 10.1242/dev.124.15.2935 (1997).

52. Martinez-Morales, J. R. & Wittbrodt, J. Shaping the vertebrate eye. *Current opinion in genetics & development* **19,** 511–517; 10.1016/j.gde.2009.08.003 (2009).

53. Eiraku, M. *et al.* Self-organizing optic-cup morphogenesis in three-dimensional culture. *Nature* **472,** 51–56; 10.1038/nature09941 (2011).

54. Saint-Geniez, M. & D'Amore, P. A. Development and pathology of the hyaloid, choroidal and retinal vasculature. *The International journal of developmental biology* **48,** 1045–1058; 10.1387/ijdb.041895ms (2004).

55. Servetnick, M. & Grainger, R. M. Changes in neural and lens competence in Xenopus ectoderm: evidence for an autonomous developmental timer. *Development* **112,** 177–188; 10.1242/dev.112.1.177 (1991).

56. Liu, W., Lagutin, O. V., Mende, M., Streit, A. & Oliver, G. Six3 activation of Pax6 expression is essential for mammalian lens induction and specification. *The EMBO journal* **25,** 5383–5395; 10.1038/sj.emboj.7601398 (2006).

57. Kamachi, Y., Uchikawa, M., Tanouchi, A., Sekido, R. & Kondoh, H. Pax6 and SOX2 form a co-DNA-binding partner complex that regulates initiation of lens development. *Genes & development* **15,** 1272–1286; 10.1101/gad.887101 (2001).

58. Henry, J. J. & Grainger, R. M. Early tissue interactions leading to embryonic lens formation in Xenopus laevis. *Developmental biology* **141,** 149–163; 10.1016/0012-1606(90)90110-5 (1990).

59. Graw, J. Eye development. *Current topics in developmental biology* **90,** 343–386; 10.1016/S0070-2153(10)90010-0 (2010).

60. Cvekl, A. & Tamm, E. R. Anterior eye development and ocular mesenchyme: new insights from mouse models and human diseases. *BioEssays : news and reviews in molecular, cellular and developmental biology* **26,** 374–386; 10.1002/bies.20009 (2004).

61. Gollisch, T. & Meister, M. Eye smarter than scientists believed: neural computations in circuits of the retina. *Neuron* **65,** 150–164; 10.1016/j.neuron.2009.12.009 (2010).

62. Reese, B. E. Development of the retina and optic pathway. *Vision Research* **51,** 613–632; 10.1016/j.visres.2010.07.010 (2011).

63. Masland, R. H. The Neuronal Organization of the Retina. *Neuron* **76,** 266–280; 10.1016/j.neuron.2012.10.002 (2012).

64. Strauss, O. The retinal pigment epithelium in visual function. *Physiological reviews* **85,** 845–881; 10.1152/physrev.00021.2004 (2005).

65. Guymer, R., Luthert, P. & Bird, A. Changes in Bruch's membrane and related structures with age. *Progress in Retinal and Eye Research* **18,** 59–90; 10.1016/S1350-9462(98)00012-3 (1999).

66. Bassett, E. A. & Wallace, V. A. Cell fate determination in the vertebrate retina. *Trends in Neurosciences* **35,** 565–573; 10.1016/j.tins.2012.05.004 (2012).

67. Cepko, C. L., Austin, C. P., Yang, X., Alexiades, M. & Ezzeddine, D. Cell fate determination in the vertebrate retina. *Proceedings of the National Academy of Sciences of the United States of America* **93,** 589–595; 10.1073/pnas.93.2.589 (1996).

68. La Vail, M. M., Rapaport, D. H. & Rakic, P. Cytogenesis in the monkey retina. *The Journal of comparative neurology* **309,** 86–114; 10.1002/cne.903090107 (1991).

69. Stiemke, M. M. & Hollyfield, J. G. Cell birthdays in Xenopus laevis retina. *Differentiation; research in biological diversity* **58,** 189–193; 10.1046/j.1432-0436.1995.5830189.x (1995).

70. Livesey, F. J. & Cepko, C. L. Vertebrate neural cell-fate determination: lessons from the retina. *Nat Rev Neurosci* **2,** 109–118; 10.1038/35053522 (2001).

71. Turner, D. L., Snyder, E. Y. & Cepko, C. L. Lineage-independent determination of cell type in the embryonic mouse retina. *Neuron* **4,** 833–845; 10.1016/0896-6273(90)90136-4 (1990).

72. Alexiades, M. R. & Cepko, C. Quantitative analysis of proliferation and cell cycle length during development of the rat retina. *Dev. Dyn.* **205,** 293–307; 10.1002/(SICI)1097-0177(199603)205:3<293::AID-AJA9>3.0.CO;2-D (1996).

73. Cepko, C. Intrinsically different retinal progenitor cells produce specific types of progeny. *Nat Rev Neurosci* **15,** 615–627; 10.1038/nrn3767 (2014).

74. Desai, A. R. & McConnell, S. K. Progressive restriction in fate potential by neural progenitors during cerebral cortical development. *Development* **127,** 2863–2872; 10.1242/dev.127.13.2863 (2000).

75. Austin, C. P., Feldman, D. E., Ida, J. A. & Cepko, C. L. Vertebrate retinal ganglion cells are selected from competent progenitors by the action of Notch. *Development* **121,** 3637–3650; 10.1242/dev.121.11.3637 (1995).

76. Belliveau, M. J., Young, T. L. & Cepko, C. L. Late retinal progenitor cells show intrinsic limitations in the production of cell types and the kinetics of opsin synthesis. *J. Neurosci.* **20,** 2247–2254; 10.1523/JNEUROSCI.20-06-02247.2000 (2000).

77. Lillien, L. & Cepko, C. Control of proliferation in the retina: temporal changes in responsiveness to FGF and TGF alpha. *Development* **115,** 253–266; 10.1242/dev.115.1.253 (1992).

78. Lillien, L. Changes in retinal cell fate induced by overexpression of EGF receptor. *Nature* **377,** 158–162; 10.1038/377158a0 (1995).

79. Marquardt, T. *et al.* Pax6 is required for the multipotent state of retinal progenitor cells. *Cell* **105,** 43–55; 10.1016/S0092-8674(01)00295-1 (2001).

80. Riesenberg, A. N. *et al.* Pax6 regulation of Math5 during mouse retinal neurogenesis. *genesis* **47,** 175–187; 10.1002/dvg.20479 (2009).

81. Brown, N. L., Patel, S., Brzezinski, J. & Glaser, T. Math5 is required for retinal ganglion cell and optic nerve formation. *Development* **128,** 2497–2508; 10.1242/dev.128.13.2497 (2001).

82. Feng, L. *et al.* MATH5 controls the acquisition of multiple retinal cell fates. *Mol Brain* **3,** 36; 10.1186/1756-6606-3-36 (2010).

83. Elliott, J., Jolicoeur, C., Ramamurthy, V. & Cayouette, M. Ikaros confers early temporal competence to mouse retinal progenitor cells. *Neuron* **60,** 26–39; 10.1016/j.neuron.2008.08.008 (2008).

84. Neumann, C. J. & Nuesslein-Volhard, C. Patterning of the zebrafish retina by a wave of sonic hedgehog activity. *Science (New York, N.Y.)* **289,** 2137–2139; 10.1126/science.289.5487.2137 (2000).

85. Mu, X. *et al.* Ganglion cells are required for normal progenitor- cell proliferation but not cell-fate determination or patterning in the developing mouse retina. *Current biology : CB* **15,** 525–530; 10.1016/j.cub.2005.01.043 (2005).

86. Martinez-Morales, J.-R. *et al.* Differentiation of the vertebrate retina is coordinated by an FGF signaling center. *Developmental Cell* **8,** 565–574; 10.1016/j.devcel.2005.01.022 (2005).

87. Belliveau, M. J. & Cepko, C. L. Extrinsic and intrinsic factors control the genesis of amacrine and cone cells in the rat retina. *Development* **126,** 555–566; 10.1242/dev.126.3.555 (1999).

88. Ezzeddine, Z. D., Yang, X., DeChiara, T., Yancopoulos, G. & Cepko, C. L. Postmitotic cells fated to become rod photoreceptors can be respecified by CNTF treatment of the retina. *Development* **124,** 1055–1067; 10.1242/dev.124.5.1055 (1997).

89. Altshuler, D., Lo Turco, J. J., Rush, J. & Cepko, C. Taurine promotes the differentiation of a vertebrate retinal cell type in vitro. *Development* **119,** 1317–1328; 10.1242/dev.119.4.1317 (1993).

90. Sjöqvist, M. & Andersson, E. R. Do as I say, Not(ch) as I do: Lateral control of cell fate. *Developmental biology* **447,** 58–70; 10.1016/j.ydbio.2017.09.032 (2019).

91. Dorsky, R. I., Rapaport, D. H. & Harris, W. A. Xotch inhibits cell differentiation in the xenopus retina. *Neuron* **14,** 487–496; 10.1016/0896-6273(95)90305-4 (1995).

92. Furukawa, T., Mukherjee, S., Bao, Z. Z., Morrow, E. M. & Cepko, C. L. rax, Hes1, and notch1 promote the formation of Müller glia by postnatal retinal progenitor cells. *Neuron* **26,** 383–394; 10.1016/s0896-6273(00)81171-x (2000).

93. Frade, J. Chapter 5 Interkinetic nuclear movement in the vertebrate neuroepithelium: encounters with an old acquaintance. In *Progress in Brain Research : Changing Views of Cajal's Neuron* (Elsevier2002), Vol. 136, pp. 67–71.

94. Sauer, F. C. Mitosis in the neural tube. *Journal of Comparative Neurology* **62,** 377–405; 10.1002/cne.900620207 (1935).

95. Baye, L. M. & Link, B. A. Nuclear migration during retinal development. *Brain Research* **1192,** 29–36; 10.1016/j.brainres.2007.05.021 (2008).

96. Schroer, T. A. Dynactin. *Annual review of cell and developmental biology* **20,** 759–779; 10.1146/annurev.cellbio.20.012103.094623 (2004).

97. Fan, S. S. & Ready, D. F. Glued participates in distinct microtubule-based activities in Drosophila eye development. *Development* **124,** 1497–1507; 10.1242/dev.124.8.1497 (1997).

98. Whited, J. L., Cassell, A., Brouillette, M. & Garrity, P. A. Dynactin is required to maintain nuclear position within postmitotic Drosophila photoreceptor neurons. *Development* **131,** 4677–4686; 10.1242/dev.01366 (2004).

99. Pearson, R. A., Lüneborg, N. L., Becker, D. L. & Mobbs, P. Gap junctions modulate interkinetic nuclear movement in retinal progenitor cells. *J. Neurosci.* **25,** 10803–10814; 10.1523/JNEUROSCI.2312-05.2005 (2005).

100. Baye, L. M. & Link, B. A. The disarrayed mutation results in cell cycle and neurogenesis defects during retinal development in zebrafish. *BMC Dev Biol* **7,** 28; 10.1186/1471-213X-7-28 (2007).

101. Messier, P. E. Microtubules, interkinetic nuclear migration and neurulation. *Experientia* **34,** 289–296; 10.1007/BF01922992 (1978).

102. Malicki, J. Cell fate decisions and patterning in the vertebrate retina: the importance of timing, asymmetry, polarity and waves. *Current Opinion in Neurobiology* **14,** 15–21; 10.1016/j.conb.2004.01.015 (2004).

103. Wozniak, M. A., Modzelewska, K., Kwong, L. & Keely, P. J. Focal adhesion regulation of cell behavior. *Biochimica et biophysica acta* **1692,** 103–119; 10.1016/j.bbamcr.2004.04.007 (2004).

104. Masland, R. H. The fundamental plan of the retina. *Nat Neurosci* **4,** 877–886; 10.1038/nn0901-877 (2001).

105. Roorda, A. & Williams, D. R. The arrangement of the three cone classes in the living human eye. *Nature* **397,** 520–522; 10.1038/17383 (1999).

106. Wässle, H., Puller, C., Müller, F. & Haverkamp, S. Cone contacts, mosaics, and territories of bipolar cells in the mouse retina. *J. Neurosci.* **29,** 106–117; 10.1523/JNEUROSCI.4442-08.2009 (2009).

107. Nawy, S. & Jahr, C. E. Suppression by glutamate of cGMP-activated conductance in retinal bipolar cells. *Nature* **346,** 269–271; 10.1038/346269a0 (1990).

108. Nawy, S. & Jahr, C. E. cGMP-gated conductance in retinal bipolar cells is suppressed by the photoreceptor transmitter. *Neuron* **7,** 677–683; 10.1016/0896-6273(91)90380-i (1991).

109. MacNeil, M. A. & Masland, R. H. Extreme diversity among amacrine cells: implications for function. *Neuron* **20,** 971–982; 10.1016/S0896-6273(00)80478-X (1998).

110. Vaney, D. I. Patterns of neuronal coupling in the retina. *Progress in Retinal and Eye Research* **13,** 301–355; 10.1016/1350-9462(94)90014-0 (1994).

111. Witkovsky, P. & Dearry, A. Chapter 10 Functional roles of dopamine in the vertebrate retina. *Progress in Retinal Research* **11,** 247–292; 10.1016/0278-4327(91)90031-V (1991).

112. Hoon, M., Okawa, H., Della Santina, L. & Wong, R. O. L. Functional architecture of the retina: development and disease. *Progress in Retinal and Eye Research* **42,** 44–84; 10.1016/j.preteyeres.2014.06.003 (2014).

113. Trojan, P. *et al.* Centrins in retinal photoreceptor cells: regulators in the connecting cilium. *Progress in Retinal and Eye Research* **27,** 237–259; 10.1016/j.preteyeres.2008.01.003 (2008).

114. Luo, D.-G., Xue, T. & Yau, K.-W. How vision begins: an odyssey. *Proceedings of the National Academy of Sciences of the United States of America* **105,** 9855–9862; 10.1073/pnas.0708405105 (2008).

115. Swaroop, A., Kim, D. & Forrest, D. Transcriptional regulation of photoreceptor development and homeostasis in the mammalian retina. *Nat Rev Neurosci* **11,** 563–576; 10.1038/nrn2880 (2010).

116. Nathans, J., Thomas, D. & Hogness, D. S. Molecular genetics of human color vision: the genes encoding blue, green, and red pigments. *Science (New York, N.Y.)* **232,** 193–202; 10.1126/science.2937147 (1986).

117. Deeb, S. S. Genetics of variation in human color vision and the retinal cone mosaic. *Current opinion in genetics & development* **16,** 301–307; 10.1016/j.gde.2006.04.002 (2006).

118. Nishida, A. *et al.* Otx2 homeobox gene controls retinal photoreceptor cell fate and pineal gland development. *Nature neuroscience* **6,** 1255–1263; 10.1038/nn1155 (2003).

119. Koike, C. *et al.* Functional roles of Otx2 transcription factor in postnatal mouse retinal development. *Molecular and cellular biology* **27,** 8318–8329; 10.1128/MCB.01209-07 (2007).

120. Furukawa, T., Morrow, E. M. & Cepko, C. L. Crx, a novel otx-like homeobox gene, shows photoreceptor-specific expression and regulates photoreceptor differentiation. *Cell* **91,** 531–541; 10.1016/S0092-8674(00)80439-0 (1997).

121. Furukawa, T., Morrow, E. M., Li, T., Davis, F. C. & Cepko, C. L. Retinopathy and attenuated circadian entrainment in Crx-deficient mice. *Nature genetics* **23,** 466–470; 10.1038/70591 (1999).

122. Hennig, A. K., Peng, G.-H. & Chen, S. Regulation of photoreceptor gene expression by Crx-associated transcription factor network. *Brain Research* **1192,** 114–133; 10.1016/j.brainres.2007.06.036 (2008).

123. Mitton, K. P. *et al.* The leucine zipper of NRL interacts with the CRX homeodomain. A possible mechanism of transcriptional synergy in rhodopsin regulation. *Journal of Biological Chemistry* **275,** 29794–29799; 10.1074/jbc.M003658200 (2000).

124. Oh, E. C. T. *et al.* Rod differentiation factor NRL activates the expression of nuclear receptor NR2E3 to suppress the development of cone photoreceptors. *Brain Research* **1236,** 16–29; 10.1016/j.brainres.2008.01.028 (2008).

125. Chen, J., Rattner, A. & Nathans, J. The rod photoreceptor-specific nuclear receptor Nr2e3 represses transcription of multiple cone-specific genes. *J. Neurosci.* **25,** 118–129; 10.1523/JNEUROSCI.3571-04.2005 (2005).

126. Cheng, H. *et al.* In vivo function of the orphan nuclear receptor NR2E3 in establishing photoreceptor identity during mammalian retinal development. *Hum Mol Genet* **15,** 2588–2602; 10.1093/hmg/ddl185 (2006).

127. Peng, G.-H., Ahmad, O., Ahmad, F., Liu, J. & Chen, S. The photoreceptor-specific nuclear receptor Nr2e3 interacts with Crx and exerts opposing effects on the transcription of rod versus cone genes. *Hum Mol Genet* **14,** 747–764; 10.1093/hmg/ddi070 (2005).

128. Jia, L. *et al.* Retinoid-related orphan nuclear receptor RORbeta is an early-acting factor in rod photoreceptor development. *Proceedings of the National Academy of Sciences of the United States of America* **106,** 17534–17539; 10.1073/pnas.0902425106 (2009).

129. Srinivas, M., Ng, L., Liu, H., Jia, L. & Forrest, D. Activation of the blue opsin gene in cone photoreceptor development by retinoid-related orphan receptor beta. *Mol Endocrinol* **20,** 1728–1741; 10.1210/me.2005-0505 (2006).

130. Ng, L. *et al.* A thyroid hormone receptor that is required for the development of green cone photoreceptors. *Nature genetics* **27,** 94–98; 10.1038/83829 (2001).

131. Wang, Y. *et al.* A locus control region adjacent to the human red and green visual pigment genes. *Neuron* **9,** 429–440; 10.1016/0896-6273(92)90181-C (1992).

132. Smallwood, P. M., Wang, Y. & Nathans, J. Role of a locus control region in the mutually exclusive expression of human red and green cone pigment genes. *Proceedings of the National Academy of Sciences of the United States of America* **99,** 1008–1011; 10.1073/pnas.022629799 (2002).

133. Khanna, H. *et al.* Retinoic Acid Regulates the Expression of Photoreceptor Transcription Factor NRL. *Journal of Biological Chemistry* **281,** 27327–27334; 10.1074/jbc.M605500200 (2006).

134. LaVail, M. M. *et al.* Protection of mouse photoreceptors by survival factors in retinal degenerations. *Investigative ophthalmology & visual science* **39,** 592–602 (1998).

135. Rhee, K. D., Goureau, O., Chen, S. & Yang, X.-J. Cytokine-induced activation of signal transducer and activator of transcription in photoreceptor precursors regulates rod differentiation in the developing mouse retina. *J. Neurosci.* **24,** 9779–9788; 10.1523/JNEUROSCI.1785-04.2004 (2004).

136. Arshavsky, V. Y., Lamb, T. D. & Pugh, E. N. G proteins and phototransduction. *Annu. Rev. Physiol.* **64,** 153–187; 10.1146/annurev.physiol.64.082701.102229 (2002).

137. Koutalos, Y. & Ebrey, T. G. Recent progress in vertebrate photoreception. *Photochemistry and photobiology* **44,** 809–817; 10.1111/j.1751-1097.1986.tb05541.x (1986).

138. Yingbin Fu. Phototransduction in Rods and Cones. In *Webvision: The Organization of the Retina and Visual System [Internet],* edited by Y. Fu (University of Utah Health Sciences Center2010).

139. Fain, G. L., Hardie, R. & Laughlin, S. B. Phototransduction and the evolution of photoreceptors. *Current biology : CB* **20,** R114-24; 10.1016/j.cub.2009.12.006 (2010).

140. Dacheux, R. F. & Miller, R. F. Photoreceptor-bipolar cell transmission in the perfused retina eyecup of the mudpuppy. *Science (New York, N.Y.)* **191,** 963–964; 10.1126/science.175443 (1976).

141. Chen, C. K., Inglese, J., Lefkowitz, R. J. & Hurley, J. B. Ca(2+)-dependent interaction of recoverin with rhodopsin kinase. *Journal of Biological Chemistry* **270,** 18060–18066; 10.1074/jbc.270.30.18060 (1995).

142. Klenchin, V. A., Calvert, P. D. & Bownds, M. D. Inhibition of rhodopsin kinase by recoverin. Further evidence for a negative feedback system in phototransduction. *Journal of Biological Chemistry* **270,** 16147–16152; 10.1074/jbc.270.27.16147 (1995).

143. Kühn, H. & Wilden, U. Deactivation of photoactivated rhodopsin by rhodopsin-kinase and arrestin. *Journal of receptor research* **7,** 283–298; 10.3109/10799898709054990 (1987).

144. Fain, G. L., Matthews, H. R., Cornwall, M. C. & Koutalos, Y. Adaptation in vertebrate photoreceptors. *Physiological reviews* **81,** 117–151; 10.1152/physrev.2001.81.1.117 (2001).

145. Kutuzov, M. A. & Bennett, N. Calcium-activated opsin phosphatase activity in retinal rod outer segments. *European Journal of Biochemistry* **238,** 613–622; 10.1111/j.1432-1033.1996.0613w.x (1996).

146. Klumpp, S. *et al.* Protein phosphatase type-2C isozymes present in vertebrate retinae: Purification, characterization, and localization in photoreceptors. *J. Neurosci. Res.* **51,** 328–338; 10.1002/(SICI)1097-4547(19980201)51:3<328::AID-JNR6>3.0.CO;2-I (1998).

147. Yang, S. D., Benovic, J. L., Fong, Y. L., Caron, M. G. & Lefkowitz, R. J. Cyclic phosphorylation-dephosphorylation of rhodopsin in retina by protein kinase FA (the activator of ATP.Mg-dependent protein phosphatase). *Biochemical and Biophysical Research Communications* **178,** 1306–1311; 10.1016/0006-291x(91)91036-c (1991).

148. Hsieh, C.-L., Yao, Y., Gurevich, V. V. & Chen, J. Arrestin Facilitates Rhodopsin Dephosphorylation in Vivo. *J. Neurosci.* **42,** 3537–3545; 10.1523/JNEUROSCI.0141-22.2022 (2022).

149. Bok, D. The retinal pigment epithelium: a versatile partner in vision. *Journal of cell science. Supplement* **17,** 189–195; 10.1242/jcs.1993.Supplement_17.27 (1993).

150. Hamann, S. Molecular mechanisms of water transport in the eye. In *International Review of Cytology : Molecular Mechanisms of Water Transport Across Biological Membranes* (Academic Press2002), Vol. 215, pp. 395–431.

151. La Dornonville de Cour, M. Ion transport in the retinal pigment epithelium. A study with double barrelled ion-selective microelectrodes. *Acta ophthalmologica. Supplement,* 1–32 (1993).

152. Boulton, M. & Dayhaw-Barker, P. The role of the retinal pigment epithelium: topographical variation and ageing changes. *Eye (London, England)* **15,** 384–389; 10.1038/eye.2001.141 (2001).

153. Miesfeld, J. B. & Brown, N. L. Eye organogenesis: A hierarchical view of ocular development. *Current topics in developmental biology* **132,** 351–393; 10.1016/bs.ctdb.2018.12.008 (2019).

154. Bharti, K., Liu, W., Csermely, T., Bertuzzi, S. & Arnheiter, H. Alternative promoter use in eye development: the complex role and regulation of the transcription factor MITF. *Development* **135,** 1169–1178; 10.1242/dev.014142 (2008).

155. Westenskow, P., Piccolo, S. & Fuhrmann, S. Beta-catenin controls differentiation of the retinal pigment epithelium in the mouse optic cup by regulating Mitf and Otx2 expression. *Development* **136,** 2505–2510; 10.1242/dev.032136 (2009).

156. Fujimura, N., Taketo, M. M., Mori, M., Korinek, V. & Kozmik, Z. Spatial and temporal regulation of Wnt/beta-catenin signaling is essential for development of the retinal pigment epithelium. *Developmental biology* **334,** 31–45; 10.1016/j.ydbio.2009.07.002 (2009).

157. Hägglund, A.-C., Berghard, A. & Carlsson, L. Canonical Wnt/β-catenin signalling is essential for optic cup formation. *PLOS ONE* **8,** e81158; 10.1371/journal.pone.0081158 (2013).

158. Kim, J. Y. *et al.* Yap is essential for retinal progenitor cell cycle progression and RPE cell fate acquisition in the developing mouse eye. *Developmental biology* **419,** 336–347; 10.1016/j.ydbio.2016.09.001 (2016).

159. Steinfeld, J. *et al.* RPE specification in the chick is mediated by surface ectoderm-derived BMP and Wnt signalling. *Development* **140,** 4959–4969; 10.1242/dev.096990 (2013).

160. Saari, J. C. & Bredberg, D. L. Purification of cellular retinaldehyde-binding protein from bovine retina and retinal pigment epithelium. *Experimental Eye Research* **46,** 569–578; 10.1016/S0014-4835(88)80013-7 (1988).

161. Mendelsohn, C., Ruberte, E., LeMeur, M., Morriss-Kay, G. & Chambon, P. Developmental analysis of the retinoic acid-inducible RAR-beta 2 promoter in transgenic animals. *Development* **113,** 723–734; 10.1242/dev.113.3.723 (1991).

162. Gonzalez-Fernandez, F. Interphotoreceptor retinoid-binding protein--an old gene for new eyes. *Vision Research* **43,** 3021–3036; 10.1016/j.visres.2003.09.019 (2003).

163. Raviv, S. *et al.* PAX6 regulates melanogenesis in the retinal pigmented epithelium through feed-forward regulatory interactions with MITF. *PLOS Genetics* **10,** e1004360; 10.1371/journal.pgen.1004360 (2014).

164. Cavodeassi, F. & Bovolenta, P. New functions for old genes: Pax6 and Mitf in eye pigment biogenesis. *Pigment Cell & Melanoma Research* **27,** 1005–1007; 10.1111/pcmr.12308 (2014).

165. Dakubo, G. D. *et al.* Indian hedgehog signaling from endothelial cells is required for sclera and retinal pigment epithelium development in the mouse eye. *Developmental biology* **320,** 242–255; 10.1016/j.ydbio.2008.05.528 (2008).

166. Perron, M. *et al.* A novel function for Hedgehog signalling in retinal pigment epithelium differentiation. *Development* **130,** 1565–1577; 10.1242/dev.00391 (2003).

167. Masuda, T. & Esumi, N. SOX9, through interaction with microphthalmia-associated transcription factor (MITF) and OTX2, regulates BEST1 expression in the retinal pigment epithelium. *The Journal of biological chemistry* **285,** 26933–26944; 10.1074/jbc.M110.130294 (2010).

168. Masuda, T. *et al.* Transcription factor SOX9 plays a key role in the regulation of visual cycle gene expression in the retinal pigment epithelium. *The Journal of biological chemistry* **289,** 12908–12921; 10.1074/jbc.M114.556738 (2014).

169. Bakall, B. *et al.* Expression and localization of bestrophin during normal mouse development. *Invest. Ophthalmol. Vis. Sci.* **44,** 3622–3628; 10.1167/iovs.03-0030 (2003).

170. Marmorstein, A. D. The polarity of the retinal pigment epithelium. *Traffic* **2,** 867–872; 10.1034/j.1600-0854.2001.21202.x (2001).

171. Bonilha, V. L., Finnemann, S. C. & Rodriguez-Boulan, E. Ezrin promotes morphogenesis of apical microvilli and basal infoldings in retinal pigment epithelium. *J Cell Biol* **147,** 1533–1548; 10.1083/jcb.147.7.1533 (1999).

172. Rizzolo, L. J. Polarity and the development of the outer blood-retinal barrier. *Histology and histopathology* **12,** 1057–1067 (1997).

173. Rahner, C., Fukuhara, M., Peng, S., Kojima, S. & Rizzolo, L. J. The apical and basal environments of the retinal pigment epithelium regulate the maturation of tight junctions during development. *J Cell Sci* **117,** 3307–3318; 10.1242/jcs.01181 (2004).

174. Chihara, E. & Nao-i, N. Resorption of subretinal fluid by transepithelial flow of the retinal pigment epithelium. *Graefe's archive for clinical and experimental ophthalmology = Albrecht von Graefes Archiv fur klinische und experimentelle Ophthalmologie* **223,** 202–204; 10.1007/BF02174060 (1985).

175. Hamann, S. *et al.* Aquaporins in complex tissues: distribution of aquaporins 1-5 in human and rat eye. *The American journal of physiology* **274,** C1332-45; 10.1152/ajpcell.1998.274.5.C1332 (1998).

176. Adler, A. J. & Southwick, R. E. Distribution of glucose and lactate in the interphotoreceptor matrix. *ORE* **24,** 243–252; 10.1159/000267174 (1992).

177. Ban, Y. & Rizzolo, L. J. Regulation of glucose transporters during development of the retinal pigment epithelium. *Developmental Brain Research* **121,** 89–95; 10.1016/S0165-3806(00)00028-6 (2000).

178. Pfeffer, B. A., Clark, V. M., Flannery, J. G. & Bok, D. Membrane receptors for retinol-binding protein in cultured human retinal pigment epithelium. *Investigative ophthalmology & visual science* **27,** 1031–1040 (1986).

179. Steinberg, R. H. Interactions between the retinal pigment epithelium and the neural retina. *Doc Ophthalmol* **60,** 327–346; 10.1007/BF00158922 (1985).

180. Snodderly, D. M., Sandstrom, M. M., Leung, I. Y.-F., Zucker, C. L. & Neuringer, M. Retinal pigment epithelial cell distribution in central retina of rhesus monkeys. *Investigative ophthalmology & visual science* **43,** 2815–2818 (2002).

181. Boulton, M., Moriarty, P., Jarvis-Evans, J. & Marcyniuk, B. Regional variation and age-related changes of lysosomal enzymes in the human retinal pigment epithelium. *The British journal of ophthalmology* **78,** 125–129; 10.1136/bjo.78.2.125 (1994).

182. Hayasaka, S., Shiono, T., Hara, S. & Mizuno, K. Regional distribution of lysosomal enzymes in the retina and choroid of human eyes. *Albrecht von Graefes Archiv fur klinische und experimentelle Ophthalmologie. Albrecht von Graefe's archive for clinical and experimental ophthalmology* **216,** 269–273; 10.1007/BF00455034 (1981).

183. Tanihara, H., Inatani, M. & Honda, Y. Growth factors and their receptors in the retina and pigment epithelium. *Progress in Retinal and Eye Research* **16,** 271–301; 10.1016/S1350-9462(96)00028-6 (1997).

184. Witmer, A. N., Vrensen, G. F. J. M., van Noorden, C. J. F. & Schlingemann, R. O. Vascular endothelial growth factors and angiogenesis in eye disease. *Progress in Retinal and Eye Research* **22,** 1–29; 10.1016/S1350-9462(02)00043-5 (2003).

185. Steele, F. R., Chader, G. J., Johnson, L. V. & Tombran-Tink, J. Pigment epithelium-derived factor: neurotrophic activity and identification as a member of the serine protease inhibitor gene family. *Proceedings of the National Academy of Sciences of the United States of America* **90,** 1526–1530; 10.1073/pnas.90.4.1526 (1993).

186. Cao, W. *et al.* In vivo protection of photoreceptors from light damage by pigment epithelium-derived factor. *Investigative ophthalmology & visual science* **42,** 1646–1652 (2001).

187. Adamis, A. P. *et al.* Synthesis and secretion of vascular permeability factor/vascular endothelial growth factor by human retinal pigment epithelial cells. *Biochemical and Biophysical Research Communications* **193,** 631–638; 10.1006/bbrc.1993.1671 (1993).

188. Frank, R. N. Growth factors in age-related macular degeneration: pathogenic and therapeutic implications. *ORE* **29,** 341–353; 10.1159/000268032 (1997).

189. Alm, A. & Bill, A. The oxygen supply to the retina. II. Effects of high intraocular pressure and of increased arterial carbon dioxide tension on uveal and retinal blood flow in cats. A study with radioactively labelled microspheres including flow determinations in brain and some other tissues. *Acta Physiologica Scandinavica* **84,** 306–319; 10.1111/j.1748-1716.1972.tb05182.x (1972).

190. Miceli, M. V., Liles, M. R. & Newsome, D. A. Evaluation of oxidative processes in human pigment epithelial cells associated with retinal outer segment phagocytosis. *Experimental Cell Research* **214,** 242–249; 10.1006/excr.1994.1254 (1994).

191. *The role of melanin in the RPE* (1998).

192. Handelman, G. J., Dratz, E. A., Reay, C. C. & van Kuijk, J. G. Carotenoids in the human macula and whole retina. *Investigative ophthalmology & visual science* **29,** 850–855 (1988).

193. Handelman, G. J., Max Snodderly, D., Adler, A. J., Russett, M. D. & Dratz, E. A. [19] Measurement of carotenoids in human and monkey retinas. In *Methods in Enzymology : Oxidants and Antioxidants Part A* (Academic Press1999), Vol. 213, pp. 220–230.

194. Landrum, J. T., Bone, R. A., Moore, L. L. & Gomez, C. M. [40] Analysis of zeaxanthin distribution within individual human retinas. In *Methods in Enzymology : Oxidants and Antioxidants Part A* (Academic Press1999), Vol. 299, pp. 457–467.

195. Rózanowska, M. *et al.* Blue light-induced reactivity of retinal age pigment. In vitro generation of oxygen-reactive species. *Journal of Biological Chemistry* **270,** 18825–18830; 10.1074/jbc.270.32.18825 (1995).

196. Sparrow, J. R., Nakanishi, K. & Parish, C. A. The lipofuscin fluorophore A2E mediates blue light-induced damage to retinal pigmented epithelial cells. *Investigative ophthalmology & visual science* **41,** 1981–1989 (2000).

197. Beatty, S., Koh, H., Phil, M., Henson, D. & Boulton, M. The role of oxidative stress in the pathogenesis of age-related macular degeneration. *Survey of Ophthalmology* **45,** 115–134; 10.1016/S0039-6257(00)00140-5 (2000).

198. Newsome, D. A., Miceli, M. V., Liles, M. R., Tate, D. J. & Oliver, P. D. Antioxidants in the retinal pigment epithelium. *Progress in Retinal and Eye Research* **13,** 101–123; 10.1016/1350-9462(94)90006-X (1994).

199. Newsome, D. A., Dobard, E. P., Liles, M. R. & Oliver, P. D. Human retinal pigment epithelium contains two distinct species of superoxide dismutase. *Investigative ophthalmology & visual science* **31,** 2508–2513 (1990).

200. Tate, D. J., Miceli, M. V. & Newsome, D. A. Phagocytosis and H2O2 induce catalase and metallothionein gene expression in human retinal pigment epithelial cells. *Investigative ophthalmology & visual science* **36,** 1271–1279 (1995).

201. Nguyen-Legros, J. & Hicks, D. Renewal of photoreceptor outer segments and their phagocytosis by theretinal pigment epithelium. In *International Review of Cytology : Molecular Mechanisms of Water Transport Across Biological Membranes* (Academic Press2002), Vol. 196, pp. 245–313.

202. Gao, H. & Hollyfield, J. G. Aging of the human retina. Differential loss of neurons and retinal pigment epithelial cells. *Investigative ophthalmology & visual science* **33,** 1–17 (1992).

203. Young, R. W. Shedding of discs from rod outer segments in the rhesus monkey. *Journal of Ultrastructure Research* **34,** 190–203; 10.1016/S0022-5320(71)90014-1 (1971).

204. Finnemann, S. C., Bonilha, V. L., Marmorstein, A. D. & Rodriguez-Boulan, E. Phagocytosis of rod outer segments by retinal pigment epithelial cells requires alpha(v)beta5 integrin for binding but not for internalization. *Proceedings of the National Academy of Sciences of the United States of America* **94,** 12932–12937; 10.1073/pnas.94.24.12932 (1997).

205. Finnemann, S. C. Focal adhesion kinase signaling promotes phagocytosis of integrin-bound photoreceptors. *The EMBO journal* **22,** 4143–4154; 10.1093/emboj/cdg416 (2003).

206. Feng, W., Yasumura, D., Matthes, M. T., LaVail, M. M. & Vollrath, D. Mertk triggers uptake of photoreceptor outer segments during phagocytosis by cultured retinal pigment epithelial cells. *Journal of Biological Chemistry* **277,** 17016–17022; 10.1074/jbc.M107876200 (2002).

207. Hall, M. O. & Abrams, T. Kinetic studies of rod outer segment binding and ingestion by cultured rat RPE cells. *Experimental Eye Research* **45,** 907–922; 10.1016/S0014-4835(87)80105-7 (1987).

208. Finnemann, S. C. & Silverstein, R. L. Differential roles of CD36 and alphavbeta5 integrin in photoreceptor phagocytosis by the retinal pigment epithelium. *J Exp Med* **194,** 1289–1298; 10.1084/jem.194.9.1289 (2001).

209. Xue, L., Gollapalli, D. R., Maiti, P., Jahng, W. J. & Rando, R. R. A palmitoylation switch mechanism in the regulation of the visual cycle. *Cell* **117,** 761–771; 10.1016/j.cell.2004.05.016 (2004).

210. Nicoletti, A. *et al.* Molecular characterization of the human gene encoding an abundant 61 kDa protein specific to the retinal pigment epithelium. *Hum Mol Genet* **4,** 641–649; 10.1093/hmg/4.4.641 (1995).

211. Redmond, T. M. *et al.* Rpe65 is necessary for production of 11-cis-vitamin A in the retinal visual cycle. *Nature genetics* **20,** 344–351; 10.1038/3813 (1998).

212. Jang, G. F. *et al.* Characterization of a dehydrogenase activity responsible for oxidation of 11-cis-retinol in the retinal pigment epithelium of mice with a disrupted RDH5 gene. A model for the human hereditary disease fundus albipunctatus. *Journal of Biological Chemistry* **276,** 32456–32465; 10.1074/jbc.M104949200 (2001).

213. Saari, J. C. *et al.* Visual cycle impairment in cellular retinaldehyde binding protein (CRALBP) knockout mice results in delayed dark adaptation. *Neuron* **29,** 739–748; 10.1016/S0896-6273(01)00248-3 (2001).

214. Joshi, R., Sipani, R. & Bakshi, A. Roles of Drosophila Hox Genes in the Assembly of Neuromuscular Networks and Behavior. *Front. Cell Dev. Biol.* **9,** 786993; 10.3389/fcell.2021.786993 (2021).

215. Lui, J. H., Hansen, D. V. & Kriegstein, A. R. Development and evolution of the human neocortex. *Cell* **146,** 18–36; 10.1016/j.cell.2011.06.030 (2011).

216. Sanoh, S. *et al.* Predictability of metabolism of ibuprofen and naproxen using chimeric mice with human hepatocytes. *Drug metabolism and disposition: the biological fate of chemicals* **40,** 2267–2272; 10.1124/dmd.112.047555 (2012).

217. Duval, K. *et al.* Modeling Physiological Events in 2D vs. 3D Cell Culture. *Physiology (Bethesda, Md.)* **32,** 266–277; 10.1152/physiol.00036.2016 (2017).

218. Maqsood, M. I., Matin, M. M., Bahrami, A. R. & Ghasroldasht, M. M. Immortality of cell lines: challenges and advantages of establishment. *Cell Biology International* **37,** 1038–1045; 10.1002/cbin.10137 (2013).

219. Schutgens, F. & Clevers, H. Human Organoids: Tools for Understanding Biology and Treating Diseases. *Annual review of pathology* **15,** 211–234; 10.1146/annurev-pathmechdis-012419-032611 (2020).

220. Martin, G. R. Isolation of a pluripotent cell line from early mouse embryos cultured in medium conditioned by teratocarcinoma stem cells. *Proceedings of the National Academy of Sciences of the United States of America* **78,** 7634–7638; 10.1073/pnas.78.12.7634 (1981).

221. Thomson, J. A. *et al.* Embryonic stem cell lines derived from human blastocysts. *Science (New York, N.Y.)* **282,** 1145–1147; 10.1126/science.282.5391.1145 (1998).

222. Takahashi, K. & Yamanaka, S. Induction of pluripotent stem cells from mouse embryonic and adult fibroblast cultures by defined factors. *Cell* **126,** 663–676; 10.1016/j.cell.2006.07.024 (2006).

223. Takahashi, K. *et al.* Induction of pluripotent stem cells from adult human fibroblasts by defined factors. *Cell* **131,** 861–872; 10.1016/j.cell.2007.11.019 (2007).

224. Lancaster, M. A. & Knoblich, J. A. Organogenesis in a dish: modeling development and disease using organoid technologies. *Science (New York, N.Y.)* **345,** 1247125; 10.1126/science.1247125 (2014).

225. Huch, M., Knoblich, J. A., Lutolf, M. P. & Martinez-Arias, A. The hope and the hype of organoid research. *Development* **144,** 938–941; 10.1242/dev.150201 (2017).

226. Kim, J., Koo, B.-K. & Knoblich, J. A. Human organoids: model systems for human biology and medicine. *Nat Rev Mol Cell Biol* **21,** 571–584; 10.1038/s41580-020-0259-3 (2020).

227. Sato, T. *et al.* Single Lgr5 stem cells build crypt-villus structures in vitro without a mesenchymal niche. *Nature* **459,** 262–265; 10.1038/nature07935 (2009).

228. van de Wetering, M. *et al.* Prospective derivation of a living organoid biobank of colorectal cancer patients. *Cell* **161,** 933–945; 10.1016/j.cell.2015.03.053 (2015).

229. Huch, M. *et al.* Long-term culture of genome-stable bipotent stem cells from adult human liver. *Cell* **160,** 299–312; 10.1016/j.cell.2014.11.050 (2015).

230. Lancaster, M. A. *et al.* Cerebral organoids model human brain development and microcephaly. *Nature* **501,** 373–379; 10.1038/nature12517 (2013).

231. Berkers, G. *et al.* Rectal Organoids Enable Personalized Treatment of Cystic Fibrosis. *Cell Reports* **26,** 1701-1708.e3; 10.1016/j.celrep.2019.01.068 (2019).

232. Dekkers, J. F. *et al.* Characterizing responses to CFTR-modulating drugs using rectal organoids derived from subjects with cystic fibrosis. *Science translational medicine* **8,** 344ra84; 10.1126/scitranslmed.aad8278 (2016).

233. Kuwahara, A. *et al.* Generation of a ciliary margin-like stem cell niche from self-organizing human retinal tissue. *Nat Commun* **6,** 6286; 10.1038/ncomms7286 (2015).

234. Nakano, T. *et al.* Self-formation of optic cups and storable stratified neural retina from human ESCs. *Cell Stem Cell* **10,** 771–785; 10.1016/j.stem.2012.05.009 (2012).

235. Singh, R. K. *et al.* Characterization of Three-Dimensional Retinal Tissue Derived from Human Embryonic Stem Cells in Adherent Monolayer Cultures. *Stem cells and development* **24,** 2778–2795; 10.1089/scd.2015.0144 (2015).

236. Reichman, S. *et al.* From confluent human iPS cells to self-forming neural retina and retinal pigmented epithelium. *Proceedings of the National Academy of Sciences of the United States of America* **111,** 8518–8523; 10.1073/pnas.1324212111 (2014).

237. Zhong, X. *et al.* Generation of three-dimensional retinal tissue with functional photoreceptors from human iPSCs. *Nat Commun* **5,** 4047; 10.1038/ncomms5047 (2014).

238. Sridhar, A. *et al.* Single-Cell Transcriptomic Comparison of Human Fetal Retina, hPSC-Derived Retinal Organoids, and Long-Term Retinal Cultures. *Cell Reports* **30,** 1644-1659.e4; 10.1016/j.celrep.2020.01.007 (2020).

239. Cowan, C. S. *et al.* Cell Types of the Human Retina and Its Organoids at Single-Cell Resolution. *Cell* **182,** 1623-1640.e34; 10.1016/j.cell.2020.08.013 (2020).

240. Wahlin, K. J. *et al.* Photoreceptor Outer Segment-like Structures in Long-Term 3D Retinas from Human Pluripotent Stem Cells. *Sci Rep* **7,** 766; 10.1038/s41598-017-00774-9 (2017).

241. Cora, V. *et al.* A Cleared View on Retinal Organoids. *Cells* **8,** 391; 10.3390/cells8050391 (2019).

242. O'Hara-Wright, M. & Gonzalez-Cordero, A. Retinal organoids: a window into human retinal development. *Development* **147**; 10.1242/dev.189746 (2020).

243. Kaewkhaw, R. *et al.* Transcriptome Dynamics of Developing Photoreceptors in Three-Dimensional Retina Cultures Recapitulates Temporal Sequence of Human Cone and Rod Differentiation Revealing Cell Surface Markers and Gene Networks. *Stem cells (Dayton, Ohio)* **33,** 3504–3518; 10.1002/stem.2122 (2015).

244. Kallman, A. *et al.* Investigating cone photoreceptor development using patient-derived NRL null retinal organoids. *Communications biology* **3,** 82; 10.1038/s42003-020-0808-5 (2020).

245. Phillips, M. J. *et al.* Modeling human retinal development with patient-specific induced pluripotent stem cells reveals multiple roles for visual system homeobox 2. *Stem cells (Dayton, Ohio)* **32,** 1480–1492; 10.1002/stem.1667 (2014).

246. Achberger, K. *et al.* Merging organoid and organ-on-a-chip technology to generate complex multi-layer tissue models in a human retina-on-a-chip platform. *eLife* **8**; 10.7554/eLife.46188 (2019).

247. Iwasaki, Y. *et al.* Differentiation/Purification Protocol for Retinal Pigment Epithelium from Mouse Induced Pluripotent Stem Cells as a Research Tool. *PLOS ONE* **11,** e0158282; 10.1371/journal.pone.0158282 (2016).

248. Kai Richler. Differentiation of retinal pigment epithelium from mouse embryonic stem cells. Master thesis. Karlsruher Institut für Technologie, 2019.

249. Capowski, E. E. *et al.* Reproducibility and staging of 3D human retinal organoids across multiple pluripotent stem cell lines. *Development* **146**; 10.1242/dev.171686 (2019).

250. Kilpinen, H. *et al.* Common genetic variation drives molecular heterogeneity in human iPSCs. *Nature* **546,** 370–375; 10.1038/nature22403 (2017).

251. Williams, R. L. *et al.* Myeloid leukaemia inhibitory factor maintains the developmental potential of embryonic stem cells. *Nature* **336,** 684–687; 10.1038/336684a0 (1988).

252. Smith, A. G. *et al.* Inhibition of pluripotential embryonic stem cell differentiation by purified polypeptides. *Nature* **336,** 688–690; 10.1038/336688a0 (1988).

253. Burdon, T., Stracey, C., Chambers, I., Nichols, J. & Smith, A. Suppression of SHP-2 and ERK signalling promotes self-renewal of mouse embryonic stem cells. *Developmental biology* **210,** 30–43; 10.1006/dbio.1999.9265 (1999).

254. Weinberger, L., Ayyash, M., Novershtern, N. & Hanna, J. H. Dynamic stem cell states: naive to primed pluripotency in rodents and humans. *Nat Rev Mol Cell Biol* **17,** 155–169; 10.1038/nrm.2015.28 (2016).

255. Hanna, J. *et al.* Metastable pluripotent states in NOD-mouse-derived ESCs. *Cell Stem Cell* **4,** 513–524; 10.1016/j.stem.2009.04.015 (2009).

256. Kawasaki, H. *et al.* Induction of midbrain dopaminergic neurons from ES cells by stromal cell-derived inducing activity. *Neuron* **28,** 31–40; 10.1016/S0896-6273(00)00083-0 (2000).

257. CELL SEARCH SYSTEM -CELL BANK- (RIKEN BRC) [AES0145 : Rx-GFP K/I EB5]. Available at https://cellbank.brc.riken.jp/cell_bank/CellInfo/?cellNo=AES0145&lang=En (2022).

258. Völkner, M. *et al.* Retinal Organoids from Pluripotent Stem Cells Efficiently Recapitulate Retinogenesis. *Stem Cell Reports* **6,** 525–538; 10.1016/j.stemcr.2016.03.001 (2016).

259. Stephan Keppler. Differentiation and Cultivation of Retinal Cells in a Defined 3D Environment. Doctoral thesis. Karlsruher Institut für Technologie, 2021.

260. Hudson, C., Darras, S., Caillol, D., Yasuo, H. & Lemaire, P. A conserved role for the MEK signalling pathway in neural tissue specification and posteriorisation in the invertebrate chordate, the ascidian Ciona intestinalis. *Development* **130,** 147–159; 10.1242/dev.00200 (2003).

261. Kyriakis, J. M. & Avruch, J. Mammalian MAPK signal transduction pathways activated by stress and inflammation: a 10-year update. *Physiological reviews* **92,** 689–737; 10.1152/physrev.00028.2011 (2012).

262. Kudoh, T., Wilson, S. W. & Dawid, I. B. Distinct roles for Fgf, Wnt and retinoic acid in posteriorizing the neural ectoderm. *Development* **129,** 4335–4346; 10.1242/dev.129.18.4335 (2002).

263. Vukicevic, S. *et al.* Identification of multiple active growth factors in basement membrane Matrigel suggests caution in interpretation of cellular activity related to extracellular matrix components. *Experimental Cell Research* **202,** 1–8; 10.1016/0014-4827(92)90397-q (1992).

264. Matrigel Matrix | Extracellular Matrix | Corning. Available at https://www.corning.com/emea/de/products/life-sciences/products/surfaces/matrigel-matrix.html (2022).

265. Eiraku, M. & Sasai, Y. Mouse embryonic stem cell culture for generation of three-dimensional retinal and cortical tissues. *Nat Protoc* **7,** 69–79; 10.1038/nprot.2011.429 (2011).

266. Fujiwara, H. *et al.* Regulation of mesodermal differentiation of mouse embryonic stem cells by basement membranes. *Journal of Biological Chemistry* **282,** 29701–29711; 10.1074/jbc.M611452200 (2007).

267. Chichagova, V. *et al.* Human iPSC differentiation to retinal organoids in response to IGF1 and BMP4 activation is line- and method-dependent. *Stem cells (Dayton, Ohio)* **38,** 195–201; 10.1002/stem.3116 (2020).

268. Cai, Z., Feng, G.-S. & Zhang, X. Temporal requirement of the protein tyrosine phosphatase Shp2 in establishing the neuronal fate in early retinal development. *J. Neurosci.* **30,** 4110–4119; 10.1523/JNEUROSCI.4364-09.2010 (2010).

269. Srinivasan, B. *et al.* TEER measurement techniques for in vitro barrier model systems. *Journal of laboratory automation* **20,** 107–126; 10.1177/2211068214561025 (2015).

270. Benson, K., Cramer, S. & Galla, H.-J. Impedance-based cell monitoring: barrier properties and beyond. *Fluids and Barriers of the CNS* **10,** 5; 10.1186/2045-8118-10-5 (2013).

271. Magdalena Winklhofer. Gene expression profile of retinal pigment epithelium derived from mouse embryonic stem cells. Master thesis. Karlsruher Institut für Technologie, 2021.

272. Stern, J. & Temple, S. Retinal pigment epithelial cell proliferation. *Experimental biology and medicine (Maywood, N.J.)* **240,** 1079–1086; 10.1177/1535370215587530 (2015).

273. Westenskow, P., Sedillo, Z., Barnett, A. & Friedlander, M. Efficient derivation of retinal pigment epithelium cells from stem cells. *Journal of visualized experiments : JoVE*; 10.3791/52214 (2015).

274. Leach, L. L. *et al.* Induced Pluripotent Stem Cell-Derived Retinal Pigmented Epithelium: A Comparative Study Between Cell Lines and Differentiation Methods. *Journal of ocular pharmacology and therapeutics : the official journal of the Association for Ocular Pharmacology and Therapeutics* **32,** 317–330; 10.1089/jop.2016.0022 (2016).

275. Foltz, L. P. & Clegg, D. O. Rapid, Directed Differentiation of Retinal Pigment Epithelial Cells from Human Embryonic or Induced Pluripotent Stem Cells. *Journal of visualized experiments : JoVE*; 10.3791/56274 (2017).

276. Grebenyuk, S. & Ranga, A. Engineering Organoid Vascularization. *Frontiers in Bioengineering and Biotechnology* **7,** 39; 10.3389/fbioe.2019.00039 (2019).

277. Gaucher, D. *et al.* Taurine deficiency damages retinal neurones: cone photoreceptors and retinal ganglion cells. *Amino Acids* **43,** 1979–1993; 10.1007/s00726-012-1273-3 (2012).

278. Castelli, V. *et al.* Taurine and oxidative stress in retinal health and disease. *CNS Neuroscience & Therapeutics* **27,** 403–412; 10.1111/cns.13610 (2021).

279. Völkner, M. *et al.* Mouse Retinal Organoid Growth and Maintenance in Longer-Term Culture. *Front. Cell Dev. Biol.* **9,** 645704; 10.3389/fcell.2021.645704 (2021).

280. Heger, J. I. *et al.* Human serum alters cell culture behavior and improves spheroid formation in comparison to fetal bovine serum. *Experimental Cell Research* **365,** 57–65; 10.1016/j.yexcr.2018.02.017 (2018).

281. Shang, P., Stepicheva, N. A., Hose, S., Zigler, J. S. & Sinha, D. Primary Cell Cultures from the Mouse Retinal Pigment Epithelium. *Journal of visualized experiments : JoVE*; 10.3791/56997 (2018).

282. Lynn, S. A. *et al.* A convenient protocol for establishing a human cell culture model of the outer retina. *F1000Research* **7,** 1107; 10.12688/f1000research.15409.1 (2018).

283. Zhaeentan, S. *et al.* The effects of hydrocortisone on tight junction genes in an in vitro model of the human fallopian epithelial cells. *European journal of obstetrics, gynecology, and reproductive biology* **229,** 127–131; 10.1016/j.ejogrb.2018.05.034 (2018).

284. Förster, C. *et al.* Differential effects of hydrocortisone and TNFalpha on tight junction proteins in an in vitro model of the human blood-brain barrier. *The Journal of physiology* **586,** 1937–1949; 10.1113/jphysiol.2007.146852 (2008).

285. Harpavat, S. & Cepko, C. L. Thyroid hormone and retinal development: an emerging field. *Thyroid : official journal of the American Thyroid Association* **13,** 1013–1019; 10.1089/105072503770867183 (2003).

286. Forrest, D., Reh, T. A. & Rüsch, A. Neurodevelopmental control by thyroid hormone receptors. *Current opinion in neurobiology* **12,** 49–56; 10.1016/s0959-4388(02)00289-1 (2002).

287. Ng, L., Ma, M., Curran, T. & Forrest, D. Developmental expression of thyroid hormone receptor beta2 protein in cone photoreceptors in the mouse. *Neuroreport* **20,** 627–631; 10.1097/WNR.0b013e32832a2c63 (2009).

288. Arbogast, P., Flamant, F., Godement, P., Glösmann, M. & Peichl, L. Thyroid Hormone Signaling in the Mouse Retina. *PLOS ONE* **11,** e0168003; 10.1371/journal.pone.0168003 (2016).

289. Yang, F., Ma, H. & Ding, X.-Q. Thyroid Hormone Signaling in Retinal Development, Survival, and Disease. *Vitamins and hormones* **106,** 333–349; 10.1016/bs.vh.2017.05.001 (2018).

290. Fields, M. A., Del Priore, L. V., Adelman, R. A. & Rizzolo, L. J. Interactions of the choroid, Bruch's membrane, retinal pigment epithelium, and neurosensory retina collaborate to form the outer blood-retinal-barrier. *Progress in Retinal and Eye Research* **76,** 100803; 10.1016/j.preteyeres.2019.100803 (2020).

291. Chen, L.-J. *et al.* Microfluidic co-cultures of retinal pigment epithelial cells and vascular endothelial cells to investigate choroidal angiogenesis. *Sci Rep* **7,** 3538; 10.1038/s41598-017-03788-5 (2017).

292. Moscona, A. Cell suspensions from organ rudiments of chick embryos. *Experimental Cell Research* **3,** 535–539; 10.1016/0014-4827(52)90077-3 (1952).

293. Layer, P. G., Rothermel, A. & Willbold, E. From stem cells towards neural layers: a lesson from re-aggregated embryonic retinal cells. *Neuroreport* **12,** A39-46; 10.1097/00001756-200105250-00001 (2001).

294. Rothermel, A. & Layer, P. G. Photoreceptor plasticity in reaggregates of embryonic chick retina: rods depend on proximal cones and on tissue organization. *The European journal of neuroscience* **13,** 949–958; 10.1046/j.1460-9568.2001.01469.x (2001).

295. Vollmer, G., Layer, P. G. & Gierer, A. Reaggregation of embryonic chick retina cells: pigment epithelial cells induce a high order of stratification. *Neuroscience Letters* **48,** 191–196; 10.1016/0304-3940(84)90018-1 (1984).

296. Rothermel, A., Willbold, E., Degrip, W. J. & Layer, P. G. Pigmented epithelium induces complete retinal reconstitution from dispersed embryonic chick retinae in reaggregation culture. *Proceedings. Biological sciences* **264,** 1293–1302; 10.1098/rspb.1997.0179 (1997).

297. Layer, P. G., Alber, R., Mansky, P., Vollmer, G. & Willbold, E. Regeneration of a chimeric retina from single cells in vitro: cell-lineage-dependent formation of radial cell columns by segregated chick and quail cells. *Cell and tissue research* **259,** 187–198; 10.1007/BF00318440 (1990).

298. Carter-Dawson, L. D. & LaVail, M. M. Rods and cones in the mouse retina. II. Autoradiographic analysis of cell generation using tritiated thymidine. *The Journal of comparative neurology* **188,** 263–272; 10.1002/cne.901880205 (1979).

299. Cui, Z. *et al.* Transcriptomic Analysis of the Developmental Similarities and Differences Between the Native Retina and Retinal Organoids. *Invest. Ophthalmol. Vis. Sci.* **61,** 6; 10.1167/iovs.61.3.6 (2020).

300. Chen, H. Y., Kaya, K. D., Dong, L. & Swaroop, A. Three-dimensional retinal organoids from mouse pluripotent stem cells mimic in vivo development with enhanced stratification and rod photoreceptor differentiation. *Molecular Vision* **22,** 1077–1094 (2016).

301. Akhtar, T. *et al.* Accelerated photoreceptor differentiation of hiPSC-derived retinal organoids by contact co-culture with retinal pigment epithelium. *Stem Cell Research* **39,** 101491; 10.1016/j.scr.2019.101491 (2019).

302. Burmeister, M. *et al.* Ocular retardation mouse caused by Chx10 homeobox null allele: impaired retinal progenitor proliferation and bipolar cell differentiation. *Nature genetics* **12,** 376–384; 10.1038/ng0496-376 (1996).

303. Livne-bar, I. *et al.* Chx10 is required to block photoreceptor differentiation but is dispensable for progenitor proliferation in the postnatal retina. *Proceedings of the National Academy of Sciences of the United States of America* **103,** 4988–4993; 10.1073/pnas.0600083103 (2006).

304. Yamamoto, H., Kon, T., Omori, Y. & Furukawa, T. Functional and Evolutionary Diversification of Otx2 and Crx in Vertebrate Retinal Photoreceptor and Bipolar Cell Development. *Cell Reports* **30,** 658-671.e5; 10.1016/j.celrep.2019.12.072 (2020).

305. Peng, S., Adelman, R. A. & Rizzolo, L. J. Minimal effects of VEGF and anti-VEGF drugs on the permeability or selectivity of RPE tight junctions. *Invest. Ophthalmol. Vis. Sci.* **51,** 3216–3225; 10.1167/iovs.09-4162 (2010).

306. Pearson, R. A., Dale, N., Llaudet, E. & Mobbs, P. ATP released via gap junction hemichannels from the pigment epithelium regulates neural retinal progenitor proliferation. *Neuron* **46,** 731–744; 10.1016/j.neuron.2005.04.024 (2005).

307. Wen, R. *et al.* Regulation of rod phototransduction machinery by ciliary neurotrophic factor. *J. Neurosci.* **26,** 13523–13530; 10.1523/JNEUROSCI.4021-06.2006 (2006).

308. Rhee, K. D. & Yang, X.-J. Function and mechanism of CNTF/LIF signaling in retinogenesis. *Advances in experimental medicine and biology* **664,** 647–654; 10.1007/978-1-4419-1399-9_74 (2010).

309. Ivan Rebustini & S Patricia Becerra. PEDF protects photoreceptors via a CRX-dependent mechanism. *Invest. Ophthalmol. Vis. Sci.* **62,** 2966 (2021).

310. Polato, F. & Becerra, S. P. Pigment Epithelium-Derived Factor, a Protective Factor for Photoreceptors in Vivo. *Advances in experimental medicine and biology* **854,** 699–706; 10.1007/978-3-319-17121-0_93 (2016).

311. Dorgau, B. *et al.* Decellularised extracellular matrix-derived peptides from neural retina and retinal pigment epithelium enhance the expression of synaptic markers and light responsiveness of human pluripotent stem cell derived retinal organoids. *Biomaterials* **199,** 63–75; 10.1016/j.biomaterials.2019.01.028 (2019).

312. Ghareeb, A. E., Lako, M. & Steel, D. H. Coculture techniques for modeling retinal development and disease, and enabling regenerative medicine. *STEM CELLS Translational Medicine* **9,** 1531–1548; 10.1002/sctm.20-0201 (2020).

313. Layer, P. G. & Willbold, E. Embryonic chicken retinal cells can regenerate all cell layers in vitro, but ciliary pigmented cells induce their correct polarity. *Cell and tissue research* **258,** 233–242; 10.1007/bf00239443 (1989).

314. Wolburg, H., Willbold, E. & Layer, P. G. Müller glia endfeet, a basal lamina and the polarity of retinal layers form properly in vitro only in the presence of marginal pigmented epithelium. *Cell and tissue research* **264,** 437–451; 10.1007/BF00319034 (1991).

315. Shiau, F., Ruzycki, P. A. & Clark, B. S. A single-cell guide to retinal development: Cell fate decisions of multipotent retinal progenitors in scRNA-seq. *Developmental biology* **478,** 41–58; 10.1016/j.ydbio.2021.06.005 (2021).

316. Lyu, P. *et al.* Gene regulatory networks controlling temporal patterning, neurogenesis, and cell-fate specification in mammalian retina. *Cell Reports* **37,** 109994; 10.1016/j.celrep.2021.109994 (2021).

317. Sun, R., Peng, S., Chen, X., Zhang, H. & Rizzolo, L. J. Diffusible retinal secretions regulate the expression of tight junctions and other diverse functions of the retinal pigment epithelium. *Molecular Vision* **14,** 2237–2262 (2008).

318. Fridolfsson, H. N., Ly, N., Meyerzon, M. & Starr, D. A. UNC-83 coordinates kinesin-1 and dynein activities at the nuclear envelope during nuclear migration. *Developmental biology* **338,** 237–250; 10.1016/j.ydbio.2009.12.004 (2010).

319. Perron, M. & Harris, W. A. Determination of vertebrate retinal progenitor cell fate by the Notch pathway and basic helix-loop-helix transcription factors. *Cellular and molecular life sciences : CMLS* **57,** 215–223; 10.1007/PL00000685 (2000).

320. Del Bene, F., Wehman, A. M., Link, B. A. & Baier, H. Regulation of neurogenesis by interkinetic nuclear migration through an apical-basal notch gradient. *Cell* **134,** 1055–1065; 10.1016/j.cell.2008.07.017 (2008).

321. Baye, L. M. & Link, B. A. Interkinetic nuclear migration and the selection of neurogenic cell divisions during vertebrate retinogenesis. *J. Neurosci.* **27,** 10143–10152; 10.1523/JNEUROSCI.2754-07.2007 (2007).

322. Ha, T. *et al.* The Retinal Pigment Epithelium Is a Notch Signaling Niche in the Mouse Retina. *Cell Reports* **19,** 351–363; 10.1016/j.celrep.2017.03.040 (2017).

323. Bray, S. J. Notch signalling in context. *Nat Rev Mol Cell Biol* **17,** 722–735; 10.1038/nrm.2016.94 (2016).

324. Pearson, R. A., Lüneborg, N. L., Becker, D. L. & Mobbs, P. Gap junctions modulate interkinetic nuclear movement in retinal progenitor cells. *J. Neurosci.* **25,** 10803–10814; 10.1523/JNEUROSCI.2312-05.2005 (2005).

325. Cullen, P. J. & Lockyer, P. J. Integration of calcium and Ras signalling. *Nature reviews. Molecular cell biology* **3,** 339–348; 10.1038/nrm808 (2002).

326. Moscat, J. & Diaz-Meco, M. T. The atypical protein kinase Cs. Functional specificity mediated by specific protein adapters. *EMBO Reports* **1,** 399–403; 10.1093/embo-reports/kvd098 (2000).

327. Aghaizu, N. D. *et al.* Repeated nuclear translocations underlie photoreceptor positioning and lamination of the outer nuclear layer in the mammalian retina. *Cell Reports* **36,** 109461; 10.1016/j.celrep.2021.109461 (2021).

328. Hans, F. & Dimitrov, S. Histone H3 phosphorylation and cell division. *Oncogene* **20,** 3021–3027; 10.1038/sj.onc.1204326 (2001).

329. Das, T., Payer, B., Cayouette, M. & Harris, W. A. In vivo time-lapse imaging of cell divisions during neurogenesis in the developing zebrafish retina. *Neuron* **37,** 597–609; 10.1016/s0896-6273(03)00066-7 (2003).

330. Pacal, M. & Bremner, R. Mapping differentiation kinetics in the mouse retina reveals an extensive period of cell cycle protein expression in post-mitotic newborn neurons. *Developmental Dynamics* **241,** 1525–1544; 10.1002/dvdy.23840 (2012).

331. Sharma, R. K. & Netland, P. A. Early born lineage of retinal neurons express class III beta-tubulin isotype. *Brain Research* **1176,** 11–17; 10.1016/j.brainres.2007.07.090 (2007).

332. Yanai, A., Laver, C. R. J., Gregory-Evans, C. Y., Liu, R. R. & Gregory-Evans, K. Enhanced functional integration of human photoreceptor precursors into human and rodent retina in an ex vivo retinal explant model system. *Tissue engineering. Part A* **21,** 1763–1771; 10.1089/ten.tea.2014.0669 (2015).